MODELLING THE EFFECT OF NUTRIENT SUPPLY, TEMPERATURE AND LIGHT INTENSITY ON CNIDARIAN-ALGAE SYMBIOSIS

MALIN GUSTAFSSON

February 2014

A THESIS SUBMITTED IN FULFILMENT OF THE REQUIERMENTS FOR THE DEGREE OF DOCTOR OF PHILOSOPHY IN SCIENCE

DEPARTMENT OF ENVIRONMENTAL SCIENCE,

PLANT FUNCTIONAL BIOLOGY AND CLIMATE CHANGE CLUSTER

UNIVERSITY OF TECHNOLOGY, SYDNEY

i. CERTIFICATE OF ORIGINAL AUTHORSHIP

I certify that the work in this thesis has not previously been submitted for a degree nor has it been submitted as part of requirements for a degree except as fully acknowledged within the text.

I also certify that the thesis has been written by me. Any help that I have received in my research work and the preparation of the thesis itself has been acknowledged. In addition, I certify that all information sources and literature used are indicated in the thesis.

Production Note:
Signature removed prior to publication.

07/08/2013

Malin Gustafsson

i. ACKNOLEDGMENTS

Foremost, I would like to thank my supervisors Professor Peter Ralph and Dr. Mark Baird for their continuous support over the past years. It has been a challenging but rewarding experience, which would not have been possible without their assistance. Thank you Peter for all the encouragement and for being an endless source of ideas. I would also like to extend a special thanks to Mark Baird for spending hours and hours on Skype discussing the project, he has been an invaluable source of knowledge and support throughout my candidature.

Furthermore, I would like to thank Mathieu Pernice and Mathieu Mongin for their collaboration and contribution towards this project. Additionally, I would like to extend my appreciation to Ross Hill, David Suggett and Kay Bishof for supplying experimental data to this project.

I would also like to thank all my colleges at UTS whom have come with ideas and suggestions to aid the progress of this project. I would particularly like to thank John Moore for helping out with the administration, and Verena Schrameyer for bringing me along to Heron Island.

During my candidature I have spent time at CSIRO in Hobart and would like to thank Richard Matear everyone else there that have taken an interest in my project, and taking time to discuss and give valuable feedback, particularly during the model development phase.

I also thank the Australian Research Council (DP110105200) and the University of Technology, Sydney for providing funds for the University of Technology, Sydney President's scholarship and the International Postgraduate Research Scholarship.

Last but not least, I would like to thank my family and friends for their support and understanding throughout my candidature, particularly my parents, my sister and Martin for listening and discussing all aspects of my project. It is a privilege to have you all in my life. Here I would also like to extend a warm thank you to Noni, Puj, Ginny, Miriam, James and Mark for taking me into their homes and making me feel like family. I will miss my visits to Sydney and to Hobart.

ii. PUBLICATIONS

PEER REVIEWED JOURNAL ARTICLES ARISING DIRECTLY FROM THIS THESIS

Chapter 2:

Gustafsson, M. S. M., M. E. Baird, and P. J. Ralph. 2013. The interchangeability of autotrophic and heterotrophic nitrogen sources in Scleractinian coral symbiotic relationships: A numerical study. Ecological Modelling **250:** 183-194.

Chapter 3:

Gustafsson, M. S. M., M. E. Baird, and P. J. Ralph. (in press). Modeling photoinhibition and bleaching in Scleractinian coral as a function of light, temperature and heterotrophy. Limnology and Oceanography.

iii. TABLE OF CONTENT

iv. LIST OF FIGURES

two DIN uptake rates (V_{DIN}^{H}: 0.5 and 5 µg N cm^{-2} d^{-1}) and two feeding rates (Z_N: 0.5 and 5 µg N cm^{-2} d^{-1}). Panel A and B show the C_F^H and C_R^H respectively. Panel C and D show C_F^S and C_R^S for the entire symbiont population (S). Panels E and F show C_F^S and C_R^S for one symbiont cell. Panels G and H show the chlorophyll concentration for the symbiont population and for an individual symbiont cell respectively. Note that the scale on the y-axis differ between panels.

Figure 2.4: Average daily coral N fluxes at steady state and a light level of 1000 µmol photon m^{-2} s^{-1} for the four nutrent cases: A) high Z_N + high V_{DIN}^{H} B) high Z_N + low V_{DIN}^{H} C) low Z_N + high V_{DIN}^{H} D) low Z_N + low V_{DIN}^{H}. Blue and green boxes represent host and symbiont state variables respectively. The size of the boxes indicates the size of the individual N state variables, with the numerical value given in µg N cm^{-2}. The arrows show the direction of the fluxes and the thickness of the arrow and numerical value in µg N cm^{-2} d^{-1} quantifying the magnitude of the flux.

Figure 2.5: Average daily coral C fluxes at steady state and a light level of 1000 µmol photon m^{-2} s^{-1} for the four nutrient cases: A) high Z_N + high V_{DIN}^{H} B) high Z_N + low V_{DIN}^{H} C) low Z_N + high V_{DIN}^{H} D) low Z_N + low V_{DIN}^{H}. Blue and green boxes represent host and symbiont state variables respectively. The size of the boxes indicates the size of the individual C state variables, with the numerical value given in µg C cm^{-2}. The arrows show the direction of the fluxes and the thickness of the arrow and numerical value in µg C cm^{-2} d^{-1} quantifying the magnitude of the flux.

Figure 2.6: Percentage of change in host (C_F^H) and symbiont population biomass ($C_F^S S$) between the four nutrient cases; high feeding rate on prey (Z_N) + high DIN diffusion rate (V_{DIN}^{H}), high Z_N + low V_{DIN}^{H}, low Z_N + high V_{DIN}^{H}, low Z_N + low V_{DIN}^{H}.

The arrows indicate the direction of comparison, and the number the percentage decreases (negative numbers) or increase (positive numbers) in the state variable.

Figure 3.1: Schematic of photoinhibition model, boxes indicate state variables and arrows are fluxes. ΔRO_f is not considered a state variable, as we assume that it will immediately react with symbiont tissues at the site of formation, hence inhibit the photosystem. The numbers in the brackets correspond to the equation number in Table 3.3. The dashed arrow and box refereeing to ROS in the host are not included in the model.

Figure 3.2: Model fitted to data from Hill et al. (2012). Solid lines represented the 25°C model run over a 2 day period. Dashed line is the model run at 31°C. Filled markers indicate the experimental data for the 25°C treatment and open markers the 31°C treatment with ±standard deviation (SD). (A) is diurnal light oscillation. (B) F_v:F_m data with corresponding $Q_a: Q_t$ in the model. (C) Photochemistry Y(II) corresponding in model was $Q_{ox}: Q_t$. (D) Y(NPQ) corresponding in the model $D_t: (D_t + D_d + \text{Chl})$. (E) Y(NO) calculated using the assumption Y(II)+Y(NPQ)+Y(NO)=1.

Figure 3.3: F_v:F_m at (A) 10:30 h and (B) 05:30 h for the modeled and Borell and Bischof (2008) experimental data during the ten day feeding experiment. Closed and open markers show the measured F_v:F_m for fed and unfed coral, respectively. Black and grey lines indicate the modeled F_v:F_m ($Q_a: Q_t$) for fed and unfed coral, respectively.

Figure 3.4: Symbiont population size after two days acclimation under non-stress and non-feeding conditions (Reference) and after 10 days of elevated temperature for fed and starved corals. Light grey bar shows the measurements ±standard error (SE) from Borell and Bischof (2008).

Figure 3.5: Concentration of reactive oxygen species per symbiont cell (RO_S) and H_2O_2 measurements (mean ±SE) from two *Symbiodinium* clades (A1 and B1) in culture, from Suggett et al. (2008). (A) 100 μmol photon m^{-2} s^{-1} treatment. (B) 1000 μmol photon m^{-2} s^{-1} treatment.

Figure 3.6: Percentage of chlorophyll concentration remaining per coral unit surface area as a function of heat stress and heterotrophic feeding over time. Vertical dashed lines indicate 100 DHD. (A) 90 day simulation at T_{mean} (28°C) for corals feeding heterotrophically at a range of rates. (B) 2°C above T_{mean}. (C) 3°C above T_{mean}. (D) 4°C above T_{mean}. (D) Legend gives line shading for heterotrophic the feeding rates.

Figure 3.7: (A) Concentration of ROS (RO_S) and (B) reserves (C_R^S) in the symbiont for T_{mean}, +2°C, +3°C and +4°C heating over 90 days and a heterotrophic feeding rate of 100 μg N cm^{-2} d^{-1}.

Figure 4.1: Schematic over C fluxes between the environment, host and the symbiont. Symbols and abbreviations are explained in Table 4.1 and 4.2.

Figure 4.2: Accumulation rate of C in the symbiont (A) and host tissues (B). The model values correspond to the lines and are the sum of the change in the functional and the reserve pools. The circles shows the measured ^{13}C accumulation rate at four hours for the 200 µmol photon m^{-2} s^{-1} light treatment (closed circle) and 50 µmol photon m^{-2} s^{-1} light treatment (open circle) ± 1 SD.

Figure 4.3: Modelled carbon budget diagram for the sea anemone *Aiptasia pulchella*, rates are given in µg C mg^{-1} h^{-1}, and percentages of internal fluxes to the total photosynthates rate in brackets. Light intensity of 200 (A) and 50 µmol photon m^{-2} s^{-1} (B). Dashed arrow marked mC corresponds to the carbon the host acquired from dead symbiont that died due to natural mortality.

Figure 4.4: Modelled carbon budget diagram for the coral, rates are given in µg C cm^{-2} h^{-1}.

Figure 5.1: Location of Heron Reef, Wistari Reef and One Tree Reef on the Great Barrier Reef (A). Heron Reef with the three different coral zones (B): Black= bommies, dark gray = crest, light gray = slope .

Figure 5.2: Red line represents the surface elevation, dashed the water velocity and the solid black line the intensity at 420 nm for two sites on the reef: Coral slope (top panel) and bommies (bottom panel). The red boxes show the two selected periods: 7-8th ($P^{high}_{velocity}$) and 18-19th ($P^{low}_{velocity}$).

Figure 5.3: Tidal height for $P_{velocity}^{high}$ and $P_{velocity}^{low}$. Letters indicate the output points and the black and white bars represent night and day, respectively. The x-axis shows the date and local time of day.

Figure 5.4: PON at the surface of the water column for $P_{velocity}^{high}$ in unit mg N m^{-3}. The title of each panel states the time point letter as well as the date and time of day. Arrows represent the current direction and strength. The black contour marks the rim of the reefs.

Figure 5.5: PON at the surface of the water column for $P_{velocity}^{low}$ in unit mg N m^{-3}. The title of each panel states the time point letter as well as the date and time of day. Arrows represent the current direction and strength. The black contour marks the rim of the reefs.

Figure 5.6: DIN at the surface of the water column for $P_{velocity}^{high}$, unit mg N m^{-3}. The title of each panel states the time point letter as well as the date and time of day. Arrows represent the current direction and strength. The black contour marks the rim of the reefs.

Figure 5.7: DIN at the surface of the water column for $P_{velocity}^{low}$, unit mg N m-3. The title of each panel states the time point letter as well as the date and time of day. Arrows represent the current direction and strength. The black contour marks the rim of the reefs.

Figure 5.8: Vertical profiles of PON, DIN, Age and water velocity from three sites on the reef (lagoon, bommies and reef slope). The top row of panels represents the values from
$P_{velocity}^{high}$ and the bottom row $P_{velocity}^{low}$.

Figure 5.9: Age of water at the surface over the reef for $P_{velocity}^{high}$, unit hours.

Figure 5.10: Age of water at the surface over the reef for $P_{velocity}^{low}$, unit hours.

Figure 5.11: Mean biomass of coral host and symbiont popuation for $P_{velocity}^{high}$ (I and III) column) and $P_{velocity}^{low}$ (II and IV) in mg N m^{-2}. The star in IV shows the location of the point evaluated in Figure 5.12.

Figure 5.12: Simulated change in coral biomass, PON concentration, DIN concentration, tidal height and water velocity for one point at the bommies during the month of January, the location of the point is shown in Figure (5.11 IV). The rectangles show two periods of coral growth, one "enhanced" and one "reduced".

Figure 5.13: Uptake rate of inorganic nitrogen by corals (mg N m^{-2} d^{-1}).

Figure 5.14: Mass transfer rate coefficient (m d^{-1}) over the corals for output point with DIN uptake for both periods.

Figure 5.15: Uptake rate of organic nitrogen by corals through heterotrophic feeding (mg N m^{-2} d^{-1}). Note that the letter representing each panel corresponds to the time point identification in Figure 5.3.

Figure 5.16: Potential uptake rate of organic nitrogen by corals through heterotrophic feeding (mg N m^{-2} d^{-1}). Note that the letter representing each panel corresponds to the time point identification in Figure 5.3.

Figure 5.17: Surface water pH during $P_{velocity}^{high}$.

Figure 5.18: Surface water pH during $P_{velocity}^{low}$.

Figure 5.19: Profile of DIN uptake by the coral community, and change DIN concentration, pH and water age at the surface of the water column, as well as water velocity directly over the substrate. A) red line shows the location of the profile over Heron Reef. Water velocity, pH, water age, DIN concentration in the water column, DIN uptake over the coral population and coral host N biomass along the transect for $P_{velocity}^{high}$ (B), and $P_{velocity}^{low}$ (C). The arrow in indicate the direction of the current. At the bottom of the panels showing biomass different colour bars indicate different parts of the reef; black=reef slope, gray=reef crest and dashed=bommies.

v. LIST OF TABLES

Table 3.3: State variable equations from the GBR13 model, where Eqs. 9-12 include the alterations made for this model. Equation numbers are given in brackets, and equation numbers following GBR13 indicate which equation it refers to in Gustafsson et al. (2013).

Table 3.4: Photoinhibition model equations, the number in brackets refers to the equation numbers used in the text.

Table 3.5: Description and value of model parameters.

Table 3.6: Equations from Gustafsson et al. (2013) (GBR13) relevant to this photoinhibition model. The numbers in brackets refers to the equation numbers in GBR13.

Table 3.7: Parameters from Gustafsson et al. (2013) (GBR13) relevant to this photoinhibition model.

Table 8: Definition of state variables and initial conditions for *Pocillopora damicornis* and *Stylophora pistillata.* The initial values for the symbiont population size and pigment pools for *P. damicornis* were derived from Hill et al. (2012) whereas the initial total values of the RCII pools were estimated from Suggett et al. (2008) and divided into the three pools so that initial F_v:F_m and Y(II) values

corresponded with those in Hill et al. (2012). For *S. pistillata* the initial values were derived by spinning up the model for 2 days using a smaller symbiont cell size.

Table 4.1: Model equations

Table 4.2: Model parameters, variables and rates used in the anemone model and the coral model. Bracketed values represented the parameters different in the coral-model.

Table 4.3: Initial conditions for Tremblay et al. (2012).

Table 4.4: Experimental dataset: Uptake rate of ^{13}C by different tissues, and total C content of the host and the symbiont (average of three samples). The light levels were HL: 200 µmol photon m^{-2} s^{-1} and LL: 50 µmol photon m^{-2} s^{-1} (Pernice pers. comm.).

Table 5.1: Ecology state variables

Table 5.2: Model equations associated with corals

Table 5.3: Model parameters.

vi. ABBREVIATIONS

APX	Ascorbate peroxidises
C	Carbon
CCM	Carbon Concentrating Mechanism
Chl	Chlorophyll
CSIRO	Commonwealth Scientific and Industrial Research Organisation
DIC	Dissolved Inorganic Carbon
DIN	Dissolved Inorganic Nitrogen
DOM	Dissolved Organic Matter
ETC	Electron Transport Chain
e^-	Electron
Fv/Fm	Maximum quantum yield of photosystem II
IPCC	Intergovernmental Panel of Climate Change
H_2O_2	Hydrogen peroxide
MTL	Mass Transfer Limited
N	Nitrogen
NOAA	National Oceanic and Atmospheric Administration
NPQ	Non-photochemical quenching
O_2^-	Superoxide

$^1O_2$*	Singlet oxygen
OEC	Oxygen Evolution Complex
POC	Particulate Organic Carbon
POM	Particulate Organic Matter
PON	Particulate Organic Nitrogen
ROS	Reactive Oxygen Species
PQ	Plastoquinone
PSII	Photosystem II
PSI	Photosystem I
SHOC	Spares Hydrodynamic Ocean Code
SOD	Superoxide dismutase
SST	Sea Surface Temperature

vii. ABSTRACT

Understanding the symbiotic association between a coral host and their algae symbiont is essential if we are to be able to simulate and predict how expected changes in ocean sea surface temperatures and other environmental conditions associated with climate change may influence coral reefs in the future. In this thesis a mechanistic coral-algae symbiosis model is proposed, a model which captures the interaction between a heterotrophic host and an autotrophic symbiont with varying sources of nutrients, and various temperature and light intensities. This modelling effort includes mathematical representations of important physiological processes, such as growth, respiration, photosynthesis, calcification, translocation of photosynthates, mortality and mucus production, as well as photoinhibition, ROS production and bleaching. Validating the model using experimental data, showed the model capable of capturing the nutrient dynamics between the environment, the cnidarian host and the symbiotic algae, photoinhibition and bleaching as a function of elevated temperature and light, as well as the mitigating effects heterotrophic feeding may have during elevated thermal stress.

The basic coral symbiosis model, first developed, considered the nutrient dynamics of the symbiosis. The coral acquires nitrogen (N) through two processes, uptake of dissolved inorganic nitrogen (V_{DIN}^{H}) and heterotrophic feeding (Z_N). Numerical experiments were used to highlight the importance of these different sources of N for coral survival and growth. The model outputs showed the importance of the algae symbionts to the coral host as a source of both N and C when the feeding rate was limited. In contrast, with no light or low light, conditions under which the symbiont population dies, the host was able to survive if Z_N was sufficient to sustain its metabolic requirements. Translocation and recycling of nutrient were shown to be two of the most important features of this model, emphasizing why it is essential to resolve host and symbiont in a coral model.

During the second phase of this thesis a photoinhibition and bleaching model was added to the basic symbiosis model. The resulting modelled rate of bleaching depended on temperature, light intensity and the potential for heterotrophic feeding. The validation showed that the model was capable of capturing both the diurnal change in the state of the photosystem, as well as changes in the symbiont population and the coral host caused by different temperature, light and feeding treatments. Elevated temperatures and light led to a degradation of the photosystem and the expulsion of symbiont cells. If the coral fed heterotrophically, this degradation of the photosynthetic apparatus due to temperature and light stress was reduced, but still a clear decrease in Fv/Fm and cell numbers was observed when the coral was exposed to elevated temperature.

During the first two phases of this modelling effort it was noted that translocation and the uptake of inorganic nutrients needed more consideration. These processes were redefined using experimental (nanoSIMS) data of uptake and translocation in the symbiotic sea anemone *Aiptasia pulchella*. The new definitions proposed that the uptake of DIN and DIC from the environment were symbiont driven and directly associated with photosynthetic activity. The new translocation definition has two components including a representation of the "host release factor" as well as a release of excess photosynthates. This exercise also allowed us to show that the model worked well for a symbiotic association other than the corals.

The final part of this project was to incorporate the coral symbiosis model into a reef scale fully coupled hydrodynamic biogeochemical model of Heron Island Reef. Due to the high complexity of the model a simplified version of the basic symbiosis model was included. Even so the month long model runs showed how the coral influenced the nutrient dynamics over the reef and how changes in water column properties, water velocity and bottom friction influenced coral uptake of nutrients.

The model developed in this thesis highlights that the interchangeability of N sources, and the ability to exchange and recycle nutrients in the host-symbiont system, is the key to coral survival in nutrient poor environments. The photoinhibition model showed that heterotrophic feeding can mitigate the effect of

temperature and light stress as it enhances repair rates and tissue synthesis. The model is also applicable to other host-symbiont associations (such as the sea anemone) and it can be decoupled and used for the animal or the algae part separately. This model is a good tool to explore host-symbiont interactions, however there is always room for improvement and further development.

CHAPTER 1:

GENERAL INTRODUCTION

1. General Introduction

Coral reefs are among the most productive marine ecosystems in the world, providing habitat for a diverse range of organisms (Hughes 1989; Roberts et al. 2002). Hermatypic or reef-building (Scleractinian) corals are colony-forming sessile organisms most commonly found in tropical marine oligotrophic environments, where they lay down a calcium carbonate skeleton which acts as the foundation of the reef (Falkowski et al. 1993; Muller-Parker and D'elia 1997; Lesser 2004; Davy et al. 2006). The success of corals in these nutrient-poor waters depends largely on a symbiotic relationship between a cnidarian host and a unicellular dinoflagellate algae from the genus *Symbiodinium* often referred to as 'zooxanthellae' (Muscatine and Porter 1977; Titlyanov and Titlyanova 2002; Venn et al. 2008).

This symbiotic relationship is based on the heterotrophic animal host providing the autotrophic zooxanthellae with a protected environment within its tissues and a steady influx of nutrient-rich compounds from the host's metabolic processes, typically consisting of carbon dioxide, ammonium, urea and polyphosphates (Wang and Douglas 1999; Venn et al. 2008; Pernice et al. 2012). The zooxanthellae in turn provide the host with photosynthates such as glycerol, glycerides and amino acids, which are important for the host's metabolic functions (Sutton and Hoegh-Guldberg 1990; Titlyanov and Titlyanova 2002). This symbiosis is not just found in corals, but can also be seen in several other anthozoans such as clams, anemones and jellyfish which have a similar association with the zooxanthellae (Davy and Cook 2001a; Venn et al. 2008). Scleractinian corals and the coral-algae interaction have received a great deal of attention due to the threat that climate change poses for the future existence of coral reefs (Hoegh-Guldberg 2004).

Global sea surface temperatures (SST) have increased during the past two centuries as a result of climate change (IPCC, 2007). These climatic changes are

thought to be at least partly caused by an increase in greenhouse gases such as carbon dioxide (CO_2) resulting from anthropogenic activities (IPCC, 2007). In a response to climate change, SST and ocean acidification are expected to increase in the future (Mackay and Khalil 2000). The effects that these changes may have on coral reefs have been widely debated over the past few decades (Gattuso et al. 1999; Kleypas et al. 1999; Kleypas et al. 2001; Anthony et al. 2008; De'ath et al. 2009; Doney et al. 2009). Coral bleaching events are expected to increase in frequency and severity as the oceans warm, with a predicted loss of 30-90% of the total coral population by 2050 (Hoegh-Guldberg 2004). Such a loss of corals is likely to lead to the extinction, of less resilient coral species and a shift in the coral reef community structure (Loya et al. 2001). This prediction of future coral loss is based on the assumption that the change in temperature is too rapid for the coral to adapt to the changing conditions. It is argued that the generation time of the corals is too long and the gene flow is too great, and hence prevents local adaptations. The extended generation time is linked to long life span, late maturation and colony fission of the Scleractinian coral (Hughes et al., 1992).

Baird et al. (2009) discuss the possibility that the assumption of limited local adaptation as a result of great dispersion may be inaccurate. For example, genetic studies have shown subdivision on a local scale indicating restricted genetic flow (Ayre and Hughes, 2004). There is also the 'adaptive bleaching hypothesis' (Buddemeier and Fautin, 1993), which suggests that the coral can adapt to stress in matter of weeks rather than generations, by switching its current clade (subset) of symbionts to a more temperature tolerant partner (Buddemeier and Fautin, 1993). To understand and predict the future of coral reefs, the corals ability to adapt to local conditions needs to be understood, including the role of both partners in the symbiotic relationship (Baird et al. 2009).

The loss of coral reefs would be devastating, as coral reefs are of both biological and socio-economic importance, with approximately 500 million people directly dependent on coral reefs for their livelihood (Hoegh-Guldberg 2004; Wilkinson [ed.]. 2002). Coral reefs also harbour a diverse range of organisms, with representatives from 32 of the 34 known animal phyla (Hoegh-Guldberg 1999),

which are likely to be adversely effected by the loss of scleractinian corals and eventually the reef structure. Additionally, coral reefs can act as an important physical barrier protecting coastal areas from wave action and subsequent erosion.

To understand how the corals are affected by changes in their environment we need to identify the physiological implications and responses to such changes. The process of identifying these physiological responses is complicated by the symbiotic interaction, which can both amplify or diminish the effect of stressors. To be able to understand and predict how corals will respond to climate change in to the future, we first need to understand the basics of the symbiosis and dynamic interactions which occur under non-stress conditions. In the following sections, general coral physiology, nutrient acquisition, photobiology, calcification and the role of corals in a reef environment will be described.

1.1 CORAL PHYSIOLOGY

Cnidarians have a relatively simple body construction, with a diploblastic (two cell layer) body pattern composed of the epidermis and the gastrodermis (Berking 2007). These two layers are derived from germ layers, the ectoderm and the endoderm, which are formed during embryonic gastrulation and separated by a cellular matrix often referred to as mesoglea (Epp et al. 1986). The gastrodermal cell layers surround the gastrovascular cavity (coelenteron) which opens to the seawater via the mouth of the polyp. In coral, gastrodemal cells above and below the coelenteron harbour the symbiotic zooxanthellae (Fig. 1.1). The gastrovascular cavity of a polyp is interconnected with cavities of adjacent polyps forming a complex system. The interconnected cavities are to a certain extent divided into compartments by mesenteries and water exchange within the cavity can be induced by ciliar movement. The process of calcification occurs in the aboral ectoderm cells, called the calicoblastic epithelium (Fig. 1.1) (Gattuso et al. 1999). Processes like calcification and photosynthesis are strongly influenced by the chemistry of the water within the gastrovascular cavity (Furla et al. 2000; Al-

Horani et al. 2003). The chemistry (pH) of this water is altered by respiration, calcification, photosynthesis and exchange with the external seawater (Furla et al. 2000).

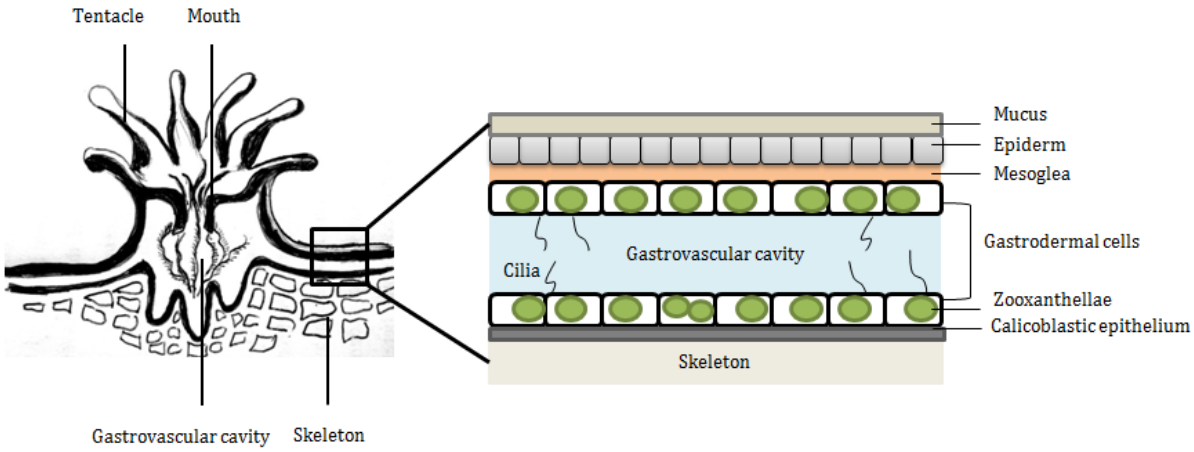

Figure 1.1: Schematic of coral body plan, with a coral polyp to the left and the organization of coral tissue to the right.

The surface of the coral host is covered by a mucus layer composed of a complex mixture of polysaccharide, protein and lipids (Bythell and Wild 2011). The mucus layer is vital for processes such as heterotrophic feeding and sediment cleansing, as well as a defense against a large number of environmental stresses (Anthony and Connolly 2004; Bythell and Wild 2011). The mucus is mainly secreted from mucocyte cells in the oral ectoderm (Marshall and Wright 1993). The composition of the mucus varies greatly according to irradiance, environmental contaminants, age and species (Crossland 1987; Edmunds and Davies 1989; Brown and Bythell 2005). The presence of zooxanthellae also play an essential role in determining the composition of mucus, with 20 to 45% of daily net photosynthate production being released as mucus and dissolved organic carbon (Crossland 1987; Edmunds and Davies 1989; Brown and Bythell 2005).

There is a second partner associated with the coral which is often overlooked and that is the coral microbial consortium. The coral microbial consortium includes microorganisms such as bacteria and Archaea (Rosenberg et al. 2007). There is a large diverse population of Archaea present in coral tissues (Kellogg 2004;

Webster et al. 2004). However, distinct populations of bacteria can be found in the surface mucus layer of the coral, the coral tissue and within the calcium carbonate skeleton (Rosenberg et al., 2007). Early studies into the coral-bacteria partnership focused on the bacterial communities in the surface mucus layer describing their beneficial characteristics such as nitrogen fixation and chitin decomposition (Ducklow and Mitchell 1979; Shashar et al. 1994). It has also been suggested that an endolithic community of bacteria living inside the corals skeleton can provide the coral with 50% of its nitrogen requirement (Ferrer and Szmant 1988). The coral-algae-bacteria association has not yet been included in any models of coral energetic. However, the associated bacterial community may prove to play a vital role to coral health and probably should not be forgotten.

1.2 HETEROTROPHY VS. AUTOTROPHY

The mixotrophic character of corals (that they acquire nutrient both through autotrophy and heterotrophy) has been known since the early twentieth Century (Yonge and Nicholls 1931). The success of Scleractinian corals in nutrient-poor environments was originally thought to solely depend on the translocation of photosynthates from the symbiont to the host, as it was observed that approximately 60-80% of the daily photosynthate production were translocated to the host (Muscatine et al. 1981; Edmunds and Davies 1986). However, now it is recognized that corals have varied and adaptable trophic capacity (Houlbrèque and Ferrier-Pagès 2009). Corals can feed on a wide range of prey items from zooplankton to particulate and dissolved organic matter (POM and DOM). Corals can capture prey items by tentacle grabbing, nematocyst discharges or mucus adhesion (Lewis and Price 1975; Sebens et al. 1998; Houlbrèque and Ferrier-Pagès 2009). It has been demonstrated that feeding on zooplankton can increase pigment concentration, as well as symbiont population size within the coral (Houlbrèque et al. 2003). Though, the concentration of zooplankton over a reef is generally varied in both space and time (Houlbrèque and Ferrier-Pagès 2009), planktonic microorganisms are relatively abundant in reef environments. This may be a

significant source of nitrogen and carbon for the coral community and have been suggested as one of the major nutrient sources sustaining the reefs within these oligotrophic waters (Houlbreque et al. 2004b).

1.3 PHOTOSYNTHESIS, PHOTOINHIBITION AND BLEACHING

Corals often live close to their upper thermal limit during the summer months, and an increase in summer mean SST of only 1-3°C can cause photoinhibition and bleaching (Hoegh-Guldberg 1999). Bleaching is the loss of symbiont pigments and/or expulsion of symbionts allowing the white skeleton to become visible through the un-pigmented animal tissue (Brown 1997). A physical trigger of photoinhibition is the temperature-induced breakdown of the Ribulose bisphosphate carboxylase/oygenase (Rubisco) enzyme (Lilley et al. 2010). The Rubisco is essential for the fixation of CO_2 for photosynthesis; if inactive it causes a blockage of the electron transport chain (ETC) leading to a buildup of electrons which are free to form reactive oxygen species (ROS) (Falkowski et al. 2007).

Figure 1.2A shows a schematic of the flow of electrons through the ETC, with photons being captured by photosynthetic pigments in the light harvesting complex (LHC). Photosynthetic pigment captures one photon and loses one electron (e^-) which is passed via the oxygen evolution complex (OEC) to a quinone molecule in photosystem II (PSII) initiating the electron flow through the ETC. At the OEC, molecular oxygen is generated through photo-oxidation of water via the following reaction: $2H_2O + 4e^- \rightarrow O_2 + 4H^+$ (Falkowski et al. 2007). The free H^+ will change the pH of the lumen, additionally the H^+ can be used for the production of ATP (not shown in Fig. 1.2). Blocking the ETC, due to temperature inactivation of Rubisco, hence blocks the Calvin-Benson cycle, causes a buildup of electrons which can react with O_2 forming superoxide (O_2^-) at the site of photosystem I (PSI) (Fig. 1.2B-C) (Venn et al. 2008). Superoxide dismutase (SOD) catalyzes the formation of hydrogen peroxide (H_2O_2), whereas the enzyme ascorbate peroxidase (APX) can reduce the H_2O_2 to water (Asada 2006). The production of O_2^- and H_2O_2 is called the Mehler reaction (Mehler and Brown 1952). In addition to the Mehlar reaction,

ROS can form as singlet oxygen ($^1O_2$*), which is produced due to the highly reactive triplet states of chlorophyll (Chl) reacting with O_2 (Fig. 1.2C). Triple excited Chl is a result of restricting the rate of the electron flow through the ETC causing maximal reduction of the plastoquinone (PQ) which causes a buildup of excess excitation energy (Jones et al. 1998). As $^1O_2$* forms at PSII it can prompt the degradation of the D1 protein (Asada 1996), as well as cause damage and bleaching of pigments in the light harvesting complex (Halliwell 1991; Venn et al. 2006).

The D1 protein has a vital role in the reaction centre of PSII, binding components for charge separation and electron transport (Warner et al. 1999). When the rate of damage to the D1 protein exceeds the repair rate, the photosystem becomes inhibited. Likewise, there is a continuous production of ROS even under non-stress conditions; however it is not until the rate of ROS generation exceeds the rate of detoxification that oxidative damage can occur. Where $^1O_2$* foremost causes damage to PSII, H_2O_2 and O_2^- are thought to be able to cross the symbionts cell membrane and enter the host where it can cause oxidative damage which can trigger the expulsion of symbiont cells (Venn et al. 2008; Wooldridge 2009).

The effect of elevated temperature and light stress can be reduced if the coral is able to feed heterotrophically; additionally it has been found that artificially fed corals may recover to a greater extent and faster after a bleaching event (Borell et al., 2008; Hughes et al., 2008). The likely reason behind this mitigating effect of heterotrophy is that more energy can be used to detoxify and generate new tissues which may replace damage tissues. If sufficient nutrient supply is available, a coral can live without its symbiont population, for example deep sea corals are aposymbiotic (Roberts et al., 2006) and corals which have been almost entirely bleached are known to recover if provided a sufficient food source (Connolly et al., 2012).

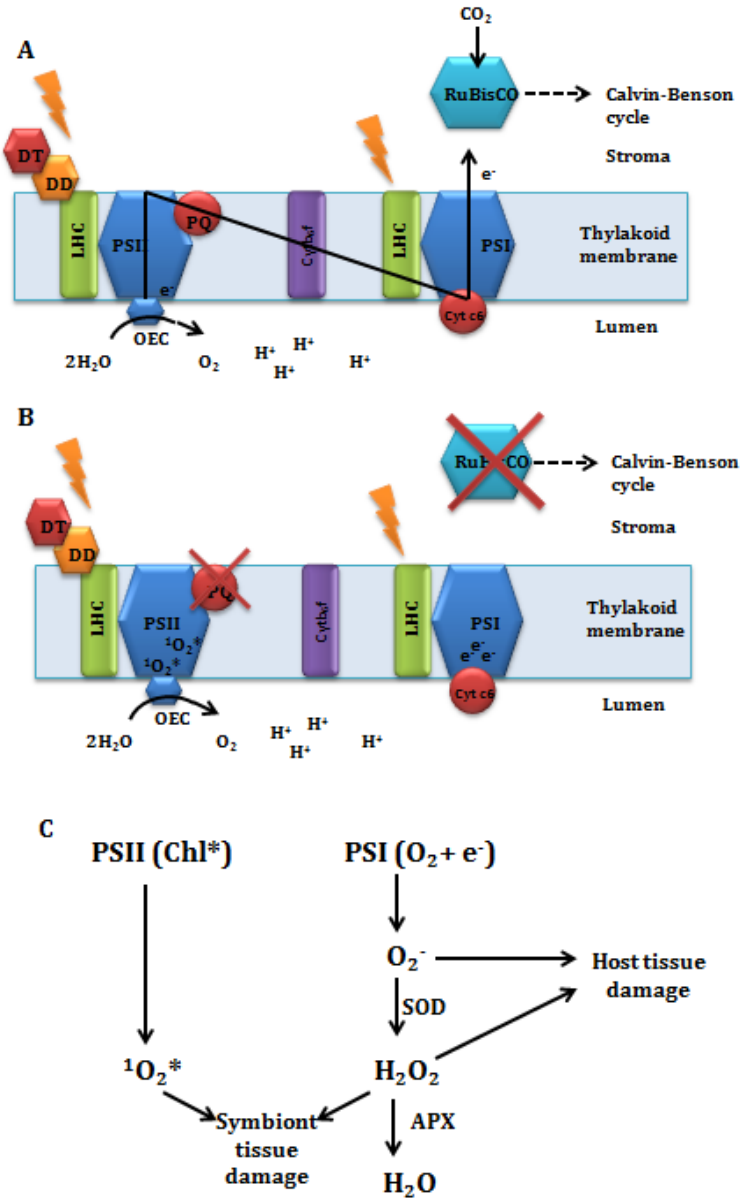

Figure 1.2: A) Diagram of photosynthetic electron flow from the absorption of light at the light harvesting complex (LHC) through photosystem II (PSII) via the oxygen evolution complex (OEC) to photosystem I and the Calvin-Benson cycle. B) Temperature dependent inactivation of Rubisco blocks the ETC resulting in accumulation of electron. C) Sites of ROS production and reactions. SOD and APX represents the presence of superoxide dismutase and ascorbate peroxidise, respectively.

1.4 OCEAN ACIDIFICATION AND CORAL CALCIFICATION

Carbon is the core element for life as we know it, playing a key part in biological processes. Even if only small amount are present in the atmosphere (0.03%) it still plays a major part in the regulation of global climate. The world's ocean acts as a buffer for atmospheric CO_2 concentrations, with a global sea-air CO_2 flux of 1.6 ±1 Gt C yr^{-1} year 1995 (IPCC, 2007). A synthesis of global data indicates an increase in CO_2 flux in the recent past of 0.1-0.6 Gt C yr^{-1} (IPCC, 2007). The high variability in these numbers depends on the difficulty to measure CO_2 fluxes, as these are highly dependent on regional conditions. Atmospheric CO_2 is diffuse into the ocean surface layer and dissolves into CO_2(aq) (Gattuso et al., 1999). Only a small fraction of the dissolved CO_2 will remain in this form, the rest reacts with water to form carbonic acid (H_2CO_3) (eq. 1.1). Carbon acid is unstable and will break down into bicarbonate ions and hydrogen ions (eq. 1.2). Further, the bicarbonate ions can be reduced to carbonate ions and hydrogen ions (eq. 1.3).

$$CO_2(aq) + H_2O \rightarrow H_2CO_3 \quad (1.1)$$

$$H_2CO_3 \rightarrow HCO_3^- + H^+ \quad (1.2)$$

$$HCO_2^- \rightarrow CO_3^{2-} + H^+ \quad (1.3)$$

These reactions give the three main dissolved inorganic carbon (DIC) species involved in the photosynthesis and calcification processes. The hydrogen ions resulting from these reactions are also important for the pH of the seawater (eq. 1.4). CO_3^{2-} consumed in the carbonic cycle results in the reduction of ocean acidity, hence balancing the pH of the seawater (Guinotte and Fabry 2008) At present surface pH is 0.1 units lower than pre-industrial levels, and is expected to decrease another 0.3-0.4 units by 2100 (IPCC, 2007).

$$pH = -\log10[H+] \quad (1.4)$$

Due to the additional CO_2 being dissolved in the oceans as a result of human activities this pH regulating system will become unbalanced, and subsequently

lead to a reduction in the ability for the oceans to dissolve atmospheric CO_2 hence leaving more CO_2 in the atmosphere. A decrease in carbonate ions lead to undersaturation of calcium carbonate which in turn effects the calcification rates in marine organisms. Projections indicate that undersaturation in respect to calcium carbonate may occur within a few centuries. For example, it is predicated that the Southern Ocean will reach undersaturation with regards to aragonite when the atmospheric CO_2 concentrations reach 600 ppm which is likely to occur by year 2050 (Orr et al., 2005).

The three main species of DIC; HCO_3^-, CO_3^{2-} and CO_2(aq) represent 90, 10 and <1% respectively of the total DIC (Gattuso et al., 1999). The composition of DIC is dependent on the acidity of the seawater. With the expected changes in pH the composition of DIC is likely to change as well, with an increase in bicarbonate and dissolved carbon dioxide and a reduction in carbonate ions (Orr et al. 2005).

Calcium and inorganic carbon are the two key players in the calcification process. Both compounds need to be transported to the calicoblastic epithelium cells in the aboral ectoderm where calcification occurs (Gattuso et al., 1999, Furla et al., 2000, Allemand et al., 2004). The overall reaction of calcification that takes place in the calicoblastic cells is as follows:

$$Ca^{2+} + 2HCO_3^- \rightarrow CaCO_3 + CO_2 + H_2O \qquad (1.5)$$

There are two sources of DIC for calcification; metabolic waste products from the host animal and the surrounding medium (Furla et al., 2000, Allemand et al., 2004). Furla et al. (2000) found that 70-75% of the CO_2 use for skeletogenisis came from the host. It should be taken into consideration that the DIC taken from the surround usually comes from the gastrovascular cavity rather than the open ocean (Gattuso et al., 1999). The chemistry of the gastrovascular fluid is different from the open water, and is dependent on the advective flux of seawater through the mouth, the photosynthetic process and the calcification (Gattuso et al. 1999; Kleypas et al. 1999).

The transport of Ca^{2+} to the site of calcification is not yet well understood. There are three main potential pathways for the Ca^{2+} to reach the site of skeletogenisis; by transcellular transport which is an energy dependent process, by paracellular diffusion or advection (reviewed by Gattuso et al., 1999). The last two processes are energy independent. It is also possible that all three processes occur in combination. The actual incorporation of Ca^{2+} into the skeleton requires an active process most likely mediated by an enzyme (Tambutte et al. 1996).

Carbonic anhydrases (CA) are known to play a key role in biomineralization in scleractinian coral (Tambutte et al. 1996; Furla et al. 2000; Al-Horani et al. 2003; Tambutté et al. 2007; Moya et al. 2008). The CA is thought to provide DIC to and/or remove carbonic acid from the site of skeletogenisis. However the exact function of CAs still remains uncertain (see review by Allemand et al, 2004; Gattuso et al, 1999). An additional feature of calcification in symbiotic corals is "light-enhanced calcification", indicating a link between photosynthesis and calcification rate. The mechanism behind this phenomenon is still uncertain (Allemand et al. 2004).

1.5 CORALS IN THEIR ENVIRONMENT

The physical environment of a coral reef varies greatly both in terms of the location of the reef, as well as between locations on an individual reef. Several of the same coral species can be found in the warm waters close to the equator, as well as in more southern and northern latitudes where the mean summer sea surface temperatures are a few degrees lower (Veron and Stafford-Smith 2000). Similarly, on one particular reef coral residing on the reef slope often experiences different physical and chemical conditions to a coral growing inside the reef lagoon. A reef lagoon often does not have the same flow or exchange of water as reef slopes, and may under low tide be fully enclosed (Koop et al. 2001). This may result in altered temperatures and water chemistry within the lagoon. The corals themselves play an important role in altering the chemistry of the water and the nutrient environment over the reef (Roberts et al., 2002). Physical processes such as calcification, photosynthesis and respiration will change the concentration of

dissolved inorganic carbon (DIC), dissolved inorganic nitrogen (DIN), the pH and the aragonite saturation state of the water. There is often a net uptake of DIC and DIN by the coral community (Koop et al., 2001), whereas the coral generally contributes to a net release of dissolved inorganic matter (DOM) and particulate organic matter (POM) (Bythell and Wild, 2011; Naumann et al., 2010). Heterotrophic feeding reduces the plankton and POM concentration in the surrounding water; however, over 70% of exuded mucus (which forms a protective layer over the coral) is immediately released into the water column as DOM and POM (Naumann et al., 2010; Wild et al., 2010). This release influences the nutrient status over the reef and provides a food source for the reef community (Haas et al., 2010; Naumann et al., 2010; Wild et al., 2010). Organisms such as zooplankton (Richman et al., 1975), bivalve (Shafir and Loya, 1983), crabs (Marsden and Meeuwig, 1990), shrimp (Patton, 1994) and fish (Benson and Muscatine, 1974) are known to feed on coral mucus.

Corals have been observed excreting large quantities of mucus when under temperature (CO_2-limitation), light stress (Wooldridge, 2009a), or if exposed to air at low tide. Altered photosynthetic rates, calcification rates and mucus release as a result of coral photoinhibition and bleaching can change the nutritional and chemical status of the reef, and therefore also affect other reef-dwelling organisms.

1.6 MODELLING BIOLOGICAL SYSTEMS

Mathematical models have become an increasingly popular tool for understanding and simulating scenarios for a wide range of natural systems, from global climate and ocean chemistry models, to ecosystem dynamics and population models, to biological and physiological models concerned with the interactions among and within organisms as a response to external forcings. As described above, coupled ocean-atmospheric climate models suggest an increase in SST and changing ocean chemistry over the coming century, and ecosystem scale models have indicated that under these scenarios a severe decline in coral health can be expected (Leclercq et al. 2002; Reynaud et al. 2003; Anthony et al. 2008). However, to fully

understand how corals will respond to climate-driven changes, we need to understand the actual physiological response within the coral and how the symbiont-host interaction may be influenced by these drivers. As the health of corals is dependent on the health of the symbiont and vice versa, any dysfunction to either party may have a cascading negative effect (Hoegh-Guldberg, 1999). There are only a few existing mathematical models relating the internal coral response to external forcing (Anthony et al. 2009; Muller et al. 2009; Eynaud et al. 2011). However, coral models often consider only one organism, rather than a dynamic symbiotic relationship between a cindarian and dinoflagellates (Anthony 2009) or lacking some of the basic coral features, such as mucus production and calcification (Muller et al. 2009; Eynaud et al. 2011).

Muller et al. (2009) developed a dynamic energy budget model describing the syntrophic relationship between a heterotrophic host and a photoautotrophic symbiont. This model aimed to describe the movement of energy and nutrient between the symbiont, host and the surrounding environment. The authors intended to minimize the complexity of the model without diminishing the attributes of the key processes of acquisition and processing of energy and nutrient. This model is however not specifically developed for scleractinian coral, and hence lacks some of the basic features of scleractinian physiology. For instance, the model does not include any temperature dependence, skeletal growth, reproduction or the formation of the surface mucus layer. It does not include active process such as photoinhibition, digestion or expulsion of symbiont.

Models that have been developed to simulate how a system/organism will be influenced by changes in external forcings, such as CO_2 emissions or changes in SST, are based on observational and experimental data which have been synthesized into mathematical representations of physical and chemical processes. These types of projection models are first written to simulate a known system, for example a biological system, which can be verified using real data. These mathematical representations of the system are then used to simulate what happens if one or several of the forcing variables, such as light, temperature or nutrient, changes. The equations are formulated from the existing literature and

thereafter tested by attempting to simulate real-world events. Modelling gives the advantage of being able to synthesise many individual pieces of information into something more comprehensive and interactive. However, it is important to acknowledge that the outputs from these model simulations are estimates and simulations of reality, rather than reality itself.

Even though there has only been a few attempts to model physiological responses in coral to external forcings, there have been several models created to describe energetic, carbon budget, photo-acclimation and photoinhibition in marine phytoplankton (Geider et al. 1998; Marshall et al. 2000; Kroon and Thoms 2006; Ross et al. 2008; Ross and Geider 2009). For example, Marshall et al. (2000) created a mechanistic model of photoinhibition in marine algae. They assumed a time dependent change in the initial slope of the photosynthesis-irradiance curve associated with the light induced damage to photosystem II. This model, which was coupled to an ammonium-nitrate interaction model, also included mathematical representations of non-photochemical quenching (NPQ). Their model was capable of simulating the effect of light and nutritional status on photosynthetic output and changes in biomass. A more complex model of the photosystem was presented by Kroon and Thoms (2006). They modelled linear and cyclic electron flow through photosystem I and II in marine phytoplankton, describing the rate of photochemistry in terms of generated electrons becoming available for cellular metabolism. This model gave a detailed description of the electron flow, but it may be considered overly complex as many of the processes within the photosystem are still not fully understood. Yet another model of the photosystem of phytoplankton was proposed by Ross et al. (2008) who modelled the electron turnover at photosystem II. Downstream limitations were taken into consideration and slow processes like photoinhibition and photo-protection was empirically accounted for. In contrast to the model by Kroon and Thoms (2006) the model by Ross et al. (2008) had a simpler structure; however both models are valid in their own right as they aim to simulate different aspects of photosynthesis.

As the zooxanthellae are dinoflagellates capable of living outside the host, these models could to some extent be useful when deriving a coral-algae symbiosis

model. However, the algae *in situ* would be constrained to the environment of the host tissues, resulting in physiological differences to free-living zooxanthellae. *Symbiodinium* residing in coral tissue generally have slow cell division, they are nutrient limited in terms of nitrogen, and "host release factors" cause the symbiont to leak a large fraction of the photosynthetic fixed carbon to the host (Sutton and Hoegh-Guldberg 1990). Additionally, none of the models mentioned above included any temperature dependence. Temperature induced photoinhibition has been shown to be an important component of the coral bleaching process, and should therefore be included in a coral bleaching model.

There are several large-scale models that simulate coral bleaching events, for example the forecast models *ReefTemp* and Coral Reef Watch, which both uses SST to predict coral bleaching on a weekly to seasonal timescale (Maynard et al. 2008b). There are also the coupled models CM2.0 and CM2.1 from the Geophysical Fluid Dynamics Laboratory which have been used to conduct climate change simulations for the 2007 Intergovernmental Panel on Climate Change (IPCC) report, and have been used to simulate previous bleaching events (Donner et al. 2007). All of these large-scale models assume a direct relationship between coral bleaching and SST and the duration of a heating event (Maynard et al. 2008a). At the scale of a single reef this way of estimating bleaching becomes rather crude, as there are numerous factors which influence the onset, degree of bleaching and recovery (discussed above). As of yet, there are no ocean models that contain any mechanistic representation of the coral, including their response to the environment, as well as their influence on the surroundings. To understand the impact of increasing SST on a reef system we first need to identify the corals role within the ecosystem and how the coral community alter the reef environment.

1.7 SCOPE OF THESIS

The overall goal of this thesis was to create a mechanistic coral symbiosis model which could capture the interaction between the heterotrophic host and autotrophic symbiont with varying sources of nutrients, temperature and light

intensities. The modelling effort included mathematical representations of important physiological processes, such as growth, respiration, photosynthesis, calcification, translocation of photosynthates, mortality and mucus production, as well as photoinhibition, ROS production and bleaching. The model was validated using experimental data, kindly provided by fellow researchers. The aim was to develop the model in such a way that it was, with only minor changes, applicable to other symbiotic organisms or could be decoupled and used to describe the energetics and photosystem of a unicellular phytoplankton. The last major goal was the incorporate the coral model into a large-scale reef model.

In more detail, the first goal was to create a mechanistic coral-algae symbiosis model exploring the implications of having two potential sources of nutrients, with the host feeding heterotrophically and the symbiont binding inorganic C and N into organic material. For chapter 2, the aim was to understand and be able to simulate the host-symbiont system under non-stress conditions. This basic model included the major physical processes of a coral and was written to act as a foundation for further model development.

After completing the basic symbiosis model, the second goal was to further develop the model to be able to simulate photoinhibition and coral bleaching as a function of temperature, light and nutrient. This required the introduction of temperature dependence into the model and a much more detailed description of the photosystem. The model was tested against experimental data and used to explore the effect of heterotrophy and the outcome was discussed in the context of 'degree heating days' which has been used in large scale bleaching predictions (Chapter 3).

Developing the basic model and the photoinhibition model led to the conclusion that the processes of the uptake of inorganic C and N and the translocation of photosynthates from the symbiont to the host was an essential processes, which required further investigation. A new experimental NanoSIMS dataset looking at the uptake and translocation of DIC between the environment, a cindarian host and symbiont of the genus *Symbiodinium*, made it possible to develop and validate a

more detailed and accurate definition of uptake and translocation. This data was from the anemone *Aiptasia pulchella* which allowed us to test the model for another organism (Chapter 4).

The final goal of this thesis was to incorporate the coral model into a bio-geochemical model of Heron Island Reef and explore the influence that the coral community had on its environment and how nutrient, water chemistry and hydrodynamic processes affected the corals and their symbionts (Chapter 5).

CHAPTER 2:

THE INTERCHANGEABILITY OF AUTOTROPHIC AND HETEROTROPHIC NITROGEN SOURCES IN SCLERACTINIAN CORAL SYMBIOTIC RELATIONSHIPS: A NUMERICAL STUDY

2. The interchangeability of autotrophic and heterotrophic nitrogen sources in Scleractinian coral symbiotic relationships: a numerical study

This chapter in inserted without abstract as published in Ecological Modelling:

Gustafsson, M. S. M., M. E. Baird, and P. J. Ralph. 2013. The interchangeability of autotrophic and heterotrophic nitrogen sources in Scleractinian coral symbiotic relationships: A numerical study. Ecological Modelling **250:** 183-194.

Model development, experimental design and model evaluation and validation was performed by Malin Gustafsson who also wrote the paper. Intellectual contributions and technical assistant were made by Mark Baird and Peter Ralph.

2.1 INTRODUCTION

Reef building coral (Scleractinian) are keystone organisms in tropical marine ecosystems, providing a structural foundation and habitats for a wide range of organisms. Scleractinian corals are sensitive to changes in their surrounding environment, and are under threat from climate change and human exploitation (Brown 1997; Hoegh-Guldberg 1999; Marshall and Baird 2000; Hoegh-Guldberg 2004). Understanding how the coral responds to environmental change is complicated by their symbiotic relationship with dinoflagellate algae (zooxanthellae) from the genus *Symbiodinium* (Peng et al. 2008; Weis 2008; Venn et al. 2008). Any dysfunction in either the host coral or symbiotic zooxanthellae, or in their exchange of metabolites, will have an almost immediate impact on the health of the zooxanthellae (Baird et al. 2009).

The success of corals in oligotrophic tropical waters depends largely on their symbiotic relationship with the zooxanthellae (Muscatine and Porter 1977;

Titlyanov and Titlyanova 2002). This symbiotic relationship is based on the cnidarian host providing a protective environment for the zooxanthellae within its tissues (Fig. 2.1) and a steady influx of nutrient-rich compounds from the host's metabolic processes, typically consisting of carbon dioxide, ammonium, urea and polyphosphates (Falkowski et al. 1993; Titlyanov and Titlyanova 2002). The zooxanthellae in turn provide the host with photosynthates, photosythetically fixed carbon (C) bound to nitrogen (N) forming amino acids and fatty acids, important for the host's metabolic functions (Muscatine 1990; Sutton and Hoegh-Guldberg 1990; Wang and Douglas 1999). The symbiont uses dissolved inorganic carbon (DIC) and dissolved inorganic nitrogen (DIN) taken up from the surrounding host tissues during this process. The concentration of DIC and DIN in the host tissues depends on the uptake from the overlying water column (Atkinson and Bilger 1992) as well as the production of respiration waste products from the host and symbiont (Furla et al. 2000).

In addition to the translocated photosynthates, the host acquires organic C and N from heterotrophic feeding. Corals can feed on a range of prey from zooplankton to bacteria and capture particulate organic matter using its tentacle or through mucus adhesion (Anthony and Fabricius 2000; Houlbrèque and Ferrier-Pagès 2009). The importance of heterotrophy versus autotrophic nutrition varies greatly depending on coral health. In non-bleached coral, heterotrophy meets as little as 15% of the coral's daily metabolic requirement. If bleached, the zooxanthellae are expelled or the photosynthetic pigments are degraded inhibiting photosynthesis, and heterotrophy must provide 100% of the coral metabolic requirements (Edmunds and Davies 1986; Grottoli et al. 2006b).

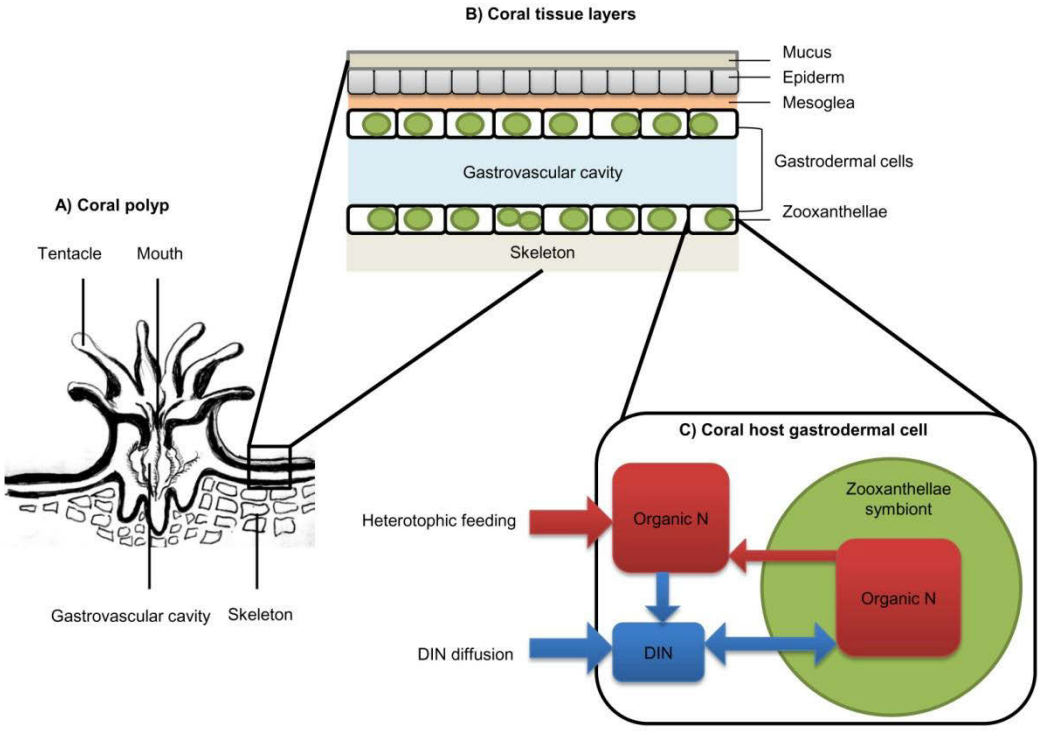

Figure 2.1: Schematic of coral tissue organization. A) General drawing of a coral polyp. B) Coral tissue layers and organization of zooxanthellae within the gastrodermal cells. C) Flux of organic and inorganic nitrogen between the coral host and the zooxanthellae symbiont.

Due to the low N availability and the generally high light regime that coral experience, the coral-algae symbiosis can be regarded as being N limited and C unlimited. Both C and N are required to form new biomass, hence there will likely be an excess of organic C in the system due to photosynthesis. This excess C can to some extent be stored as a reserve energy source (Al-Moghrabi et al. 1995), alternatively it can be excreted as mucus, with a low N:C ratio, from the coral surface via mucocytes (Bythell and Wild 2011).

Respiration waste products from coral and algae metabolic processes can be recycled within the coral. Metabolism includes the breakdown of organic matter (catabolism) to release energy. The energy is then used for cellular respiration or

for building new structural tissues (anabolism). The degraded organic material will be released as waste products or recycled by the symbiont, making it available to the host as organic compounds (Horton et al. 2002).

Ecosystem scale models have suggested a decline in coral health and calcification over the coming century (Leclercq et al. 2002; Reynaud et al. 2003; Anthony et al. 2008). Models at this large scale do not capture the dynamics of an individual coral, knowledge which is essential if we want to predict how corals will respond to environmental stressors, such as changes in nutrients availability, water temperatures (Warner et al. 1999) and irradiance (Brown et al. 2000). There are only a few existing energetic models that examine the individual coral response to stress (Anthony et al. 2009; Muller et al. 2009; Eynaud et al. 2011). However, before trying to simulate the effect climate change may have on corals it is essential to first have an understanding of, and ability to, simulate the basic features of the coral-algae symbiosis under non-stress conditions, so that we can evaluate the benefits and drawback of this relationship.

Here, we present a numerical model of coral symbiosis, which calculates changes in the physiology of a cnidarian host and an autotrophic symbiont with respect to different nitrogen sources and under different light regimes. We use steady-state solutions, biogeochemical budgets and a sensitivity analysis to show the importance of the different nitrogen and carbon sources for coral survival and growth under non-bleaching conditions.

2.2 METHODS

2.2.1 Model structure

The model describes the uptake and exchange of N and C between the environment, cnidarian host and the zooxanthellae (hereafter referred to as the symbiont). The host biomass was quantified per coral unit surface area (µg cm^{-2}). The symbiont state variables were quantified for one cell, which then was used as a

representative of all cells in the entire symbiont assembly. When a parameter or variable was related to the host or symbiont they were denoted *H* and *S*, respectively.

Table 2.1: Model equation for symbiont. Each rate or state calculation is given a number which corresponds to a number in figure 2.

Equation	No.	Description	Units
$R_C^S = \begin{cases} V_C^S \eta^S + \delta^S \, C_F^S & if \;\; C_{thres}^S > 0 \\ \delta^S \, C_F^S & else \end{cases}$	(1)	Cost of biosynthesis and respiration symbiont (C)	µg C cell^{-1} d^{-1}
$R_N^S = \begin{cases} V_N^S \eta^S + \delta^S \, N_F^S & if \;\; C_{thres}^S > 0 \\ \delta^S \, N_F^S & else \end{cases}$	(2)	Cost of biosynthesis and respiration symbiont (N)	µg N cell^{-1} d^{-1}
$C_{R,max}^S = \frac{N_F^S}{Q_{min}^S} - C_F^S$	(3)	Max size of C_R^S	µg C cell^{-1}
$T_N^S = P_{cell}\left(\frac{C_R^S}{C_R^S + C_{thres}^S}\right) Q_t \left(1 - \frac{C_R^H}{C_{R,max}^H}\right)$	(4)	Translocated N from N_F^S to N_F^H	µg N cell^{-1} d^{-1}
$T_{CF}^S = \frac{T_N^S}{Q_F^S}$	(5)	Translocated C from C_R^S to C_R^H	µg C cell^{-1} d^{-1}
$T_{CR}^S = \left(\frac{T_N^S}{Q_t} - T_{CF}^S\right)$	(6)	Translocated C from C_F^S to C_R^H	µg C cell^{-1} d^{-1}
$T_C^S = T_{CF}^S + T_{CR}^S$	(7)	Total translocated C	µg C cell^{-1} d^{-1}
$mS = \; m^S \mu_{max}^S S$	(8)	Natural symbiont mortality	cell cm^{-2} d^{-1}
$mN_F^S = m^S \mu_{max}^S N_F^S$	(9)	Mortality N_F^S	µg N cell^{-1} d^{-1}
$mC_F^S = m^S \mu_{max}^S C_F^S$	(10)	Mortality C_F^S	µg C cell^{-1} d^{-1}
$mC_R^S = m^S \mu_{max}^S C_R^S$	(11)	Mortality C_R^S	µg C cell^{-1} d^{-1}
$mN_{host}^S = mN_F^S\left(1 - \frac{C_R^H}{C_{R,max}^H}\right)$	(12)	N from dead symbiont cells re-ingested by host	µg N cell^{-1} d^{-1}
$mC_{host}^S = (mC_F^S + mC_R^S)\left(1 - \frac{C_R^H}{C_{R,max}^H}\right)$	(13)	C from dead symbiont cells re-ingested by host	µg C cell^{-1} d^{-1}
$mN_{out}^S = mN_F^S - mN_{host}^S$	(14)	N from dead symbiont expelled	µg N cell^{-1} d^{-1}
$mC_{out}^S = mC_F^S + mC_R^S - mC_{host}^S$	(15)	C from dead symbiont expelled	µg C cell^{-1} d^{-1}
$aA = \pi r^2\left(1 - \frac{2(1 - (1 + 2\gamma Cr)e^{-2\gamma Cr}}{(2\gamma Cr)^2}\right)$	(16)	Absorption cross-section	m^2 cell^{-1}
$P_C^{max} = \mu_{max}^S\left(\frac{24}{L}\right)(1 + (\eta^S + \delta^S))C_F^S$	(17)	Maximum C specific photosynthesis	µg C cell^{-1} d^{-1}
$P_{cell} = \left(\frac{P_C^{max} I}{(P_C^{max}/aA) + I}\right)\left(\frac{DIC^H}{DIC^H + DIC_{min}}\right)$	(18)	Photosynthesis	µg C cell^{-1} d^{-1}
$\varphi = 1 - \frac{P_{cell}}{P_C^{max}}$	(19)	Regulatory term	-

Table 2.1 Continued.

Equation	No.	Description	Units
$\Omega = \varphi \frac{\Pi^L_{max}\theta^C_{max}}{\theta^C}$	(20)	Acceleration term	-
$S_{max} = A_{coral}/\pi \left(3\frac{N^S_F}{\rho}/4\pi^{1/3}\right)^2$	(21)	Maximum number of symbiont cells per unit surface area	cell cm^{-2}
$V^S_{N,max} = \begin{cases} \mu^S_{max} N^S_F[(1-\alpha)\left(\frac{24}{L}\right)+\alpha] & if\ I>0 \\ \alpha\mu^S_{max}N^S_F & if\ I=0 \end{cases}$	(22)	Maximum N uptake by symbiont	µg N cell^{-1} d^{-1}
$V^S_N = V^S_{N,max}\frac{DIN^H}{DIN^H+K_n}\left(\frac{C^S_R}{C^S_R+C^S_{thres}}\right)\left(1-\frac{S}{S_{max}}\right)$	(23)	Actual N uptake rate by symbiont	µg N cell^{-1} d^{-1}
$V^S_C = \frac{V^S_N}{Q^S_F}$	(24)	C from C^S_R to C^S_F	µg C cell^{-1} d^{-1}
$\mu^S = \frac{dC^S_F}{dt}/C^S_F$	(25)	Symbiont growth rate	d^{-1}
$\frac{dN^S_F}{dt} = \begin{cases} V^S_N - R^S_N - T^S_N - mN^S_F - \mu^S N^S_F & if\ \mu^S>0\ N^S_F > N^S_{F,max} \\ V^S_N - R^S_N - T^S_N - mN^S_F & else \end{cases}$	(26)	Change in N^S_F	µg N cell^{-1} d^{-1}
$\frac{dC^S_F}{dt} = \begin{cases} V^S_C - R^S_C - T^S_{CF} - mC^S_F - \mu^S C^S_F & if\ \mu^S>0\ N^S_F > N^S_{F,max} \\ V^S_C - R^S_C - T^S_{CF} - mC^S_F & else \end{cases}$	(27)	Change in C^S_F	µg C cell^{-1} d^{-1}
$\frac{dC^S_R}{dt} = \begin{cases} P_{cell}\left(1-\frac{C^S_R}{C^S_{R,max}}\right) - V^S_C - mC^S_R & if\ \mu^S>0\ N^S_F > N^S_{F,max} \\ -T^S_{CR} - \mu^S C^S_R & \\ P_{cell}\left(1-\frac{C^S_R}{C^S_{R,max}}\right) - V^S_C - mC^S_R & else \end{cases}$	(28)	Change in C^S_R	µg C cell^{-1} d^{-1}
$\frac{dChl}{dt} = \begin{cases} \frac{V^S_N}{Q^S_F}\Pi^L_{max}\theta^C_{max}\Omega\varphi\left(1-\frac{Chl}{Chl_{max}}\right) & if\ I>0\ C^S_R > C^S_{thres} \\ \frac{V^S_N}{Q^S_F}\Pi^L_{max}\theta^C_{max}\left(1-\frac{Chl}{Chl_{max}}\right) & if\ I=0\ C^S_R > C^S_{thres} \\ -R^S_m\theta^C\ \ S & if\ C^S_R = 0 \\ 0 & else \end{cases}$	(29a)	Change in symbiont chlorophyll	µg Chl cell^{-1} d^{-1}
$\frac{dChl}{dt} = \begin{cases} \frac{dChl}{dt} - \mu^S Chl & if\ \mu^S>0\ N^S_F > N^S_{F,max} \\ \frac{dChl}{dt} & else \end{cases}$	(29b)	Change in chlorophyll taking cell division into account	µg Chl cell^{-1} d^{-1}
$\frac{dS}{dt} = \begin{cases} \mu^S S - mS & if\ \mu^S>0\ \ N^S_F > N^S_{F,max} \\ -mS & else \end{cases}$	(30)	Change in symbiont population size	cell cm^{-2} d^{-1}

The basic energetic features of this model were adapted from Ross and Geider (2009), a cell-based phytoplankton model. In accordance with their model, each of the components (host and symbiont) had two C pools; one functional (C^H_F, C^S_F) and one reserve (C^H_R, C^S_R) (Fig. 2). The state variables C^H_F and C^S_F (eq. 44 and 27 respectively, Tables 2.1 and 2.2) represented the physical structure (cell material and tissues) of the host and symbiont and were assumed to be bound to N at the Redfield ratio (Q_F=0.176 g N g C^{-1}), giving the N^H_F and N^S_F pools (eq. 43 and 26).

The C reserves, C_R^H and C_R^S, (eq. 45 and 28) were made up of C alone. Organic C from feeding in the host, and photosynthesis in case of the symbiont, entered the C reserves first, wherefrom it was incorporated into biomass, translocated between host and symbiont, or excreted as mucus. The host had two additional state variables which represented the inorganic C and N, DIC^H and DIN^H, existing in the host tissues (eq. 46 and 47 respectively). Likewise, the symbiont had one additional state variable representing the cell chlorophyll concentration (eq. 29).

2.2.2 Model parametertisation

2.2.2.1 Sources of N

We explore two different external sources and pathways of N that a coral can utilize; heterotrophic feeding and diffusion of DIN through tissues. Heterotrophic feeding provides a source of both organic N (Z_N) and C (Z_C). Coral can feed on a range of food items; in this model we have represented heterotrophic feeding with one rate, which was assumed to have a set N: C ratio (Q_Z), corresponding to the Redfield ratio. We assumed that the coral feed heterotrophically only during night (Heidelberg et al. 2004), whereas DIN diffusion (V_{DIN}^H) through the host cell walls from surrounding environment occurred throughout the day and night.

2.2.2.2 DIN^H and DIC^H

DIN diffused into the host tissues was incorporated into the host's DIN^H pool from which it could be taken up by the symbiont (V_N^S) (eq. 22 and 23). To calculate V_N^S a Michaelis-Menten style equation was used, taking into account that there must be enough C in the reserve pool to bind to the newly attained N at the Q_F ratio, as well as space limitation imposed when the symbiont population grows towards its maximum size per unit surface area ($S_{\max}$, eq. 21). Similarly, the DIC^H pool in the host tissue was replenished through the diffusion of DIC (V_{DIC}^H) from the environment (eq. 31) and used for calcification, or taken up by the symbiont to provide DIC for photosynthesis. In addition to diffusion, DIC^H and DIN^H were replenished by metabolic waste products from the host and the symbiont (eq. 46

and 47). To avoid the DIC^H and the DIN^H accumulating to unrealistic concentrations, we introduced two equilibration terms ($eqDIN^H$ and $eqDIC^H$) (eq. 32 and 33).

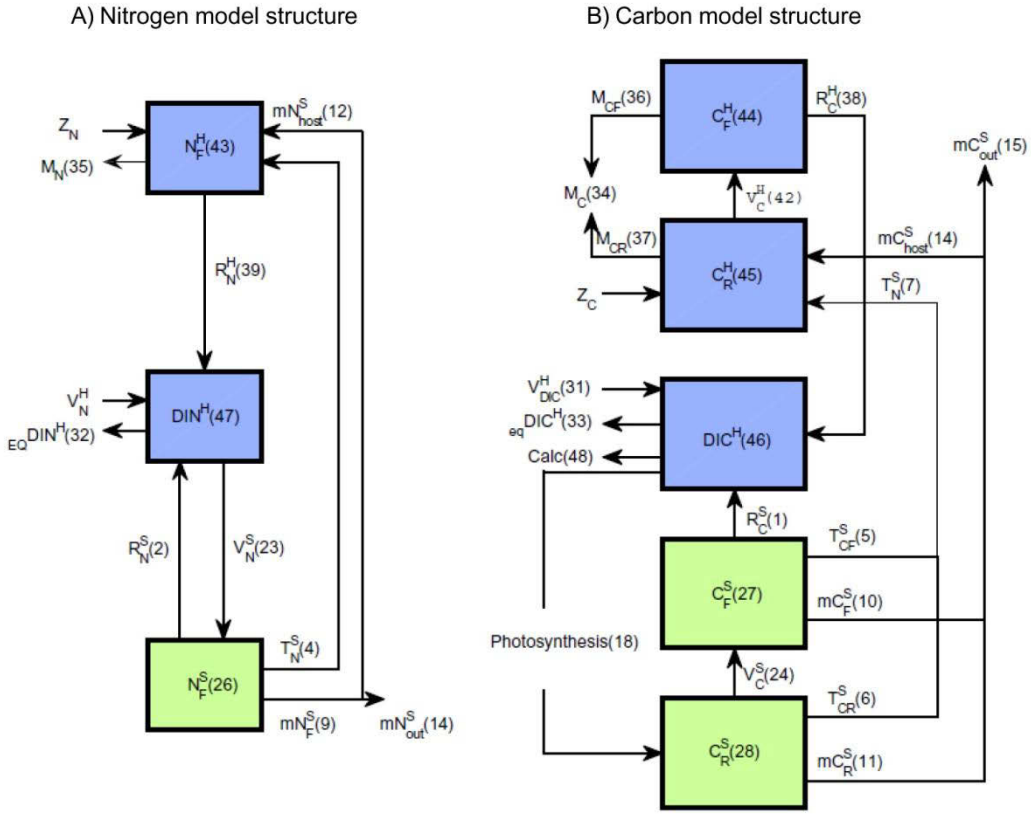

Figure 2.2: Schematic of coral nitrogen (A) and carbon (B) model. Boxes represent state variables and arrows fluxes. Blues and green boxes indicate that the pool belongs to the host and symbiont respectively. The numbers inside the brackets indicate the corresponding equation in Table 2.1 and 2.2.

Table 2.2: Model equations for coral host: Each rate or state calculation is given a number which corresponds to a number in figure 2.1.

Equation		Description	Units
$V_{DIC}^{H} = \varepsilon_{dic} C_F^H \frac{DIC^E}{DIC^E + K_{dic}}$	(31)	Host DIC uptake	µg C cm^{-2} d^{-1}
$eqDIN^H = \tau DIN^H \left(\frac{DIN^H}{DIN_{max}^H}\right)^4$	(32)	Equilibration DIN in host	µg N cm^{-2} d^{-1}
$eqDIC^H = \tau DIC^H \left(\frac{DIC^H}{DIC_{max}^H}\right)^4$	(33)	Equilibration DIC in host	µg C cm^{-2} d^{-1}
$M_C = \varepsilon_M C_R^H \left(\frac{C_R^H}{C_{R,max}^H}\right)$	(34)	Total mucus C	µg C cm^{-2} d^{-1}
$M_N = \varepsilon_M \beta_N N_F^H$	(35)	N in mucus	µg N cm^{-2} d^{-1}
$M_{CF} = \frac{M_N}{Q_F^H}$	(36)	C from C_F^H to mucus	µg C cm^{-2} d^{-1}
$M_{CR} = M_C - M_{CF}$	(37)	C from C_R^H to mucus	µg C cm^{-2} d^{-1}
$R_C^H = \begin{cases} V_C^H \eta^H + \delta^H C_F^H & if\ C_{thres}^H > 0 \\ \delta^H C_F^H & else \end{cases}$	(38)	Cost of biosynthesis and respiration host (C)	µg C cm^{-2} d^{-1}
$R_N^H = \begin{cases} V_N^H \eta^H + \delta^H N_F^H & if\ C_{thres}^H > 0 \\ \delta^H N_F^H & else \end{cases}$	(39)	Cost of biosynthesis and respiration host (N)	µg N cm^{-2} d^{-1}
$C_{R,max}^H = \frac{N_F^H}{Q_{min}^H} - C_F^H$	(40)	Max size of host C_R^H	µg C cm^{-2}
$V_N^H = Z_N + S\left(mN_{host}^S + T_N^S\right)$	(41)	Total N to host	µg C cm^{-2} d^{-1}
$V_C^H = \frac{V_N^H}{Q_F^H}$	(42)	Carbon from host reserve to host functional pool	µg C cm^{-2} d^{-1}
$\frac{dN_F^H}{dt} = Z_N - R_N^H - M_N$	(43)	Change in host N_F^H	µg N cm^{-2} d^{-1}
$\frac{dC_F^H}{dt} = V_C^H - R_C^H - M_{CF}$	(44)	Change in host C_F^H	µg C cm^{-2} d^{-1}
$\frac{dC_R^H}{dt} = Z_C + S(mC_{host}^S + T_C^S) - M_{CR} - V_C^H$	(45)	Change in host C_R^H	µg C cm^{-2} d^{-1}
$\frac{dDIC^H}{dt} = V_{DIC}^H + R_C^H + R_C^S S - P_{cell} S\left(1 - \frac{C_R^S}{C_{R,max}^S}\right) - \frac{dCalc}{dt} - eqDIC^H$	(46)	Change in host DIC^H	µg C cm^{-2} d^{-1}
$\frac{dDIN^H}{dt} = V_{DIN}^H + R_N^H + S(R_N^S - V_N^S) - eqDIN^H$	(47)	Change in host DIN^H	µg N cm^{-2} d^{-1}
$\frac{dCalc}{dt} = \begin{cases} \frac{\delta_L R_C^H}{\omega} & if\ I > 0 \\ \frac{\delta_D R_C^H}{\omega} & if\ I < 0 \end{cases}$	(48)	Calcification rate	µg C cm^{-2} d^{-1}

2.2.2.3 Symbiont growth and cell division

As mentioned above, the symbiont state variables were calculated on a per cell basis. To achieve a change in the symbiont population, and not just for an

individual cell, we assumed that when the symbiont structural biomass reached a maximum size ($N_{F,max}^{S}$ = 80 pg N cell^{-1}) at a cell diameter of 10 µm (Domotor and D'elia 1986; Muller-Parker et al. 1994a) the cell started to divide according to the growth rate (eq. 25 and 30). Hence, when the symbiont structural biomass reached $N_{F,max}^{S}$ the population of symbiont cells increased, but inside the individual cell the functional C and N concentration remained the same, meaning that when increasing the biomass of one cell by 50% over the maximum biomass half a new cell was formed (see first statement in eq.26-28, 29b and 30). If the symbiont did not receive enough light and/or nutrient, the cell population size decreased at the rate of natural mortality (eq. 8), at the same time the functional material inside each cell and the cell size decreased according to the negative growth rate (eq. 25).

The symbiont population was potentially space limited, as we assumed symbionts existed in two one-cell-thick layers in the host gastrodermal cells above and below the gastrovascular cavity (Fig. 1). $S_{\max}$ was calculated using the maximum packing of symbionts in these two layers, assuming symbionts were packed side-by-side in each layer leaving no space between cells. At a symbiont cell diameter of 10 µm, $S_{\max}$=2.55 x 10^6 cell cm^{-2}, which is in accordance with the higher values of symbiont concentrations (Stimson 1997; Ferrier-Pagès et al. 2003; Ferrier-Pagès et al. 2010; Hill et al. 2011).

2.2.2.4 Photosynthesis

Through photosynthesis the symbiont binds inorganic C into organic compounds (eq. 16-18). To estimate the photosynthetic output, we calculated the cell absorption cross section (aA) (eq. 16) and the maximum C specific photosynthetic rate (P_C^{max}) (Kirk 1994). P_C^{max} was assumed to be the amount of C needed to provide for symbiont maximum growth rate ($\mu_{\max}^{S}$) including respiration and cost of biosynthesis (eq. 17). A $\mu_{\max}^{S}$ of 0.4 d^{-1} was used, as free-living zooxanthellae under ideal light and nutrient condition are known to have a $\mu_{\max}^{S}$ of 0.3-0.4 d^{-1} (Domotor and D'elia 1986; Falkowski et al. 1993; Falkowski et al. 2007). The absorption cross-section (aA) multiplied by areal photon flux, I, gives an estimate of light absorption due to the chlorophyll within the cell. As the bracketed

component of the aA equation (eq. 16) approached one, all the light entering the cell was absorbed. This gives us an opportunity to estimate a maximum chlorophyll concentration (Chl_{max}) in the cell, as it would be energy inefficient to create more chlorophyll above that which absorbs all the light. The Chl_{max} was set to be the concentration for which less than 1% of the light passes through and out the other side of the cell (eq. 29).

2.2.2.5 Translocation of N and C from symbiont to host

One of the key features of the translocation of N and C in the coral was considered to be the transfer of amino acids and fatty acids from symbiont to the host (T_N^S and T_C^S) (eq. 4-7). The symbiont used the fixed C from photosynthesis to provide energy for its metabolic requirements, with the remainder being translocated to the host depending on the size of the host reserve pool. As C_R^H approaches $C_{R,max}^H$ the translocation subsided. Additionally, if the C_R^S was reduced to near depletion, the amount of translocated photosynthates was reduced to prevent the symbiont from starving to death (first bracketed term in eq. 4). In the model the translocated photosynthates had a low, but fixed N: C ratio (Q_t=0.037 g N g C^{-1}) (Falkowski et al. 1993). These criteria allowed for high translocation under high light conditions reducing symbiont growth rate but never to the point where it could not survive.

The second pathway for the host to acquire N and C from the symbiont was through the re-ingestion of dead symbiont cells. The symbiont population was assumed to have a natural mortality rate, which must lie between 0 and $\mu_{\max}^S$. We assigned the mortality rate to be 10% of $\mu_{\max}^S$ (eq. 8-15) (Haney 1996). Symbiont cells lost through natural mortality were either re-absorbed by the host, giving the host an additional supply of organic N and C (eq. 13, 41 and 42), or expelled from the coral tissue (eq. 12).

2.2.2.6 Respiration and cell maintenance

Transfer of N and C from the host to the symbiont occurred through the recycling of respiration waste products. The production of respiratory waste depended on the host and symbiont metabolic rates. To account for the host and symbiont

metabolic requirements both in providing energy for respiration and maintenance (Falkowski et al. 1993), as well as the energy required to form new structural biomass (biosynthesis), we formulated a set of simple equations following Ross and Geider (2009) based on biomass and growth rate (eq. 1-2 and 38-39). Biosynthesis, and hence the cost of biosynthesis, only occurred when there was enough N and C to support respiration and maintenance through the night. These thresholds were defined as: $C_{thres}^{S} = \frac{24-L}{24} R_C^S$ and $C_{thres}^{H} = \frac{24-L}{24} R_C^H$ for the symbiont and host respectively, where L represented the hours of daylight, R_C^S the respiration and cellular maintenance costs of the symbiont, and R_C^H the respiration and maintenance requirements of the host (Ross and Geider 2009).

2.2.2.7 Mucus Production and Calcification

Two additional processes which are characteristic of a coral are the production and release of mucus and the deposition of a calcium carbonate skeleton. The rate of mucus released from the coral surface (M_C) was set so it could nearly equal the entire C_R^H pool in one day (eq. 34). Coral mucus is known to have a varying N:C ratio (Bythell and Wild 2011), which becomes smaller when the photosynthetic rate is high, hence more C rich photosynthates are translocated from the symbiont to the host. To represent this in the model, we assumed that a fraction of the N_F^H was released as mucus (eq. 35). The C was taken from both C_F^H and C_R^H, where C from the C_F^H was taken out at a rate which maintained the N:C ratio between N_F^H and C_F^H (eq. 36). The remaining C part was taken from C_R^H (eq. 37). This gave a variable N:C ratio of the mucus with a maximum corresponding to the Redfield ratio if C_R^H was depleted.

Calcification was described as storage of C following the description below (eq. 48). Furla and colleges suggested that 70% of the C used for calcification came from the host respiration and the remaining part from diffusion from the environment. Their study also concluded that 17% during day time and 4.4% during the night of the C from the host respiration was sequestered into the skeleton (Furla et al. 2000).

Table 2.3: Model parameters

Symbol	Description	Value	Unit	Source
I	Irradiance	0-1000	µmol photon m^{-2} s^{-1}	-
L	No. daylight hours	12	hr	-
Π^L_{max}	Maximum proportion of C^S_F allocated to light harvesting	0.33	-	(Ross and Geider 2009)
θ^C_{max}	Maximum Chl:C ratio of light harvesting pool	0.265	g Chl g C^{-1}	(Ross and Geider 2009)
μ^S_{max}	Maximum specific growth rate symbiont	0.4	d^{-1}	(Domotor and D'elia 1986; Falkowski et al. 2007)
δ^S	Symbiont C specific respiration and maintenance rate	0.06	g C g C^{-1} d^{-1}	See text
η^S	Symbiont C specific cost of biosynthesis	0.1	g C g C^{-1}	See text
Q^S_{min}	Minimum N:C ratio in symbiont	0.05	g N g C^{-1}	(Ross and Geider 2009)
α	Factor by which dark N uptake rate is reduced	0.55	-	(Ross and Geider 2009)
K_n	Half saturation constant symbiont DIN uptake	1.4	µM N	(Muscatine and D'elia 1978)
$N^S_{F,max}$	Maximum symbiont biomass (N^S_F)	80	pg N $cell^{-1}$	(Muller-Parker et al. 1994a)
r_i	Initial symbiont cell radius	5	µm	(Domotor and D'elia 1986)
ρ	Density of N in symbiont cell	$1.53x10^5$	g N m^{-3}	See text
γ	Chlorophyll absorption coefficient	0.04	m^{-1}	(Kirk 1994)
Q_t	N:C of translocated photosynthates	0.0373	g N g C^{-1}	(Falkowski et al. 1993)
m^S	Symbiont C specific mortality rate	0.1	g C g C^{-1} d^{-1}	See text
δ^H	Host C specific respiration and maintenance rate	0.06	g C g C^{-1} d^{-1}	See text
η^H	Host C specific cost of biosynthesis	0.1	g C g C^{-1}	See text
Q^H_{min}	Minimum N:C ratio in host	0.05	g N g C^{-1}	See text
β_N	Fraction of host N released as mucus	0.05	-	(Bythell and Wild 2011)
ε_M	C specific mucus release rate	1	g C g C^{-1} d^{-1}	-
DIN^H_{max}	Maximum DIN concentration in host tissues	0.8 N^H_F	µg N cm^{-2}	See text
ε_{dic}	C specific DIC uptake rate by host	6	g C g C^{-1} d^{-1}	(Muller et al. 2009)
K_{dic}	Half saturation constant host DIC uptake	400	µM C	(Al-Moghrabi et al. 1996)
DIC^H_{max}	Maximum DIC concentration in host tissues	0.8 C^H_F	µg C cm^{-2}	See text
τ	Equilibration time constant	1	d^{-1}	-
DIC_{min}	Minimum DIC concentration in host tissues	5	µg C cm^{-2}	See text
DIC^E	DIC concentration in the environment	2000	µM C	Standard sea water
A_{coral}	Coral surface area	1	cm^2	See text
δ_L	Fraction of host respiration waste products to calcification during light	0.17	-	(Furla et al. 2000)
δ_D	Fraction of host respiration waste products to calcification during darkness	0.044	-	(Furla et al. 2000)
ω	Fraction of C to calcification from respiration	0.7	-	(Furla et al. 2000)

2.2.3 Numerical experimental design

Rather than calculating the rates of heterotrophic feeding, Z_N, and DIN diffusion, V_{DIN}^H, based on environmental concentrations, these rates were predetermined to reduce complexity, and to ease the interpretation of how N and C moved through the system. The external environment was assumed to remain unaffected by the coral. To analyze the effect of heterotrophic feeding versus DIN diffusion, the model was run to steady-state for two feeding rates (low Z_N =0.5 and high Z_N =5 µg N cm^{-2} d^{-1}) and two DIN diffusion rates (low V_{DIN}^H =0.5 and high V_{DIN}^H =5 µg N cm^{-2} d^{-1}), giving a total of four different nutrient scenarios. We denote these four nutrient cases; high Z_N + high V_{DIN}^H, high Z_N + low V_{DIN}^H, low Z_N + high V_{DIN}^H, low Z_N + low V_{DIN}^H (Fig. 2). The model was run to steady state for each nutrient scenario for a range of light intensities (0-1000 µmol photon m^{-2} s^{-1}), and the values of state variables and fluxes were presented as a daily averages.

Will the outcome of the model changes depending on which N pathway is dominant? To illustrate this, the model was evaluated using C and N budgets for the four nutrient cases at the highest light intensity (1000 µmol photon m^{-2} s^{-1}).

For all simulations the model derivatives were integrated over time until reaching steady state, which could take up to 200 simulation days. The initial state variable values were estimated from literature, and the model was run on a standard laptop using the Matlab programming language.

2.2.4 Sensitivity analysis

The parameters used for this model were based on information from different sources and may involve assumptions that make them somewhat uncertain. A sensitivity analysis was conducted for the high Z_N + low V_{DIN}^H and low Z_N + high V_{DIN}^H nutrient cases, quantifying the relationship between the state variables at steady state and each of the model parameters. These two N scenarios were

selected as they had the same total N uptake, but different dominant N sources. The parameters are defined in Table 2.3. Each parameter was changed one at the time +/- 10%, and for each change, the model was run to steady-state (Baird et al. 2003). The percentage difference between each run and the original model output (unperturbed parameter values) were calculated(Murray and Parslow 1997). Assuming a general power law relationship between parameter values and model state variables, the power can be calculated as:

$$p = \frac{\log\left(\frac{1 + y_{0.9}}{1 + y_{1.1}}\right)}{\log\left(\frac{0.9}{1.1}\right)}$$

Where p is the power, $y_{0.9}$ and $y_{1.1}$ are the values of the state variable when the parameter is at 90% and 110% respectively of its initial value. A value of p = 2 implied a doubling, or 100% change, of the parameter, and a change in model state variable of $(2^2) = 4$ or a 400% change. Parameters with a p of less than 0.3 (-0.3 < < 0.3) for all state variables were considered insensitive and not included in further analysis.

2.3 RESULTS

2.3.1 Variation in nitrogen source and irradiance

The numerical experiments analyzing the effect of nutrient sources and light intensity showed that for the high heterotrophic feeding rate (Z_N = 5 µg N cm^{-2} d^{-1}) both the host and the symbiont functional (C_F^H and C_F^S) and reserve (C_R^H and C_R^S) state variables resulted in similar values for both low and high DIN uptake V_{DIN}^H (Fig. 2.3A, B, E, F). Whereas for the low feeding rate (Z_N = 0.5 µg N cm^{-2} d^{-1}) V_{DIN}^H became an important source of N for both the host and the symbiont, as shown by the higher C_F^H for the low Z_N + high V_{DIN}^H case than for the low Z_N + low V_{DIN}^H case (Fig. 2.3B). The symbiont associated state variables approached zero with decreasing irradiance. However, this was not the case for the host when the

feeding rate was high, Z_N = 5 µg N cm^{-2} d^{-1}, showing that the host could survive without the symbiont as long as Z_N was sufficient.

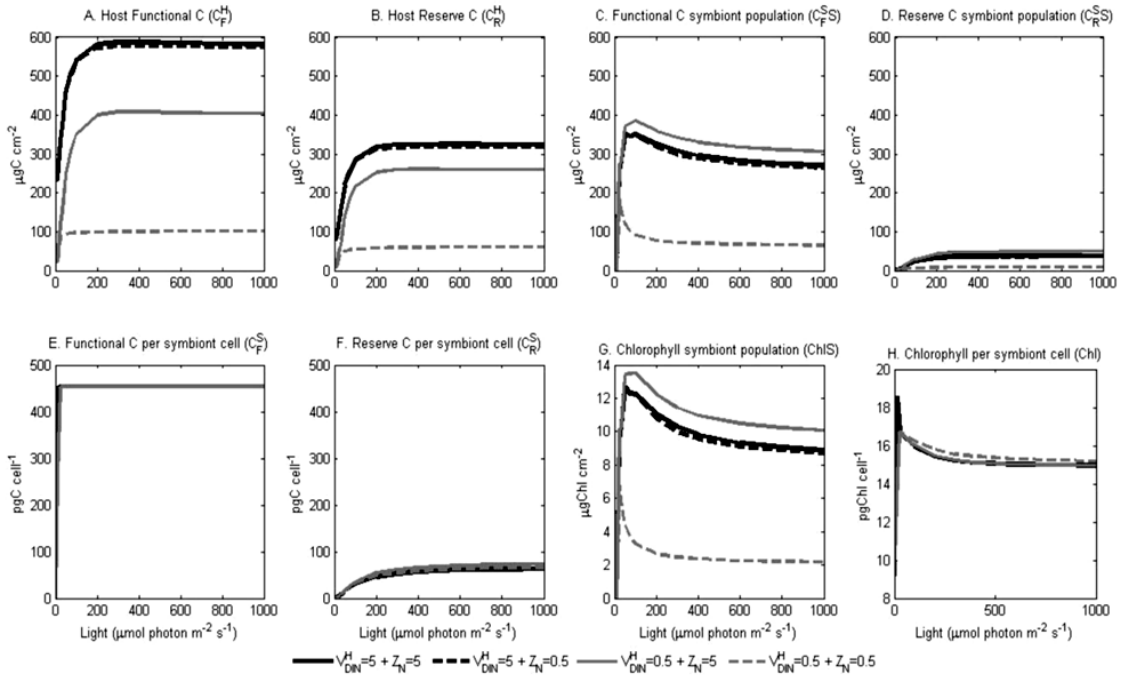

Figure 2.3: Steady state values of model state variables as a function of irradiance, ranging between 0-1000 µmol photon m^{-2} s^{-1} (0, 1, 10, 25, 35, 50, 75, 100, 200, 300, 400, 600, 800, 1000 µmol photon m^{-2} s^{-1}), and four N-scenarios; combinations of two DIN uptake rates (V_{DIN}^H: 0.5 and 5 µg N cm^{-2} d^{-1}) and two feeding rates (Z_N: 0.5 and 5 µg N cm^{-2} d^{-1}). Panel A and B show the C_F^H and C_R^H respectively. Panel C and D show C_F^S and C_R^S for the entire symbiont population (S). Panels E and F show C_F^S and C_R^S for one symbiont cell. Panels G and H show the chlorophyll concentration for the symbiont population and for an individual symbiont cell respectively. Note that the scale on the y-axis differ between panels.

High Z_N resulted in a C_F^H pool 30% greater in size than for the low Z_N (Fig. 2.3A), whereas the C_F^S pool was seemingly unaffected by all changes in nutrient uptake (Fig. 2.3E). Additionally, the size of the C_F^S pool had become light-saturated at 20 µmol photon m^{-2} s^{-1}, at which it had reached values corresponding to the maximum size of this pool ($C_{F,max}^S = N_{F,max}^S / Q_F$ = 454 pg C cm^{-2}). The combined functional C for the symbiont population ($C_F^S S$) shows that even though C_F^S was independent of

N uptake and the light saturated quickly, the number of cells changed as a function of irradiance, Z_N and V_{DIN}^H (Fig. 3C) . An interesting feature, seen in Figure 2.3C, was that the $C_F^S S$ for the low Z_N + high V_{DIN}^H case indicated the highest symbiont population size (S). The increased symbiont population size for the low Z_N + high V_{DIN}^H scenario occurred because of a slightly reduced translocation rate in relation to the photosynthetic rate, with 68.8% of the photosynthetically fixed C being translocated to the host for the high Z_N + high V_{DIN}^H scenario and 67.3% for the low Z_N + high V_{DIN}^H case. This difference of 1.5% in turns changed $C_{R,max}^H$ (eq. 3), resulting in a host induced reduction of the translocation rate.

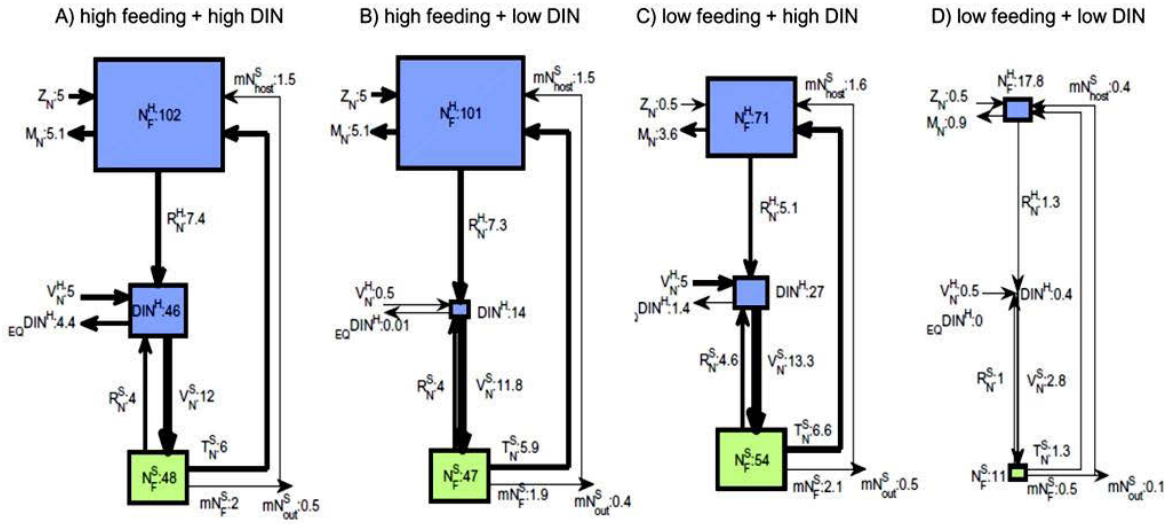

Figure 2.4: Average daily coral N fluxes at steady state and a light level of 1000 µmol photon m^{-2} s^{-1} for the four nutrent cases: A) high Z_N + high V_{DIN}^H B) high Z_N + low V_{DIN}^H C) low Z_N + high V_{DIN}^H D) low Z_N + low V_{DIN}^H. Blue and green boxes represent host and symbiont state variables respectively. The size of the boxes indicates the size of the individual N state variables, with the numerical value given in µg N cm^{-2}. The arrows show the direction of the fluxes and the thickness of the arrow and numerical value in µg N cm^{-2} d^{-1} quantifying the magnitude of the flux.

The modelled chlorophyll concentration per cell (*Chl*) showed little sensitivity to either V_{DIN}^H or Z_N. The highest *Chl* concentration was at 20 µmol photon m^{-2} s^{-1} after which it declined and leveled out (Fig. 2.3H). The reason for lower per cell *Chl* concentrations below 10 µmol photon m^{-2} s^{-1} was that for lower light levels the

symbiont cell was reduced in size due to starvation. The population chlorophyll concentration (*ChlS*) at high light on the other hand ranged between 2.5 to 11.5 µg Chl cm^{-2}, with high values associated with high Z_N and high V_{DIN}^H, and vice versa for the low values.

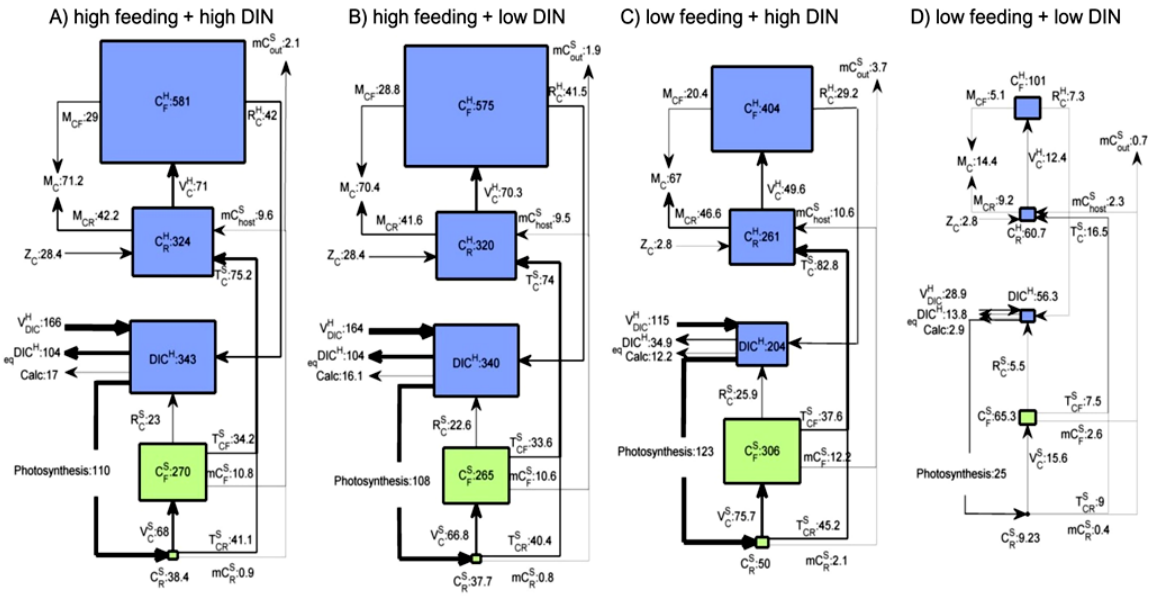

Figure 2.5: Average daily coral C fluxes at steady state and a light level of 1000 µmol photon m^{-2} s^{-1} for the four nutrient cases: A) high Z_N + high V_{DIN}^H B) high Z_N + low V_{DIN}^H C) low Z_N + high V_{DIN}^H D) low Z_N + low V_{DIN}^H. Blue and green boxes represent host and symbiont state variables respectively. The size of the boxes indicates the size of the individual C state variables, with the numerical value given in µg C cm^{-2}. The arrows show the direction of the fluxes and the thickness of the arrow and numerical value in µg C cm^{-2} d^{-1} quantifying the magnitude of the flux.

2.3.2 Nitrogen and carbon budgets at steady-state

To further investigate the effect of the two different N sources all the rates at model steady state for 1000 µmol photon m^{-2} s^{-1} were calculated. Figure 2.4 and 2.5 shows the N and C budgets for the four nutrient cases, giving the size of the state variables and all the fluxes between them averaged over 24 hours.

Additionally, to visualize the effect Z_N versus V_{DIN}^H may have had on the biomass, the percentage change in host and symbiont biomass between the four N cases were calculated (Fig. 6).

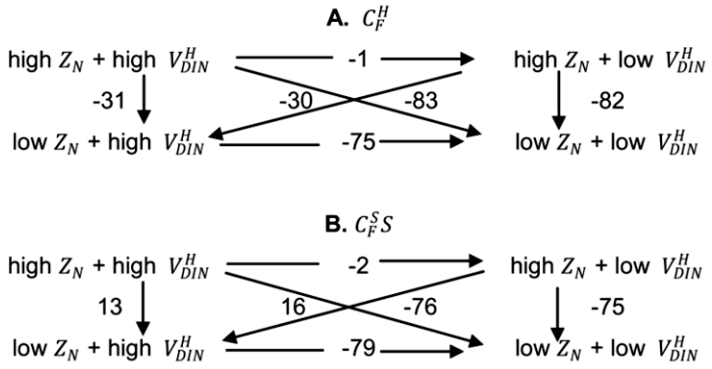

Figure 2.6: Percentage of change in host (C_F^H) and symbiont population biomass ($C_F^S S$) between the four nutrient cases; high feeding rate on prey (Z_N) + high DIN diffusion rate (V_{DIN}^H), high Z_N + low V_{DIN}^H, low Z_N + high V_{DIN}^H, low Z_N + low V_{DIN}^H. The arrows indicate the direction of comparison, and the number the percentage decreases (negative numbers) or increase (positive numbers) in the state variable.

The relatively similar size of the host and the symbiont state variables for all but the low Z_N + low V_{DIN}^H case (Fig. 2.4A, B, C, 5A, B, C and 6) showed that the N source was interchangeable due to the host-symbiont relationship. For high Z_N the host was independent of V_{DIN}^H as a source of N, indicated by the 1% change in biomass between scenarios (Fig. 2.6A). When the Z_N was reduced by an order of magnitude, but V_{DIN}^H was high, the host biomass was reduced by only 31% due to increased translocation of photosynthates from the symbiont and reduced mucus production. Similarly, under high feeding conditions, symbiont biomass was independent of DIN uptake, indicated by the small difference in N_F^S between the high Z_N + high V_{DIN}^H and the high Z_N + low V_{DIN}^H scenario (48 and 47 µg N cm^{-2} respectively) and a 2% reduction in biomass (Fig. 2.6B). This suggests that DIN from metabolic processes were sufficient to maintain the symbiont population as long as the host had the high feeding rate. When Z_N was low, high V_{DIN}^Hwere able to compensate for the lost source of organic N and were capable of maintaining both

the symbiont and the host at a relatively high biomass. For the symbiont low Z_N + high V_{DIN}^H actually resulted in a 13% increase in biomass compared to the high Z_N + high V_{DIN}^H scenario. If the DIN uptake was low as well, all the state variables decreased to a fraction of the other cases (Fig, 2.4D, 2.5D).

Another important feature shown in Figure 2.4 is the internal recycling of N between the host and the symbiont. We defined internal recycling, $Q_{N,in}$, as the ratio between N moving from the symbiont to the host and the total amount of N available to the host:

$$Q_{N,in} = \frac{(T_N^S + mN_F^S)}{(Z_N + T_N^S + mN_F^S)}$$

The percentage of translocated N and re-ingested N from dead cells was 44%, 58%, 62% and 64% of the total N available to the host for the four cases in Figure 2.4 respectively. Consequently, translocation was nearly 40% and 45% more important for low Z_N+ high V_{DIN}^H and low Z_N+ low V_{DIN}^H, respectively, compared to high Z_N+ high V_{DIN}^H.

2.3.3 Sensitivity to parameter values

To investigate the relationship between host and symbiont it was instructive to consider the sensitivity of host state variables (C_F^H and C_R^H) to symbiont parameters (μ_{max}^S, $N_{F,max}^S$, δ^S and m^S), and symbiont state variables (C_F^S, C_R^S and S) to host parameters (δ^H, Q_{min}^H and β_N) (Table 2.4). In the high Z_N + low V_{DIN}^H scenario host state variables were less sensitive to symbiont parameters than in the low Z_N + high V_{DIN}^H scenario. This was due to host biomass being determined by the feeding rate rather than translocated photosynthates from the symbiont. A similar trend could be seen for the symbiont, with a lower sensitivity of symbiont state variables to host parameters Q_{min}^H and β_N under the high Z_N + low V_{DIN}^H. However, for the high Z_N + low V_{DIN}^H scenario, host respiration (δ^H) rate positively

influenced the symbiont as increased δ^H meant a larger DIN pool, whereas for the low Z_N + high V_{DIN}^H scenario the host contribution to the DIN pool becomes less important.

Table 2.4: Sensitivity of model parameters under two of the nutrient scenarios; high Z_N + low V_{DIN}^H, low Z_N + high V_{DIN}^H. Each model parameter was changed +/- 10% separately and the power to which the model state variables changed due to the change in one parameter is seen here. The red colours indicate positive changes in the state variable when increasing the parameter and vice versa for the blue colours. Colour intensity indicates strength of the response. Parameters with a power law exponent of less than 0.3 (-0.3<p<0.3) were excluded.

			Host		Symbiont		
	Parameter	Scenario	C_F^H	C_R^H	C_F^S	C_R^S	S
Symbiont	μ_{max}^S	high Z_N +low V_{DIN}^H	0.81	1.00	0.36	1.35	0.36
		low Z_N +high V_{DIN}^H	1.97	2.03	1.00	1.93	1.00
	δ^S	high Z_N +low V_{DIN}^H	-0.48	-0.60	-0.71	-1.02	-0.71
		low Z_N +high V_{DIN}^H	-1.14	-1.18	-1.07	-1.39	-1.07
	$N_{F.max}^S$	high Z_N +low V_{DIN}^H	0.32	0.38	0.60	0.59	-0.40
		low Z_N +high V_{DIN}^H	0.96	0.98	1.05	1.03	0.05
	m^S	high Z_N +low V_{DIN}^H	-0.26	-0.39	-0.55	-1.35	-0.55
		low Z_N +high V_{DIN}^H	-0.49	-0.57	-0.68	-1.38	-0.68
Translocation	Q_t	high Z_N +low V_{DIN}^H	-0.54	-1.14	-1.77	-2.63	-1.77
		low Z_N +high V_{DIN}^H	-1.07	-1.67	-2.06	-2.95	-2.06
Host	δ^H	high Z_N +low V_{DIN}^H	-0.26	-0.04	0.54	0.74	0.54
		low Z_N +high V_{DIN}^H	-0.43	-0.23	0.17	0.39	0.17
	Q_{min}^H	high Z_N +low V_{DIN}^H	0.12	-0.53	0.29	1.12	0.29
		low Z_N +high V_{DIN}^H	0.37	-0.31	0.55	1.41	0.55
	β_N	high Z_N +low V_{DIN}^H	-0.63	-0.32	-0.25	0.05	-0.25
		low Z_N +high V_{DIN}^H	-0.27	0.05	0.26	0.64	0.26

In the low Z_N + high V_{DIN}^H scenario the host state variables (C_F^H and C_R^H) had an approximately quadratic sensitivity to the change of μ_{max}^S (p=1.97 and 2.03 respectively) and linear, or less than linear, sensitivity to $N_{F,max}^S$ (p=0.81 and 1.00 respectively). This dependency can be tracked through the translocation pathway. Three traits of the symbiont were directly influenced by changes in μ_{max}^S; the maximum rate of photosynthesis (P_C^{max}), the symbiont maximum N uptake rate ($V_{N,max}^S$), as well as the symbiont mortality terms (eq. 8-13). $N_{F,max}^S$ influenced the total biomass of the symbiont population, hence also total photosynthesis. As the symbiont natural mortality term was based on symbiont biomass, a larger biomass due to positive change in $N_{F,max}^S$ will increase the mortality rate. Effectively, increasing μ_{max}^S or $N_{F,max}^S$ enhanced the rate of photosynthesis for the symbiont population which resulted in an increase in the translocation of photosynthates to the host. Increasing μ_{max}^S and $N_{F,max}^S$ by 10% individually, under low Z_N + high V_{DIN}^H conditions, changed the C translocation ($T_C^S S$) from 82.8 to 99.9 µg C cm^{-2} d^{-1} and 82.8 to 91.2 µg C cm^{-2} d^{-1} respectively. Additionally, increasing μ_{max}^S or $N_{F,max}^S$ resulted in a higher symbiont natural mortality rate, hence there was more symbiont biomass which the host could reabsorb. Under low Z_N + high V_{DIN}^H conditions this resulted in an increase of the dead cell absorption ($mC_{host}^S S$) from 10.6 to 12.8 µg C cm^{-2} d^{-1} and from 10.6 to 11.7 µg C cm^{-2} d^{-1} when increasing μ_{max}^S or $N_{F,max}^S$ with 10% respectively. However, host state variables were relatively insensitivity to changes in the symbiont C specific mortality rate (m^S), indicating that changes in the rate of photsynthate translocation may be the most important.

The sensitivity analysis also showed the effect of translocation on both the host and the symbiont. Changes to the N:C ratio of transferred photosynthates (Q_t) caused the greatest response in the state variables of all the parameters, with a linear or more negative response ($p < -1$) in almost all host and symbiont state variables for both nutrient scenarios. Increasing Q_t forced the symbiont to release more N to the host, N which otherwise would have become symbiont biomass, hence reducing the symbiont population biomass which results in a reduction of total translocation of N to the host.

2.4 DISCUSSION

The output of this model describes a N dependent system in which N was exchanged between the environment and the coral, as well as internally recycled between the host and the symbiont. The numerical experiments, sensitivity analysis and the calculations (Fig. 6) all indicate that the host heterotrophic feeding was the most efficient way to retain nutrients, rendering the coral animal independent of DIN uptake, and hence the symbiont, when prey was readily available. The light experiments showed that if the light was 0 or 1 μmol photon m^{-2} s^{-1} the host survived if heterotrophic feeding was high, whereas the symbiont population died (Fig. 2.3). This model response is realistic as coral lacking dinoflagellate symbionts are known to survive in places where prey is plentiful, for example in deep nutrient-rich water where light is limited and photosynthetic activity is insignificant (Roberts et al. 2006). The symbiont on the other hand seemed to be less sensitive to the source of N; rather it depended on the concentration of DIN and DIC in the host tissues which function as the symbiont's environment.

When heterotrophic feeding was limited but DIN available the animal host could survive due to the translocated photosynthates from the symbiont (Fig. 2.4C). This was consistent with the generally accepted idea that coral living in high-light oligotrophic waters are dependent on their symbionts to provide an additional source of nitrogen (Grottoli et al. 2006b; Hughes et al. 2008). Under these conditions a loss of symbionts means that the host may starve and eventually die if conditions are persistent. This was also shown in the model outputs, however the model had no lower limit that determined the amount of biomass the coral needs to survive.

We could use the model to calculate to what extent the host could sustain itself, at a certain biomass, on heterotrophic feeding in the absence of symbiont. Based on the parameterization of the model we were able to relate feeding rate to the biomass of the host at steady state creating an equation which could be used to

calculate the feeding rate needed to sustain a certain biomass from equations 39, 41 and 43 (Table 2.2):

$$Z_N = \frac{N_F^H(\delta^H + \beta_N)}{2(1-\eta^H)}$$

Where Z_N was the feeding rate, δ^H was the biomass specific respiration and maintenance rate, β_N the fraction of N_F^H released as mucus, and η^H the N specific cost of biosynthesis. In the low Z_N + low V_{DIN}^H scenario the host had a N_F^H of 17.8 µg N cm^{-2} and received 0.5 µg N cm^{-2} d^{-1} from feeding. According to the above calculation to sustain this biomass without the symbiont the feeding rate would have to have been 0.9 µg N cm^{-2} d^{-1}. Thus, only 56.8% of the N needed was supplied through feeding.

Similarly, for the low Z_N + high V_{DIN}^H case with an N_F^H of 71.2 µg N cm^{-2} the host needed a feeding rate of 3.5 µg N cm^{-2} d^{-1} without zooxanthellae, instead of 0.5 µg N cm^{-2} d^{-1} to sustain that biomass. Thus, translocation supplied 86% of the N required, with only 14% coming from heterotrophic feeding. For the high feeding scenarios (high Z_N + low V_{DIN}^H and high Z_N + high V_{DIN}^H) the actual Z_N and the calculated Z_N were the same (5 µg N cm^{-2} d^{-1}), hence 100% of the N needed came from feeding. This numerical exercise stresses again the importance of the algal symbionts to the coral host as a source of both N and C when the feeding rate was limited, and support that with high feeding the host becomes independent of the symbiont as a source of N.

Even though the model was not fitted to a particular data set the range of model rates and state variable values agreed well with published experimental data. The size of the total C and N pools for the host and the symbiont were within the same range as the results from experimental observation of Muller-Parker et al. (1994a). Similar to the model outputs they also found that an increase in DIN resulted in a greater increase in symbiont biomass than for the animal fraction.

The modelled rate of photosynthesis corresponded well with values from the literature (Muller-Parker et al. 1994a; Houlbrèque et al. 2003; Houlbreque et al. 2004a). The model output for high light scenarios ranged between 25 to 132 µg C cm^{-2} d^{-1} with the lowest values associated with the low feeding rate and DIN uptake rate. This was in accordance with Houlbrèque and colleagues who found that starved corals had a photosynthetic rate of 57.6 ± 23.1 µg C cm^{-2} d^{-1} and fed corals 357.4 ± 216.2 µg C cm^{-2} d^{-1} (Houlbrèque et al. 2003). In a later study they noted an average photosynthetic rate of 164.3 ± 17.3 µg C cm^{-2} d^{-1} (Houlbreque et al. 2004a). The modelled chlorophyll concentration at steady state, ranging between 2.2 to 10.1 µg Chl cm^{-2}, also agreed with literature. For example Houlbrèque et al. (2003) recorded chlorophyll concentration between 7 and 21 µg Chl cm^{-2}, Muller-Parker at al. reported a somewhat lower range of 2-11 µg Chl cm^{-2} (Muller-Parker et al. 1994b).

Some of the other modelled rates were more difficult to compare to existing experimental data such as respiration and maintenance. Experimental measurements of respiration are often produced by measuring O_2 released from the coral (Al-Horani et al. 2003; Borell et al. 2008). This definition of respiration is not the same as the internal respiration rates calculated in this model; rather the $eqDIC^H$ rate would be the corresponding term. Assuming C from the DIC pool was released as CO_2 the values of $eqDIC^H$ were well in agreement with measured coral respiration rates which commonly range between 8.6-177 µg C cm^{-2} d^{-1} (Gattuso et al. 1999; Leclercq et al. 2002; Borell et al. 2008). Our $eqDIC^H$ rates ranged between 13.8 and 104 µg C cm^{-2} d^{-1} for the four nutrient scenarios.

In this model, mucus production served as a way to release excess C in the form of high C and low N compounds. The release of mucus was enhanced when excess C accumulates in the reserve pools, often as a result of increasing photosynthesis. The exact process and quantity of mucus production under different environmental conditions is still not well understood (Bythell and Wild 2011). A few studies attempting to quantify mucus production have divided the measurements into particulate organic carbon (POC), particulate organic nitrogen (PON) and dissolved organic carbon (DOC). Naumann and colleagues showed that

6 coral species on average released 6.24 ± 1.2 µg POC cm^{-2} d^{-1} and 0.648 ± 0.77 µg PON cm^{-2} d^{-1}, DOC released was much more variable ranging between -263 ± 245 µg DOC cm^{-2} d^{-1} (net uptake) for *Pocillopora* to 73.7 ± 66 µg DOC cm^{-2} d^{-1} for *Acropora* (Naumann et al. 2010). The combined high POC and DOC release values were of the same order of magnitude as the model output which had values varying between 14.4 and 71.6 µg C cm^{-2} d^{-1}. Due to the uncertainty in the experimental result we argue that to avoid unnecessary model complexity we kept the mucus calculations as simple as possible. In future version of the model exploring the function of mucus more in depth and adding positive feedbacks is desirable.

The model proved to be relative insensitive to many of the parameters used in the model (Table 2.3 and 2.4). Two of the parameters which the model outputs were sensitive to were μ_{max}^{S} and $N_{F,max}^{S}$ estimated from the literature. One of the likely reasons behind the model sensitivity to μ_{max}^{S} depended on the accumulated effect this parameter had on three separate model processes (as mentioned in section 2.3.3), indicating that further exploration into these parameters could prove useful. The high model sensitivity to Q_t highlights the importance of knowing the internal exchanges of N and C occurring within the coral, if we want to predict coral growth. There is a gap in our knowledge about exactly what compounds are being transferred from the symbiont to the host. Assuming a large fraction is amino acids the N:C ratio would lie somewhere between 0.1 - 0.3 g N g C^{-1} (range of essential amino acids) (Hughes 2011). However, Falkowski (1993) suggested a Q_t of 0.03 g N g C^{-1}. We used 0.08 g N g C^{-1} as a compromise, but the high sensitivity to this parameter suggests that more research into the internal exchange between the symbiont and coral host is needed.

The model indicated that close to 60%, or more, of the N available to the host had previously been recycled by the symbiont for all N scenarios with the exception of the high Z_N + high V_{DIN}^{H}. Even though we saw an increase in the importance of recycled N when N uptake was limited, it could have been expected that this response should have been stronger, as coral reefs are generally considered to

have a high internal recycling rate (Wilkinson et al. 1984). However on the scale of coral-algae symbiosis it has been suggested that internal recycling cannot occur indefinitely without any influx of new N species (Fitt and Cook 2001). The importance of translocation and internal recycling highlights why it is central to resolve host and symbiont in a coral model, and instead of giving fixed recycling rates keeping the system dynamic.

2.5 SUMMARY

This model gives a basic framework of coral host and algae symbiont interaction, and proved to be a useful tool for exploring the effect two different nutrient sources had on the system. The numerical experiments and the sensitivity analysis showed that the host could survive without the symbiont if heterotrophic feeding was high. The symbiont retained a high biomass as long as there was enough DIN in the host tissue independent of whether the DIN came from the environment or metabolic waste products. The model yielded state variable values and model rates similar to experimental data from the literature. However, the parameterization of the model should be considered with care, and should be updated if new more suitable experimental data becomes available.

The model highlights that being able to acquire N and C from two different sources and have an internal exchange and recycling is the key to the success of the coral in oligotrophic environments. In the future this model will be extended to incorporate a more detailed photosystem model, with the aim to simulate photoinhibition and subsequent bleaching, how having different nutrient sources will influence these processes, and to test the theory that heterotrophy reduces the risk of bleaching and enhances the rate of recovery.

CHAPTER 3:

MODELLING PHOTOINHIBITION AND BLEACHING IN SCLERACTINIAN CORAL AS A FUNCTION OF LIGHT, TEMPERATURE AND HETEROTROPHY

3. Modelling photoinhibition and bleaching in Scleractinian coral as a function of light, temperature and heterotrophy

This chapter in inserted without abstract as published in Limnology and Oceanography:

Gustafsson, M. S. M., M. E. Baird, and P. J. Ralph. (in press). Modeling photoinhibition and bleaching in Scleractinian coral as a function of light, temperature and heterotrophy. Limnology and Oceanography.

Model development, experimental design and model evaluation and validation was performed by Malin Gustafsson who also wrote the paper. Intellectual contributions and technical assistant were made by Mark Baird and Peter Ralph.

3.1 INTRODUCTION

Reef building corals (Scleractinian) live close to their observed upper thermal limit during summer months (Lesser and Farrell 2004). As a consequence of increasing sea surface temperatures (SST) mass coral bleaching events have become more frequent (Hughes et al. 2003; Wilkinson [ed.]. 2002). Most corals living in the photic-zone of the ocean are known to harbor symbiotic unicellular dinoflagellate algae from the genus *Symbiodinium* within their tissues. Coral bleaching is caused by a breakdown of the coral-algae symbiosis, resulting in the loss of photosynthetic pigments or expulsion of the algae symbionts from the coral host tissues (Brown 1997; Jones 2008).

The symbiotic relationship between the coral host and the symbiotic algae depends upon the autotrophic symbiont fixing carbon (C) through photosynthesis,

which is used to synthesize products such as glycerol, glycerides, amino acids, and fatty acids (Falkowski et al. 1984; Muscatine 1990; Sutton and Hoegh-Guldberg 1990). Glycerol and glycerides can be produced in large quantities causing a high C:N ratio of photosynthetic products (Sutton and Hoegh-Guldberg 1990; Grant et al. 1997). These photosynthates can be translocated to the host, providing a source of nutrients (Wang and Douglas 1999). Additionally, the corals can feed on a wide range of prey items from zooplankton to particulate and dissolved organic matter (POM and DOM). Corals can capture prey items by tentacle grabbing, nematocyst discharges, or mucus adhesion (Houlbrèque and Ferrier-Pagès 2009). The metabolic byproducts of the host in turn provide the symbiont population with a steady supply of inorganic compounds, such as carbon dioxide, ammonium, urea, and polyphosphates (Titlyanov and Titlyanova 2002).

When the coral is exposed to high light and elevated temperature, the photosystem of the symbiotic algae may become photoinhibited (Hoegh-Guldberg and Jones 1999; Venn et al. 2008). Photoinhibition can be caused by oxidative stress, which usually involves the accumulation of reactive oxygen species (ROS) at photosystem II (PSII) in the electron transport chain (ETC), resulting in the degradation of the DI protein, inhibiting the zooxanthellae's ability to photosynthesize (Lesser 2006). Photosynthesis and cell respiration will continuously produce low levels of reactive oxygen species (ROS), such as singlet oxygen ($^1O_2$), hydroxyl radical (OH^-), superoxide (O_2^-), and hydrogen peroxide (H_2O_2) (Asada 2006; Lesser 2006). However, oxidative stress only occurs when the production of ROS exceeds the ability of the organisms to quench or eliminate the ROS using cellular products such as antioxidants (Lesser 2006; Levy et al. 2006). Accumulated ROS may cause damage to the photosystem, as well as to both symbiont and host tissues (Smith et al. 2005; Asada 2006; Venn et al. 2008). The presence of highly reactive oxygen species such as $^1O_2$, with an average lifetime of 3.7 μs, commonly result in specific damage to protein in close association with the site where the ROS was formed (Lesser 2006). Other ROS such as H_2O_2, which is uncharged, have longer lifetimes and can therefore move across cell membranes to other parts of the alga cell or

even into the host (Downs et al. 2002; Saragosti et al. 2010). These ROS can affect tissue and proteins that are remote from the formation site.

The sensitivity of the symbiont photosystem to temperature may be associated with the relative rates of damage and repair of PSII which changes the rate of fixation of inorganic carbon (Venn et al. 2008). There are several protective mechanisms the algae may use to counteract or reduce the damaging effects of light and temperature stress, such as non-photochemical quenching and alternative electron transport path ways (Kirk 1994).

When the coral is exposed to elevated light and temperature, the photosystem of the symbiotic algae may become photoinhibited (Hoegh-Guldberg and Jones 1999; Venn et al. 2008). Photoinhibition may lead to damage to the photosystem and eventually bleaching due to oxidative stress, involving the production and accumulation of reactive oxygen species (ROS) (Lesser 2006; Venn et al. 2008). A physical trigger of photoinhibition is the temperature induced breakdown of the Ribulose bisphosphate carboxylase oygenase (Rubisco) enzyme (Lilley et al. 2010). Rubisco is essential for the fixation of CO_2 for photosynthesis; if inactive it causes a blockage of the electron transport chain (ETC) leading to a build-up of electrons which can react with O_2 forming superoxide (O_2^-) at the site of photosystem I (PSI) (Venn et al. 2008). Superoxide dismutase (SOD) catalyzes the reaction turning O_2^- of hydrogen peroxide (H_2O_2), whereas the detoxifying enzymes ascorbate peroxidases (APX) can reduce the H_2O_2 to water (Asada 2006). The production of O_2^- and H_2O_2 is called the Mehler reaction (Mehler and Brown 1952). In addition to the Mehlar reaction, ROS can form as singlet oxygen ($^1O_2^*$), which is produced due to the highly reactive triplet states of chlorophyll (^{3}Chl) reacting with O_2. Triple excited Chl is a result of restricting the rate of the electron flow through the ETC causing maximal reduction of the plastoquinone (PQ) which causes a buildup of excess excitation energy (Jones et al. 1998).

Photosynthesis and cell respiration will continuously produce low levels of ROS, such as singlet oxygen ($^1O_2^*$), hydroxyl radical (OH^-), superoxide (O_2^-), and hydrogen peroxide (H_2O_2) (Asada 2006; Lesser 2006). However, oxidative stress

only occurs when the production of ROS exceeds the ability of the organisms to eliminate the ROS using cellular products such as antioxidants (Lesser 2006). Accumulated ROS may cause damage to the photosystem, as well as to both symbiont and host tissues (Asada 2006; Venn et al. 2008). The presence of highly reactive oxygen species such as $^1O_2^*$, with an average lifetime of 3.7 μs, commonly results in specific damage to protein in close association with the site where the ROS was formed (Lesser 2006). As $^1O_2^*$ forms at PSII it can prompt the degradation of the D1 protein (Asada 1996), as well as cause damage and bleaching of pigments in the light harvesting complex (Venn et al. 2006). Other ROS such as H_2O_2, which is uncharged, have longer lifetimes and can therefore move across cell membranes to other parts of the algal cell or even into the host (Saragosti et al. 2010).

When a photon is absorbed by a chlorophyll *a* molecule, it excites the chlorophyll from the ground state to the single excited state. The energy from the excited molecule may then have one of four fates; 1) the energy may be passed to the reaction center, in photosystem I or II, where it will be used for photochemical quenching (photosynthesis); 2) the energy can be dissipated as heat returning the chlorophyll molecule to the ground state (non-photochemical quenching); 3) the chlorophyll can re-emit the energy as a longer wavelength photon (fluorescence); or 4) as mentioned above, the chlorophyll excited state (Chl^*) can be converted into a triplet spin configuration (^3Chl), which is a potent sensitizer of $^1O_2^*$, a process which does not include any transfer of electrons, but results in molecular damage (Apel and Hirt 2004).There are several additional sites within the symbiont and the host where ROS can form, such as the mitochondria (Dunn et al. 2012), however is this study we focus on ROS production associated with the photosystem.

There are several protective mechanisms the algae may use to counteract or reduce the damaging effects of light and temperature stress, such as non-photochemical quenching, and detoxification of ROS (Kirk 1994). Non-photochemical quenching (NPQ) involves the fast modification of auxiliary pigments to switch their photochemical function from light absorbing to heat dissipating under high light conditions and reverses under low light, and is

referred to as the xanthophyll cycle. In dinoflagellates, the pigment diadinoxanthin is converted to diatoxanthin through the removal of an epoxy group under high light.

It has also been suggested that repair rates of the photosystem may be temperature dependent; Hill et al. (2011) showed an up-regulation of D1 repair, whereas other studies showed a down regulation (Hill et al. 2004; Murata et al. 2007; Takahashi et al. 2009). Similarly, the antioxidant activity may be up-regulated during elevated temperature (Flores-Ramírez and Liñán-Cabello 2007), yet this regulation varies between symbiont clades (Mcginty et al. 2012).

The effect of elevated temperature on the coral symbiosis is linked to the D1 repair process and antioxidant systems, but it is also influenced by the host's ability to feed heterotrophically. An increased acquisition of nitrogen from heterotrophy has been shown to reduce photoinhibition and bleaching damage (Grottoli et al. 2006; Ferrier-Pagès et al. 2010; Hoogenboom et al. 2012). Heterotrophic feeding increased the host metabolism, hence supplying the symbiont with additional inorganic carbon and nitrogen, providing an additional source of energy which can be used to enhance the repair of damaged PSII. In addition, the host's need for translocated photosynthates decreases with increasing supply of heterotrophic food (Falkowski et al. 1984). An additional process that may be of importance, although not considered in this study, is the temperature-dependent changes in the microbial consortium associated with the coral (Gilbert et al. 2012).

The complexities associated with the dinoflagellate photosystem, and the processes leading to photoinhibition and coral bleaching are still not fully understood. A process-based numerical model of this system may help to understand some of these complexities. Gustafsson et al. (2013) developed a coral symbiosis model, hereafter referred to as the GBR13 model, which described the symbiosis between an autotrophic algae symbiont and a heterotrophic cnidarian host under different light and nutrient conditions (Gustafsson et al. 2013). The GBR13 model showed that being able to utilize both inorganic and organic sources of nutrients allowed for a stable host-symbiont population under low and variable

nutrient fluxes. This model did not, however, include any temperature dependence or sensitivity to high light of the symbiont photosystem, and thus could not simulate the temperature and light dependent breakdown of the coral symbiosis which may lead to coral bleaching.

Here we present a numerical model of coral photosynthesis building upon the GBR13 model to simulate photoinhibition and subsequent bleaching. Evidence clearly indicates that the key trigger of thermal bleaching is the impairment of the photosystem (Venn et al. 2008). However, uncertainty remains concerning the sequence of events. There are three proposed effects of elevated temperature; energetic decoupling of the thylakoid membrane (Tchernov et al. 2004), impairment of the Calvin cycle through temperature induced inactivation of Rubisco (Jones et al. 1998; Lilley et al. 2010), and dysfunction of PSII and degradation the DI protein (Iglesias-Prieto et al. 1992). We chose to focus on the hypothesis that temperature-dependent inactivation of the Rubisco protein would impair the CO_2 uptake, causing a backlog of electrons which could result in the formation of ROS. This hypothesis was chosen due to the clear relationship between temperature and Rubisco activity and the availability of experimental data for model parameterization (Lilley et al. 2010).

The formation of $^1O_2$ through the excitation of chlorophyll was accounted for in the model due to the reduction of PSII, but not given a separate state variable, rather being incorporated in the pool of ROS. In accordance with experimental studies, the ROS caused damage to the photosystem, as well as other cell tissues, if it was not eliminated by the antioxidant system or other detoxifying processes. Damaged PSII protein could be repaired, but when the photo-damage exceeded the repair rate, then photoinhibition occurred. A build up of H_2O_2 caused general tissue damage and expulsion of symbiont cells.

The model was fitted to the experimental photo-biological dataset of Hill et al. (2012) to derive the unknown parameters associated with D1 protein repair, detoxification and re-oxidation state of the photosystem. The model was assessed using the experimental ROS data from Suggett et al. (2008), and the effect of

feeding vs. starvation on photoinhibition and bleaching were simulated and compared to the experimental dataset by Borell and Bischof (2008). Finally, the temperature dependence of bleaching in the model was compared to general field observations using the bleaching index Degree Heating Days (Maynard et al. 2008*a*), a tool used to predict onset and severity of coral bleaching.

3.2 METHODS

The photoinhibition model developed in this paper builds on the coral symbiosis model of Gustafsson et al. (2013), hereafter GBR13. The processes of nutrient cycling, respiration, cell division, mucus production, synthesis of tissues and chlorophyll, calcification and more were based on the GBR13 model. One important alteration to the GBR13 model was redefining the translocation of photosynthates (T_C^S) from the symbiont to the host, where a new definition was needed:

$$T_C^S = \frac{(C_F^H(\mu_{\max}^H + \eta^H + \delta^H \mu_{\max}^H) - Z_C)\left(\frac{C_R^S}{C_{R,\max}^S}\right)}{S} \quad (1)$$

Where T_C^S is the translocation of carbon (C) from the symbiont to the host, $\mu_{\max}^H$ is the maximum host growth rate, η^H represents respiration and cell maintenance of the host, δ^H is the host C specific cost of biosynthesis, Z_C is the rate of C acquisition through heterotrophic feeding, C_R^S is the symbiont C reserve, S is the number of symbiont cells, and $C_{R,\max}^S$ is the maximum size of the symbiont C reserve. Equation 1 replaces eq. 4 in GBR13. This new definition resulted in a host-controlled translocation rate, where the host's need for energy set the rate, as long as the symbiont had sufficient energy to maintain its own cellular demands. The change was made to include the 'host factor' a chemical agent present in the host tissues (Gates et al. 1995), and is based on the observation that starved cnidarian hosts have been shown to extract a larger fraction of the newly produced photosynthates than fed hosts (Davy and Cook 2001b).

The photoinhibition model described in this paper was linked to the GBR13 model, adding a much more detailed description of not just the photosystem, but also several associated processes such as antioxidant systems, the nutritional cost of repairing the photosystem and producing antioxidants, as well as synthesis of diadinoxanthin and diatoxanthin pigments and the loss of symbionts due to damage caused by ROS production. However, not all processes of the photosystem were included due to our desire to constrain the complexity and as several of these processes are not yet fully understood. An example of such a process was the transfer of ROS from the symbiont cell to the host tissues and the host's ability to detoxify using its antioxidant system. We acknowledge that these processes will be important under some circumstances and should ideally be included into the model in the future. The major assumptions made deriving this model are stated in Table 3.1.

Table 3.1: Assumptions made while deriving the photoinhibition model.

- Temperature dependent inactivation of Rubisco as the primary site affected by elivated temperatures.
- Reactive oxygen is not transferred across cell mambranes to the host.
- Exocytosis: symbiont cells are expelled without causing damage to the host.
- Translocation of photosynthates are influenced by the host's need of nutrient, a representation of the 'host release factor'.
- Synthesis of new reaction centers (RCII) and xanthophyll pigments are assumed to occur at the same rate as chlorophyll synthesis.
- The presence of three pigments was assumed; chlorophyll, diadinoxanthin, and diatoxanthin.

3.2.1 Model structure

The photoinhibition model described here included six new state variables (Fig. 3.1, Table 3.2), in addition to the twelve described in GBR13 (Table 3.3). The first three new state variables included the different states of the photosystem defined as the number of reaction centers (RCII) per cell that were oxidized (Q_{ox}), reduced

(Q_r), or inhibited (Q_i) (Eqs. 3-5). Oxidized RCII (Q_{ox}) could pass the captured electron on through the ETC. However, one of the first steps in the ETC was the light-driven reduction of the primary acceptor plastoquinone in RCII, which was then balanced by its re-oxidation (Eqs. 3 and 4). The fourth and fifth state variables were the concentration of two xanthophyll pigments, diadinoxanthin (D_d) which could absorb photons and contribute to capturing light for photosynthesis, and diatoxanthin (D_t) which could dissipate heat, hence it protected the cell when exposed to excessive light (Eqs. 6 and 7). The last state variable was the concentration of ROS formed after stress (RO_s) (Eq. 8). This pool only contained ROS that had a relatively slow reaction rate such as H_2O_2 as we assume that highly reactive ROS (such as $^1O_2{}^*$) would react with the surrounding tissues immediately, hence they would not accumulate.

State variables from GBR13 which were altered during the coupling of the two models through the addition of a bleaching associated loss term are redefined in the first part of Table 3.3 (Eqs. 9-12). The reduction term represented the energetic cost of repairing damage to the photosystem (B_{k_i}), as well as the cost of reducing ROS concentrations through detoxification ($B_{A_{\mathrm{RO}}}$). The second half of Table 3.3 shows the state variables for the coral-algae symbiosis model presented in GBR13.

Figure 3.1 shows a schematic of the photoinhibition model. We will go through each process shown in Fig. 3.1, as well as the process of calibrating the model to a dataset collected by Hill et al. (2012), with an emphasis on deriving the unknown parameters, and as a means of using the model framework and observations to better describe these poorly understood processes. Model equations are presented in Table 3.2 – 3.4 with associated parameters in Table 3.5, and relevant equations and parameters from GBR13 in Table 3.6 and 3.7.

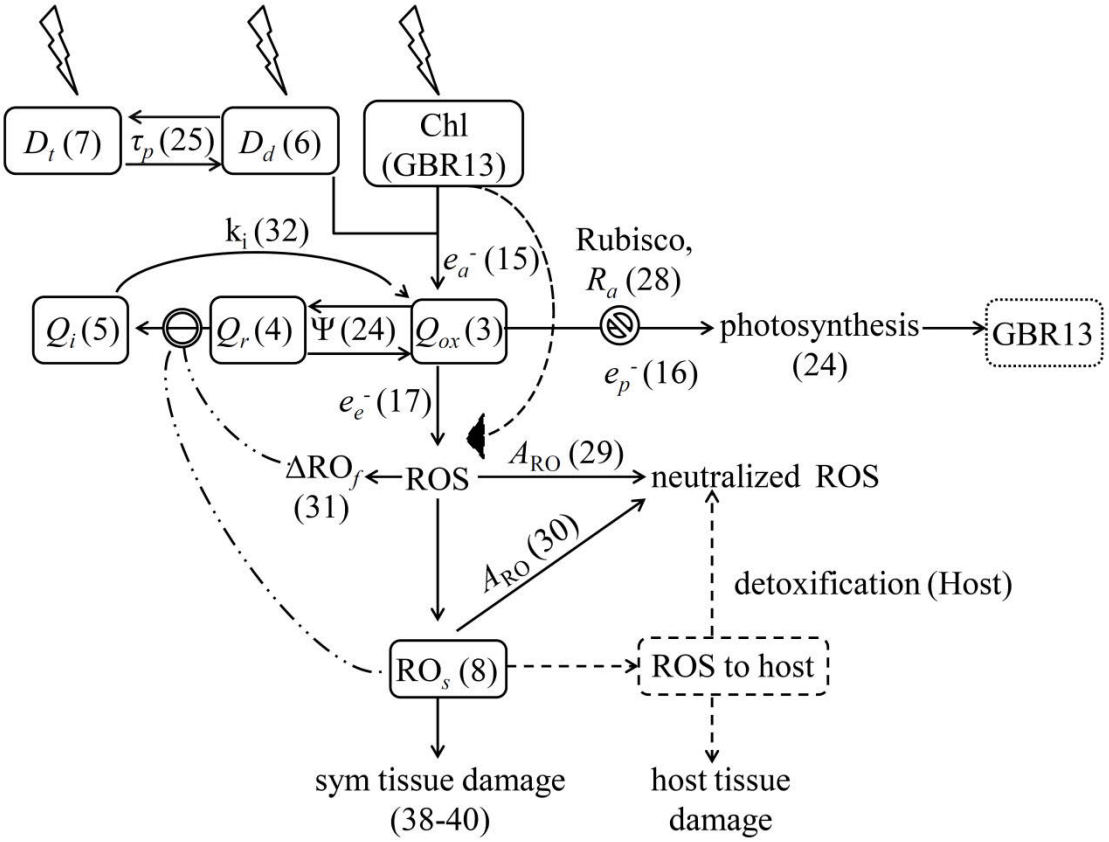

Figure 3.1: Schematic of photoinhibition model, boxes indicate state variables and arrows are fluxes. ΔRO_f is not considered a state variable, as we assume that it will immediately react with symbiont tissues at the site of formation, hence inhibit the photosystem. The numbers in the brackets correspond to the equation number in Table 3.2 and 3.4. The dashed arrow and box refereeing to ROS in the host are not included in the model.

Table 3.2: New state variable equations for the photoinhibition model. The number in brackets refers to the equation numbers used in the text.

Equation	Eq.	Description	Unit
$\frac{dQ_{ox}}{dt} = -\Psi - \Delta\mathrm{RO}_f \frac{Q_{ox}}{Q_t} + k_i Q_i + \mu^{\mathrm{Chl}} Q_t - \mu^S Q_{ox}$	(3)	oxidizes RCII	μmol RCII cell^{-1}d^{-1}
$\frac{dQ_r}{dt} = \Psi - \Delta\mathrm{RO}_f \frac{Q_r}{Q_t} - \mu^S Q_r$	(4)	reduced RCII	μmol RCII cell^{-1}d^{-1}
$\frac{dQ_i}{dt} = \Delta\mathrm{RO}_f \frac{Q_a}{Q_t} - k_i Q_i - \mu^S Q_i$	(5)	inhibited RCII	μmol RCII cell^{-1}d^{-1}
$\frac{dD_d}{dt} = \varsigma(D_d + D_t) - \tau_p - \mu^S D_d$	(6)	diadinoxanthin	μg D_d cell^{-1}d^{-1}
$\frac{dD_t}{dt} = \tau_p - \mu^S D_t$	(7)	diatoxanthin	μg D_t cell^{-1}d^{-1}
$\frac{d\mathrm{RO}_s}{dt} = \begin{cases} f_{\mathrm{RO}_s}\mathrm{RO} - f_{\mathrm{RO}_s} A_{\mathrm{RO}} + \Delta\mathrm{RO}_f \left(1 - \frac{Q_a}{Q_t}\right) & if\ I > 0 \\ -\beta\mathrm{RO}_s - \mu^S \mathrm{RO}_s & \\ -A_{\mathrm{RO}} - \beta\mathrm{RO}_s - \mu^S \mathrm{RO}_s & \text{else} \end{cases}$	(8)	slow ROS	μmol ROS cell^{-1}d^{-1}

3.2.2 Electron transport

For the purpose of this photoinhibition model, electron energy, which could be converted to ROS or C while moving through the model processes, were used as a form of model currency. The rate of electrons generated within the cell (e_a^-) depended on the cells absorption cross sectional area (σ'), light intensity (I) and the quantum efficiency of PSII (φ_{PSII}) (Eq. 15) (Table 3.4). The electrons could pass through the ETC and contribute to photosynthesis, e_p^- (Eq. 16), or, if there was any downstream blockage, or if e_a^- exceeds the maximum capacity of the electron transport (e_{max}^-), the electrons were produced in excess (e_e^-), which was the first step towards the production of ROS (Eq. 17). The process described above corresponded to the Mehler reaction (Mehler and Brown 1952) and was defined in a way that there were always some formation of e_e^- and hence ROS; however, under low light and optimal temperatures the antioxidant and repair systems in the model were able to counteract the production of the ROS.

Table 3.3: State variable equations from the GBR13 model, where Eqs. 9-12 include the alterations made for this model. Equation numbers are given in brackets, and equation numbers following GBR13 indicate which equation it refers to in Gustafsson et al. (2013).

Equation	Eq. No.	Description	Unit
$\frac{dN_F^S}{dt} = \begin{cases} V_N^S - R_N^S - T_N^S - mN_F^S - \mu^S N_F^S - B_N^S & \text{if } \mu^S > 0 \; N_F^S > N_{F,\max}^S \\ V_N^S - R_N^S - T_N^S - mN_F^S - \delta_N^S & \text{else} \end{cases}$	(9)	change in N_F^S	μg N cell^{-1} d^{-1}
$\frac{dC_F^S}{dt} = \begin{cases} V_C^S - R_C^S - T_{CF}^S - mC_F^S - \mu^S C_F^S - B_{CF}^S & \text{if } \mu^S > 0 \; N_F^S > N_{F,\max}^S \\ V_C^S - R_C^S - T_{CF}^S - mC_F^S - B_{CF}^S & \text{else} \end{cases}$	(10)	change in C_F^S	μg C cell^{-1} d^{-1}
$\frac{dC_R^S}{dt} = \begin{cases} P_{\text{cell}}\left(1 - \frac{C_R^S}{C_{R,\max}^S}\right) - V_C^S - mC_R^S & \text{if } \mu^S > 0 \; N_F^S > N_{F,\max}^S \\ \quad - T_{CR}^S - \mu^S C_R^S - B_{CR}^S & \\ P_{\text{cell}}\left(1 - \frac{C_R^S}{C_{R,\max}^S}\right) - V_C^S - mC_R^S - B_{CR}^S & \text{else} \end{cases}$	(11)	change in C_R^S	μg C cell^{-1} d^{-1}
$\frac{dS}{dt} = \begin{cases} \mu^S S - mS - m_S^{exp} & \text{if } \mu^S > 0 \quad N_F^S > N_{F,\max}^S \\ -mS - m_S^{exp} & \text{else} \end{cases}$	(12)	change in symbiont population size	cell cm^{-2} d^{-1}
$\frac{d\text{Chl}}{dt} = \begin{cases} \frac{V_N^S}{Q_F^S}\Pi_{\max}^L \theta_{\max}^C \Omega\varphi\left(1 - \frac{\text{Chl}}{\text{Chl}_{\max}}\right) & \text{if } I > 0 \; C_R^S > C_{\text{thres}}^S \\ \frac{V_N^S}{Q_F^S}\Pi_{\max}^L \theta_{\max}^C \left(1 - \frac{\text{Chl}}{\text{Chl}_{\max}}\right) & \text{if } I = 0 \; C_R^S > C_{\text{thres}}^S \\ -R_m^S \theta^C S & if \; C_R^S = 0 \\ 0 & \text{else} \end{cases}$	GBR13 (29a)	change in symbiont chlorophyll	μg Chl cell^{-1} d^{-1}
$\frac{dN_F^H}{dt} = Z_N - R_N^H - M_N$	GBR13 (43)	change in host N_F^H	μg N cm^{-2} d^{-1}
$\frac{dC_F^H}{dt} = V_C^H - R_C^H - M_{CF}$	GBR13 (44)	change in host C_F^H	μg C cm^{-2} d^{-1}
$\frac{dC_R^H}{dt} = Z_C + T_C^S S - M_{CR} - V_C^H$	GBR13 (45)	change in host C_R^H	μg C cm^{-2} d^{-1}
$\frac{d\text{DIC}^H}{dt} = V_{\text{DIC}}^H + R_C^H + R_C^S S - P_{\text{cell}} S\left(1 - \frac{C_R^S}{C_{R,\max}^S}\right) - \frac{d\text{Calc}}{dt} - eq\text{DIC}^H$	GBR13 (46)	change in host DIC^H	μg C cm^{-2} d^{-1}
$\frac{d\text{DIN}^H}{dt} = V_{\text{DIN}}^H + R_N^H + S(R_N^S - V_N^S) - eq\,\text{DIN}^H$	GBR13 (47)	change in host DIN^H	μg N cm^{-2} d^{-1}

The parameter $e_{\max}^-$ was defined as the rate of electrons that could pass through the ETC given the maximum number of photosystem II reaction centers per cell ($Q_{\max}$) present in the oxidized form and in the absence of any downstream blockages (Eqs. 18-20). To estimate $e_{\max}^-$ we assumed a maximum light intensity ($I_Q^{\max}$) where all electrons could pass through the ETC (Eq. 18). To determine the maximum electrons per RCII (Eq. 19), the maximum number of absorbed photons

($I_Q^{\max}\sigma'\varphi_{\mathrm{PSII}}$) was divided by $Q_{\max}$ (Eq. 20). $Q_{\max}$ was calculated assuming a linear relationship between chlorophyll concentration and the number of RCIIs, using a RCII:Chl ratio established for *Symbiodinium* by Suggett et al. (2008). Hence, $Q_{\max}$ was achieved when the chlorophyll concentration was at its maximum, which was defined as the chlorophyll concentration required to absorb more than 95% of the light incident upon the cell.

3.2.3 Photon absorption and the xanthophyll cycle

There are several types of pigments present within the symbiont cell. Some, such as chlorophyll, absorb light and pass the photons on through the photosystem, whereas others such as diatoxanthin, absorb light and dissipate it as heat. Including all of the details of pigments present in the symbiont cell and their respective functions in the model was not feasible. Therefore, we focused on the processes considered most important for photo-protection and photoinhibition, and only three pigments were described as state variables in the model; chlorophyll *a* (Chl *a*) as it acts as the primary donor of electrons to the ETC, as well as diadinoxanthin and diatoxanthin due to their photo-protective role in the xanthophyll cycle (Falkowski et al. 2007).

Absorption of light (σI) was calculated in the same manner as in GBR13; however, there are now three pigments rather than one (Eq. 21). The absorption cross section was calculated for all pigments (σ) (Eq. 22) and then the absorption cross section for the absorbing pigments Chl *a* and diatoxanthin (σ') (Eq. 23). The photosynthetic output was set to correspond to e_p^- as long as it did not exceed the maximum photosynthetic rate ($P_C^{\max}$) (Eq. 24). $P_C^{\max}$ was set to be the amount of C needed to provide for symbiont maximum growth rate ($\mu_{\max}^S$) including respiration and cost of biosynthesis, as photosynthesis above this rate would be energy inefficient (Table 3.6). The photosynthetic output was also limited by the availability of dissolved inorganic carbon (DIC) in the host tissue (Gattuso et al. 1999), represented by the bracketed term in Eq. 24.

Table 3.4: Photoinhibition model equations, the number in brackets refers to the equation numbers used in the text.

Equation	Eq. No.	Description	Unit
$Q_t = Q_{ox} + Q_r + Q_i$	(13)	total RCII	μmol RCII cell^{-1}
$Q_a = Q_{ox} + Q_r$	(14)	active RCII	μmol RCII cell^{-1}
$e_a^- = \sigma' \varphi_{\mathrm{PSII}} I$	(15)	electron absorption rate	μmol e$^-$cell^{-1} d^{-1}
$e_p^- = min \begin{cases} e_a^- \dfrac{Q_{ox}}{Q_t} R_a \\ e_{\max}^- R_a \end{cases}$	(16)	electrons leading to C fixation	μmol e$^-$cell^{-1}d^{-1}
$e_e^- = e_a^- - e_p^-$	(17)	electrons diverted from C fixation.	μmol e$^-$cell^{-1}d^{-1}
$e_{\max}^- = 6Q_t$	(18)	max. e transport rate	mol e$^-$ cell^{-1} d^{-1}
$6 = \dfrac{I_Q^{\max} \sigma' \varphi_{\mathrm{PSII}}}{Q_{\max}}$	(19)	max. e transfer per RCII	mol e$^-$ mol RCII^{-1} d^{-1}
$Q_{\max} = \mathrm{Chl}_{\max} \theta_{\mathrm{Chl}}^{\mathrm{RCII}}$	(20)	max. RCII per cell	μmol RCII cell^{-1}
$P = \mathrm{Chl} + D_d + D_t$	(21)	total pigment pool	μg P m^{-3}
$\sigma = \pi r^2 \left(1 - \dfrac{2(1-(1+2\gamma Pr)e^{-2\gamma Pr}}{(2\gamma Pr)^2}\right)$	(22)	absorption cross section	m^2 cell^{-1}
$\sigma' = \sigma \dfrac{\mathrm{Chl} + D_d}{P}$	(23)	effective absorption cross section	m^2 cell^{-1}
$P_{\mathrm{cell}} = min \begin{cases} P_C^{\max} \left(\dfrac{\mathrm{DIC}^H}{\mathrm{DIC}^H + k_{\mathrm{DIC}}}\right) \\ \theta_C^{e^-} e_p^- \left(\dfrac{DIC^H}{\mathrm{DIC}^H + k_{\mathrm{DIC}}}\right) \end{cases}$	(24)	photosynthetic rate	μg C cell^{-1}d^{-1}
$\tau_p = \begin{cases} D_d \alpha^X f_T^I & \text{if } I > 0 \\ -D_t \alpha^X (1 - R_a) & \text{else} \end{cases}$	(25)	switching between absorbing and heat dissipating xanthophylls pigments	μg D$_x$ cell^{-1}d^{-1}
$\Psi = \begin{cases} \dfrac{e_a^-}{6} \dfrac{Q_{ox}}{Q_t} (1 - R_a) & \text{if } I > 0 \\ -Q_r \dfrac{Q_r}{Q_t} R_a & \text{else} \end{cases}$	(26)	reduction or oxidation of active RCII	μmol RCII cell^{-1}d^{-1}
$\mu^{\mathrm{Chl}} = \dfrac{d\mathrm{Chl}}{dt} / \mathrm{Chl}$	(27)	chlorophyll growth rate	d^{-1}
$R_a = 0.058(T - T_i) + 1$	(28)	active fraction of Rubisco	-
$\Delta\mathrm{ROS} = \dfrac{e_e^-}{\theta_{\mathrm{RO}}^{e^-(R_a)}}$	(29)	rate of ROS formed by e_e^-	μmol ROS cell^{-1}d^{-1}
$A_{\mathrm{RO}} = \Delta\mathrm{ROS} \left(\dfrac{N_F^S}{N_F^S + N_{\mathrm{thres}}^S}\right) \left(\dfrac{C_R^S}{C_{R,\max}^S}\right)$	(30)	rate of detoxification	μmol e$^-$cell^{-1}d^{-1}
$\Delta\mathrm{RO}_f = \begin{cases} f_{\Delta\mathrm{RO}_f} \Delta\mathrm{ROS} - f_{\Delta\mathrm{RO}_f} A_{\mathrm{RO}} & if\ I > 0 \\ 0 & else \end{cases}$	(31)	electrons that form fast ROS.	μmol RO$_f$ cell^{-1}d^{-1}
$k_i = \begin{cases} \alpha_d^K f_T^I Q_i \dfrac{C_R^S}{C_R^S + k_D} & if\ I > 0 \\ \alpha_n^K Q_i \dfrac{C_R^S}{C_R^S + C_{\mathrm{thres}}^S} & else \end{cases}$	(32)	repair rate of Q_i to Q_{ox}	μmol RCII cell^{-1}d^{-1}
$B_{k_i} = k_i \omega_{\mathrm{D1}} f_\delta$	(33)	carbon cost of D1 repair	μg C cell^{-1}d^{-1}
$B_{A_{\mathrm{RO}}} = A_{\mathrm{RO}} \omega_A f_\delta$	(34)	carbon cost of antioxidant activity	μg C cell^{-1}d^{-1}
$B_{CF}^S = \left(B_{A_{\mathrm{RO}}} + B_{k_i}\right) \left(1 - \dfrac{C_R^S}{C_R^S + k_B}\right)$	(35)	total cost of D1 repair and detoxification taken from C_F^S	μg C cell^{-1}d^{-1}
$B_{CR}^S = \left(B_{A_{\mathrm{RO}}} + B_{k_i}\right) \left(\dfrac{C_R^S}{C_R^S + k_B}\right)$	(36)	total cost of D1 repair and detoxification taken from C_R^S	μg C cell^{-1}d^{-1}

Table 3.4. Continued.

Equation	Eq. No.	Description	Unit
$B_N^S = \delta_{CF}^S Q_F^S$	(37)	total cost of D1 repair and detoxification taken from N_F^S	μg N cell^{-1}d^{-1}
$m_C^{exp} = \beta \mathrm{RO}_s \theta_{\mathrm{RO}}^C \omega_C$	(38)	rate of C loss due to symbiont expulsion	μg C cell^{-1}d^{-1}
$m_S^{exp} = \frac{m_C^{exp}}{C_F^S} S$	(39)	rate of symbiont expulsion	cell cm^{-2}d^{-1}
$f_T^I = \left(\frac{I}{I_{\mathrm{noon}}}\right)^{(1-R_a)}$	(40)	light and temperature dependent shape factor	-

The description of the xanthophyll cycle in the model captured the interchange of xanthophyll pigments to minimize the damage due to light stress or maximize photosynthetic activity under low light conditions (Eqs. 6 and 7). The rate at which the xanthophyll pigments converted from one pool to the other (τ_p) was assumed to be light-dependent and temperature dependent (Havaux and Tardy 1996) (Eq. 25). To achieve this light and temperature dependence we used the diurnal light and temperature function f_T^I (*see* section Model evaluation) derived from Hill et al. (2012) dataset.

3.2.1 Reduction and re-oxidation of RCII

The rate of reduction and re-oxidation of Q_{ox} and Q_r, Ψ, was a function of the amount of light the RCII were exposed to, e_a^-, divided by the maximal capacity of the RCII to pass electrons through to the ETC (6) (Eq. 26). This formulation means that increasing light resulted in increasing RCII reduction; hence fewer electrons were able to pass through to the ETC reducing the potential production of ROS. The current oxidative state of the RCII pool (Q_{ox}: Q_t) was used to prevent Q_{ox} from ever becoming negative by slowing the reduction rate as Q_{ox} approached zero. The reduction rate coefficients of Ψ (α_d^Q) and the temperature dependence of Ψ are described in the model evaluation section below.

Table 3.5: Description and value of model parameters.

	Description	Parameter value	Unit	Source
f_{RO_s}	fraction of ΔROS to RO_s after detoxification	0.5	-	*see* text
$f_{\Delta\mathrm{RO}_f}$	fraction of ΔROS to $\Delta\mathrm{RO}_f$ after detoxification	0.5	-	*see* text
β	reaction rate of RO_s with symbiont tissues	3	d^{-1}	*see* text
$I_Q^{\max}$	max. I where all photons can pass through the ETC	500	μmol photon $\mathrm{m}^{-2}\mathrm{s}^{-1}$	(Gorbunov et al. 2001)
φ_{PSII}	quantum efficiency of charge separation at PSII	1	$1\mathrm{e}^-$ photon^{-1}	(Ross et al. 2008)
$\theta_C^{e^-}$	mol of electrons needed to make one mol of C	10	mol e^- mol C^{-1}	(Kirk 1994)
$\theta_{\mathrm{Chl}}^{\mathrm{RCII}}$	RCII to Chl ratio	1.92 x10^{-6}	mol RCII mol Chl^{-1}	(Suggett et al. 2008)
$T_{\max}$	temperature where Rubisco activity is zero	38	°C	(Lilley et al. 2010)
θ_{RO}^{C}	ROS to carbon ratio	1	mol C mol RO^{-1}	*see* text
I_{noon}	light intensity at midday	1500 (600)	μmol photon m^{-2} s^{-1}	(Borell and Bischof 2008; Hill et al. 2012)
k_B	half saturation constant for energy requirement of repair and detoxification of the photosystem	$10C_{\mathrm{thres}}^{S}$	μg C cell^{-1}	-
k_{DIC}	half saturation constant for DIC uptake by symbiont	0.5	pg C cell^{-1}	-
ω_{D1}	D1 molar mass	635	g C mol $\mathrm{D1}^{-1}$	-
ω_A	antioxidant molar mass	120.1	g C mol $\mathrm{D1}^{-1}$	-
ω_C	g C per mol C	12.01	g C mol C^{-1}	-
f_δ	fractional D1 repair cost of net D1 synthesis	0.008	-	(Raven 2011)
$\theta_{\mathrm{RO}}^{e^-}$	mol of e^- required to make mol ROS	7000	mol e^- mol RO^{-1}	*see* text
α^X	xanthophyll conversion rate coefficient	1	d^{-1}	*see* text
α_d^Q	temperature dependent reduction coefficient day	144	d^{-1}	*see* text
α_d^K	temperature dependent repair coefficient day	$(47T - 1151)$ (x2.3)	d^{-1}	*see* text
α_n^K	temperature dependent repair coefficient day	0.001	d^{-1}	*see* text

The rate of re-oxidation of Q_r to Q_{ox} was assumed to be able to oxidize the entire Q_r pool in one day if there was no temperature stress. In a similar manner to the reduction rate, the re-oxidation rate was reduced as Q_{red}: Q_t approached zero. In addition to the reduction and re-oxidation rate, there were other processes which could change the concentration of Q_{ox} and Q_r. Due to the limited information about RCII synthesis, we assumed a linear relationship between the synthesis of new RCII and the rate of chlorophyll production (Eq. 27). The chlorophyll synthesis was adapted from Ross et al. (2008). Newly synthesized RCII were incorporated into the Q_{ox} pool, as represented in the second last term in Eq. 3. The last term in all the

new state variables represents the reduction per cell in the density of components of the photosystem due to cell division (Eqs. 3-8).

Table 3.6: Equations and parameters from Gustafsson et al. (2013) (GBR13) relevant to this photoinhibition model. The numbers in brackets refers to the equation numbers in GBR13.

Symbol		Eq. No.	Description	Unit
$R_N^S = \begin{cases} V_N^S \eta^S + \delta^S N_F^S & \text{if } C_{\text{thres}}^S > 0 \\ \delta^S N_F^S & \text{else} \end{cases}$		(1)	cost of biosynthesis and respiration symbiont (N)	μg N cell^{-1} d^{-1}
$R_C^S = \begin{cases} V_C^S \eta^S + \delta^S C_F^S & \text{if } C_{\text{thres}}^S > 0 \\ \delta^S C_F^S & \text{else} \end{cases}$		(2)	cost of biosynthesis and respiration symbiont (C)	μg C cell^{-1} d^{-1}
$R_N^H = \begin{cases} V_N^H \eta^H + \delta^H N_F^H & \text{if } C_{\text{thres}}^H > 0 \\ \delta^H N_F^H & \text{else} \end{cases}$		(38)	cost of biosynthesis and respiration host (N)	μg N cm^{-2} d^{-1}
$R_C^H = \begin{cases} V_C^H \eta^H + \delta^H C_F^H & \text{if } C_{\text{thres}}^H > 0 \\ \delta^H C_F^H & \text{else} \end{cases}$		(39)	cost of biosynthesis and respiration host (C)	μg C cm^{-2} d^{-1}
$mN_N^S = m^S \mu_{\max}^S N_F^S$		(9)	mortality N_F^S	μg N cell^{-1} d^{-1}
$mC_F^S = m^S \mu_{\max}^S C_F^S$		(10)	mortality C_F^S	μg C cell^{-1} d^{-1}
$mC_R^S = m^S \mu_{\max}^S C_R^S$		(11)	mortality C_R^S	μg C cell^{-1} d^{-1}
$M_C = C_R^H \left(\frac{C_R^H}{C_{R,\max}^H} \right)$		(34)	total mucus C	μg C cm^{-2} d^{-1}
$M_N = \beta_N N_F^H$		(35)	N in mucus	μg N cm^{-2} d^{-1}
$M_{CF} = \beta_N N_F^H / Q_F^H$		(36)	C from C_F^H to mucus	μg C cm^{-2} d^{-1}
$M_{CR} = M_C - M_{CF}$		(37)	C from C_R^H to mucus	μg C cm^{-2} d^{-1}
$\mu^S = \frac{dC_F^S}{dt} / C_F^S$		(25)	symbiont growth rate	d^{-1}
$C_{\text{thres}}^S = \frac{24 - L}{24} R_C^S, R_N^S$		text	symbiont C requirement to last through one night	μg C cell^{-1}
$C_{R,\max}^S = N_F^S / Q_{\min}^S - C_F^S$		(3)	max. size of C_R^S	μg C cell^{-1}
$S_{\max} = A_{\text{coral}} / \pi \left(3 \frac{N_F^S}{\rho} / 4\pi^{1/3} \right)^2$		(21)	max. number of symbiont cells per unit surface area	cell cm^{-2}
$P_C^{\max} = \mu_{max}^S \left(\frac{24}{L} \right) (1 + (\eta^S + \delta^S)) C_F^S$		(17)	max. C specific photosynthesis	µg C cell^{-1} d^{-1}
$V_{\text{DIC}}^H = \varepsilon_{\text{dic}} C_F^H \frac{\text{DIC}^E}{\text{DIC}^E + K_{\text{dic}}}$		(31)	host DIC uptake	μg C cm^{-2} d^{-1}
$eq\text{DIN}^H = \text{DIN}^H \left(\frac{\text{DIN}^H}{\text{DIN}_{\max}^H} \right)^4$		(32)	equilibration DIN in host	μg N cm^{-2} d^{-1}
$eq\text{DIC}^H = \text{DIC}^H \left(\frac{\text{DIC}^H}{\text{DIC}_{\max}^H} \right)^4$		(33)	equilibration DIC in host	μg C cm^{-2} d^{-1}
$V_{N,max}^S = \begin{cases} \mu_{\max}^S N_F^S [(1 - \alpha) \left(\frac{24}{L} \right) + \alpha] & if\ I > 0 \\ \alpha \mu_{\max}^S N_F^S & if\ I = 0 \end{cases}$		(22)	max. N uptake by symbiont	μg N cell^{-1} d^{-1}
$V_N^S = V_{N,\max}^S \frac{\text{DIN}^H}{\text{DIN}^H + K_n} \left(\frac{C_R^S}{C_R^S + C_{\text{thres}}^S} \right) \left(1 - \frac{S}{S_{\max}} \right)$		(23)	actual N uptake rate by symbiont	μg N cell^{-1} d^{-1}
$\varphi = 1 - \frac{P_{\text{cell}}}{P_C^{\max}}$		(19)	regulatory term	-
$\Omega = \varphi \frac{\Pi_{\max}^L \theta_{\max}^C}{\theta^C}$		(20)	acceleration term	-

3.2.2 Reactive oxygen production

When temperature increased, the amount of active Rubisco decreased (Eq. 28) causing a reduction of electrons able to pass through the ETC leading to a buildup of excess electrons (e_e^-). The process of the formation of triplet excited ^{3}Chl was not included as a separate mechanism in the model. However, absorbed photons that did not pass through the RCII due to reduction or inhibition of Q_{ox} were assumed to excite Chl causing the production of $^1O_2{}^*$, hence all electrons absorbed but not used for photosynthesis became in excess (e_e^-) and contributed to ROS production (Eq. 29). The ROS could have one of three fates: 1) it could be detoxified and be neutralized (Eq. 30); 2) it could form fast ROS (ΔRO_f) which were assumed to be highly reactive and therefore causing immediate damage to the photosystem (Eq. 31); or 3) it could form long-lived slow ROS (RO_S), with a slower reaction rate, which could accumulate in the symbionts tissue and potentially react with any part of the cell causing structural damage and cell death (Eq. 8) (Apel and Hirt 2004). As the fast ROS was formed near the RCII the assumption was made that it primarily caused damage to the RCII resulting in a pool of inhibited RCII (Q_i). This corresponds to the breakdown of the D1 protein rendering the reaction center inoperable until it is repaired. This damage to the photosystem was represented by the second term in Eqs. 3 and 4, if Q_{ox} or Q_r were approaching zero, the rate of Q_i formation would decrease.

3.2.1 Photosystem Repair

An active repair rate (k_i) regenerated D1 protein and converted Q_i back to the Q_{ox} pool (Eq. 32). The repair rate, k_i, was set to depend upon light intensity, temperature, the size of the Q_i and the size of the symbiont N and C pools. The temperature dependent photosystem repair rate coefficients (α_d^K and α_n^K) were derived by fitting the model to the Hill et al. (2012) dataset (*see* section: Model evaluation). These up-regulating responses to light and temperature were reduced with decreasing N and C in the symbiont cell (Hill et al. 2011). Repairing the

photosystem came at an energetic cost, set to be 1% of the total C requirement needed to synthesize a new D1 protein (Raven 2011) (Eq. 33).

Table 3.7: Parameters from Gustafsson et al. (2013) (GBR13) relevant to this photoinhibition model.

Symbol	Description	Value	Source	Unit
$\mu^S_{\max}$	maximum specific symbiont growth rate	0.4	Domotor and D'elia 1986; Falkowski et al. 2007	d^{-1}
$\mathrm{Chl}_{\max}$	maximum chlorophyll concentration per cell	concentration where <95% light is absorbed		μg Chl $cell^{-1}$
$\mathrm{DIC}_{\max}$	maximum DIC concentration in host tissues	C^H_F	-	μg C cm^{-2}
δ^S, δ^H	symbiont, host C specific respiration and maintenance rate	0.06	-	g C g C^{-1} d^{-1}
η^S, η^H	symbiont, host C specific cost of biosynthesis	0.1	-	g C g C^{-1}
$Q^S_{\min}$	minimum N:C ratio in symbiont	0.05	Ross and Geider 2009	g N g C^{-1}
L	No. daylight hours	12	-	h
A_{coral}	Coral surface area	1	-	cm^2
α	factor by which dark N uptake rate is reduced	0.55	Ross and Geider 2009	-
K_n	half saturation constant symbiont DIN uptake	1.4	Muscatine and D'elia 1978	μmol N L^{-1}
Z_N	N, C uptake rate by heterotrophic feeding	-	Input parameter	μg cm^{-2} d^{-1}
$\varepsilon_{\mathrm{dic}}$	C specific DIC uptake rate by host	6	Muller et al. 2009	g C g C^{-1} d^{-1}
K_{dic}	half saturation constant host DIC uptake	400	Al-Moghrabi et al. 1996	μmol C L^{-1}
β_N	fraction of host N released as mucus	0.05	Bythell and Wild 2011	-
$\Pi^L_{\max}$	maximum proportion of C^S_F allocated to light harvesting	0.33	Ross and Geider 2009	-
$\theta^C_{\max}$	maximum Chl:C ratio of light harvesting pool	0.265	Ross and Geider 2009	g Chl g C^{-1}

3.2.2 Rubisco activity

Temperature dependent de-activation of the Rubisco enzyme caused a reduction in the sink of electrons by passing through the ETC. The de-activation of Rubisco was described by Lilley et al. (2010) to be strongly temperature-dependent, and by fitting a simple model to their data, we estimated the Rubisco activity (R_a) as a function of temperature (Eq. 28). Note, that the active fraction of Rubisco was used instead of an actual estimate of the Rubisco concentration in the cell.

3.2.3 Antioxidant activity

The ability of the antioxidant system to neutralize ROS is still not fully understood and quantitative measurements are generally not available; therefore, we decided to model antioxidant as a detoxification rate (A_{RO}) dependent upon the rate of ROS production and limited by the N and C required to maintain the detoxification process (Eq. 30). This detoxification term included all sinks of excess electrons, reducing the formation of ROS, such as photorespiration and alternative electron transport paths. During daytime, the antioxidant system was assumed to neutralize the newly formed ROS irrespective of species, the ROS remaining after detoxification was split into the fast and slow pool. During the night, there was no new formation of ROS and the fast pool was assumed to have completely reacted, leaving only the slow pool. As with the cost of photosystem repair, the detoxification process also had a cost set to be 1% of the total C cost of synthesizing a new antioxidant (Eq. 34).

3.2.4 Bleaching

The portion ROS that were not detoxified was assumed to have reacted with the surrounding symbiont tissue and damaged it (Eq. 38). The model assumed a one to one ratio of RO_S to damage functional C. The rate of cell death due to ROSs was set to be the rate of C destruction over the size of the functional C pool (Eq. 39). Cell death caused by ROS or natural mortality was assumed to be lost, and the symbiont cell expelled from the coral tissue (Gates et al. 1992). The expulsion of the cells where assumed to occur through the release of isolated symbiont cells (exocytosis), a process assumed to occur without the release of any host tissue (Steen and Muscatine 1987). This assumption should be considered with care as it has been shown that under thermal stress the expulsion of symbiont cells often involved the release of the entire host endoderm cells encasing the symbionts

(Gates et al. 1992). The decision to not include this potential damage to the host was made on the basis of constraining the complexity of the model.

3.2.5 Model evaluation

Hill and colleagues produced a data set using three coral species and two temperature levels (25°C and 31°C). Coral specimens used in Hill et al. (2012) were incubated in these two temperature treatments for two days, chlorophyll fluorescence measurements were taken at 05:00 h, 09:00 h, 13:00 h, 17:00 h, and 21:00 h hours each day, from which they calculated maximum quantum yield (F_v:F_m), effective quantum yield (Y(II)), non-photochemical quenching yield (Y(NPQ)), and non-regulated heat dissipation (Y(NO)). As the experiment was conducted outdoors, a natural light curve with a maximum of approximately 1500 μmol photon m^{-2} s^{-1} was used. The photoinhibition model was fitted to the dataset for one of the three coral species, *Pocillopora damicornis*. This species was preferred as the GBR13 model was parameterized for this species where possible. To replicate the conditions for the experiment conducted by Hill et al. (2012) a similar light field was created using the latitude where the experiment was conducted and the time of year giving a maximum light intensity of 1500 μmol photon m^{-2} s^{-1} (Fig. 3.2A).

The photosystem repair rate, reduction and re-oxidation rates, and the rate of ROS production, and detoxification are still not fully understood or agreed upon in the literature. These rates are likely to be temperature dependent (Hill et al. 2012; Mcginty et al. 2012). However, as there were no specific measurements of these rates or the effect of temperature, a temperature dependent day and night repair coefficients (α_d^K and α_n^K), a shape factor of diurnal variations in light and temperature (f_T^I), a reduction rate coefficient (α_d^Q), and a temperature dependent function ($\theta_{\mathrm{RO}}^{e^{-R_a}}$) accounting for alternative sinks of electron which may reduce the production of ROS (Eq. 27) were derived by fitting the model to the Hill et al. (2012) dataset. This would not the preferred method when specific data and

knowledge of the rate had been available; thus theses processes and rates should be considered with care and in the light of new findings or empirical data should be tested and perhaps reconsidered. In the following sections these rates and coefficients are described individually.

The Rubisco activity (R_a) was used to account for temperature dependence of reduction and re-oxidation of RCII (Ψ) meaning that the rate of RCII reduction increased towards its maximum with increasing temperature to aid photo-protection during daytime (Eq. 26). For the same reason at night elevated temperature meant a slower re-oxidation rate. The temperature dependence of the reduction and re-oxidation of the RCII pool were necessary to achieve the variation between the two temperature treatments seen in Fig. 3.2C. After an iteration process of fitting the model to the Hill et al. (2012) dataset of rate of reduction process, the adjustment of the photosystem to a new light or temperature level was assumed to be able to take place over 10 min, giving a rate coefficient (α_d^Q) of 144 d^{-1}.

To fit the modeled F_v:F_m curves to the Hill et al. (2012) dataset a daytime temperature dependant repair rate coefficient (α_d^K) was derived. The repair rate coefficient increased linearly with increasing temperature. The relationship was set to be linear as we only had two temperature levels to work from; however it is unlikely that this relationship is linear for all temperatures and should be revisited if a new more extensive dataset becomes available. The function f_T^I was created to be able to constrain the repair process which is dependent on daily variations in light intensity and temperature. The repair rate of RCII did not need to be as high under low light conditions and temperature, as the rate of photo damage was reduced. The value of f_T^I ranged between 0 and 1, and had a daily shape similar to the light curve with a maximum of 1 at midday, but the steepness of the curve depending on temperature (Eq. 40). The derived parameter f_T^I was calculated as the ratio of the current light level relative to the light level at midday and the exponential based on Rubisco activity which determined the temperature component.

The process of ROS production is still the most uncertain process in the model; we could find essentially no quantitative data defining the process of ROS production. As mentioned above the ROS production were reduced as we implicitly include processes such as singlet oxygen being quenched by carotenoids, as well as a sink of electrons due to alternative electron transport paths, such as cyclic electron flow around PSII and photo-respiration (Ulstrup et al. 2006; Crawley et al. 2010). If all excess electrons were assumed to become ROS the symbiont population became greatly damages already at low light and temperature levels. The electron to ROS conversion function was formulated such that at low temperature and light stress the alternative electron sinks removed almost all excess electrons, and as stress increased the efficiency of alternative sinks eventually became limited.

Table 3.8: Definition of state variables and initial conditions for *Pocillopora damicornis* and *Stylophora pistillata.* The initial values for the symbiont population size and pigment pools for *P. damicornis* were derived from Hill et al. (2012) whereas the initial total values of the RCII pools were estimated from Suggett et al. (2008) and divided into the three pools so that initial Fv:Fm and Y(II) values corresponded with those in Hill et al. (2012). For *S. pistillata* the initial values were derived by spinning up the model for 2 days using a smaller symbiont cell size.

Symbol	Description	*P. damicornis* initial values	*S. pistillata* initial values	Unit
Q_{ox}	oxidized RCII	4.1×10^{-3}	0.0015	pmol RCII cell^{-1}
Q_r	reduced RCII	3.4×10^{-3}	0.002	pmol RCII cell^{-1}
Q_i	inhibited RCII	6.2×10^{-3}	0.0015	pmol RCII cell^{-1}
RO_s	'slow' ROS	0	0.1	pmol ROS cell^{-1}
D_d	diadinoxanthin	7.2	0.92	pg D_d cell^{-1}
D_t	diatoxanthin	0.8	2.07	pg D_d cell^{-1}
Chl	chlorophyll *a*	8	3	pg Chl cell^{-1}
S	symbiont population size	8.5×10^5	5.2×10^6	cell cm^{-2}

The initial conditions used for the model was set to equal the Hill et al. (2012) dataset at time zero (Table 3.8). The host parameterization was left unchanged from the GBR13 model. The model state variables were used to calculate the maximum quantum yield of PSII (F_v:F_m), effective quantum yield of PSII (Y(II)), non-photochemical quenching yield (Y(NPQ)), and non-regulated heat dissipation (Y(NO)), using the following assumption that Y(II) + Y(NPQ) + Y(NO) = 1.

From the model state, F_v:F_m was defined as the maximum ability of the photosystem if all RCII in the active pool were oxidized (F_v:F_m=Q_a: Q_t). Y(II) represents the fraction of the photosystem that was capable of photosynthesis (Q_{ox}: Q_t), and Y(NPQ) was the fraction dissipating energy as heat through the xanthophyll cycle (D_t:(D_t+D_d+ Chl)). Y(NO) was calculated using the assumption above (Y(NO)=1 - Y(II) - Y(NPQ)).

3.2.6 Feeding simulations

It has been documented that heterotrophic feeding may limit the effect of elevated temperatures by reducing photoinhibition and subsequently lessening bleaching (Ferrier-Pagès et al. 2003; Borell et al. 2008; Hoogenboom et al. 2012). As this photoinhibition model was connected to the GBR13 model which originally described the exchange of nutrient between the environment, host, and symbiont simulating the effect of heterotrophic feeding, this provided an opportunity to further explore and validate both models. Borell and Bischof (2008) constructed a study where the importance of heterotrophic feeding was measured under thermal stress conditions. Borell and Bischof (2008) examined the bleaching susceptibility and photosystem activity of *Symbiodinium* in the Scleractinian coral *Sylophora pistillata* under thermal stress associated with daily temperature rise of 2 ^{o}C to 3^{o}C over a 10 day period, with a temperature increase from 28^{o}C to 29^{o}C just after dawn and a midday maximum of 32.5 ^{o}C. The studied coral specimens were collected in July-August 2005 off Barang Lompo Island (05°03' S, 119°19' E) at 3 m depth. We aimed to recreate the results from their study to further evaluate and validate our model.

In order to switch the model from *P. damicornis* to *S. pistillata* only two parameter changes were required. The first change was that of symbiont cell radius (r_i), which was reduced to accommodate a larger number of cells in each cell layer (Lajeunesse et al. 2005). As defined in the GBR13 model there were two one-cell thick layers of host cells which can harbor symbionts, this gave a maximum number of symbiont cells per coral surface area. To be able to reach the number of

symbiont cells recorded for *Stylophora pistillata,* r_i had to be reduced from 5 μm to 3 μm (changed from 10 μm to 6 μm diameter cells). Changing r_i changes the maximal amount of C, N, and chlorophyll that one cell could contain. Secondly, the repair rate coefficients α_d^k and α_n^k were doubled.

Photosystem repair is a vital process in the protection against bleaching, and it has been speculated that variations in the ability of different corals species to photo-repair underlies the difference in bleaching susceptibility (Takahashi et al. 2004; Takahashi et al. 2009; Ragni et al. 2010). In vitro bleaching 'sensitive' *Symbiodinium* have been shown to have a reduced photo-repair rate in comparison to 'tolerant' clades of *Symbiodinium* (Takahashi et al. 2009; Ragni et al. 2010). While in situ measurements of photo-repair are still sparse, it has been shown that the *Symbiodinium* associated with the bleaching tolerant *Porites astreoides* had a higher repair rate than *Symbiodinium* associated with the bleaching sensitive *Monstastraea faveolata* (Hennige et al. 2011). No such information was found for *P. damicornis* or *S. pistillata* at the time of this study.

In the Borell and Bischof (2008) experiment, corals acclimated in the experimental tanks under non-stress and non-feeding conditions for two days prior to the experiment. To get the initial conditions of the model, we ran the model for two days under these conditions. The results after these two days were then used as the initial conditions of the temperature and feeding experiment (Table 3.8).

For the temperature experiment, the model was run for 10 days with a daily temperature fluctuation corresponding to that defined by Borell and Bischof (2008) with a maximum at midday of 32.5°C and a temperature after dawn of 29°C. The model was run twice, first with, and then without, heterotrophic feeding. The feeding rate used was adapted from Ferrier-Page et al. (2010) where *S. pistillata* was recorded to have a maximum mean feeding rate of 233 μg C cm^{-2} h^{-1}. Based on this feeding rate and that the coral were fed for three hours in Borell and Bischof (2008), the daily mean rate of C uptake from heterotrophic feeding were calculated to be 698 μg C cm^{-2} d^{-1}.

As described in the GBR13, uptake of DIN and DIC from the surrounding water could be used by the symbiont binding it into organic material that could be translocated to the host providing the host with an additional source of nutrients. The water in the experimental tanks was filtered (0.5 μm) oligotrophic seawater with a DIN concentration of <0.3 μmol L^{-1}. Average daily DIN and DIC uptake rates by the host was approximated to be 3.3 μg N cm^{-2} d^{-1} and 17 μg C cm^{-2} d^{-1}, respectively, (Marubini and Thake 1999 (Marubini and Thake 1999)). The experimental corals were taken from a 6 m depth and the light levels during the experiment were adjusted to correspond to the light field at this depth with a maximum of 600 μmol photon m^{-2} s^{-1}, therefore when running the feeding simulations the I_{noon} were set to this value.

3.3 RESULTS

The photoinhibition model was successfully coupled to the GBR13 coral host-symbiont growth model. After adjusting the parameters to represent *P. damicornis* as far as possible (Table 3.5), as well as deriving the three unknown rates (Ψ, k_i, and A_{RO}), the model behaved in accordance with the *P. damicornis* dataset by Hill et al. (2012). Figure 3.2 shows the calculations of F_v:F_m, Y(II), Y(NPQ), and Y(NO) from the model, as well as the experimental dataset. The model captured both the daily variation and the trend of the photosynthetic parameters over time of the two treatments (*see* Fig. 3.2). The photosystem recovered slowly during the night for both temperature treatments. However, the damage caused during the day exceeded the ability of the system to detoxify, so there was a net D1 loss, resulting in a decrease in the modeled F_v:F_m and Y(II). For the 25°C treatment, a diurnal variation in F_v:F_m was seen, but there were no overall degradation of the photosystem over the two days. The 31°C temperature treatment in addition to the daily fluctuation showed an overall degradation of the photosystem. There was an initial reduction in the modeled F_v:F_m for the 31°C treatment relative to that seen in experimental data from the first day. The reason for this could be the presence

of greater energy reserves in the experimental coral which aids repair and delays onset of inhibition.

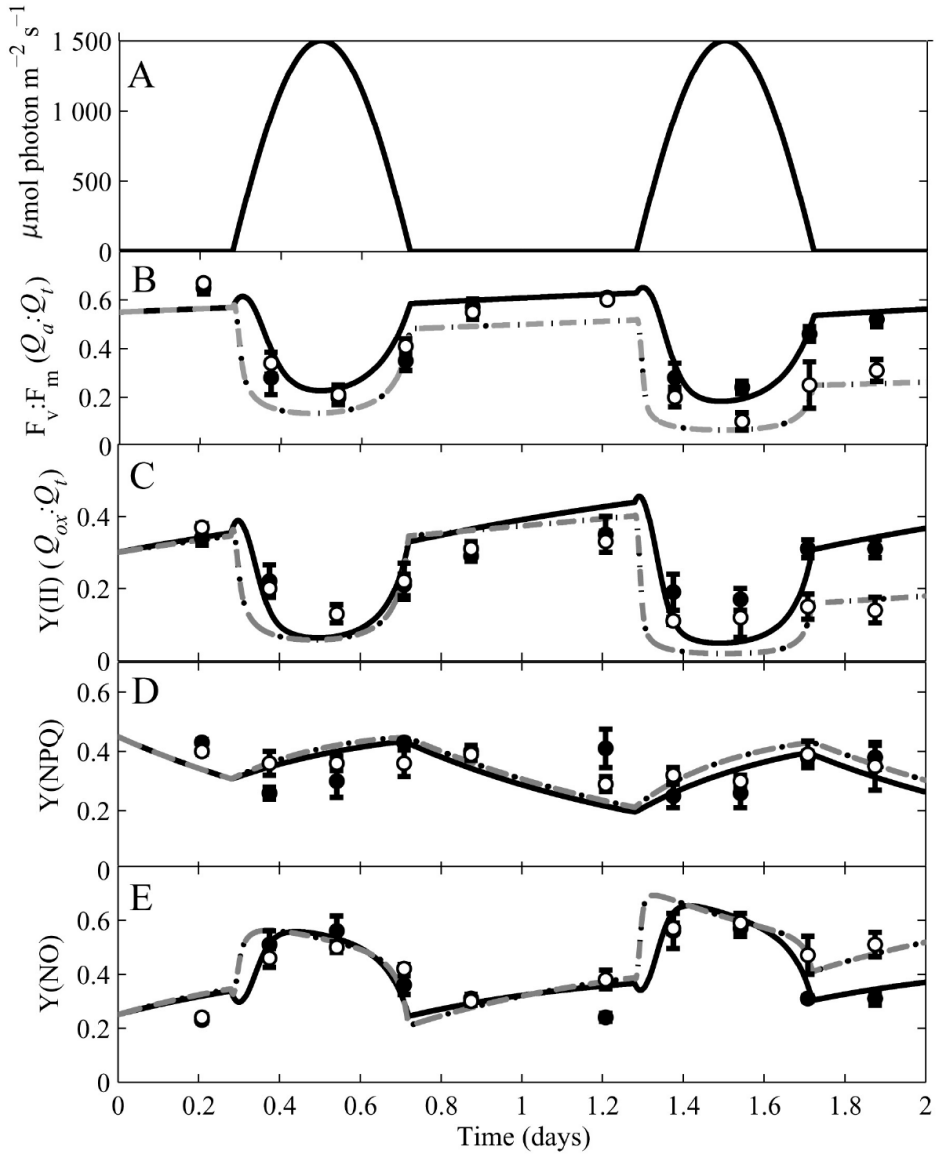

Figure 3.2: Model fitted to data from Hill et al. (2012). Solid lines represented the 25°C model run over a 2 day period. Dashed line is the model run at 31°C. Filled markers indicate the experimental data for the 25°C treatment and open markers the 31°C treatment with ±standard deviation (SD). (A) is diurnal light oscillation. (B) F_v:F_m data with corresponding $Q_a : Q_t$ in the model. (C) Photochemistry Y(II) corresponding in model was $Q_{ox} : Q_t$. (D) Y(NPQ) corresponding in the model $D_t : (D_t + D_d + \mathrm{Chl})$. (E) Y(NO) calculated using the assumption Y(II)+Y(NPQ)+Y(NO)=1.

The modeled Y(NPQ) and Y(NO) also had a daily fluctuation which increased during the daytime with a similar reduction during the night. The model showed only a small difference in Y(NPQ) and Y(NO) between temperature treatments, with the 31°C treatment being slightly higher and more so towards the end of the experiment.

3.3.1 Feeding simulations

After adjusting this model to fit Hill et al. (2012) and changing the initial conditions (Table 3.8), the Borell and Bischof (2008) dataset could be simulated, showing that the two coupled models worked well together (Figs. 3.3, 3.4) for two different coral species. Similar to the Borell and Bischof (2008) dataset, the model showed a greater reduction in F_v:F_m for the starved coral than for the fed coral for both the 10:30 h and the 05:30 h measurement (Fig. 3.3). The 10:30 h measurements and model values were lower than the 05:30 h, indicating recovery of the photosystem during night. The model value at 05:30 h overlay the Borell and Bischof (2008) data for the first four days. However, for the last day, the model calculate a F_v:F_m value approximately 0.1 lower than the data for fed coral.

After running the model ten days forward in time for the two treatments, the number of symbiont cells per coral surface area had decreased for both treatments to approximately 1.8×10^6 cell cm^{-2} and 3.28×10^6 cell cm^{-2} for the fed and starved coral respectively (Fig. 3.4). The model output corresponded well with the experimental results. The loss of symbionts in both the fed and unfed corals in the experiment was likely associated with elevation in temperature. In the model this reduction in symbiont population, even though having a good supply of nitrogen (fed coral), was found to be caused by that the symbionts maximum ability to repair and grow was exceeded by the rate of damage and natural mortality under these high temperature conditions.

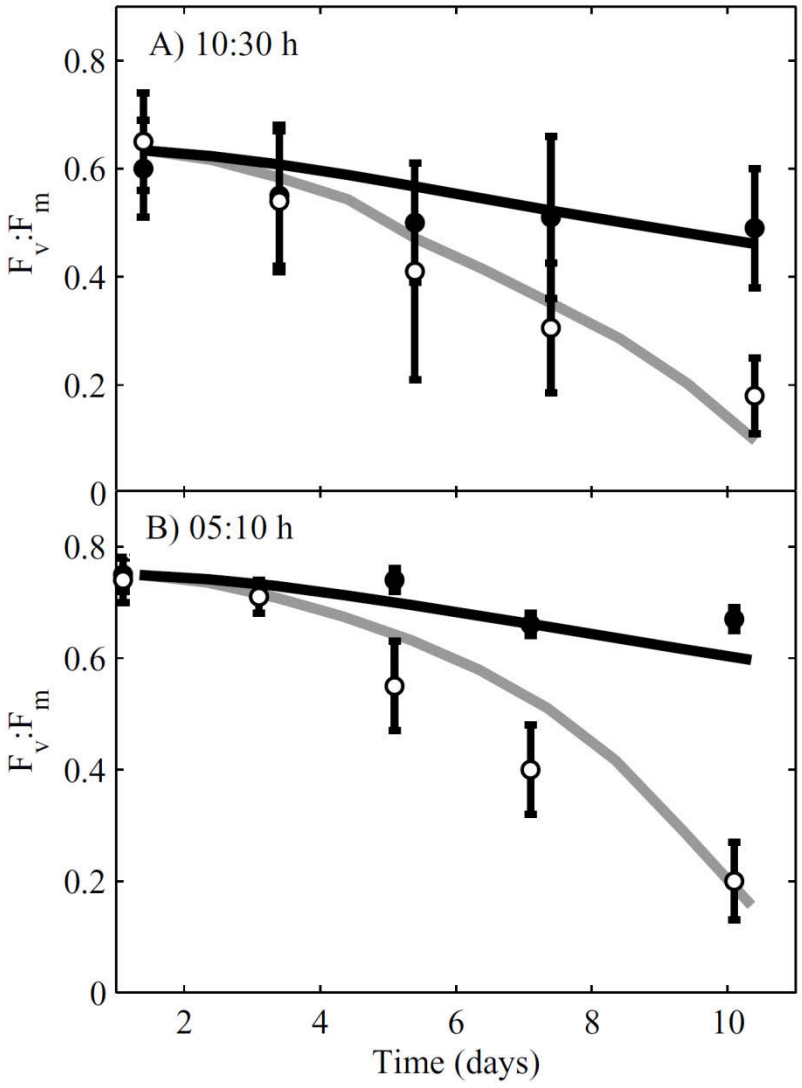

Figure 3.3: F_v:F_m at (A) 10:30 h and (B) 05:30 h for the modeled and Borell and Bischof (2008) experimental data during the ten day feeding experiment. Closed and open markers show the measured F_v:F_m for fed and unfed coral, respectively. Black and grey lines indicate the modeled F_v:F_m (Q_a:Q_t) for fed and unfed coral, respectively.

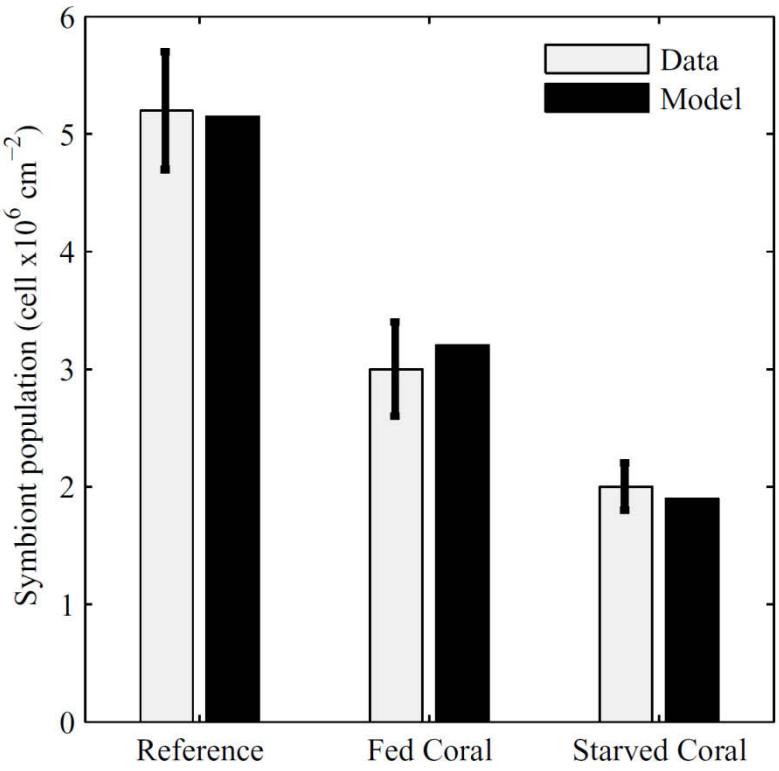

Figure 3.4: Symbiont population size after two days acclimation under non-stress and non-feeding conditions (Reference) and after 10 days of elevated temperature for fed and starved corals. Light grey bar shows the measurements ±standard error (SE) from Borell and Bischof (2008).

3.4 DISCUSSION

In this study, we developed a coral model which was able to simulate photoinhibition and the loss of the symbiont population due to temperature and light stress under different feeding regimes. The model captured both the diurnal change in the state of the photosystem, as well as overall degradation of the photosystem under temperature stress. Elevated temperatures led to a degradation of the photosystem and the loss of symbiont cells. If the coral could feed heterotrophically this degradation was reduced, but still a decrease in the health of the photosystem was apparent (Fig. 3.3).

The dynamic rates derived by fitting the model to the Hill et al. (2012) dataset probably represented more than one actual physiological function each. For example, the A_{RO} (detoxification rate) which we presented as the activity of the antioxidant system probably also accounts for alternative electron paths and ROS scavengers (Asada 2006). Similarly the parameterization of the model accounts for the process of singlet oxygen formation from triple excited chlorophyll without defining it mechanistically. In the future, it would be ideal to resolve these rates with mechanistic formulations. Even so, the current model was able with only a few parameter adjustments to reproduce an independent experiment with a different species validating that this model does capture the main dynamic processes of coral symbiosis and its response to thermal and light stress.

Modeling all aspects of the photosystem would have been unnecessarily complex and probably not to be preferred as there are many functions and responses in the photosystem of which we still have limited understanding. However, one shortcoming of this model was that ROS could not move across the symbiont cell membrane into the host tissue. The choice to exclude this process was due to the lack of experimental data (Baird et al. 2009) and our wish to not incorporate any unnecessary uncertainty into the model. Similarly the choice to use Rubisco activity, rather than having Rubisco content as a state variable changing over time reduces the model complexity. Experimental data on Rubisco in *Symbiodinium* is scarce as Rubisco extracted from *Symbiodinium* has proved to be unstable, making quantitative measurements uncertain (Lilley et al. 2010).

An interesting outcome of this modeling study was that to get the model output to correspond to the Hill et al. (2012) data, k_i (the repair rate) had to be up-regulated with increasing temperature and light. This supports the finding by Hill et al. (2011) who found a significantly higher repair rate in corals exposed to temperature and light stress. As they did not separate between light and temperature stresses, a direct comparison of their rate constants were difficult. The need to up-regulate the repair rate was interesting, as some researchers have found the opposite trend with inhibition of the repair rate associated with increasing temperature (Murata et al. 2007; Takahashi et al. 2009).

The rather complex definitions of k_i and A_{RO} indicate that further experimental investigations of these rates are needed. The need to double the k_i rate for *S. pistillata* also suggests that these rates may be species or clade specific, as found by Henning et al. (2011) as well as McGinty et al. (2012).

3.4.1 H_2O_2 production

In this model, we assume that the ROS state variable, RO_S, corresponds to the accumulated H_2O_2 in the symbiont cell. Techniques to measure other ROS with faster reaction rate are still limited; however, H_2O_2 can be estimated using for example amplex red and horseradish peroxidase assays (Suggett et al. 2008). Suggett et al. (2008) provided a study of net H_2O_2 production in two different clades of cultured *Symbiodinium* for different light and temperature treatments. To establish if the concentration of ROS produced by the model were reasonable, we ran the model using the experimental setup of Suggett et al. (2008) with a 24 hour temperature treatment (26°C and 32°C) prior to one hour of light treatment (100 and 1000 μmol photon m^{-2} s^{-1}). The model was initiated using the same settings as we used to reproduce Hill et al. (2012). The conversion between ROS for the symbiont population and ROS per cell with a diameter of 12.5 μm was used. This conversion was made as cell size of cultured zooxanthellae have been found to be larger than the cell size of in hospite zooxanthellae (Domotor and D'elia 1986).

Figure 3.5 shows the modeled slow ROS (RO_S), as well as the results for the two *Symbiodinium* clades (A1 and B1) from Suggett et al. (2008). For both temperatures for the 100 μmol photon m^{-2} s^{-1} light treatments the modeled RO_S concentration corresponded well with the measured values for both clades. Similarly, in the 32°C and 1000 μmol photon m^{-2} s^{-1} treatment the model estimate lay within the standard deviation of clade A1. However, for the 26°C and 1000 μmol photon m^{-2} s^{-1} treatment the modeled results differed notably from those measured, with modeled values close to those of the 100 μmol photon m^{-2} s^{-1} light treatment. The Suggett et al. (2008) study indicates that light intensity was a stronger inducer of H_2O_2 production than elevated temperature. This is not the

case in the model; at optimal growth temperature Rubisco activity is high and most captured energy will be used for photosynthesis. Additionally, the detoxification system effectively reduces the size of the RO_S pool. This divergence between the experimental data and the model indicates that the model definition may not capture all the dynamics of ROS production. As new measurements of ROS production in *Symbiodinium*, preferably in hospite, become available, this definition should be re-examined.

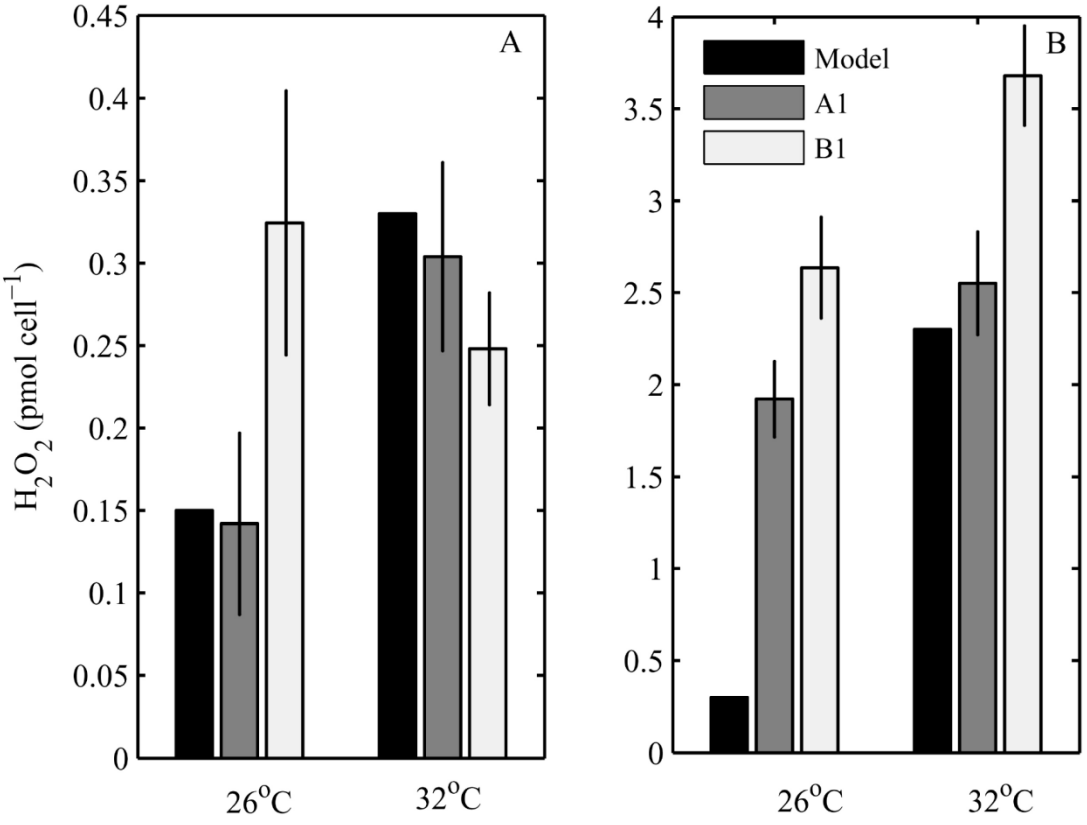

Figure 3.5: Concentration of reactive oxygen species per symbiont cell (RO_S) and H_2O_2 measurements (mean ±SE) from two *Symbiodinium* clades (A1 and B1) in culture, from Suggett et al. (2008). (A) 100 μmol photon m^{-2} s^{-1} treatment. (B) 1000 μmol photon m^{-2} s^{-1} treatment.

3.4.2 Degree Heating Days

Degree heating weeks (DHW) is a thermal stress index produced by the National Oceanic and Atmospheric Administration (NOAA) Coral Reef Watch. A few studies have use degree heating days (DHD) instead, which is a similar index but with a daily resolution (Maynard et al. 2008*a,b*). The DHD index uses sea surface temperature (SST) to predict occurrence and severity of coral bleaching as a function of temperature anomalies which exceed the mean summer SST, as well as the duration of the elevated temperature:

$$\mathrm{DHD} = \sum_{i=1}^{n}(T_i - T_{\mathrm{mean}}) \qquad (2)$$

Where T_{mean} is the mean climatological summer SST, T_i is the mean SST of day *i*, and *n* is the number of days. Two days with a temperature 2°C above T_{mean} has the same DHD as one days with a temperature 4°C above T_{mean}. The concept of DHD does not take into consideration the effect of other environmental conditions, such as light intensity, nutrient availability or species-specific physiological properties such as photosystem repair. Field derived relationships between bleaching and the DHD index provide a summary of field observations against which the photoinhibition model presented in this paper could be assessed.

To test the model's bleaching behavior at different values of the DHD index, the model was run for temperature scenarios, 2°C, 3°C, and 4°C above T_{mean} for 90 days and a range of feeding rates and DIN uptake rates. The model was forced using a light curve with a maximum intensity of 1000 μmol photon m^{-2} s^{-1} at noon and initiated with the values derived to initialize the model for the Borell and Bischof (2008) feeding experiment. These initial conditions were chosen to avoid any initial fluctuation of the model. The T_{mean} was set to 28°C. We acknowledge that the T_{mean} in the region where the coral for the Borell and Bischof (2008) study was conducted are likely to be closer to 30°C during summer; however, the corals were collected during July-August. The model was adjusted to the experimental

conditions in Borell and Bischof (2008) where 28°C was the nighttime temperature under which the coral was able to maintain its biomass as long as food was available. We decided to use 28°C as T_{mean} as the modeled coral experienced damage above this temperature, and we worked under the assumption that T_{mean} should be close to the corals upper thermal limit.

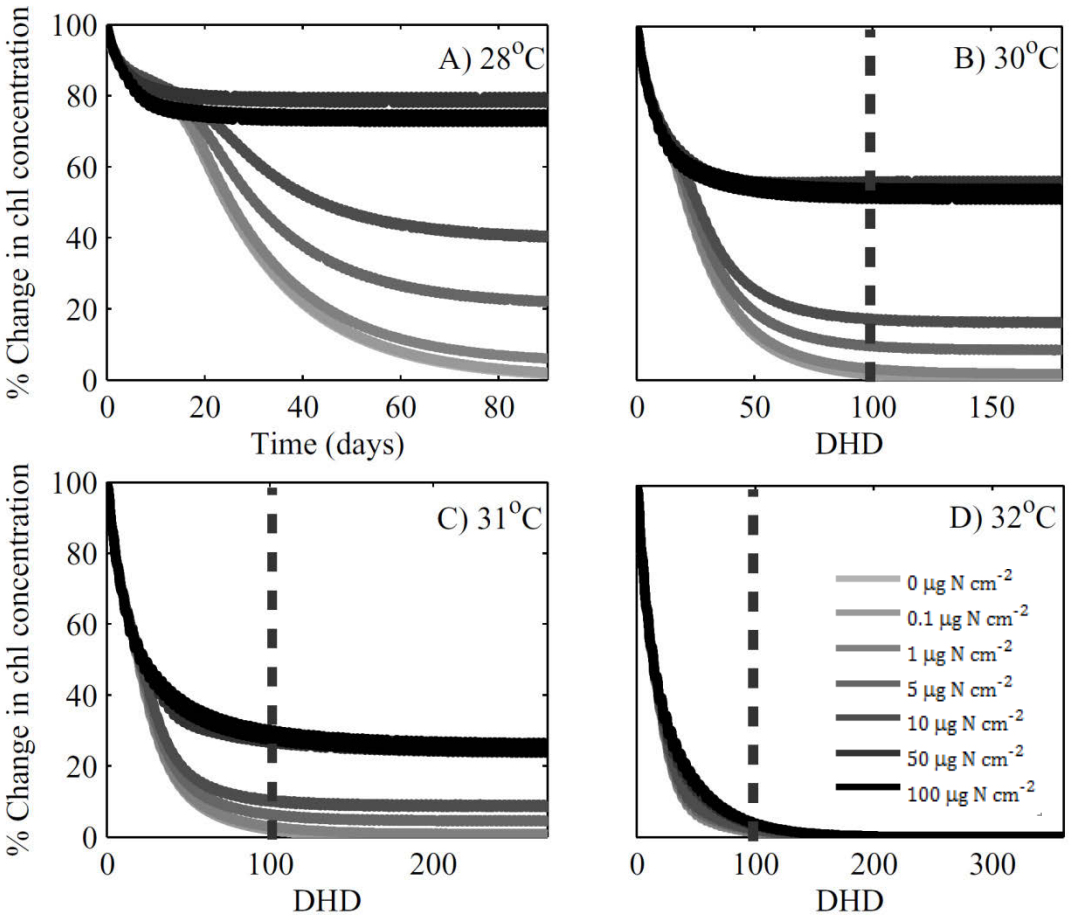

Figure 3.6: Percentage of chlorophyll concentration remaining per coral unit surface area as a function of heat stress and heterotrophic feeding over time. Vertical dashed lines indicate 100 DHD. (A) 90 day simulation at T_{mean} (28°C) for corals feeding heterotrophically at a range of rates. (B) 2°C above T_{mean}. (C) 3°C above T_{mean}. (D) 4°C above T_{mean}. (D) Legend gives line shading for heterotrophic the feeding rates.

Figure 3.6 shows the percentage of initial chlorophyll pigmentation per coral surface area still remaining after exposure to elevated temperatures and varying heterotrophic nutrient input over time. Variation in DIN uptake did not reduce the severity of bleaching in the absence of heterotrophy. The model predicted that corals were almost entirely bleached after approximately 110-120 DHD irrespective of the DIN uptake rate in the absence of heterotrophy. Heterotrophy reduced the bleaching severity; however, this mitigating effect of feeding decreased with increasing temperature (Fig. 3.6). A model simulation at T_{mean} showed that at the highest feeding rates approximately 80% of the initial condition chlorophyll concentration remains after 90 days, whereas the two lowest feeding rates approached zero (Fig. 3.6A). Interestingly, at a low heterotrophic feeding rate or at high temperature, complete bleaching occurred at the same thermal stress of approximately 110-120 DHD, as for the DIN simulations. Complete bleaching after 110-120 DHD was in agreement with literature (Maynard et al. 2008*a,b*). Maynard et al. (2008*a*) recorded complete or severe bleaching of three coral species after 120 to 140 DHD. However the onset of bleaching seemed to occur somewhat earlier in the model than shown in Maynard et al. (2008*a*), where the bleaching severity at 50 DHD ranged between 5-40% of coral bleached. Note that there are likely to be great differences in stress across a reef, with varying light regimes, and nutrient uptake depending on location, current, and depth (Lesser et al. 2010; Wyatt et al. 2010). The light intensity used in this model simulation is that of a shallow reef (<5 m), which may explain the earlier onset of bleaching in the model.

Coral bleaching is often referred to in terms of mild (<25% bleached), moderate (<50% bleached), and severe (>50% bleached) (Maynard et al. 2008a). The model output indicates that for the coral to only suffer mild to moderate bleaching during a prolonged heating event of 2°C above T_{mean} the coral had to have a heterotrophic feeding rate of approximately 50 μg N cm^{-2} d^{-1} (Fig. 3.6B). This rate was only a fraction (approx. 10%) of the calculated maximum coral feeding rate of 492 μg N cm^{-2} d^{-1} assuming that the coral mainly feed during the night and that the N:C of the ingested prey was at Redfield ratio (calculated from Ferrier-Page et al.

(2010)). However, increasing the feeding rate above 50 μg N cm^{-2} d^{-1} had no further mitigating effect on bleaching. At 3°C above T_{mean} all simulations showed severe bleaching after approximately 50 DHD (Fig. 3.6C), and for the scenarios with 4°C above T_{mean} all simulations were severely bleached after approximately 30 DHD.

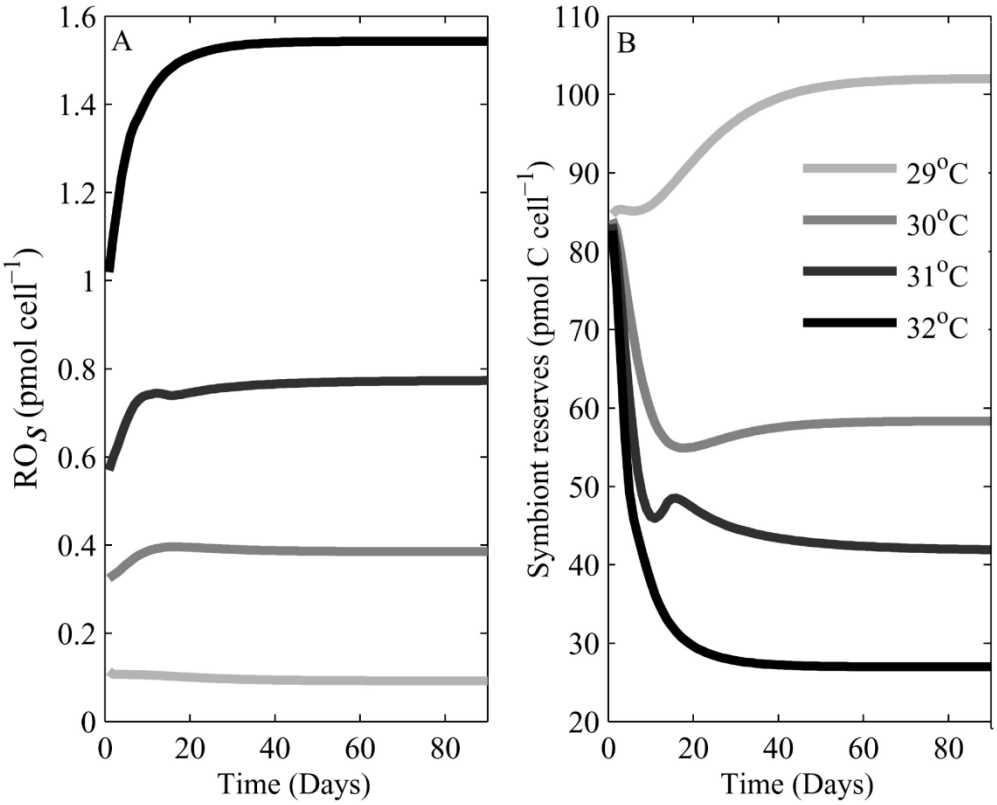

Figure 3.7: (A) Concentration of ROS (RO$_S$) and (B) reserves (C_R^S) in the symbiont for T_{mean}, +2°C, +3°C and +4°C heating over 90 days and a heterotrophic feeding rate of 100 μg N cm^{-2} d^{-1}.

The onset of bleaching was associated with a rapid loss of symbiont reserves (C_R^S) that in turn reduced the detoxifying and repair rate of the photosystem (Fig. 3.7). For the feeding rate of 100 μg N cm^{-2} d^{-1} the RO$_S$ pool increased as the C_R^S decreased, a result of ROS production exceeding detoxification and repair. The

reason why C_R^S and the concentration of RO_S for the 32°C scenario did not go to zero, depends on that the measurements were per cell and the population size still contained a few cells after 90 days (Fig. 3.7).

The reason why heterotrophic feeding delayed or prevented the depletion of the C_R^S pool was heterotrophically-fed hosts did not need to extract photosynthates from the symbiont to the same extent as when only DIN was supplied. In the GBR13 model it was shown that the host and symbiont both could survive under conditions where heterotrophy was low and DIN was high. This was not the case under temperature stress conditions, as in addition to translocation to the host more energy was also needed for photosystem repair and ROS detoxification.

The favorable comparison of the thermal stress behavior in the model and in field observations summarized using the DHD index gives some confidence that the model is capturing approximately the correct scale of thermal stress response in corals, and further that the mechanism of photoinhibition and oxidative stress are important processes in coral bleaching.

The model highlights the importance of the coral being able to feed heterotrophically and the symbionts ability to utilize host waste products. Previous studies have shown that under non-stress conditions, increasing DIN concentration in the environment may lead to increasing symbiont growth, as well as the ability to sustain the host when feeding is limited (Muller-Parker et al. 1994a). However, coral under temperature stress have been found to have a reduced DIN uptake rate from the environment (Godinot et al. 2011). Additionally, elevated DIN concentrations in the water column have been found to increase symbiont expulsion rate (Zhu et al. 2004) and corals exposed to high DIN river runoff have been found to have a lower thermal tolerance threshold (Wooldridge and Done 2009). This lack of positive response from corals exposed to elevated DIN concentrations under heat stress conditions supports the result presented here that DIN concentration had no effect on the bleaching rate. Also, in accordance with previous experiments heterotrophy was found to have a mitigating effect on the bleaching rate (Borell et al. 2008; Connolly et al. 2012;

Hoogenboom et al. 2012). We suggest that the reason why heterotrophy could reduce the effect of elevated temperatures but DIN could not, was associated with a reduction in the translocation of photosynthates from symbiont to the host with increasing feeding rates due to a reduction in the host need for an extra nutrient source. Hence the symbiont was left with more reserves of nutrients which it could use for cell maintenance, repair, and growth.

Overall, model was found to respond in a similar manner to thermal stress as observed communities, as quantified by the DHD index. The model results and experimental studies suggest that adding a mitigating effect of an organic nutrient source may be a possible improvement the prediction of coral bleaching. The difference in the onset of bleaching between the model and the data from Maynard et al. (2008*a*) may well be associated with that we were using a model written to represent a single coral, or even a specific coral surface. Whereas, a coral reef usually contains several different species of coral in a range of local habitats with varying environmental conditions.

3.4.3 Future work

This photoinhibition model was used to reproduce several datasets with only small adjustments to model settings that were required to account for different species as well as in hospite vs. cultured *Symbiodinium*, whilst still capturing the major responses to light intensity and temperature. However, as there are diverging theories how the photosystem responds to stress (Murata et al. 2007; Takahashi et al. 2008; Hill et al. 2011), further refinement of the model with the aim to pinpoint the reason behind diverging results from experimental studies would be useful. Resolving what we referred to as detoxification into antioxidant activity, photorespiration and alternative electron pathways would be useful and as experimental data becomes available these components of the model should be updated. Likewise, transfer of ROS from the symbiont to the host and the ability of the host to deal with this additional source of ROS should also be incorporated into the model as soon as data becomes available. This model has the potential to be

used for other symbiotic relationships between a heterotrophic host and an autotrophic symbiont, or to could be decoupled and used to look at free-living single cell algae.

CHAPTER 4:

UPTAKE AND TRANSLOCATION OF CARBON AND NITROGEN BETWEEN A CNIDARIAN HOST AND AUTOTROPHIC SYMBIONTS

4. Uptake and translocation of carbon and nitrogen between a Cnidarian host and autotrophic symbionts

Model development, experimental design, and model evaluation and validation were performed by Malin Gustafsson, who also wrote this chapter. Intellectual contributions and technical assistant were made by Mathieu Pernice, Peter Ralph and Mark Baird. Additionally, Mathieu Pernice contributed the experimental data used in this chapter, and wrote the supplementary section.

4.1 INTRODUCTION

In tropical marine environments there are many examples of organisms which live in symbiosis with one another to aid their survival in an environment where nutrient supplies may be episodic (Venn et al. 2008). Symbiosis between an animal host and a unicellular algae occur in a wide range of organisms belonging to several different phyla, such as giant clams, marine turbillarians, corals, anemones, jelly fish and ascidians (Sutton and Hoegh-Guldberg 1990; Lajeunesse 2002; Stat et al. 2006). The unicellular algae reside within the animal host tissues where they fix inorganic carbon (C) and nitrogen (N) through photosynthesis into photosynthates consisting mainly of carbohydrates, lipids and amino acids (Venn et al. 2008). These photosynthates are partly released to the host animal providing a source of nutrients (Wang and Douglas 1999; Titlyanov and Titlyanova 2002). The symbiont in turn is supplied with a steady influx of metabolic by-products from the host, mainly consisting of carbon dioxide, ammonia and urea (Wang and Douglas 1999; Venn et al. 2008). This symbiosis is sensitive to shifting environmental conditions and consequently, has become of great interest to climate change-oriented researchers over the past few decades, with the most attention given to reef

building corals, as the loss of the world's coral reefs would have great biological, ecological and socio-economical implications (Hoegh-Guldberg 1999).

The translocation of photosynthates from the symbiont to the host is essential to the success of corals (and other symbiotic organisms) in environments were the opportunity to feed heterotrophically is restricted (Fitt and Cook 2001; Venn et al. 2008). The current understanding of the translocation process is limited, both in terms of rates and compounds being translocated (Wang and Douglas 1998; Yellowlees et al. 2008). A free- living dinoflagellate is known to release less than 5% of their carbon fixed through photosynthesis into the water column in the form of dissolved organic carbon (DOC) and particulate organic carbon (POC); however, when living within the tissues of another organism this release (translocation) rate can increase to 90% of the algae's daily photosynthate production being released to the animal host (Muscatine et al. 1981; Davies 1991). It has been suggested that this elevated translocation rate for symbiotic dinoflagellates is induced by a chemical stimulus referred to as a "host release factor", which changes the properties of the algal cell wall making it "leaky" (Sutton and Hoegh-Guldberg 1990; Grant et al. 1997; Davy and Cook 2001a).

To predict the health of corals in a changing environment, it is essential to understand (and simulate) the contribution of the translocated photosynthates to the coral energy budget (Edmunds and Davies 1986; Edmunds and Davies 1989; Muscatine et al. 1989). In the GBR13 coral–algae symbiosis model, the translocation was defined as the leftover photosynthates produced by the symbiont after symbiont respiration, cell maintenance or growth. However, if the symbiont C reserves became depleted, the translocation rate was reduced to prevent the host from starving the symbiont to death (Chapter 2.2.2.5). The GBR13 model lacked any representation of the "host release factor". In Chapter 3 the translocation was altered to include a host-driven component, where the host, when lacking other sources of nutrient, extracted it from the symbiont. In addition, the sensitivity analysis in GBR13 showed that both the symbiont and the host were highly sensitive to changes in the fixed N to C ratio of the translocated photosynthates. These results indicated that translocation ideally should have a

dynamic N to C ratio and a release of excess photosynthates in addition to the "host release factor".

The process of taking up inorganic compounds from the environment is also uncertain. It might occur partly by diffusion through the boundary layer, or by actively pumping inorganic carbon to the site of photosynthesis. The latter process is known as a carbon concentrating mechanisms (CCMs) (Leggat et al. 1999; Raven 2003). In both the GBR13 model and the extended photoinhibition version (Gustafsson et al. in press), uptake of dissolved inorganic carbon (DIC) from the overlying water was assumed to be a function of diffusion, depending on the concentration of DIC in the water column (Al-Moghrabi et al. 1996; Goiran et al. 1996). The DIC uptake by the symbiont only depended on the concentration of DIC in the host tissues and did not influence the DIC uptake from the water. Additionally, the concentration of DIC in the host tissues was replenished by metabolic waste products from the host. Experimental studies, such as the *in situ* long- term study ENCORE at One Tree Island (Southern Great Barrier Reef) have shown that the uptake of dissolved inorganic nitrogen (DIN) from the water is associated with the presence of symbionts in corals and giant clams (*Tridacna*) (Koop et al. 2001). A similar result was deduced from the experimental dataset by Pernice (pers. comm.) examining the uptake of DIC from the environment. As CCMs are associated with the algal symbiont (Raven et al. 2008) and both DIC and DIN uptake have been shown to be linked to the presence of symbionts in the coral tissues, the definition of the DIN and the DIC uptake from the environment presented in the coupled GBR13 and photoinhibition model, hereafter referred to as the GBR13-photo model, should be redefined to account for the presence of symbionts.

In this study, we aim to improve our understanding of the translocation of photosynthates from the symbiont to the host, as well as the definition of DIC uptake from the environment. Using the recent study by Pernice (pers. comm.) in which the assimilation, storage and translocation of the isotopic labelled carbon (^{13}C) in the symbiotic anemone *Aiptasia pulchella* was examined, we aimed to

derive new definitions and equations of DIC uptake and photosynthate translocation for the GBR-photo model.

The process of redefining uptake and translocation of dissolved inorganic nitrogen (DIN) were also taken into consideration. The results by Pernice (pers. comm.) suggest that the symbionts are able enhance the uptake of DIN, fix it into organic compounds and stored within the symbiont cell. This N reserve could later be used to meet the symbionts metabolic requirements or be translocated to the host (Pernice et al. 2012). Therefore, the second goal of this study was to improve our understanding of the N pathways between the environment, host and symbiont, and to improve the GBR13-photo model accordingly.

The GBR-photo model with its new definitions of symbiont reserves, uptake and translocation were adjusted to reproduce the dataset by Pernice (pers. comm.). To test the new definition and mathematical equations of the uptake and translocation processes, and to establish if this new definition was applicable to coral-algal symbiosis, the model was used to reproduce the coral carbon budget presented by Tremblay et al (2012).

4.2 METHODS

4.2.1 Anemone symbiosis

This study was conducted on the symbiotic anemone *Aiptasia pulchella* (Anthozoa, Cnidaria). Like corals, *Aiptasia pulchella* also harbor symbiotic dinoflagellates within their tissues. Their physical structure is somewhat different from a coral in that they are individual polyps and they do not lay down a calcium carbonate skeleton. Even so, the benefit of the host-algae symbiosis is essentially the same, with the symbiont utilizing host metabolic waste products and translocating photosynthates back to the host (Wang and Douglas 1999; Venn et al. 2008).

Anemone of the genus *Aiptasia* are sessile organisms with a body form of a polyp with a pedal disk attached to the substrate, an elongated body column, and oral disc with a mouth and long tentacles (Shick 1991). *Aiptasia* can feed heterotrophically on plankton and particulate organic matter (POM) which it may capture using its tentacles. They are common in tropical marine ecosystem such as mangroves, and are considered hardy as they can cope with a wide range of salinity, water quality and nutrient input (Shick 1991). Due to its hardiness, fast reproduction and relatively simple body plan *Aiptasia* have been used for many studies of algae-cnidarian interactions (Clark and Jensen 1982; Cook et al. 1992; Davy and Cook 2001a). This symbiotic cnidarian was selected as a model organism for our study as it can be maintained (i) with individuals of a uniform size minimizing potential variability in metabolism relating to different size, and (ii) in a healthy aposymbiotic state (without symbionts) for months, offering an ideal control for experiments on symbiosis (Dunn et al. 2012).

4.2.2 *Aiptasia* experiment

The theory that DIC uptake from the environment is associated with the presence of algae symbionts, would suggest that an aposymbiotic anemone would have an insignificant uptake of DIC from the surrounding water. To assess the influence of the symbionts aposymbiotic anemones were produced using a modified "cold stripping" method to remove symbiotic dinoflagellates (Muscatine et al. 1991) and then maintained in the dark for over 3 months before being incubated in the same set of experiments as the symbotic anemone specimens (Pernice, pers. comm.). These experiments included a 4 h isotopic incubation under two different light regimes (low: 50 µmol photon m^{-2} s^{-1} and high: 200 µmol photon m^{-2} s^{-1}) in artificial seawater amended with $NaH^{13}CO_3$ powder (^{13}C isotopic abundance of 99%, commercially available from Sigma) to a final concentration of 2 mM (see supplementary material). NanoSIMS analysis was then used to quantify newly fixed ^{13}C within the tissue of symbiotic and aposymbiotic anemones as described by Pernice (pers. comm.). As the results showed insignificant ^{13}C uptake in the

tissue of aposymbiotic anemone after the 4 h incubation, the incorporation of ^{13}C into the host tissue, seen in the symbiotic specimens, was assumed to be photosynthates translocated from the symbiont, justifying the new definition of symbiont driven DIC uptake (eq. 5).

4.2.3 Carbon content and uptake rate

Prior to carbon content analysis, *Symbiodinium* cells were separated from anemone tissue previously stored at -80°C by centrifugation (4000 g for 5 min at 4°C). The pellets of dinoflagellate cells and supernatant of anemone host tissue were freeze-dried and weighed. Carbon content (%) was then analyzed in both anemone tissue and dinoflagellate in duplicate at the UC Davis Stable Isotope Facility (Department of Plant Sciences, University of California, Davis, California) by using a combustion (950°C) method with a elemental analyzer (PDZ Europa ANCA-GSL). The carbon uptake rate per mg of host tissue or dinoflagellate (ρ) was expressed in µg C h^{-1} mg^{-1} and was calculated by normalizing the ^{13}C-incorporation measured by using NanoSIMS to the average carbon content (% of dry mass) of the animal tissue or the dinoflagellate symbiont and to the time of incubation according to the following equation (Dugdale and Wilkerson 1986; Grover et al. 2002):

$$\rho = \left(\frac{(C_{mes} - C_{nat})}{(C_{enr} - C_{nat}) \times T_{inc}}\right) \times C_{content} \times 10^3$$

Where:

C_{mes} is the measured $^{13}C/^{12}C$ ratio, C_{nat} is the natural $^{13}C/^{12}C$ ratio measured in non-labelled control *Aiptasia* samples, C_{enr} is the ^{13}C-enrichment of the incubation medium., and T_{inc} is the incubation time. $C_{content}$ is the average carbon content (%) measured by using combustion (950°C) method with elemental analyzer (PDZ Europa ANCA-GSL).

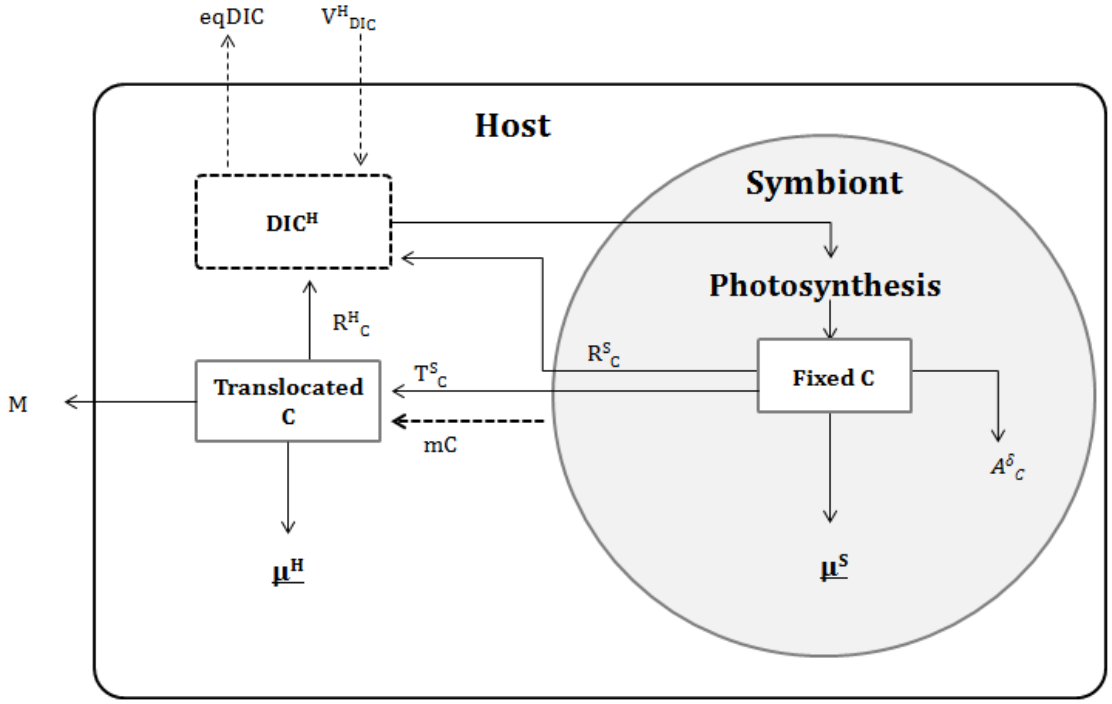

Figure 4.1: Schematic over C fluxes between the environment, host and the symbiont. Symbols and abbreviations are explained in Tables 4.1 and 4.2.

4.2.1 Anemone model

The coupled GBR13-photo model includes both the symbiosis and the photosystem. However, these two models were written for coral symbiosis and therefore required some alteration to be applicable to an anemone-algal symbiosis. First, the calcification processes were removed. Second, the model units had to be converted from being standardized to cm^2 of coral surface area to mg of anemone tissue dry weight. This conversion was done under the assumption that the tissue of the *Aiptasia* had the same properties as a coral; hence measurements of dry tissue weight per cm^2 were used to create a conversion factor. This assumption should be considered with care and possibly revisited in the light of any new evidence. At a symbiont population size of $1.4x10^6$ per cm^2 (as given in Tremblay et al. (2012) described below) a tissue dry weight of 10 mg cm^{-2} has been suggested (Fitt et al. 1993), therefore we suggest a conversion factor of 0.1. It should be

mentioned that the dry weight of tissue per unit surface area does vary with species, season and nutrient availability, however the values range by a factor of four between 5-19 mg cm^{-2} (Fitt et al. 1993; Fitt et al. 2000; Grottoli et al. 2006a).

4.2.2 Symbiont nitrogen reserves

To account for the finding that dinoflagellate symbionts are able to store N within their cells (Pernice et al. 2012; Kopp et al. 2013), a N reserve (N_R^S) state variable was added to the model (Table 4.2). The N_R^S was assumed to contain organic compounds high in N (eq. 1), which could be used for cell maintenance, growth or translocation to the host. To avoid unrealistic accumulation of N in the reserve pool, the maximum size of N_R^S ($N_{R,max}^S$ (eq. 17)) was set to be the same as the functional N pool (N_F^S); there could not be more reserves than structural material. The C and N pathways were given similar formulations, but independent of one another (Fig. 4.1, Table 4.1). Thus, changing the uptake of N does not necessarily change carbon uptake.

4.2.3 Inorganic carbon and nitrogen uptake

In the GBR13-photo model the host was given a constant uptake rate of DIN. Here it was changed to an equation calculating the uptake rate (V_{DIN}^H (eq. 11)) driven by the symbionts need for DIN, as well as the concentration in the water column (DIN^E). Therefore, the maximum DIN uptake ($V_{N,max}^S$ (eq. 8)) was set to equal the maximal need of the symbiont population to achieve its maximum growth rate (μ_{max}^S). Similarly, the maximum uptake rate of DIC (V_{DIC}^H (eq. 12)) was set to equal the maximum photosynthetic rate (P_{cell}^{max}) for the symbiont population. To calculate the uptake of DIN and DIC from the environment Michaelis–Menten style equations were used, depending on the maximal ability of the symbiont to use DIN and DIC, as well as the concentration in the water column and the half- saturation constants K_{din} and K_{dic} (eq. 11-12).

Like the GBR13-photo model, the DIC and DIN available to the symbiont (DIC^H and DIN^H) also included metabolic and respiration by-products from the host and the symbionts metabolic processes (eq. 5 and 6). To avoid accumulation of DIC and DIN in the host tissues, as well as having DIC and DIN uptake from the environment being dependent on the symbiont population, the equilibrium terms for DIC and DIN ($eqDIC$ and $eqDIN$) were defined to release any unused newly acquired DIC or DIN back into the environment (eq. 18 and 19).

We assume that all DIN and DIC uptake by the symbiont (V_{NR}^S and P_{cell}) went to N_R^S (eq. 1) and C_R^S (eq. 3) respectively, from which the N and C could be used to create new structural cell material (N_F^S (eq. 2) and C_F^S (eq. 4)), respiration and cost of biosynthesis (R_N^S and R_C^S), providing for the cost of repairing and detoxifying the photosystem due to ROS production (A_N^δ and A_C^δ), or translocation of compounds back to the host (T_N^S (eq. 13-14) and T_C^S (eq. 15-16)).

4.2.4 Translocation of photosynthates

The translocation of C and N from the symbiont to the host had two components. First, the host-driven part which involved the host actively extracting C and N from the symbiont ($T_{C,host}^S$ (Eq. 15) and $T_{N,host}^S$ (Eq. 13)), see photoinhibition model (Gustafsson et al. (submitted), Chapter 3). Second, in contrast to the GBR13-photo model as the C_R^S or N_R^S approached their maximum concentration ($C_{R,max}^S$ or $N_{R,max}^S$) the translocation rate was enhanced to get rid of excess C (T_C^S) or N (T_N^S). As the C and N were translocated independent of one another a flexible C:N ratio was achieved.

Table 4.1: Model equations

Equation	No.	Description	Unit
$\frac{dN_R^S}{dt} = V_{NR}^S\left(1-\frac{N_R^S}{N_{R,max}^S}\right) - V_{NF}^S - T_{N,host}^S - R_N^S - A_N^\delta$	(1)	Change in symbiont N reserve	pg N cell^{-1} h^{-1}
$\frac{dN_F^S}{dt} = V_{NF}^S = V_{NR}^S\left(\frac{C_R^S}{C_R^S + C_{R,thres}^S}\right)\left(1-\frac{S}{S_{max}}\right)\left(\frac{N_R^S}{N_{R,max}^S}\right)$	(2)	Change in symbiont functional N	pg N cell^{-1} h^{-1}
$\frac{dC_R^S}{dt} = P_{cell}\left(1-\frac{C_R^S}{C_{R,max}^S}\right) - V_{CF}^S - T_{C,host}^S - R_C^S - A_C^\delta$	(3)	Change in symbiont C reserve	pg C cell^{-1} h^{-1}
$\frac{dC_F^S}{dt} = V_{CF}^S$	(4)	Change in symbiont functional C	pg C cell^{-1} h^{-1}
$\frac{dDIC^H}{dt} = V_{DIC}^H + R_C^H + R_C^S S - P_{cell} S - eqDIC^H$	(5)	Change in host DIC concentration	pg DIC mg^{-1} h^{-1}
$\frac{dDIN^H}{dt} = V_{DIN}^H + R_N^H + R_N^S S - V_{NR}^S S - eqDIN^H$	(6)	Change in host DIN concentration	pg DIN mg^{-1} h^{-1}
$N_T^S = N_F^S + N_R^S$	(7)	Total symbiont N	pg N cell^{-1}
$V_{N,max}^S = \mu_{max}^S N_T^S (1 + R_N^S)$	(8)	Max symbiont uptake rate of N	pg N cell^{-1} h^{-1}
$V_{NR}^S = V_{N,max}^S\left(\frac{DIN^H}{DIN^H + K_n}\right)$	(9)	Rate of symbiont N uptake	pg N cell^{-1} h^{-1}
$V_{CF}^S = V_{NF}^S / Q_F^S$	(10)	Rate of C incorporation in new symbiont tissue	pg C cell^{-1} h^{-1}
$V_{DIN}^H = V_{N,max}^S S\left(\frac{DIN^E}{DIN^E + K_{din}}\right)$	(11)	Rate of host DIN uptake	pg DIN mg^{-1} h^{-1}
$V_{DIC}^H = P_{cell}^{max} S\left(\frac{DIC^E}{DIC^E + K_{dic}}\right)$	(12)	Rate of host DIC uptake	pg DIC mg^{-1} h^{-1}
$T_{N,host}^S = \frac{(N_F^H(\mu_{max}^H + \eta^H + \delta^H \mu_{max}^H) - Z_N - mN_{Host}^S)\left(\frac{N_R^S}{N_{R,max}^S}\right)}{S}$	(13)	Translocation rate of N from the symbiont to the host induced by the host	pg N cell^{-1} h^{-1}
$T_N^S = T_{N,host}^S\left(1 + \frac{N_R^S}{N_{R,max}^S}\right)$	(14)	Total translocation rate of N from the symbiont to the host	pg N cell^{-1} h^{-1}
$T_{C,host}^S = \frac{(C_F^H(\mu_{max}^H + \eta^H + \delta^H \mu_{max}^H) - Z_C - mC_{Host}^S)\left(\frac{C_R^S}{C_{R,max}^S}\right)}{S}$	(15)	Translocation rate of C from the symbiont to the host induced by the host	pg C cell^{-1} h^{-1}
$T_C^S = T_{C,host}^S + P_{cell}\left(\frac{C_R^S}{C_{R,max}^S}\right)$	(16)	Total translocation rate of C from the symbiont to the host	pg C cell^{-1} h^{-1}
$N_{R,max}^S = N_F^S$	(17)	Max size of N_R^S	pg N cell^{-1}
$eqDIC^H = V_{DIC}^H + R_C^H + R_C^S S - P_{cell} S$	(18)	Equilibration DIC in host	µg C cm^{-2} d^{-1}
$eqDIC^H = V_{DIN}^H + R_N^H + R_N^S S - V_{NR}^S S$	(19)	Equilibration DIN in host	µg C cm^{-2} d^{-1}

Table 4.2: Model parameters, variables and rates used in the anemone model and the coral model. Bracketed values represented the parameters which are different in the coral model.

Symbol	Description	Source/Value	units
S	Number of symbiont cells per cm^2 of host surface	Eq. 10 GBR13-photo	cell cm^{-2}
S_{max}	Maximum number of symbiont cells per unit surface area	Eq. 21 GBR13	cell cm^{-2}
P_{cell}	Rate of Photosynthesis	Eq. 22 GBR13-photo	µg C cell^{-1} d^{-1}
P_{cell}^{max}	Maximum C specific photosynthesis rate		µg C cell^{-1} d^{-1}
R_N^S	Cost of biosynthesis and respiration symbiont (N)	Eq. 2 GBR13	µg N cell^{-1} d^{-1}
R_C^S	Cost of biosynthesis and respiration symbiont (C)	Eq. 1 GBR13	µg C cell^{-1} d^{-1}
R_N^H	Cost of biosynthesis and respiration host (N)	Eq. 39 GBR13	µg N cm^{-2} d^{-1}
R_C^H	Cost of biosynthesis and respiration host (C)	Eq. 38 GBR13	µg C cell^{-1} d^{-1}
η^H	Symbiont C specific respiration and maintenance rate	0.1	g C g C^{-1} d^{-1}
δ^H	Symbiont C specific cost of biosynthesis	0.1	g C g C^{-1} d^{-1}
A_N^δ	Total N cost of D1 repair and detoxification	Eq. 35 GBR13-photo	µg N cell^{-1}d^{-1}
A_C^δ	Total C cost of D1 repair and detoxification	$\delta_{CR}^S + \delta_{CF}^S$ GBR13-photo	µg C cell^{-1}d^{-1}
$C_{R,thres}^S$	C needed to support cell functions through the night	GBR13 text	µg C cell^{-1}
$C_{R,max}^S$	Max value of C_R^S	Eq. 3 GBR13	µg C cell^{-1}
μ_{max}^S	Maximum symbiont growth rate	0.4	d^{-1}
μ_{max}^H	Maximum host growth rate	0.05	d^{-1}
K_n	Half saturation constant symbiont DIN uptake	1	mg N m^{-3}
K_{din}	Half saturation constant host DIN uptake	1	mg N m^{-3}
K_{dic}	Half saturation constant host DIN uptake	4.8	g C m^{-3}
mN_{Host}^S	N from dead symbiont cells re-ingested by host	Eq. 12 GBR13	µg N cell^{-1} d^{-1}
mC_{Host}^S	C from dead symbiont cells re-ingested by host	Eq. 13 GBR13	µg C cell^{-1} d^{-1}
Q_{min}^S	Minimum N:C ratio in symbiont	0.05 (0.1)	g N g C^{-1}
Q_F^S	N:C ratio in symbiont functional pool	0.1761	g N g C^{-1}
DIN^E	Concentration of DIN in the water column	10	mg N m^{-3}
DIC^E	Concentration of DIC in the water column	24	g C m^{-3}
Z_N	N uptake through heterotrophic feeding	0	µg N cell^{-1} d^{-1}
Z_C	C uptake through heterotrophic feeding	0	µg C cell^{-1} d^{-1}

4.2.5 Model evaluation and validation

To recreate the uptake rate of DIC, as well as the translocation rate of photosynthates for two light levels (50 and 200 µmol photon m^{-2} s^{-1}) as established by Pernice (pers. comm.) the model was first run for two model days using the

light conditions of 200 µmol photon m^{-2} s^{-1} and a 12:12 hour light:dark cycle, corresponding to the conditions under which the anemones were held prior to the experiment. This allowed any initial variability in the model to settle before the actual experiment. The experimental runs were started after the spin-up period, once with the high light level of 200 µmol photon m^{-2} s^{-1} and once with the low light level of 50 µmol photon m^{-2} s^{-1} (Fig. 4.2).

To validate the new definition of the uptake and translocation processes the model parameters were again set to represent a coral-algae symbiosis using the initial conditions as presented in Tremblay et al. (2012) and Table 4.3. The model was set to reproduce the carbon budget presented in their study. The model was spun-up for two days with a 12:12 hour light and dark cycle with a light level of 250 µmol photon m^{-2} s^{-1} as described in Tremblay et al. (2012). They estimated the symbiont and host C uptake after 48 hours at a temperature of 25°C. As the exact timing of the sampling in the light/dark cycle was not given in the Tremblay paper the modelled mean daytime rates were used.

Table 4.3: Initial conditions for Tremblay et al. (2012).

Parameter	Value	Units
Light	250	µmol photon m^{-2} s^{-1}
Temperature	25	°C
Symbiont concentration	1.4	10^6 cell cm^{-2}
Chlorophyll concentration	8.5	pg Chl $cell^{-1}$

In addition to turning on calcification and adjusting initial conditions the only parameter that was altered between the anemone and the coral version of the model was the minimum N/C ratio of the symbiont cell (Q^S_{min}). The parameter influenced the amount of C that the symbiont cell could attain and hence it also influenced the translocation of photosynthates. The Q^S_{min} was set to 0.05 to accommodate the high C uptake by the symbiont tissue in the anemone model, and to 0.1 in the coral model version to reduce this rate and enhance the translocation,

as it is known that the translocation in the coral-algae symbiosis can reach 90% of the total amount of fixed C (Davies 1991).

4.3 RESULTS

The dataset provided by Pernice (pers. comm.) gave values of C uptake by tissues in the symbiont and the host from seawater with natural levels of DIC (Table 4.4). The DIC concentration in the ocean is known to be relatively stable in time and space, hence rather than looking at different DIC environmental concentrations, different light intensities leading to different photosynthetic rates were considered in their study. The values in Pernice (pers. comm.) (Table 4.4) showed that the uptake of C into the symbionts tissues was approximately one order of magnitude greater than in the host tissue if combining gastrodermal and epidermal cells. The high-light treatment yielded an uptake rate approximately 1 μg mg^{-1} h^{-1} higher than for the low-light level in the symbiont tissue, whereas the host tissues in the high-light treatment took up almost twice as much C as in the low-light treatment. Interestingly, there was also almost twice the amount of symbiont C biomass per mg of dry tentacle tissue than there was in the coral host.

Table 4.4: Experimental dataset: Uptake rate of ^{13}C by different tissues, and total C content of the host and the symbiont (average of three samples). The light levels were HL: 200 μmol photon m^{-2} s^{-1} and LL: 50 μmol photon m^{-2} s^{-1} (Pernice pers. Comm.).

Light	Tissue	Mean ^{13}C uptake (SE) μg C mg^{-1} h^{-1}	Carbon content μg C mg^{-1}
HL	Epiderm	0.03 (0.0017)	69.3
LL	Epiderm	0.0065 (0.0007)	69.3
HL	Gastroderm	0.079 (0.0165)	69.3
LL	Gastroderm	0.044 (0.0045)	69.3
HL	Zooxanthellae	2.92 (0.117)	264.7
LL	Zooxanthellae	1.83 (0.075)	264.7

The measured uptake rates in Table 4.4 correspond to the addition of C to the symbiont and the host functional and reserve carbon pools (C_F^S, C_R^S, C_F^H and C_R^H) in the model. In addition to the definition of translocation (eq. 13-16), the initial conditions for the symbiont and host biomass were estimated using the C content information from the *Aiptasia* experiment (Table 4.4). As the model contains only one category of host tissue, experimental values for the gastroderm and epiderm were combined and the average was compared with the model.

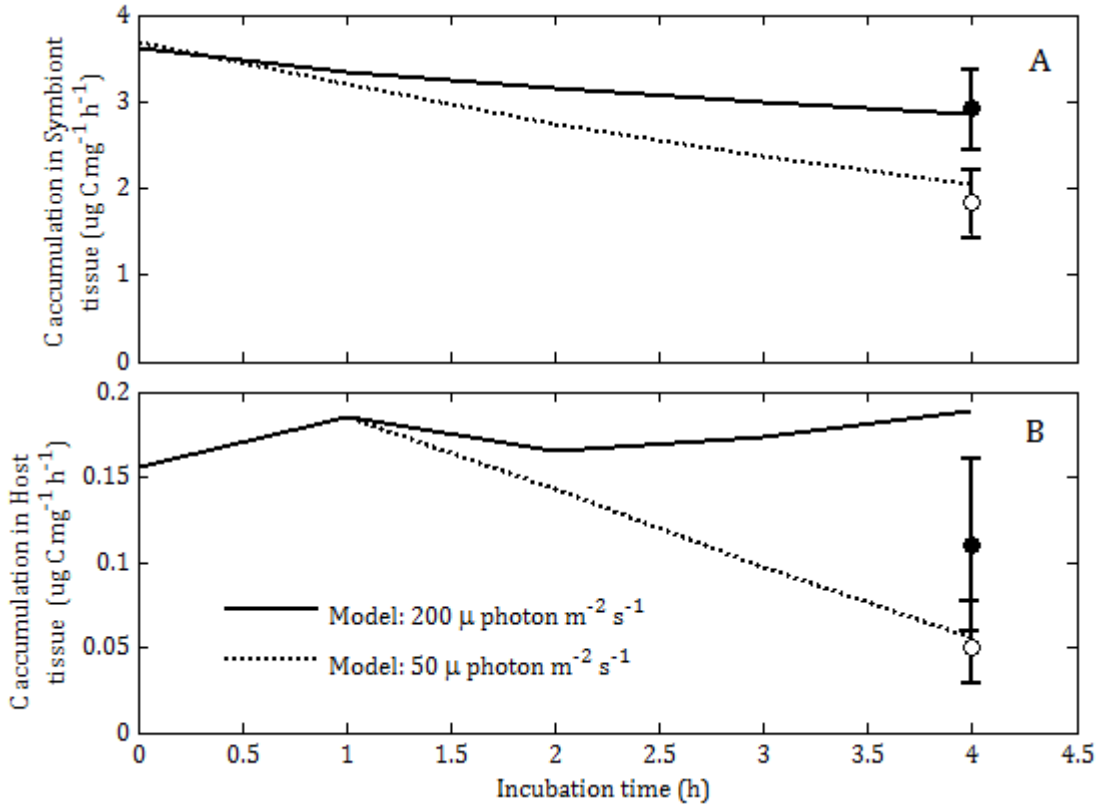

Figure 4.2: Accumulation rate of C in the symbiont (A) and host tissues (B). The model values correspond to the lines and are the sum of the change in the functional and the reserve pools. The circles shows the measured ^{13}C accumulation rate at four hours for the 200 µmol photon m^{-2} s^{-1} light treatment (closed circle) and 50 µmol photon m^{-2} s^{-1} light treatment (open circle) ± 1 SD.

The modelled symbiont uptake rate corresponded well with the measured uptake after the four hour experimental run, with an uptake rate approximately 1 μg C mg^{-1} h^{-1} higher for the high light treatment (Fig. 4.2A). The modelled host C uptake in the low-light (LL) treatment matched the measured values, whereas the modelled uptake rate for the high-light (HL) treatment were almost 0.1 μg C mg^{-1} h^{-1} higher than the measured value.

As the modelled uptake rate was calculated using the mathematical representations of physiological functions such as photosynthesis and respiration, we derived a carbon budget for the anemone host-symbiont system (Fig. 4.3). The C budget included the percentages of C fixation rate through photosynthesis incorporated into symbiont or host tissues, translocated, respired or excreted as mucus. The total rate of C incorporation into the host and the symbiont tissues was represented by μ^H and μ^S respectively. Both the HL and the LL treatment resulted in similar percentages of C being taken up by the symbiont tissues, whereas the host showed a four times higher uptake rate under the HL treatment. Translocation of fixed C was almost doubled for the HL treatment, the percentages however only varied by 4%.

As the experiment took place over a 4 hour period, the biomass of the symbiont population or the host tissues did not change noticeably, therefore rates that were dependent on the amount of biomass, such as respiration, cell maintenance and natural symbiont mortality were the same for both light treatments.

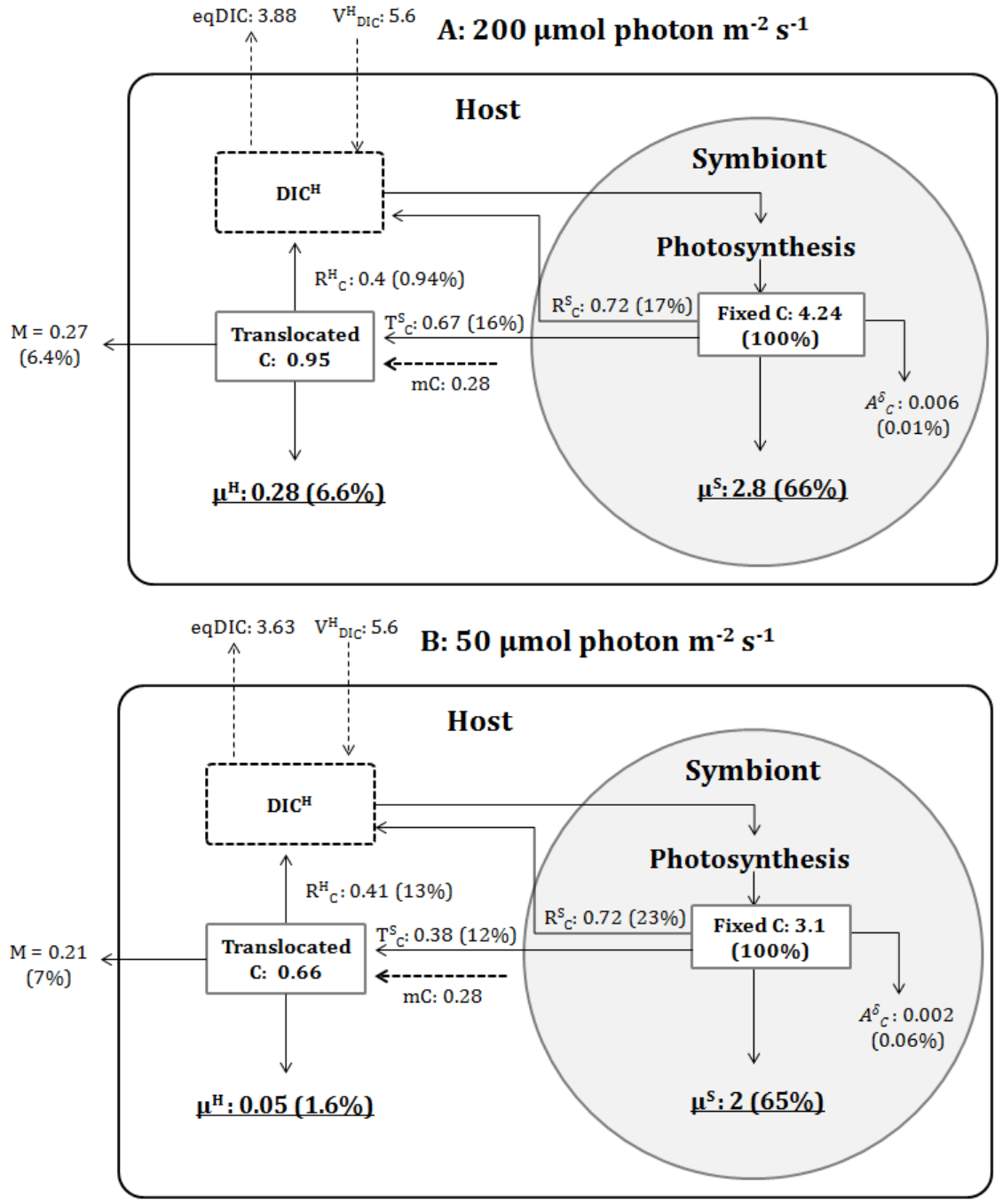

Figure 4.3: Modelled carbon budget diagram for the sea anemone *Aiptasia pulchella*. Rates are given in µg C mg^{-1} h^{-1}, and percentages of internal fluxes to the total photosynthates rate in brackets. Light intensity of 200 (A) and 50 µmol photon m^{-2} s^{-1} (B). Dashed arrow marked mC corresponds to the carbon the host acquired from dead symbionts that died due to natural mortality.

4.3.1 Coral C uptake and translocation

The results from the anemone model (with calcification turned on) and the initial conditions set to the values presented in Tremblay et al. (2012), showed that out of the fixed C, 23% was taken up by the symbiont and 13% by the host. In comparison to the anemone model, the symbiont uptake was much lower for the coral model, whereas the host's uptake was considerably higher. The translocation rate was 63% of the total fixed C for the coral, but only 12-16% for the anemone. Note that the dataset provided by Pernice (pers. comm.) was obtained using *Aiptasia* tentacle tissue only and the C translocation in this specific tissue might not reflect the metabolic exchanges occurring within the individual polyp.

Table 4.5: Comparison of modelled C rates in a coral and measured rates by Tremblay et al. (2012).

	Tremblay et al. (2012)		**Coral Model**	
Rates	**µg C cm^{-2} h^{-1}**	**% of fixed C**	**µg C cm^{-2} h^{-1}**	**% of fixed C**
Photosynthesis	15.15±1.51	100	18.36	100
Translocation	11.84±0.9	78.2±0.9	11.60	63.2
Symbiont respiration	2.13±0.12	14.0±0.8	2.44	13.3
Host respiration	5.19±0.67	34.2±4.4	4.57	24.9
Symbiont C Incorporation rate	1.36±0.21	9.0±0.8	4.30	23.4
Host C Incorporation rate	2.16±0.03	14.3±0.2	2.37	12.9
Mucus	ca. 4.3	ca. 28	5.32	29.0
Calcification	7.14±0.26	-	7.0	38.1

The coral model was compared to the study by Tremblay et al. (2012). The comparable rates are given in Table 4.5. Overall, the rates matched one another

well with the exception of the uptake by the symbiont which was somewhat overestimated in the model. The modelled translocation rate was also lower than the rate estimated the Tremblay et al. (2012). This indicates that the modelled symbiont incorporated C into new tissues rather then translocating the C to the host. The reason behind this was the initial size of the symbiont C reserve, C_R^S, which was set to 10% of the C_R^S whereas $C_{R,max}^S = C_R^S$, resulting in a restriction of translocation (eq. 15). Figure 4.4 presents the C budget for the modelled coral rates.

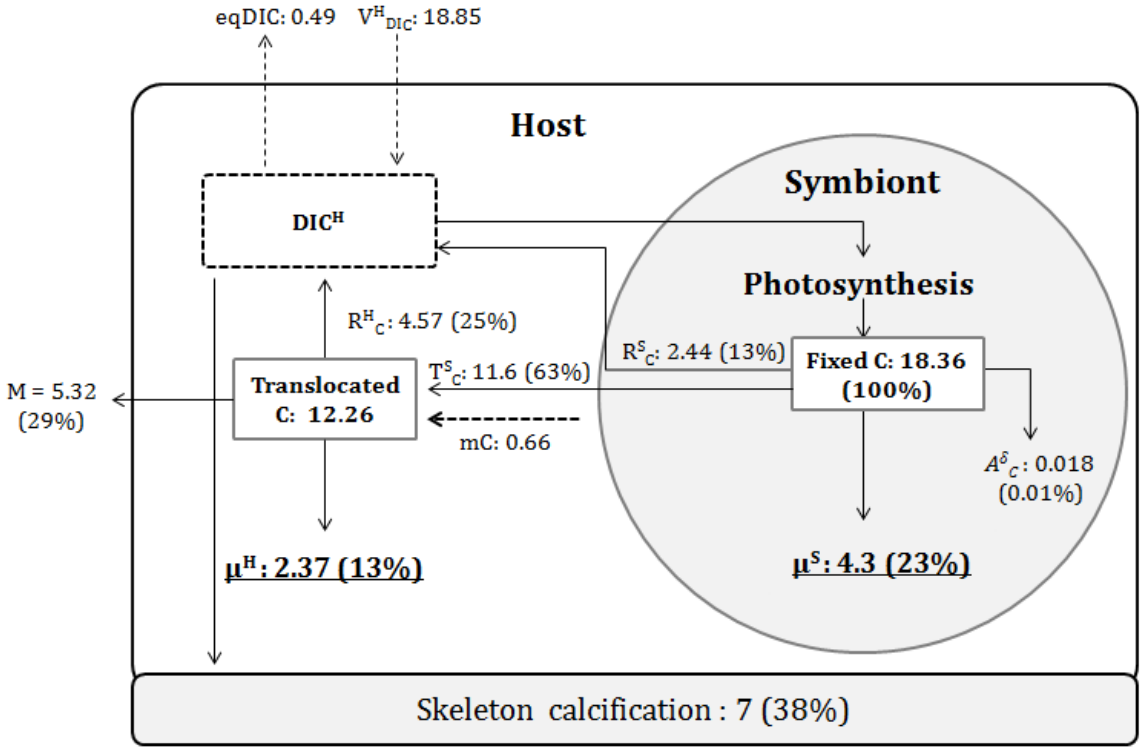

Figure 4.4: Modelled carbon budget diagram for the coral, rates are given in µg C cm^{-2} h^{-1}.

4.4 DISCUSSION

Here we provide new mathematical descriptions of inorganic nutrient uptake and translocation within the cnidarian-dinoflagellate symbiosis. The uptake rate of DIN and DIC were driven by the autotrophic symbionts (Koop et al. 2001; Pernice et al. 2012). The new model definitions only allowed for uptake during daytime as a direct result of photosynthesis. As the model now includes symbiont reserves for both N and C the lack of night time uptake of inorganic N and C from the environment was less significant. However, there have been suggestions that uptake of DIN does take place during the night, but at a significantly lower rate than during daytime (D'elia et al. 1983; Wilkerson and Trench 1986; Bythell 1990). This night-time uptake has been assumed to be a result of the recent light history; however, if exposed to prolonged periods of darkness the uptake will eventually cease and turn into net release after a few days (Szmant-Froelich and Pilson 1977; Wilkerson and Trench 1986). There may be a difference in uptake depending on DIN species. For instance different uptake rates of ammonia and nitrate have been recorded (Wilkerson and Trench 1986), and it has also recently been shown that ammonia can be taken up directly by the host (Pernice et al. 2012). However, adding this sort of complexity to the will just increase the uncertainty of the model and make interpretation more difficult as these processes are still poorly understood.

The second change made was the definition of translocation of photosynthates. The new definition captured both the “host release factor” as well as the release of excess photosynthates. There was quite a large difference between translocation rate in the anemone and the coral considered in this study. As noted above the *Aiptasia* measurements were obtained from tentacle tissue, and the C translocation in this specific tissue might not reflect the metabolic exchanges occurring across the whole individual polyp. In sea anemones, the vast majority of the C fixed by the symbiont within the tentacle can be transported via the internal fluid and stored as lipids in the polyp body column, with up to 97% of the total lipid for *Condylactis*

gigantean being stored here, hence only a small fraction of the translocated C remain in the tentacles (Kellogg and Patton 1983). As a result, a large portion of C stores may have been ineffectively detected by NanoSIMS when targeting *Aiptasia* tentacle tissue. Future studies using this model organism to investigate metabolic exchanges within cnidarian symbiosis should therefore also explore other tissues such as, for example, coelenterate tissues.

Another interesting feature of the *Aiptasia* measurements was the high symbiont biomass in comparison to the host biomass. In corals, the host biomass is generally higher than the symbiont population. For example Muller-Parker et al. (1994) showed that the symbiont population C content comprised approximately 26 % of the total biomass (Muller-Parker et al. 1994a). In the *Aiptasia* tentacle the C content of the symbiont population was almost twice that of the host; this reflects the nutritional role played by tentacles in enhancing surface area for intracellular symbiotic dinoflagellates (Fautin and Mariscal 1991).

Although not included in the present model, the light environment within the anemone and the coral tissues are likely to be different from each other due to the skeleton associated scattering of light within the coral tissue (Enríquez et al. 2005). Enríquez et al. (2005) found that symbiotic dinoflagellates associated with Scleractinian corals absorbed two to five times more light than freshly isolated symbionts. They theorized that the difference depended on the scattering of light within the coral tissue. Under low stress conditions (moderate light and temperatures) the scattering enhanced the photosynthetic output, whereas under bleaching conditions enhancements of the local light field could exacerbate the negative effect of temperature and light stress (Enríquez et al. 2005; Wangpraseurt et al. 2012). Due to the enhanced ability to measure the light field within coral tissues, it would be interesting to add a component to the model that defines the actual light field within the tissue. This could help to explain some of the differences between the anemone and the coral as seen in this study. For instance, an increase in the minimum N/C ratio (Q_{min}^{S}) was necessary to simulate the higher translocation rate in the coral compared to the anemone; this may not be needed if instead the enhanced translocation was dependent upon an enhanced light field

within the coral. Further studies incorporating these additional components into the mathematical descriptions are therefore needed to better predict the metabolic function of symbiotic corals in connection to their complex environment.

CHAPTER 5:

APPLICATION OF A MODEL OF CORAL SYMBIOSIS AT A REEF SCALE: HERON ISLAND, AUSTRALIA

5. Application of a model of coral symbiosis at a reef scale: Heron Island, Australia

Model development, experimental design, and model evaluation and validation were performed by Malin Gustafsson, who also wrote this chapter. Intellectual contributions and technical assistant were made by Mark Baird, Peter Ralph and Mathieu Mongin.

5.1 INTRODUCTION

Coral reefs provide habitat for a wide range of organisms, as well as serving as a protective boundary between coastlines and the open ocean to mitigate wave action (Hughes et al. 2003; Hoegh-Guldberg 2004). Due to climate change coral reefs are currently under threat from increasing sea surface temperatures (SST) and ocean acidification (Brown 1997; Hoegh-Guldberg 1999; Hoegh-Guldberg et al. 2007). The question of what impact elevated SST and ocean acidification may have on reef systems has received increasing attention over the past few decades. Before we can begin to comprehend the potential detrimental effects of altered properties of ocean water caused by climate change may have, it is important to understand the physical, chemical and ecological processes that occur on a reef and the interaction among them. For example, the water advected over the reef rim from the open ocean is low in nutrient. Even so, coral reefs are generally thought of as highly productive ecosystems, where nutrients are tightly recycled within the reef community (Roberts et al. 2002). The physical environment of a coral reef varies greatly between locations. For example, a coral residing on a reef slope is exposed to stronger currents and likely more stable temperatures throughout the day than a coral found within the reef lagoon, where due to shallow water depth

and tidal cycles corals may experience elevated temperatures, lower water flow and possible exposure to air.

Understanding the nutrient dynamics at a community level in a coral reef ecosystem is difficult as nutrient uptake and release occurs at many different places across the reef, and through several different processes such as animals feeding heterotrophically, plants and algae taking up inorganic nutrient through diffusion of dissolved inorganic matter (Muscatine and D'elia 1978), release of inorganic nutrients through respiration (Leclercq et al. 2002) and release of waste products and mucus as dissolved and particulate organic matter (Naumann et al. 2010; Tanaka et al. 2011). Additionally, the reef nutrient dynamics are influenced by remineralisation of organic molecules into inorganic forms, which occur both in the water column and reef sediments (Fowler and Knauer 1986; Alongi et al. 1996; Wild et al. 2004b; Wild et al. 2005a). In light of these complexities, the individual contribution by different organisms to the gross reef nutrient uptake and release has proved difficult to determine in the field, as these individual contributions are generally small (Wyatt et al. 2010). To date, several studies have shown that gross uptake and release of inorganic nutrient over a reef depends on the hydrodynamic processes and mass transfer limited (MTL) uptake, as well as the inorganic nutrient concentration in the water column (Atkinson et al. 2001; Hearn et al. 2001; Falter et al. 2004; Zhang et al. 2011; Wyatt et al. 2012).

Mass transfer limitation explains how nutrient-deplete boundary layers occur directly above the organism's surface, which controls the uptake of nutrient from the overlaying water (Atkinson and Bilger 1992; Baird and Atkinson 1997; Atkinson et al. 2001). Flume experiments have shown that nutrient uptake increases when the boundary layer is reduced due to increasing water velocity and surface roughness (Atkinson and Bilger 1992; Baird and Atkinson 1997). The nutrient flux through the boundary layer was also found to depend on the nutrient concentration in the water column above the coral (Atkinson and Bilger 1992; Baird and Atkinson 1997). In addition to the effects of water velocity and inorganic nutrient concentration, Atkinson et al. (2001) found that wave-induced water flow resulted in 2-3 times higher MTL rate constants than previously found for uniform

flow (Bilger and Atkinson 1995; Baird and Atkinson 1997). As the Atkinson et al. (2001) experiments were conducted in a closed self-sustaining system (Biosphere 2 Centre, Tucson, Arizona) and found that even though the recycling within the reef system were sufficient to sustain the gross production, the uptake of nutrients was still mass transfer limited.

Early studies of coral reef dynamics often referred to the 'coral reef paradox' of a highly productive ecosystem existing in a 'marine desert' (Johannes et al. 1972; Webb et al. 1975). Their theory suggested that there is insignificant inorganic and organic nutrient contribution from oceanic sources; however they generally included large particulate organic matter (POM). Today we are aware that the oligotrophic waters are dominated by smaller size fractions of POM, including pico- and nanoplankton, and the uptake of these small particles is ngreater than for larger size classes, indicating that the oceanic sources are important to the reef community (Houlbreque et al. 2004b; Wyatt et al. 2012).

Reef building corals (Scleractinian) harbour endo-symbiontic dinoflagellates of the genus *Symbiodinium* within their tissues. The main advantage of maintaining these symbionts is the ability to utilize both organic and inorganic sources of nutrient. Uptake of organic nutrient occurs through heterotrophic feeding, where the animal host uses tentacles and mucus to capture organic matter from the water column (Houlbrèque and Ferrier-Pagès 2009). Uptake of inorganic compounds takes place through diffusion across the gastrodermal cavity wall, which is fixed into organic compounds by the algal symbiont (Wilkerson and Trench 1986; Yellowlees et al. 2008). If either of these nutrient sources is absent, the other may sustain the coral. The symbiont is known to release up to 90% of their fixed carbon to the coral host (Davies 1991), whereas the symbionts are able to recycle metabolic waste products from the host to support the synthesis of new photosynthates.

We propose a mechanistic coral model at the reef scale based on the coral-symbiosis model by Gustafsson et al. (2013). We aim to link the coral-symbiosis model to the reef environment, accounting for the influence of hydrodynamic, chemical and biological processes. This modelling effort will increase our

understanding of the dynamics of the nutrient environment on a coral reef, considering both the effect of the environment across the coral and vice versa. As mentioned above there are different processes that may influence nutrient uptake and release over a coral reef. Measurements of a particular organism's contribution to the gross nutrient uptake and release have been difficult, due to the complex reef community composition and the variations in physical properties of the reef environment across reef zones (Wyatt et al. 2010; Wyatt et al. 2012). In this study we linked water flow velocity, tidal cycles, nutrient concentrations and carbon chemistry with uptake, release and recycling of nutrient across different reef zones. Using this model we assessed the coral's contribution to nutrient uptake and release as a function of the local hydrodynamics across the reef, and different sources of nutrient.

5.2 METHODS

5.2.1 Study site

Heron Island (151°55´E, 23°27´S) is part of the Capricorn Bunker Group in the southern Great Barrier Reef, and is located approximately 80 km off the Australian mainland, northeast of Gladstone. Heron Reef is a platform reef approximately 9.3 km long and 4.6 km wide, with Heron Island located on the northwest margin, approximately 800 x 280 m in size (Fig. 5.1). The neighbouring Wistari Reef separated from Heron Reef by the Wistari Channel, and about 20 km east of Heron Island is One Tree Island surrounded by a 5.5 km long and 3.5 km wide coral reef.

Heron Reef is composed of a number of distinct morphological and ecological zones, with a lagoon, characterised by a deep and a shallow area, surrounded by a coral dominated reef crest and slope (Fig. 5.1B) (Ahmad and Neil 1994; Roelfsema et al. 2002). The deepest part of the lagoon with a depth of approximately 3.5 m during low tide has scattered coral colonies, hereafter referred to as bommies (Fig. 5.1B). The shallow part of the lagoon with a water depth at low tide of 0.3-1 m is dominated by fine sediments (Chen and Krol 1997). The zonation of the reef has

been formed by hydrodynamic processes, such as waves, tides and currents, as well as geomorphic and ecological processes.

A)

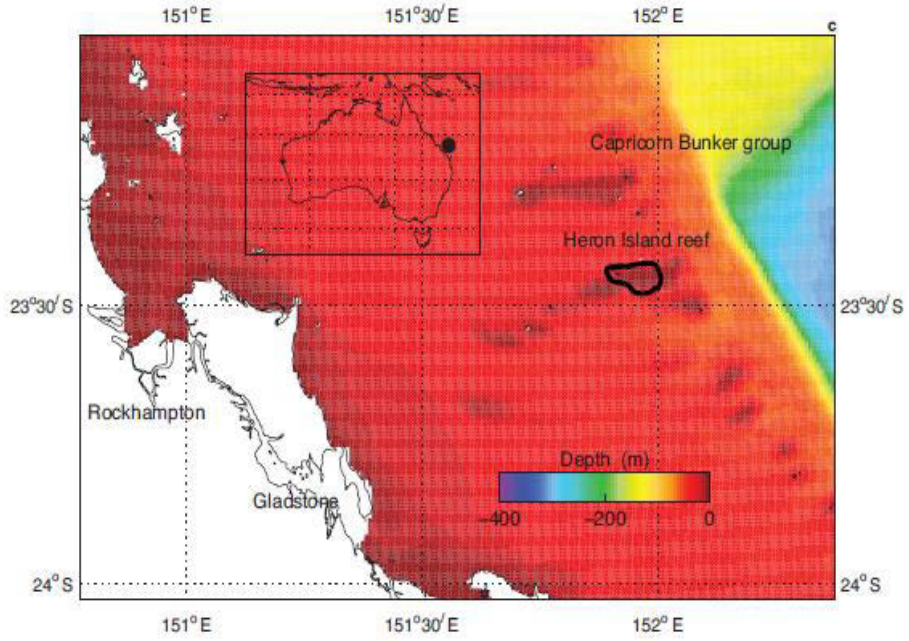

B)

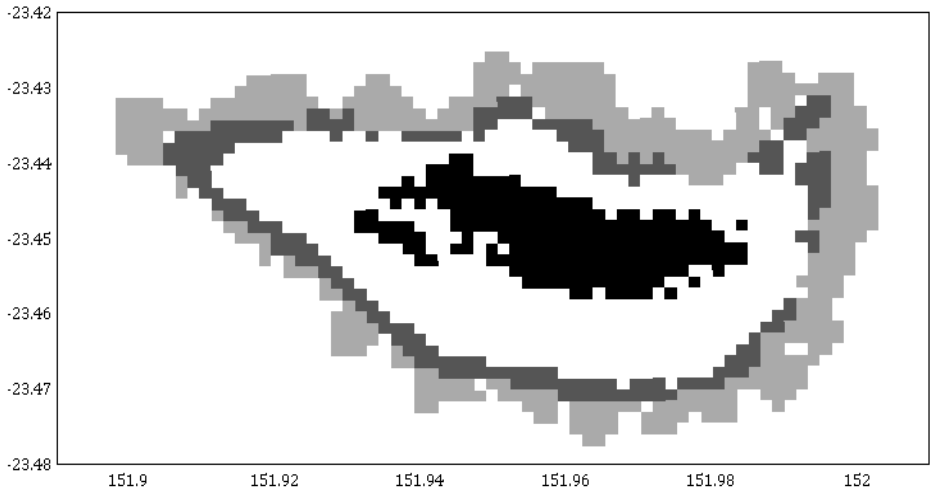

Figure 5.1: Location of Heron Reef, Wistari Reef and One Tree Reef on the Great Barrier Reef (A). Heron Reef with the three different coral zones (B): Black= isolated coral colonies (bommies), dark gray = coral crest, light gray = coral slope.

Heron Reef has a semi-diurnal tide cycle with spring tides of 2.28 m and neap tides of 1.09 m. Due to the shallow nature of Heron Reef, at times the tide may fall below the reef rim, resulting in pooling of water and a higher water level within the lagoon than the surrounding ocean (Gourlay and Hacker 1999). Additionally, the limited water depth and the protection from ocean by the reef rim resulted in wave heights on the reef of less than 0.5 m (Gourlay and Colleter 2005).

5.2.2 Model framework

Hydrodynamic processes were modelled using the Sparse Hydrodynamic Ocean Code (SHOC) (Herzfeld 2006). SHOC is a general purpose hydrodynamic model and has been successfully used for range of applications and scales ranging from estuaries to oceanic (Herzfeld et al. 2010). SHOC is a fully three-dimensional finite-difference baroclinic model based on the three dimensional equations of momentum, continuity and conservation of heat and salt, employing the hydrostatic and Boussinesq assumptions (Boussinesq 1877). The Heron Reef configuration, described in Mongin and Baird (submitted), uses a horizontal rectangular orthogonal grid and fixed vertical coordinates. The Heron Reef model uses semi-Lagrangian advection method to transport biogeochemical and ecological tracer across the reef (Mongin and Baird submitted).

A nested modelling strategy was adopted to reach a resolution of 167 m over Heron Reef. This fine grid was nested within a 1 km regional grid covering the extent of the Great Barrier Reef. In turn, this regional model was nested within a 10 km resolution global circulation model. The regional model determines the boundary conditions for the "fine Heron Reef grid". The 167 m resolution grid was generated from airborne and sonar bathymetry observations at 2m resolution (Hedley et al., 2009). The bathymetry resolves the transition between regions below mean sea level and that at the highest astronomical tide, to allow the model to capture processes in the inter-tidal zone. The model utilises wetting and drying algorithms to exploit the intertidal bathymetric resolution; wetting and drying capability involves the free surface moving through the constant z layers, allowing

a given cell to be emptied of water and remain dry for a period of time before it can be submerged again (Figure 5).

The model included a spectrally resolved optical model with wavebands of 20 nm wavelengths (λ) between 300 - 720 nm and than a waveband of 80 nm between 720 - 800 nm. In addition to the model being run for each of these wavelengths, the model included vertical layers in the water column, with 23 levels between ranging between 0.15 – 68 m below the surface within the Heron grid domain. If a grid cell had a shallower depth than 68 m only the layers above the bottom depth were evaluated for that particular cell.

5.2.3 Water column chemistry model

The water chemistry model primarily intended to understand the drivers of short time-scale variability in the water column carbon chemistry. In the shallow water reef system, benthic and air-sea fluxes are large relative to water column processes. Furthermore, the fluxes associated with changes in benthic cover are small. Thus, we only represent carbon fluxes originating from the benthic communities, in this chapter only corals were considered, on the ocean floor and do not consider changes in benthic biomass with time.

The concentration of dissolved CO_2 and carbonate system species in seawater (inorganic carbon system) can be calculated from other known parameters. Any two of the four parameters including total dissolved inorganic carbon (the total amount of dissolved CO_2, bicarbonate, and carbonate ions), total alkalinity (the excess base in seawater), pH, and the partial pressure of CO_2 can be derived from two other measured parameters.

5.2.4 Ecological model

The coral host-symbiont parameterization was based on a simplified version of the coral symbiosis model by Gustafsson et al. (2013), hereafter referred to as GBR13. The ecology model is different from GBR13 in that the zooxanthellae growth was represented by a microalgae growth model proposed by Baird et al. (2013). In order to reduce numerical/processing complexity for implementation in an ecosystem model, reserves of dissolved nutrients within the coral host and symbiont (C_R^S and C_R^S in GBR13), as well as variable elemental stoichiometry, represented in Gustafsson et al. (2013) and Baird et al. (2013) were not included in the model, hence the assumption that all tissues were in the Redfield C:N:P ratio.

We considered only three state variables associated with the coral, the nitrogen content of the coral host tissue, N^H (eq. 1), and symbiont tissues, N^S (eq. 2), as well as the intracellular chlorophyll concentration of the symbiont cells, *Chl* (eq. 3) (Table 5.1). Exchange between the coral community and overlying water significantly alters the water column concentrations of nutrient both through uptake and release. Dissolved inorganic nitrogen (DIN) (eq. 4-5) and particulate organic nitrogen (PON) (eq. 6, 18, 19) were examined to understand the coral's contribution to the reef environment. The DIN included NO_3 and NH_4. These were differentiated in the water column, but to keep the model complexity down the coral was assumed to have no particular preference for either of the two N species, therefore, contributing to just one DIN pool available for the coral.

The state variables were quantified as mg N, with the exception of Chl, as we assumed a C:N ratio of coral tissue to have a Redfield C:N:P stoichiometry (Redfield et al. 1963), as shown by Muller-Parker et al. (1994). Observations show elevated C:N ratios in nutrient-limited zooxanthellae (Muller-Parker et al. 1994a); however for simplicity we have assumed a Redfield ratio for zooxanthellae and coral tissue. Thus, fluxes of C and P with the overlying water column were directly calculated from N fluxes using the Redfield ratio. The three model state variables for the coral, as well as the changes in organic and inorganic nutrients in the environment caused by the presence of corals are defined in Table 5.1.

Table 5.1: Ecology state variables of the Heron Reef model.

Equation	No.	Description	Unit
$\frac{dN^S}{dt} = \mu_S N^S - T - \zeta_S N^S$	(1)	Change in symbiont N	mg N $m^{-2}d^{-1}$
$\frac{dN^H}{dt} = G' + T - \zeta_H N^H - M_H$	(2)	Change in host N	mg N $m^{-2}d^{-1}$
$\frac{dChl}{dt} = \left(dChl_{syn} - dChl_{dilute}\right) N_{vol}^S S - \zeta_H Chl$	(3)	Change in intracellular Chl concentration	mg Chl $m^{-3}d^{-1}$
$\frac{dNO_3}{dt} = \mu_S^{IN} N^S \frac{NO_3}{DIN}/Dz$	(4)	Change in water column NO_3 concentration	mg N $m^{-3}d^{-1}$
$\frac{dNH_4}{dt} = \mu_{CS}^{IN} N^S \frac{NH_4}{DIN}/Dz$	(5)	Change in water column NH_4 concentration	mg N $m^{-3}d^{-1}$
$\frac{dDet}{dt} = -S_{part} A_{eff} Det \frac{G'}{G} + (1 - f_{remin})\, \zeta_H N^H + M$	(6)	Change in water column labile detritus concentration	mg N $m^{-3}d^{-1}$

5.2.4.1 Coral polyp density

In the Heron Reef model, hereafter referred to as the HR model, the coral host and symbiont were quantified as area biomasses. At low biomass, the area covered by polyps was a linear function of biomass (i.e. two coral polyps cover twice the area as one polyp). As the polyp area approaches and exceeds the projected area (area of the bottom surface), the coral projected area for the calculation of water-coral exchange approaches 1, and becomes independent of biomass. Hence, the effective projected area of the coral community cannot exceed 1 even at high biomass. This is represented using:

$$A_{eff} = 1 - \exp\left(-\Omega_H N^H\right) \quad (7)$$

where A_{eff} was the effective projected area fraction of the coral community (m^2 m^{-2}) and Ω_H was the nitrogen-specific projected area of polyps (m^2 g N^{-1}) (Table 5.3). As the coral is a 3D structure and nutrient can be taken up from all coral surfaces the nitrogen-specific projected area of polyps (Ω_H) exceed the projected area, and was therefore set Ω_H to equal 2. The form of equation 7 can be shown to arise from

the cumulative sum of the probability that coral-polyps will share the same space on a horizontal surface, assuming the distribution of polyps was random implying each polyp's position was independent of all other polyps. To illustrate the behaviour of equation 7, at N^H equal to 0.1, 1, and 10 times Ω_H, the effective projected area fraction of the coral, A_{eff}, was 0.095, 0.63 and 1 respectively, while the surface area of coral to projected area ratio of benthos, $N^H/\exp(-\Omega_H N^H)$ was 1.05, 1.58 and 10 respectively.

5.2.4.1 Uptake of nutrients and particulate matter from the overlying water

The coral was able to assimilate organic nitrogen either through translocation of photosynthates from the symbiont cells or through heterotrophic feeding, capturing particulate organic matter (POM) from the water column (Fitt and Cook 2001; Houlbrèque and Ferrier-Pagès 2009). The maximum flux of organic and inorganic nutrients to the surface of the coral was specified as a mass transfer limit per projected area of coral (Atkinson and Bilger 1992; Baird et al. 2004a), with a mass transfer rate coefficient (S_{DIN}) defined in equation (8) in Table 5.2 (Falter et al. 2004; Zhang et al. 2011). To calculate S we needed to know the Schmidt number (Sc) (eq. 9), which is the ratio of the kinematic viscosity of water, v, and molecular diffusivity of NO_3, D. These two parameters may vary with temperature, salinity and nutrient species (Table 5.3). The rate constant S_{DIN} can be thought of the height of the water column cleared of mass per unit of time by the water-coral exchange.

The capture of organic particles was also represented as an areal flux (eq. 10-11). Ribes and Atkinson (2007) considered whether mass transfer limits apply to particulate matter on reefs, and found for coral rubble communities only a weak velocity dependence, suggesting that active pumping by filter feeders overcame any diffusion limitations (Monismith et al. 2010). Thus, capture of organic particles, G, was represented by a constant rate coefficient, S_{part}, multiplied by the concentration of each of the organic constituents within the water column. The calculated capture rate was limited to the maximum growth rate of the coral tissue, $\mu_H^{max} CH$. Should the potential flux of captured organic particles, G', exceed the

maximum growth rate G, then the flux from each component is multiplied by G'/G (eq. 6). The maximum flux of both nutrient and particulate from the overlying water are multiplied by the effective projected area fraction of the coral (A_{eff}).

Table 5.2: Model equations associated with corals

Equation		Description	Units
$S_{DIN} = 2850(2\tau)^{0.38}Sc^{-0.6}$	(8)	Mass transfer rate coefficient of DIN	m d^{-1}
$Sc = \frac{\omega}{D}$	(9)	Schmidt number	-
$G' = min\begin{cases}\mu_H^{max}N^H \\ G\end{cases}$	(10)	Total heterotrophic feeding rate	mg N $m^{-2}d^{-1}$
$G = S_{part}A_{eff}(PON)$	(11)	Potential heterotrophic feeding rate	mg N $m^{-2}d^{-1}$
$\mu_S = min\begin{cases}\mu_S^{max} \\ (\mu_S^{IN} + f_{remin}\zeta_H N^H)/N^S\end{cases}$	(12)	Total symbiont growth rate	d^{-1}
$\mu_S^{IN} = min\begin{cases}\mu_S^{max} \\ k_I \\ k_N/(\delta_N N^S) \\ k_P/(\delta_N N^S)\end{cases}$	(13)	Symbiont growth rate due to uptake of inorganic compounds for the water column and light absorption	d^{-1}
$k_I = k_I^S\left(\frac{R_N}{R_I}\right)S$	(14)	N equivalent photon absorption for symbiont population	mol N $m^{-2}d^{-1}$
$k_N = S_{DIN}A_{eff}DIN\delta_N$	(15)	Potential uptake rate of DIN	mol N $m^{-2}d^{-1}$
$T = (\mu_S N^S + f_{remin}\zeta_H N^H)f_{N^S 2N^H}$	(16)	Translocation of N from symbiont to host	mg N $m^{-2}d^{-1}$
$M = M_{reject} + M_H$	(17)	Total mucus	mg N $m^{-2}d^{-1}$
$M_{reject} = max\begin{cases}\mu_S N^S + f_{remin}\zeta_H N^H - \mu_S^{max}N^S \\ 0\end{cases}$	(18)	Mucus production due to unwanted host death	mg N $m^{-2}d^{-1}$
$M_H = max\begin{cases}\mu_H N^H - \mu_H^{max}N^H \\ 0\end{cases}$	(19)	Mucus production due to excess nutrient	mg N $m^{-2}d^{-1}$
$dChl_{syn} = Chl_{max}\mu_S^{max}ChlsynfactorI_q$	(20)	Rate of chlorophyll synthesis	mg Chl $m^{-3}d^{-1}$
$dChl_{dilute} = (1 - f_{N^S 2N^H})\mu_S Chl_{cell}$	(21)	Rate of chlorophyll delusion	mg Chl $m^{-3}d^{-1}$
$f_{N^S 2N^H} = \frac{S{r_S}^2\pi}{N^H\Omega_H}$	(22)	Translocation factor mediated by space limitation	-
$I_q = min\begin{cases}1 \\ k_I/(\mu_S^{max}I_{cell}) \\ k_I/(S_{DIN}A_{eff}DIN/I_{cell})\end{cases}$	(23)	Light limiting factor (0-1)	-
$S = \frac{N^S}{N_{cell}}$	(24)	Symbiont cells per m^2 coral surface	cell m^{-2}
$N_{cell} = N_m^S R_N N_{mw}$	(25)	Nitrogen content of symbiont cell	mg N $cell^{-1}$
$DIN = NO_3 + NH_4$	(26)	Total dissolved inorganic nitrogen in the water column	mg N m^{-3}
$N_{vol}^S = \frac{4\pi{r_S}^3}{3}$	(27)	Symbiont cell volume	m^3
$Chl_{cell} = \frac{Chl}{N_{vol}^S S}$	(28)	Chlorophyll concentration per symbiont cell	mg Chl $cell^{-1}$
τ	(29)	Shear stress on the bottom	N m^{-2}
$k_I^S = I\pi r_S$	(30)	Photons impacting each symbiont cell	mol photon $m^{-2}s^{-1}$
$\zeta_H = 0.01N^H$	(31)	Quadratic mortality rate of coral	s^{-1}

Table 5.3: Model parameters

Symbol	Description	Value	Unit
μ_H^{max}	Maximum coral host growth rate	0.05	d^{-1}
μ_S^{max}	Maximum coral symbiont growth rate	0.4	d^{-1}
S_{part}	Rate coefficient for particle capture	12	m d^{-1}
Dz	Depth of the water	-	m
R_N	Redfield ratio N to P	16	mol N mol P^{-1}
R_I	Redfield ratio Quanta to P	1060	mol quanta mol P^{-1}
N_{mw}	Molecular weight of nitrogen	14.01	g N mol^{-1}
δ_N	Conversion factor mg N to mol N	0.001/14.01	-
δ_P	Conversation factor mg P to mol P	0.001/30.97	-
D	Molecular diffusivity of NO_3	$f(Temp, A_{eff})$~17.5x10^{-10}	m^2s^{-1}
υ	Kinematic viscosity of water	$f(Temp, A_{eff})$~1.05x10^{-6}	m^2s^{-1}
I_{cell}	Energy content of symbiont cell	R_I/R_N	mol quanta $cell^{-1}$
r_S	Coral symbiont cell radius	5x10^{-6}	m
Ω_H	Nitrogen-specific projected area of polyp	2	m^2g N^{-1}
Chl_{max}	Maximum intracellular *Chl* concentration	3.15x10^6	mg Chl m^{-3}
f_{remin}	Remineralised fraction of coral mortality	0.5	-

5.2.4.2 Light capture by zooxanthellae

The HR model only considered one photosynthetic pigment, chlorophyll *a* (Chl). The zooxanthellae varied their intracellular chlorophyll content depending on potential light limitation of growth, and the incremental benefit of adding pigment due to the package effect (Baird et al. 2013).

5.2.4.3 Light attenuation through corals

The light incident upon the zooxanthellae, E, was assumed to be the down welling irradiance from the bottom of the overlying water column. Using scalar irradiance microprobes, Wangpraseurt et al. (2012) found in coral tissue of 1 mm thickness that the scalar irradiance at the bottom of the tissue layer was 10% of the surface irradiance. Thus, in healthy coral, absorption was much greater than scattering,

and down-welling light was a reasonable approximation of scalar irradiance incident upon the zooxanthellae. In bleached corals (no zooxanthellae), scattering of light by the coral skeleton became greater than absorption in the coral tissue, and the scalar irradiance at the coral tissue surface could reach 150% of the unbleached corals (Wangpraseurt et al. 2012). In such a case, down-welling light was a poor approximation of scalar irradiance, but bleaching was not considered in the model.

The light field experienced by all zooxanthellae within a particular model grid cell was assumed to be the same, although in reality zooxanthellae are often found in two vertically distinct layers (Berking 2007). Given this assumption of equal light exposure, and that the symbionts themselves were the dominant cause of light attenuation within the coral tissue, the average scalar irradiance at wavelength λ that the cells were exposed to, $E_{av,\lambda}$ was given by:

$$E_{av,\lambda} = \frac{E_{top,\lambda}(1-e^{\alpha_\lambda n_{N^S}})}{\alpha_\lambda n_{N^S}} \tag{32}$$

where $E_{top,\lambda}$ was the irradiance above the corals, $E_{av,\lambda}$ was the mean irradiance experienced by all zooxanthellae, $n_S = N^S/N_{cell}$ was the areal density of zooxanthellae cells, where N_{cell} was the nitrogen content of a single cell. The absorption cross-section of the zooxanthellae cells was calculated using geometric optics, and changes as a function the dynamic intracellular chlorophyll concentration as detailed in the next section.

5.2.4.4 Absorption by zooxanthellae

The absorption-cross section (α) of a spherical cell of radius (r), pigment-specific absorption coefficient (γ), and homogeneous intracellular pigment concentration

(C), was calculated using geometric optics (i.e., ray tracing) without considering internal scattering (Duyens 1956; Kirk 1975):

$$\alpha = \pi r^2 \left(1 - \frac{2(1-(1+2\gamma Cr)e^{-2\gamma Cr}}{(2\gamma Cr)^2}\right) \quad (33)$$

where πr^2 was the projected area (PA) of a sphere, and the bracketed term was 0 for no absorption (γCr = 0) and approaches 1 as the cell became fully opaque (γCr → 1). The pigment-specific absorption coefficient (γ) was wavelength-dependent. The rate of light absorption by a cell with an absorption cross-section α was αE, where E is the photon flux to the surface (μmol photon m^{-2} s^{-1}). The rate of photons absorbed across all wavelengths was given by:

$$k_I^S = \int \alpha_\lambda E_\lambda d\lambda \quad (34)$$

The rate of photon absorption per cell, k_I^S was used to calculate light absorption by the symbiont population (k_I) in equation 14 which in turn was used to determine symbiont growth rate due to light absorption (eq. 13).

5.2.4.5 Zooxanthellae growth

In the absence of internal nutrient reserves, zooxanthellae growth (μ_S^{max}) (eq. 12-15) is considered as the minimum of the maximum fluxes of nutrient and energy transferred to the cell, and the maximum growth rate (Everett et al. 2007). The potential flux of inorganic nitrogen (k_N) (eq. 15) was assumed to be equally available to each symbiont, and the flux of photons (k_I) (eq. 14) to be equal for all cells. This form of growth limitation was similar to the law of the minimum (Von

Liebig and Playfair 1840), with the difference that the maximum growth rate appears within the minimum term (eq. 12). By including μ_S^{max} within the minimum operator, the exponential temperature dependence of the maximum growth rate did not impact the temperature-independent growth under low light, or the non-linear temperature-dependent processes of diffusion of nutrient ions into the coral surface (Baird et al. 2003).

5.2.4.6 Translocation between zooxanthellae and coral tissue

The translocation of photosynthates from the coral symbiont to the host was defined by a variable fraction of the total N taken up by the symbiont (eq. 16). The translocation factor was determined by the size of the symbiont population, as it approached its maximum, the translocation fraction asymptotes to 1, hence all new carbon fixed by the symbiont is released to the host (eq. 22). Similarly, when the symbiont population approaches zero the translocation fraction reduces to zero. This definition of translocation does not take into account the host 'release factor', a chemical agent in the host tissue which allows the host to actively extract newly produced photosynthates (Gates et al. 1995; Davy and Cook 2001a). However, the current definition is a computationally less expensive option, which still provides a variable translocation rate, and for this particular study we wish to focus on the coral-environment interaction.

5.2.4.7 Mucus production

The main release of C and N from the coral occurs through the excretion of mucus from mucocytes on the coral surface (Bythell and Wild 2011). However, in the HR model the term mucus incorporates all C and N released from the coral into the water column, including unused C and N, dead tissues and respiration by-products (eq. 17). The two main drivers of mucus production were first; unwanted metabolic host waste products, where if the symbiont was unable to take up these metabolic by-products it was excreted as mucus (eq. 18). Second, all N taken up or

translocated to the host above the host's maximum growth rate was excreted as mucus (eq. 19). This may not be the ideal definition of mucus production but as the HR model did not include C or N reserves excess nutrient had to be released. All mucus was assumed to become a part of the PON concentration in the bottom water layer.

5.2.4.8 Mortality of coral polyps

Mortality in the model was represented by the mortality of the entire polyp (ζ_H) affecting both coral and zooxanthellae biomass. The polyp mortality term had a quadratic mortality coefficient, ζ_H (eq. 31), that stabilised the biomass of coral tissue to μ_H/ζ_H. As the HR model did not include any separate respiration term we assumed that the quadratic mortality term incorporated all death plus respiration by-products. The remineralisation factor (f_{remin}) represents the fraction of polyp mortality that corresponded to respiration and therefore became available to the symbiont as a source of nutrient. The remaining fraction ($1 - f_{remin}$) was set to be dead coral tissues and therefore released into the water column, where it became incorporated into the particulate organic nitrogen (PON) pool. As mentioned above, C and N released was thought of as mucus, and incorporated in the mucus term (eq. 17). The definitions and parameterisation of mortality and mucus production in the HR model are further discussed in the discussion.

5.2.4.9 Intracellular chlorophyll

Intracellular chlorophyll concentration was increased through the synthesis of pigment (eq. 20) and reduced through the sharing of pigment between offspring during cell division (eq. 21). The mortality of both the entire coral polyp and the zooxanthellae affected the chlorophyll density per m^2, although because chlorophyll was specified as an intracellular concentration, these terms do not appear explicitly in the equations in Table 2. If chlorophyll were quantified per m^2, then the loss terms for chlorophyll due to mortality would be $\zeta_H N^H Chl$. Since

chlorophyll is considered a small proportion of the cellular nitrogen, neither the synthesis nor loss appear as terms in the equations for N^S. The rate of chlorophyll synthesis was parameterised as a maximum rate, reduced by a factor representing the incremental benefit to absorption by adding further pigment, and a factor representing the degree of light limitation (Eq. 23).

5.2.5 Model setup

Forcing data, output from the regional nesting model and observations were all available for the month of January in 2010. We ran the model twice for a period of one month to spin-up the model (i.e., allowing initial fluctuations depending on initial conditions to settle before the initiating the final simulation). Thereafter the model was restarted for the same month (January 2001) with the initial conditions given at the end of the spin-up months. The 30 d simulation captures the full spring-neap tidal cycle for the Heron Island region, as well as some synoptic variability in the weather system.

To assess the change in water nutrient status as a function of water residence time over different parts of the reef, a diagnostic age tracer was used (Hall and Haine, 2002). The tracer concentration was initialised to 1 within the reef domain (corresponding to the area covered by the benthic communities). The age tracer was advected and diffused on the grid by the hydrodynamic model. When inside the reef domain, the age increased at the rate of 1 per h. When the age tracer was outside the reef region, its age is reduced at the rate of 10% per day (Mongin and Baird submitted).

The process of spinning up the model prior to the final simulation was essential as the initial conditions were difficult to establish, due to the lack of quantitative measurements of coral biomass on a reef scale. Therefore the initial condition for the coral and symbiont biomass at the start of the spin-up run were set to be 1 g N m^{-2} for the host and 0.2 g N m^{-2} for the symbiont population. Symbiont chlorophyll was set to be 0.1 g Chl m^{-2}. NH_4, NO_3 and PON advected in from the ocean were set

to have a fixed boundary condition at the edge of the fine Heron grid equal to 1, 10 and 10 mg N m^{-3} respectively (Koop et al. 2001; Wyatt et al. 2012). These fixed boundary conditions were set to ease the understanding of what are reef processes, by excluding open-ocean water processes.

5.3 RESULTS

To ease the analysis of the model output we selected two 24 h periods on the 7-8th and the 18-19th of January 2001 which were examined more closely. The 7-8th was characterised by high water velocity ($P^{high}_{velocity}$) over the reef, and the 18-19th was characterised by low water velocity ($P^{low}_{velocity}$) (Fig. 5.2). Changes in water velocity may influence nutrient concentrations in the water column as well as uptake rates (Atkinson et al. 2001). Additionally both periods had one high tide and one low tide during the day and the night. The tidal range for both periods was approximately 1.6 m and the average water velocity at the ocean surface for the 'high' velocity period ($P^{high}_{vlocity}$) was 0.35 m s^{-1} and 0.15 m s^{-1} for the 'low' velocity period ($P^{low}_{velocity}$). These water velocities are similar to measurements recorded by Wyatt et al. (2010) with values ranging between 0.1-0.25 m s^{-1} across a reef.

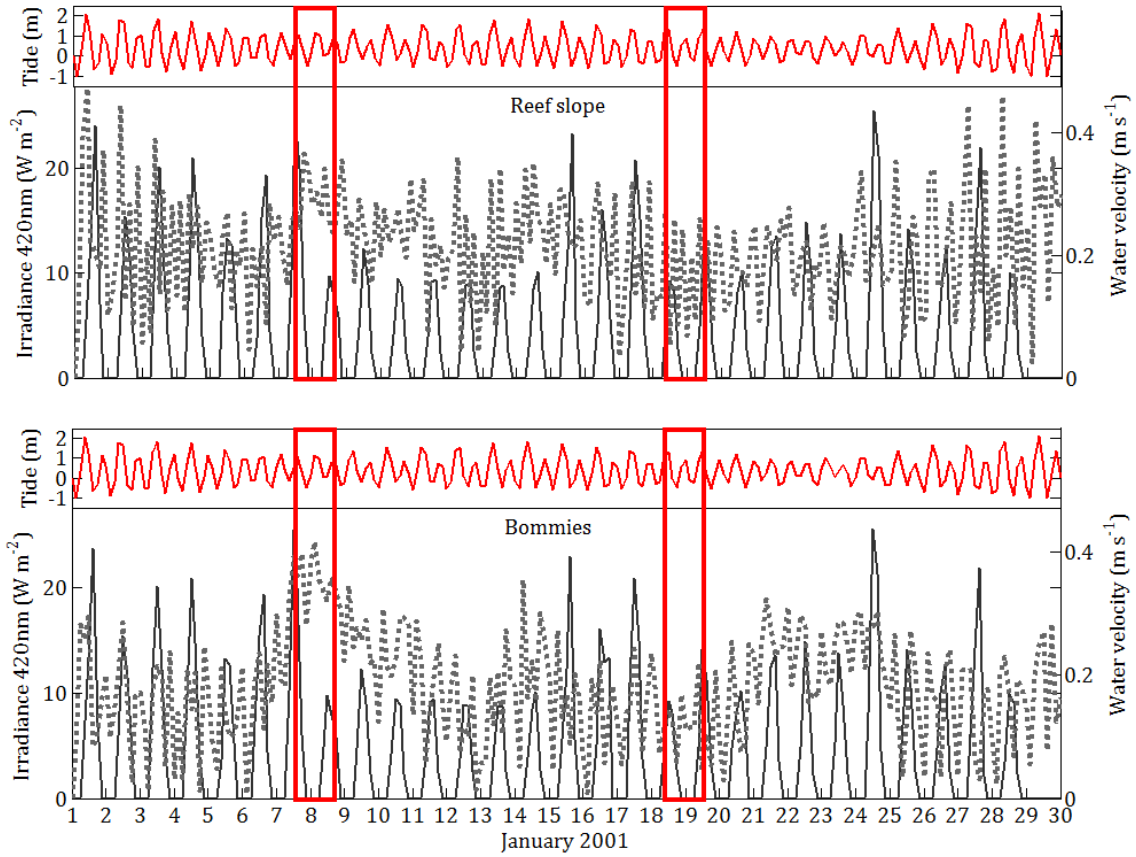

Figure 5.2: Red line represents the surface elevation, dashed the water velocity and the solid black line the solar irradiance at 420 nm for two sites on the reef: Reef slope (top panel) and bommies (bottom panel). The red boxes show the two selected periods: 7-8th ($P^{high}_{velocity}$) and 18-19th ($P^{low}_{velocity}$).

The model was set to output the rates and the state variables of the model every 3 h. This gave a total of eight output points per 24h period (Fig. 5.3). Each output point was given a letter for identification, as shown in Figure 5.3. As the modelled month was January (summer) the hours of day light exceeded the hours of darkness, hence only three of the output points took place during night and five during daylight under a 24 h period.

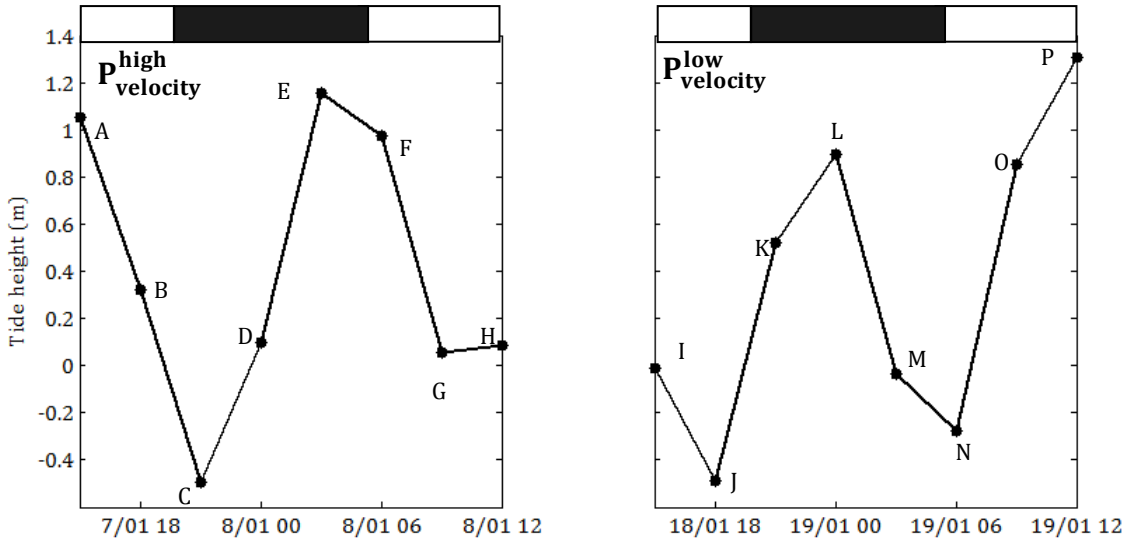

Figure 5.3: Tidal height for $P^{high}_{velocity}$ and $P^{low}_{velocity}$. Letters indicate the output points and the black and white bars represent night and day, respectively. The x-axis shows the date and local time of day.

5.3.1 Water column nutrients

5.3.1.1 PON

For $P^{high}_{velocity}$ the current moved water over Heron Reef generally in a westerly or north-westerly direction for all output points. $P^{low}_{velocity}$ on the other hand, had a more varying current direction, but was characterized by low water velocity over Heron Reef (Fig. 5.4).

At the boundary of the Heron Reef grid domain the concentration of PON was set to be 10 mg N m^{-3}. In $P^{high}_{velocity}$, water approaching the Heron Reef had a concentration of PON which reached 12 mg m^{-3} in places (Fig. 5.4). At the first two output points (3 pm and 6 pm) on the 7th January (Fig 5.4 A and B) the concentration of PON over Heron Reef was high with values approaching 12 mg N m^{-3}. The high concentration surrounding the reef indicates PON is being produced on the reef and is advected off by the currents. Just after dusk at 9 pm on the 7th of January (Fig 5.4 C) the concentration above the reef was reduced to values

between 9 and 10 mg N m^{-3}. These values were even further reduced moving into to the night (Fig 5.4 D and E), when the water over the western part of the reef was reduced to 6 mg N m^{-3}. This pattern could be explained by the current pushing PON rich water over the reef rim from the east, and due to the coral feeding heterotrophically during night. The water became depleted in PON as it moved over the reef towards the west. After dawn on the 8th January (Fig 5.4 F) the effect of the nightly reduction over the reef was still visible, but moving in to the day the concentration was increased again (Fig 5.4 G and H).

The $P_{velocity}^{high}$ case also showed a large area surrounding Heron Reef with relatively high PON concentration, whereas the $P_{velocity}^{low}$ case showed only a small area of high PON east of Heron Reef (Fig. 5.5). Additionally, the $P_{velocity}^{low}$ period showed PON reduction over large areas surrounding Heron Reef, with concentrations as low as 6-7 mg N m^{-3}. As the current version of the Heron Reef model included corals which could take up and release PON, but no other living organisms with similar processes, the change in PON was mainly caused by the coral community. Therefore, this reduction in PON depended on PON uptake by the coral community, and the advection of this PON-poor water off the reef. Low water velocity during $P_{velocity}^{low}$ as well as the preceding days was the most likely reason for this PON depletion as less PON was brought in through the grid boundaries. Above Heron Reef the concentration of PON showed a varying pattern with areas of high PON concentration (Fig. 5.5). The currents in $P_{velocity}^{low}$ did not wash PON-rich water off the reef, allowing an accumulation PON above the reef due to mucus production.

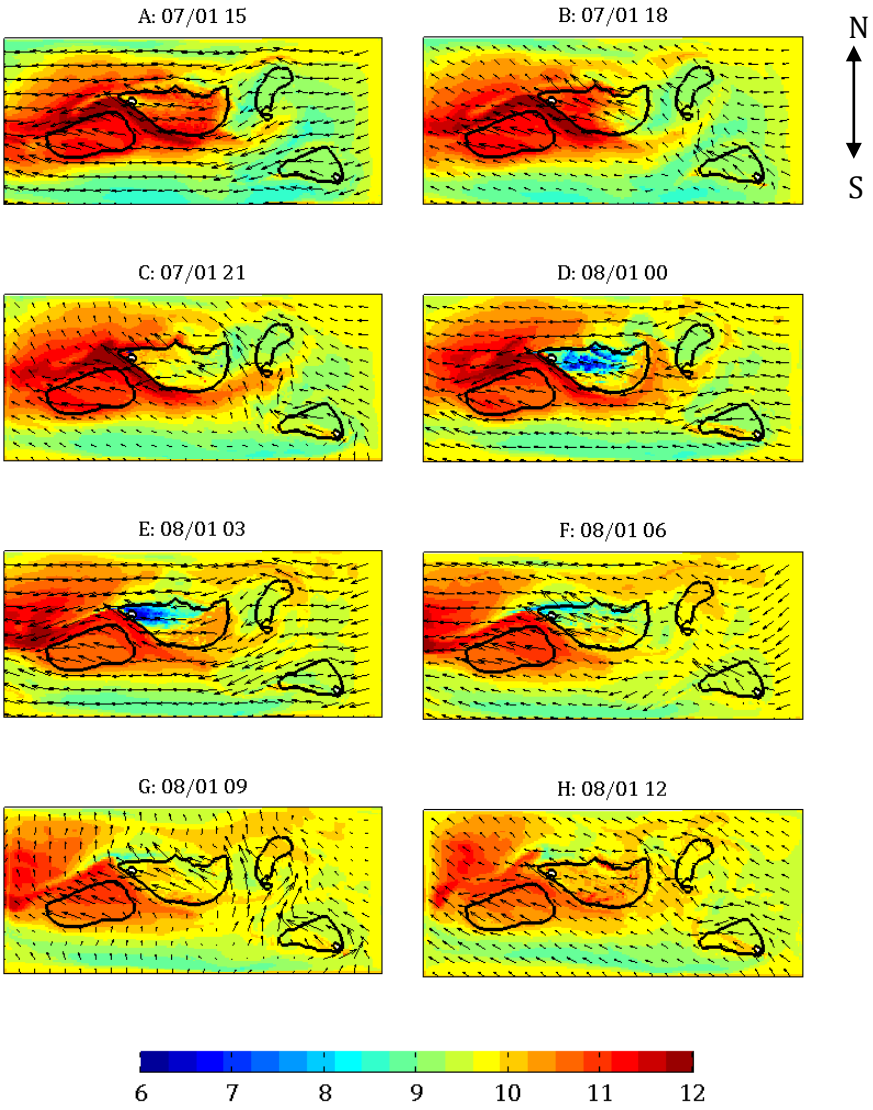

Figure 5.4: PON at the surface of the water column for $P_{velocity}^{high}$ in unit mg N m^{-3}. The title of each panel states the time point letter as well as the date and time of day. Arrows represent the current direction and strength. The black contour marks the rim of the reefs.

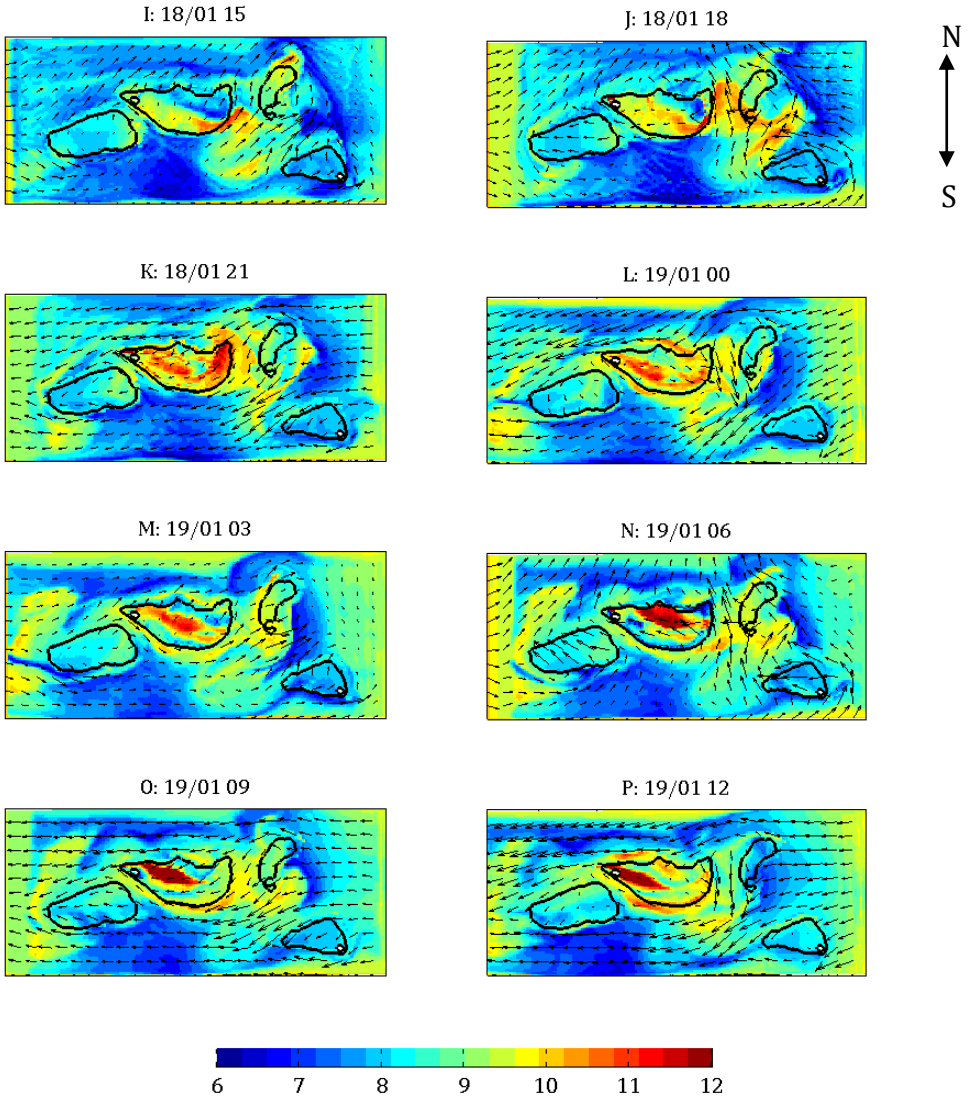

Figure 5.5: PON at the surface of the water column for $P^{low}_{velocity}$ in unit mg N m^{-3}. The title of each panel states the time point letter as well as the date and time of day. Arrows represent the current direction and strength. The black contour marks the rim of the reefs.

5.3.1.2 DIN

The concentration of DIN in the water column before moving over Heron Reef was 11 mg N m^{-3} (same as set at the Heron grid boundary). At the start of $P^{high}_{velocity}$ water moved in over the reef from the east (Fig. 5.6 A-B), the DIN concentration in the

water was reduced as it moved over the reef, due to daytime uptake by the coral community. During the first two time points after sunset, when no additional DIN uptake by the corals took place, the reduced DIN concentration over the reef was pushed off the reef towards the west (Fig. 5.6 C-D).

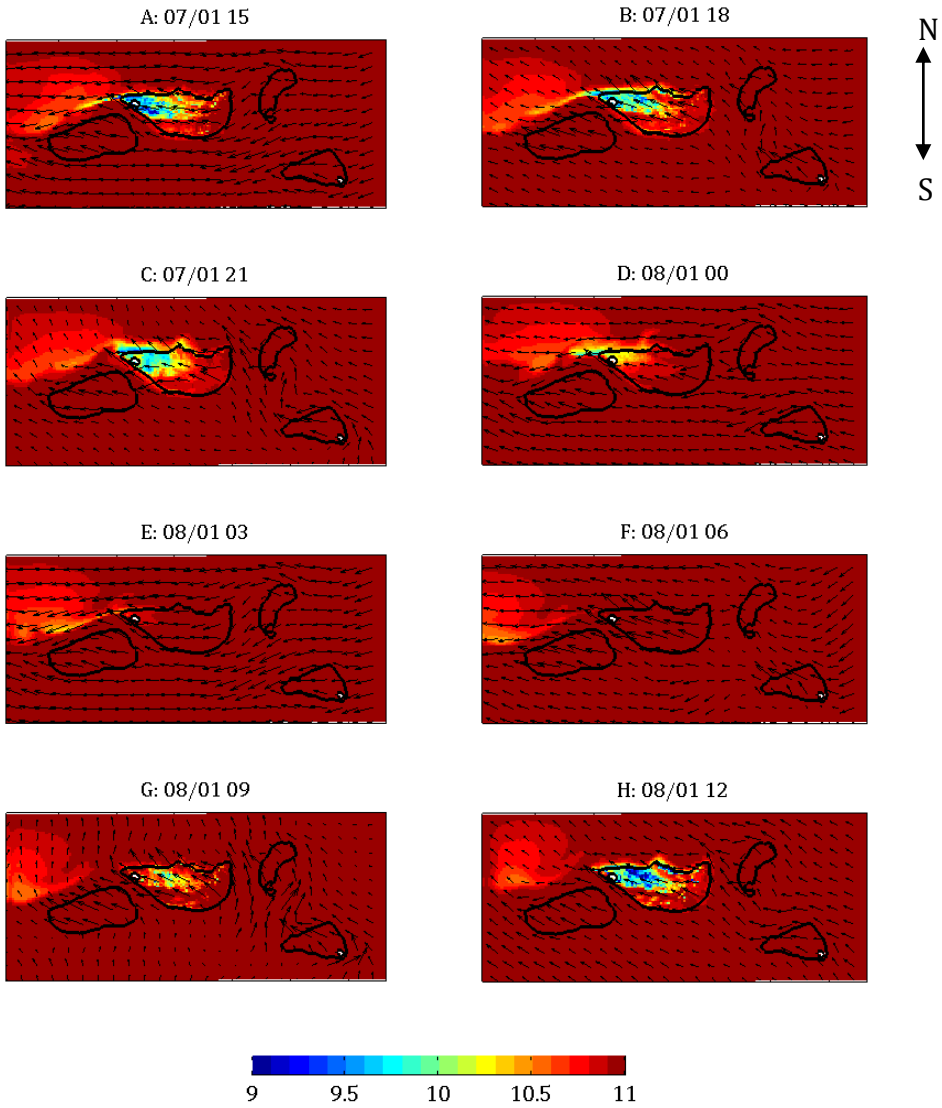

Figure 5.6: DIN at the surface of the water column for $P^{high}_{velocity}$, unit mg N m^{-3}. The title of each panel states the time point letter as well as the date and time of day.

In $P^{low}_{velocity}$ the DIN concentration over the reef, as well as a small area surrounding Heron Reef, was reduced for all time points (Fig. 5.7). The low DIN concentration

over Heron Reef in $P^{low}_{velocity}$ was associated with low exchange of ocean water over the reef caused by low water velocity, DIN uptake as well as the reversal of currents due to the tides. In contrast to PON, the coral model did not include any release of DIN, as we assumed that all loss of N from the coral were organic, therefore only reduction of DIN could take place as a result of the presence of corals.

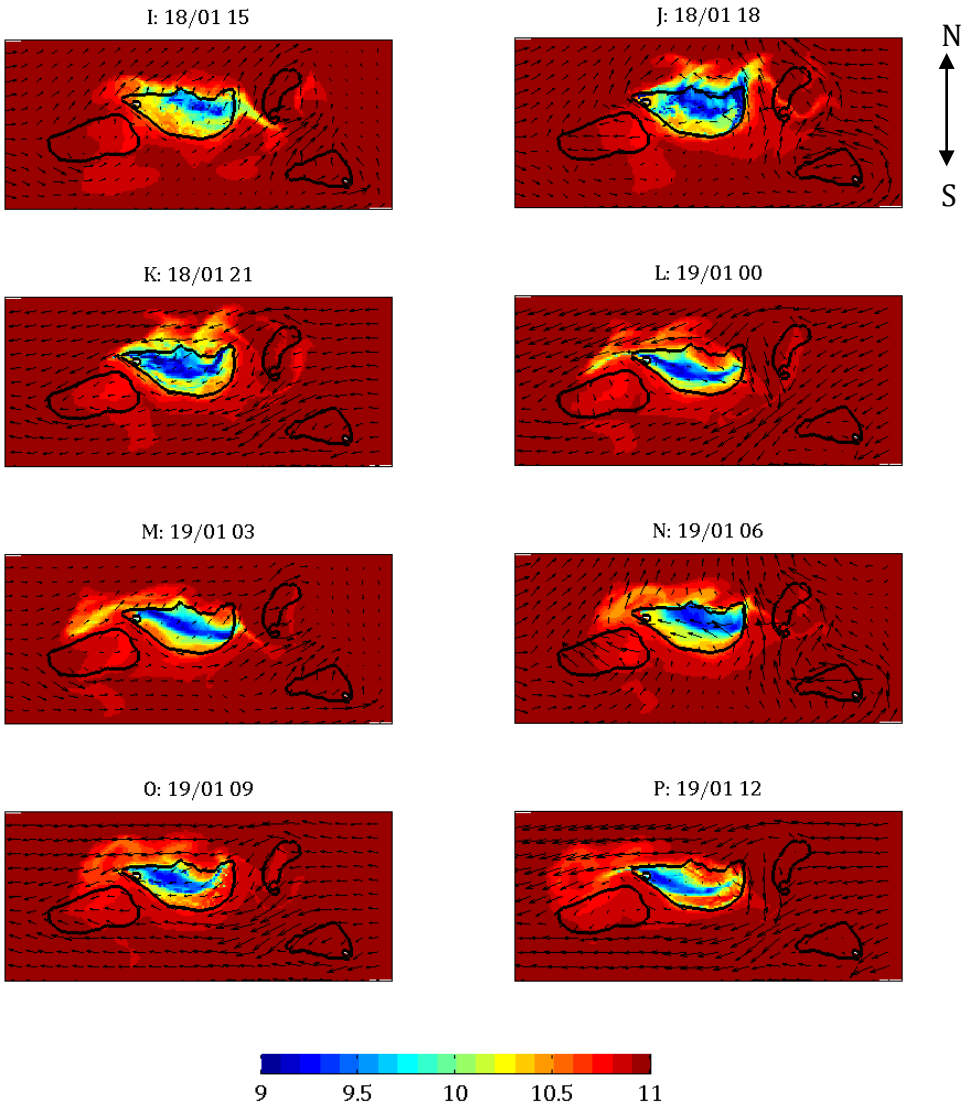

Figure 5.7: DIN at the surface of the water column for $P^{low}_{velocity}$, unit mg N m^{-3}. The title of each panel states the time point letter as well as the date and time of day. Arrows represent the current direction and strength. The black contours mark the rim of the reefs.

The concentration of PON and DIN in Figures 5.4 - 5.7, as well as the age tracer in Figures 5.9 - 5.10 used the values at the ocean surface. As many of the biological and geochemical processes take place at the ocean floor we thought it important to check whether the vertical change in nutrient concentration, age and the water velocity were negligible. Therefore, we selected three sites over the reef with different substrate (reef, bommies and sediment) and plotted the vertical profiles (Fig. 5.8). The two time points selected for these vertical profiles were F and K (see Fig. 5.3) as these had the most different concentrations of DIN and PON.

The results showed that the vertical change in DIN, PON and age were low. The lack of change with depth indicated that the vertical mixing above the reef was sufficient to eliminate any vertical stratification. The water velocity however showed a small reduction with depth for all sites and both periods, as a result of bottom friction. Therefore, when considering the uptake of nutrient by the coral the water velocity at the seabed was used rather than the surface velocity.

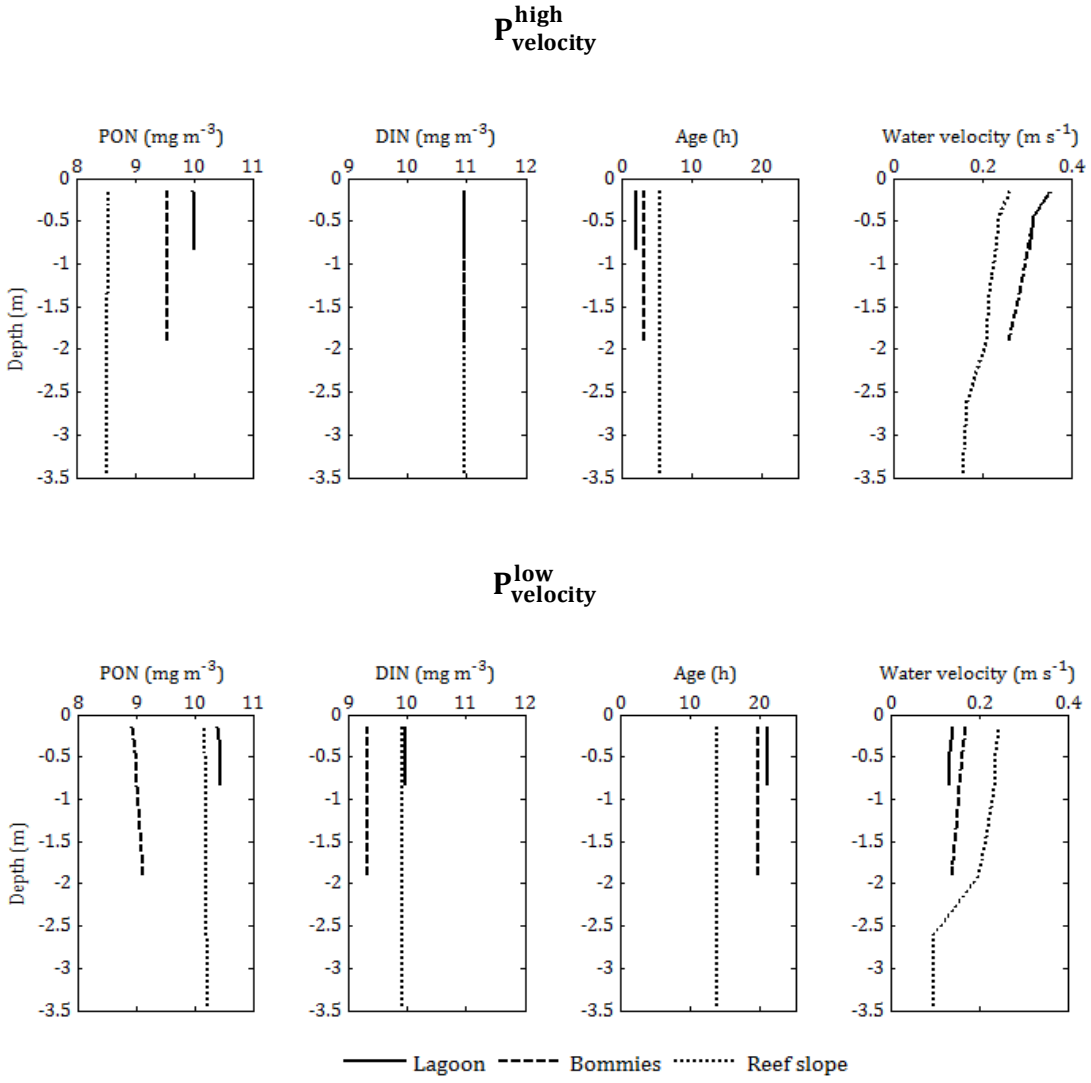

Figure 5.8: Vertical profiles of PON, DIN, Age and water velocity from three sites on the reef (lagoon, bommies and reef slope). The top row of panels represents the values from $P^{high}_{velocity}$ and the bottom row $P^{low}_{velocity}$.

5.3.2 Age tracer and water nutrient content

The $P^{high}_{velocity}$ and $P^{low}_{velocity}$ periods showed significant differences in the water residence time, here referred to as the water age, over the reef. $P^{high}_{velocity}$ had no water with an age greater than 15 h, and the average water age over the reef was

approximately 5 h for the whole period (Fig. 5.9). The greatest ages were found on the west side of the reef throughout $P_{velocity}^{high}$, as the current moved water over the reef from the east towards the west. The second period ($P_{velocity}^{low}$) had water residing over the reef with an age of up to 50 h. The water age increased throughout $P_{velocity}^{low}$ as a result of the persistent low water velocity (Fig 5.10).

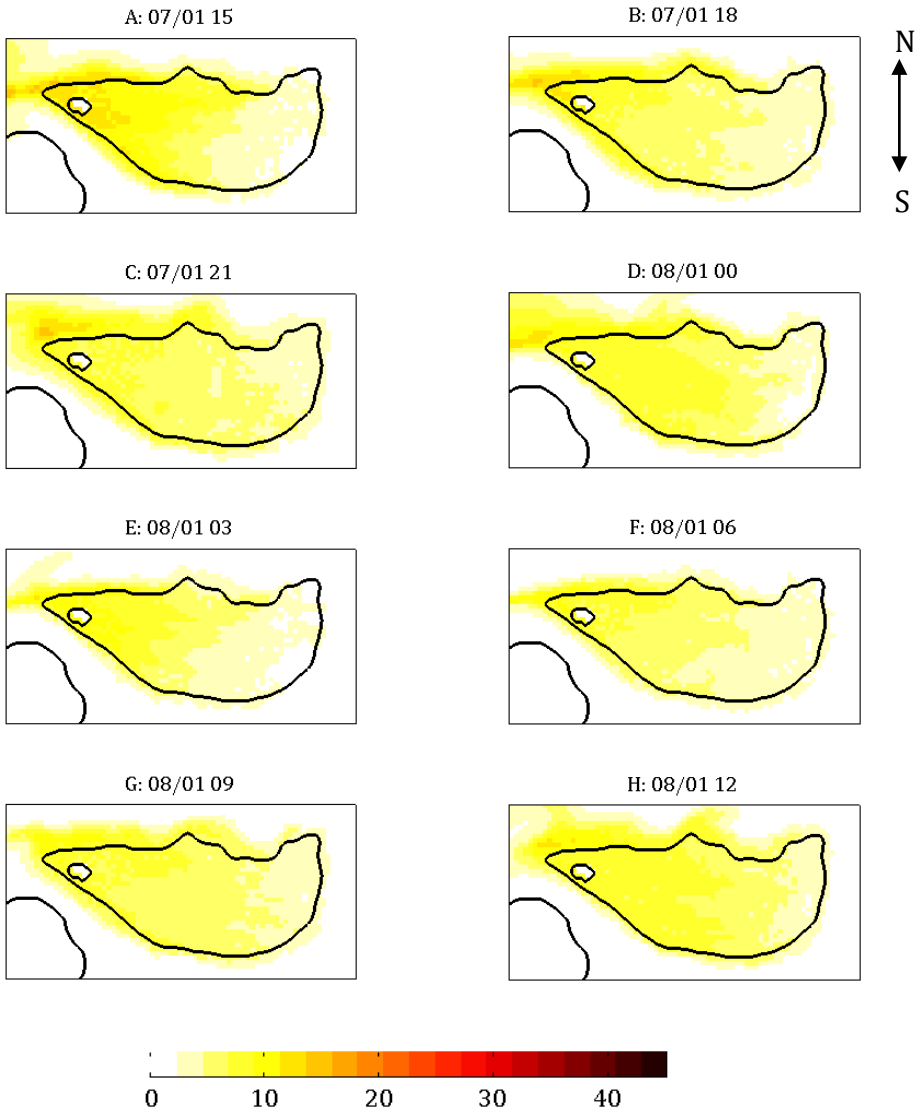

Figure 5.9: Age of water at the surface over the reef for $P_{velocity}^{high}$, units: hours.

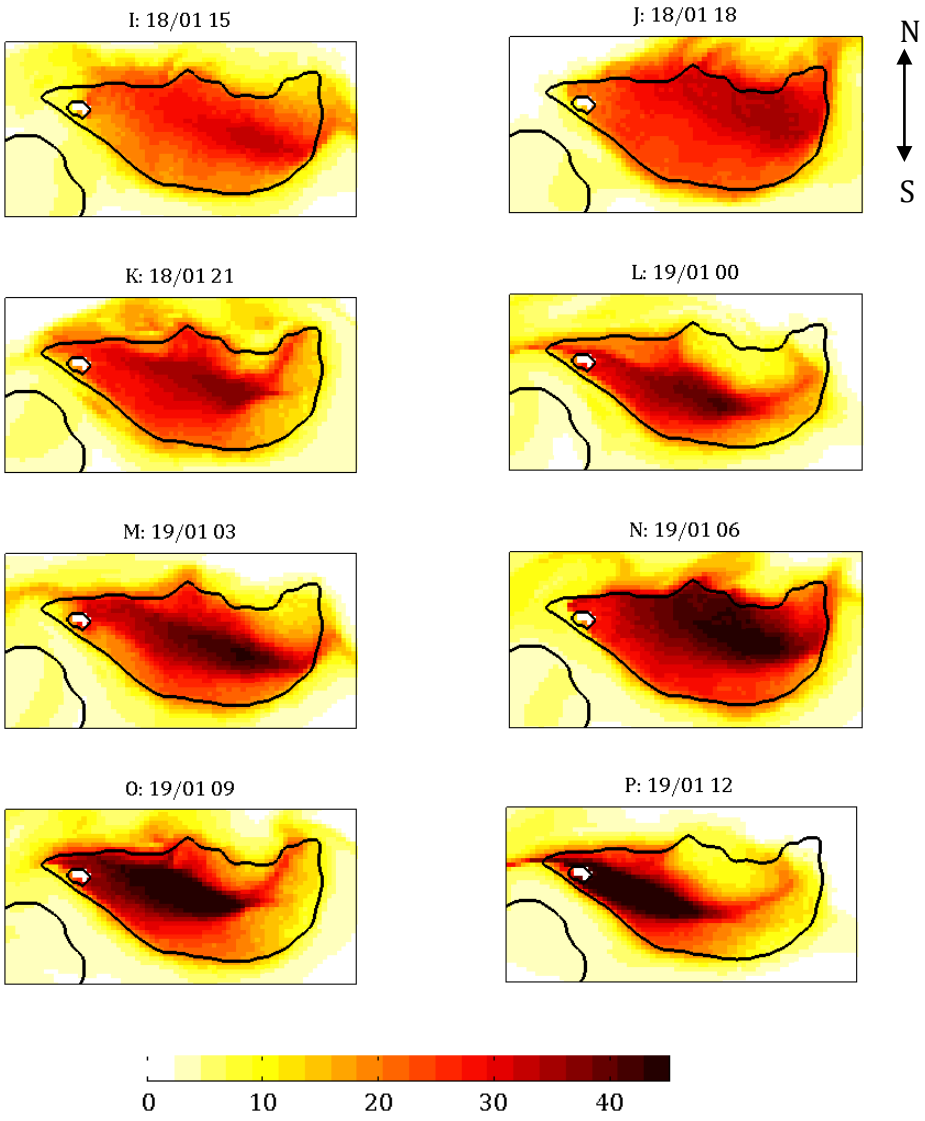

Figure 5.10: Age of water at the surface over the reef for $P^{low}_{velocity}$, units: hours.

5.3.3 Coral biomass

The biomasses of host and symbionts were relatively similar between the two periods, with 0 to 40 mg N m^{-2} higher values in $P^{low}_{velocity}$ (Fig. 5.11). In both periods the symbiont and host biomass at the crest and the slope were approximately twice the biomass of the corals growing at the bommies. The host biomass was highest at the deeper parts of the reef slope below 5 m, and the lowest biomass

was at the western part of the bommies. The symbiont population did not have the same clear increase in biomass with depth, but the western part of the slope and the inner part of crest had the highest biomass.

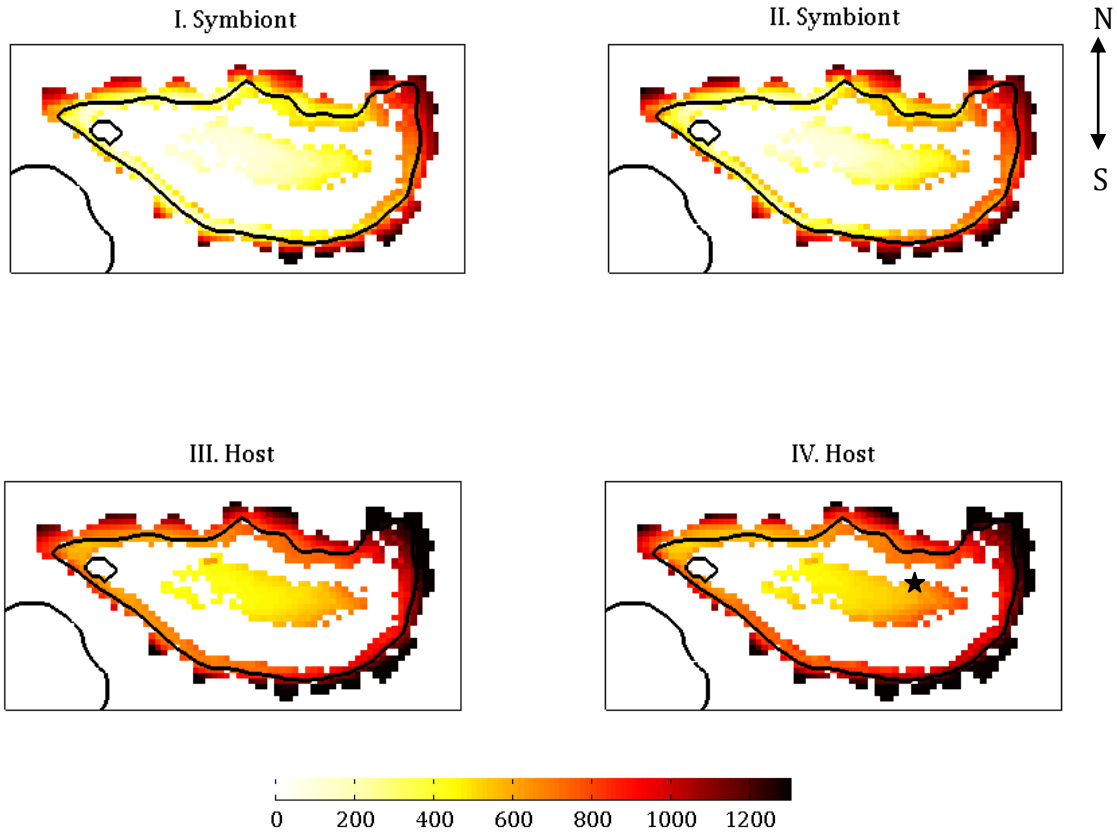

Figure 5.11: Mean biomass of coral host and symbiont popuation for $P_{velocity}^{high}$ (I and III) column) and $P_{velocity}^{low}$ (II and IV) in mg N m^{-2}. The star in IV shows the location of the point evaluated in Figure 5.12.

The results show that periods of reduced coral growth coincide with low water velocity, whereas periods of enhanced coral growth was associated with high water velocity. The PON and DIN concentration fluctuated diurnally throughout the whole month. The DIN concentration remained at approximately the same average daily values right through the month, whereas there was a slight reduction in daily mean PON concentration and a greater diurnal fluctuation associated with

spring tides. For the two periods ($P^{high}_{velocity}$ and $P^{low}_{velocity}$) considered in this study the tidal range was approximately the same, removing this tidal-dependent change in nutrient concentration. However, this may be important to consider in the future.

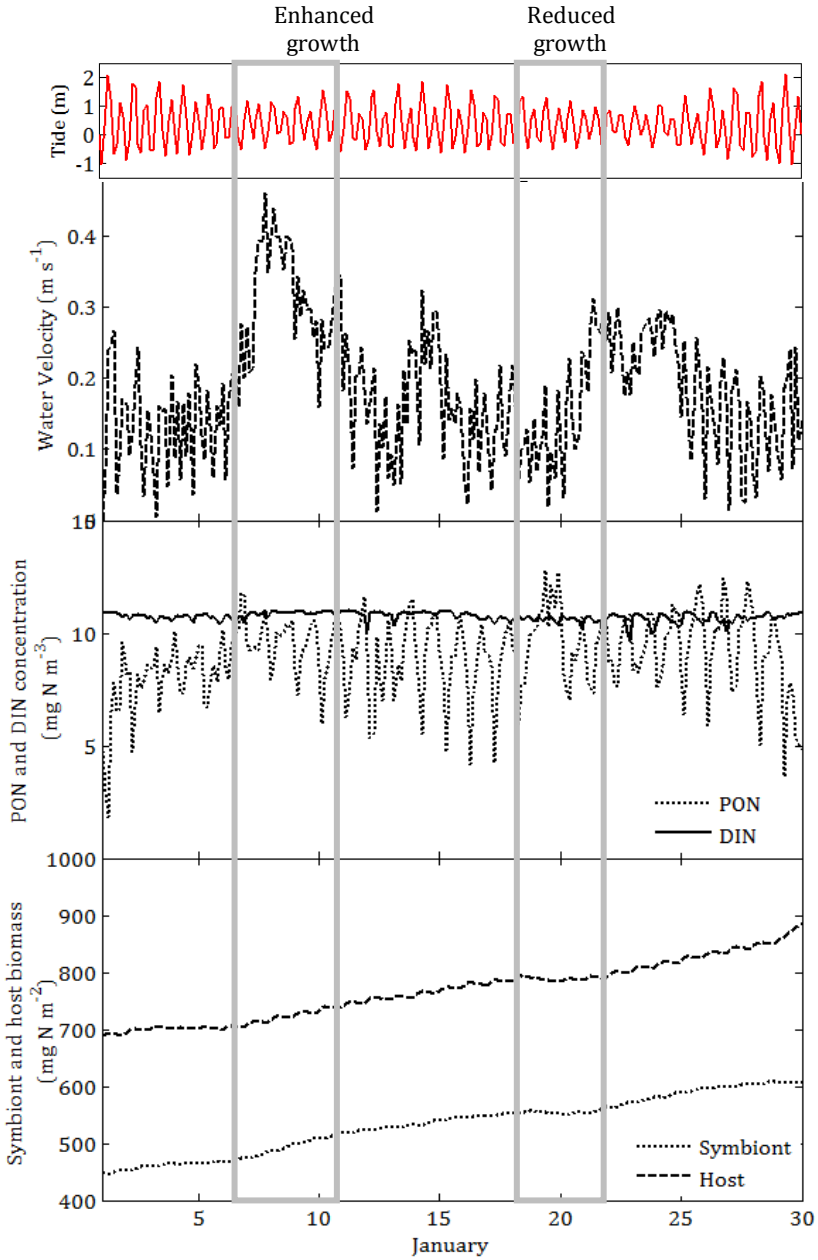

Figure 5.12: Simulated change in coral biomass, PON concentration, DIN concentration, tidal height and water velocity for one point at the bommies during the month of January, the location of the point is shown in Figure (5.11 IV). The rectangles show two periods of coral growth, one "enhanced" and one "reduced".

5.3.4 Coral nutrient uptake and release

5.3.4.1 DIN

The $P_{velocity}^{high}$ period showed higher DIN uptake rate than $P_{velocity}^{low}$, however, during both periods the highest uptake was around the reef crest, and at the eastern side of the reef slope (Fig. 5.13). The total DIN uptake at the bommies for $P_{velocity}^{high}$ ranged between 20 and 30 mg N m^{-2} d^{-1}, close to that of the reef crest (15 to 35 mg N m^{-2} d^{-1}), even though the biomass at the bommies was approximately half that of the crest. It should be noted here that the biomass in $P_{velocity}^{low}$ was 0 to 40 mg N m^{-2} higher than in $P_{velocity}^{high}$, which could reduce the difference between the two periods. This variation between the two periods depended on current strength and subsequent mass transfer rate coefficient (S_{DIN}). The variation within and between the two periods seemed to a lesser extent dependent on the DIN concentration in the water column.

The mass transfer rate coefficient, S_{DIN}, was a function of bottom shear stress, and it ranged between 1 – 5 m d-1 in $P_{velocity}^{high}$ at the bommies and the reef crest. In $P_{velocity}^{low}$, the S_{DIN} ranged between 0 – 3 m d-1 with the highest uptake occurring at the reef crest and slope (Fig. 5.14). The general S_{DIN} value was higher for $P_{velocity}^{high}$ due to the stronger currents characterizing this period, and S_{DIN} was the main cause of the coral-associated DIN uptake pattern. Back calculation of the DIN uptake rates revealed that for all daytime time points the symbiont growth was DIN uptake limited (k_N) and not limited by light (k_I). Hence the uptake in Figure (5.13) equaled $S_{DIN} A_{eff} DIN$ (eq. 15).

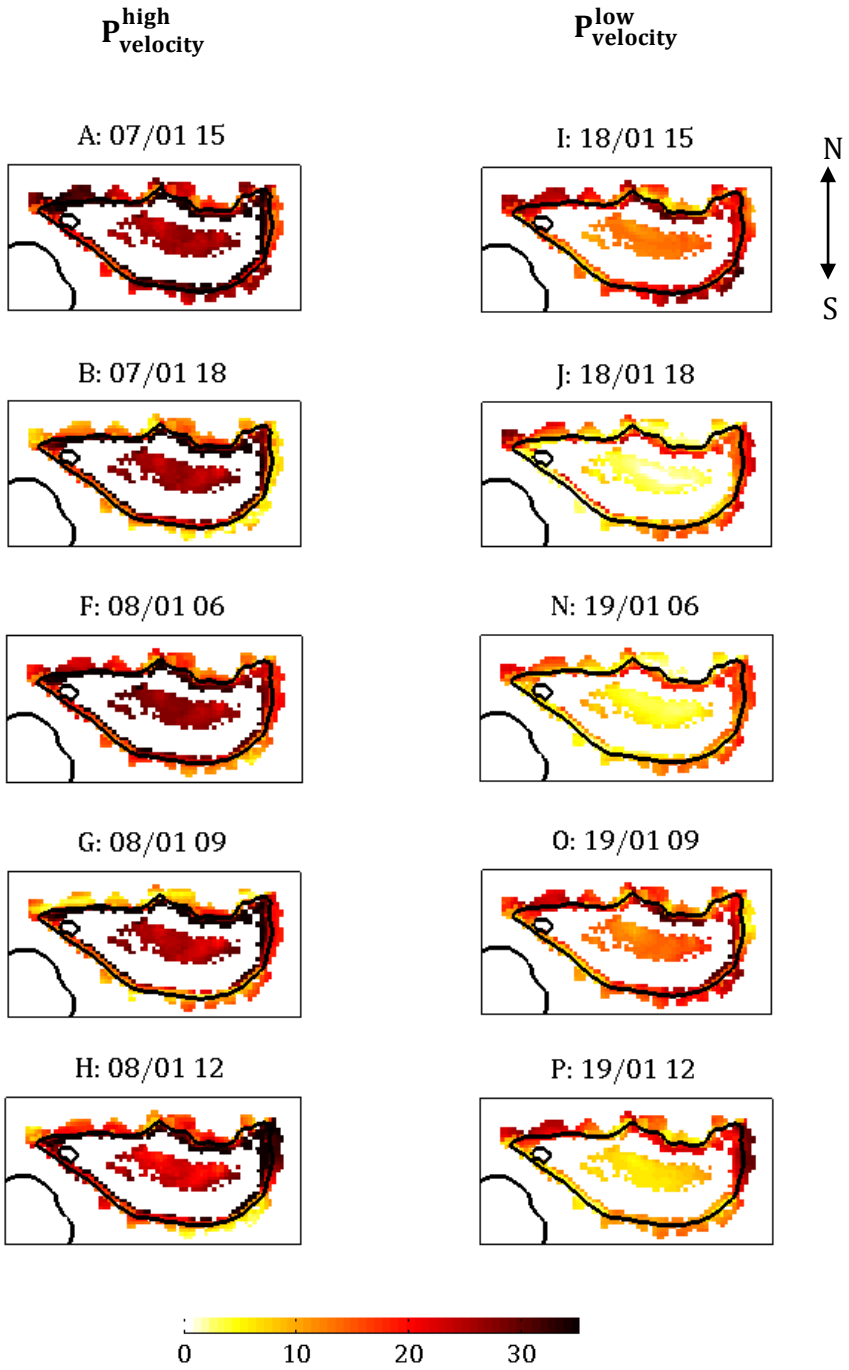

Figure 5.13: Uptake rate of inorganic nitrogen by corals (mg N m^{-2} d^{-1}).

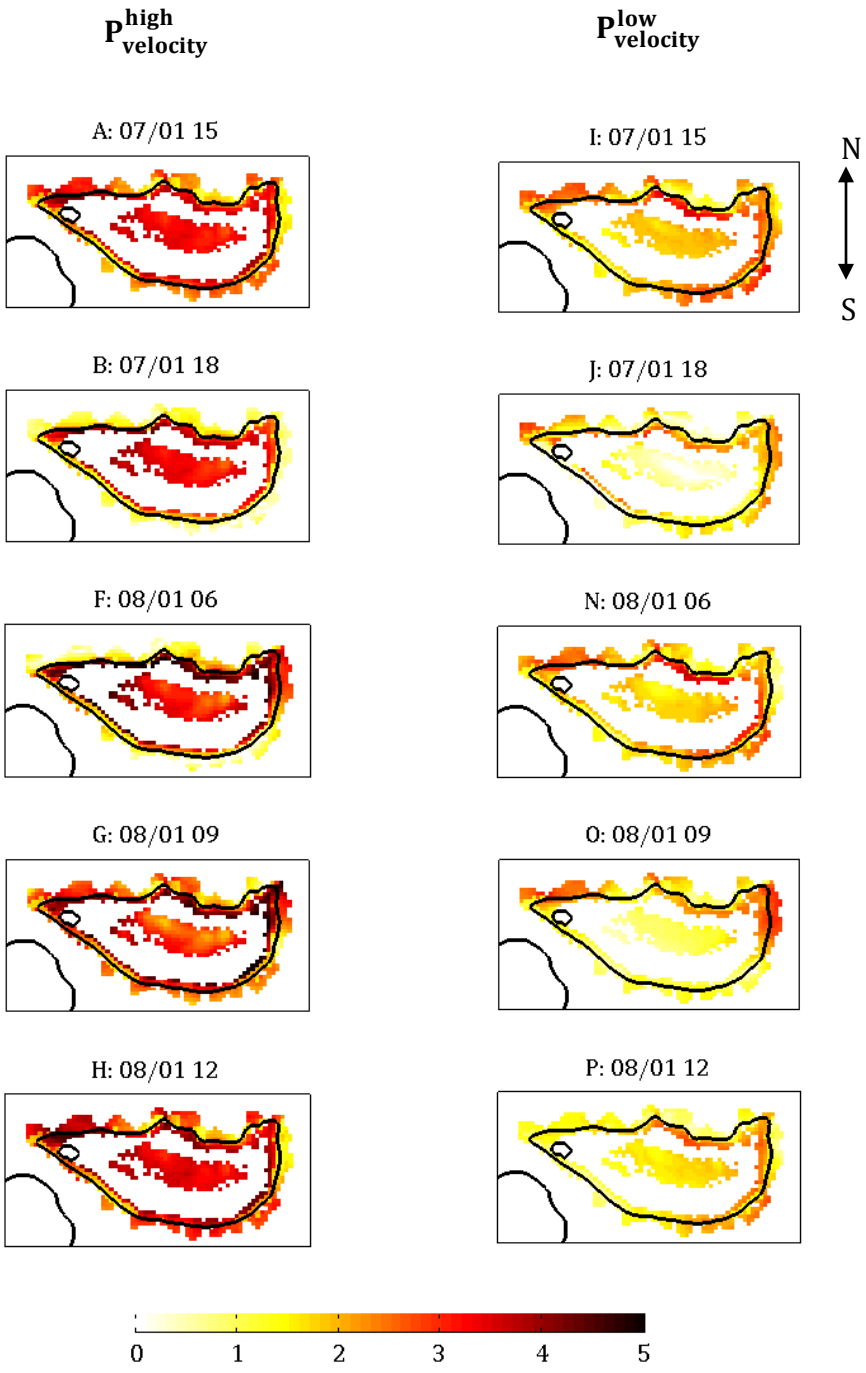

Figure 5.14: Mass transfer rate coefficient (m d^{-1}) over the corals.

5.3.4.2 PON

Total heterotrophic feeding rate (G') on PON showed similar patterns over the reef for all nighttime points in both periods (Fig. 5.15). Overall, the heterotrophic

feeding rate at the bommies was approximately half that of the crest and slope. The PON heterotrophic feeding rate was approximately 2% higher in $P^{low}_{velocity}$ than in $P^{high}_{velocity}$ across the whole reef (Fig 5.15).

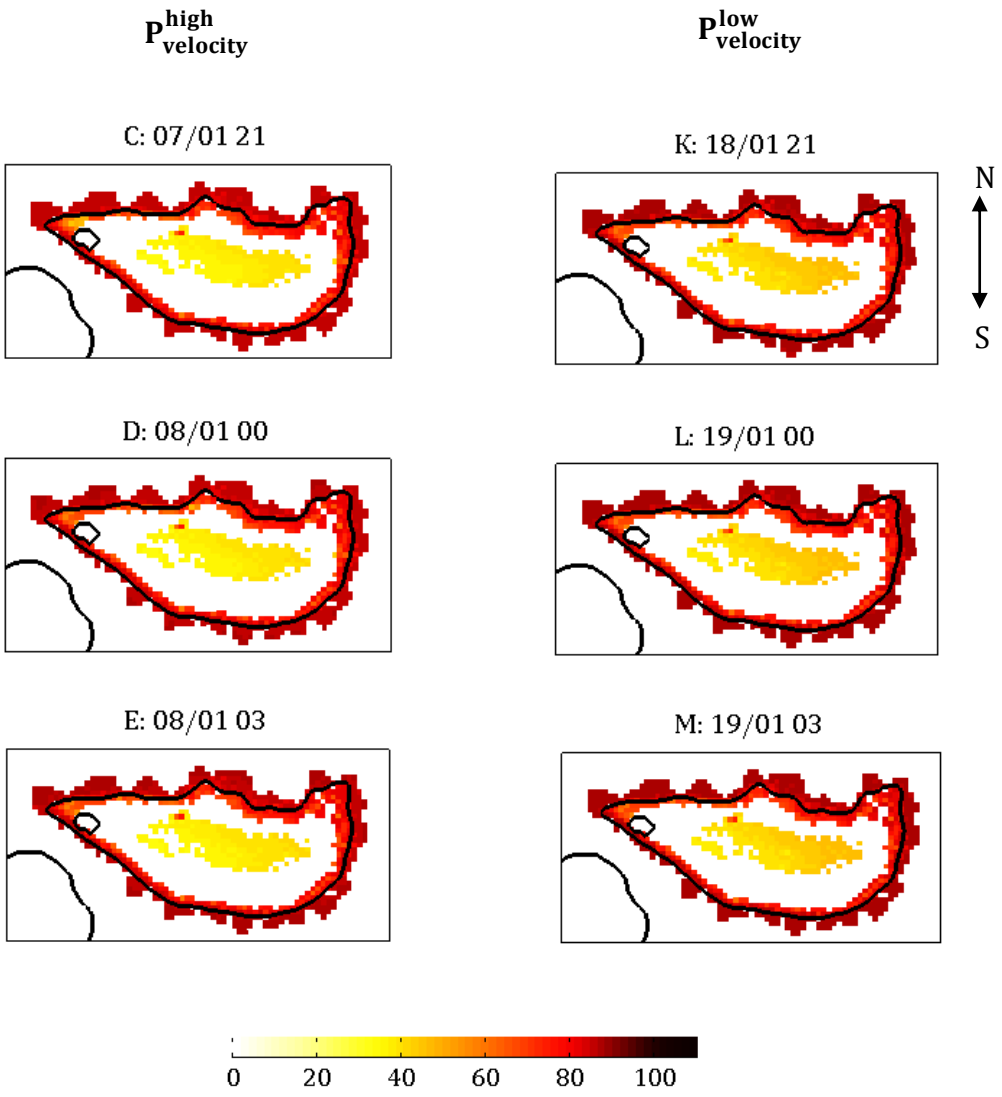

Figure 5.15: Uptake rate of organic nitrogen by corals through heterotrophic feeding (mg N m^{-2} d^{-1}). Note that the letter representing each panel corresponds to the time point identification in Figure 5.3.

The total heterotrophic feeding rate was almost 50% smaller than the potential heterotrophic feeding rate (Fig 5.16). This potential heterotrophic feeding rate during $P^{low}_{velocity}$ was almost as high at the bommies as it was at the reef crest and

slope. $P^{high}_{velocity}$ gave a similar result but here the rates were slightly lower at the bommies, particularly toward the west. This difference between total and potential heterotrophic feeding rates showed that the total heterotrophic feeding was limited by the host's maximum growth rate for that particular biomass, as the total heterotrophic feeding rate was set to equal the minimum of the host maximum growth rate and the potential heterotrophic feeding rate (eq. 10).

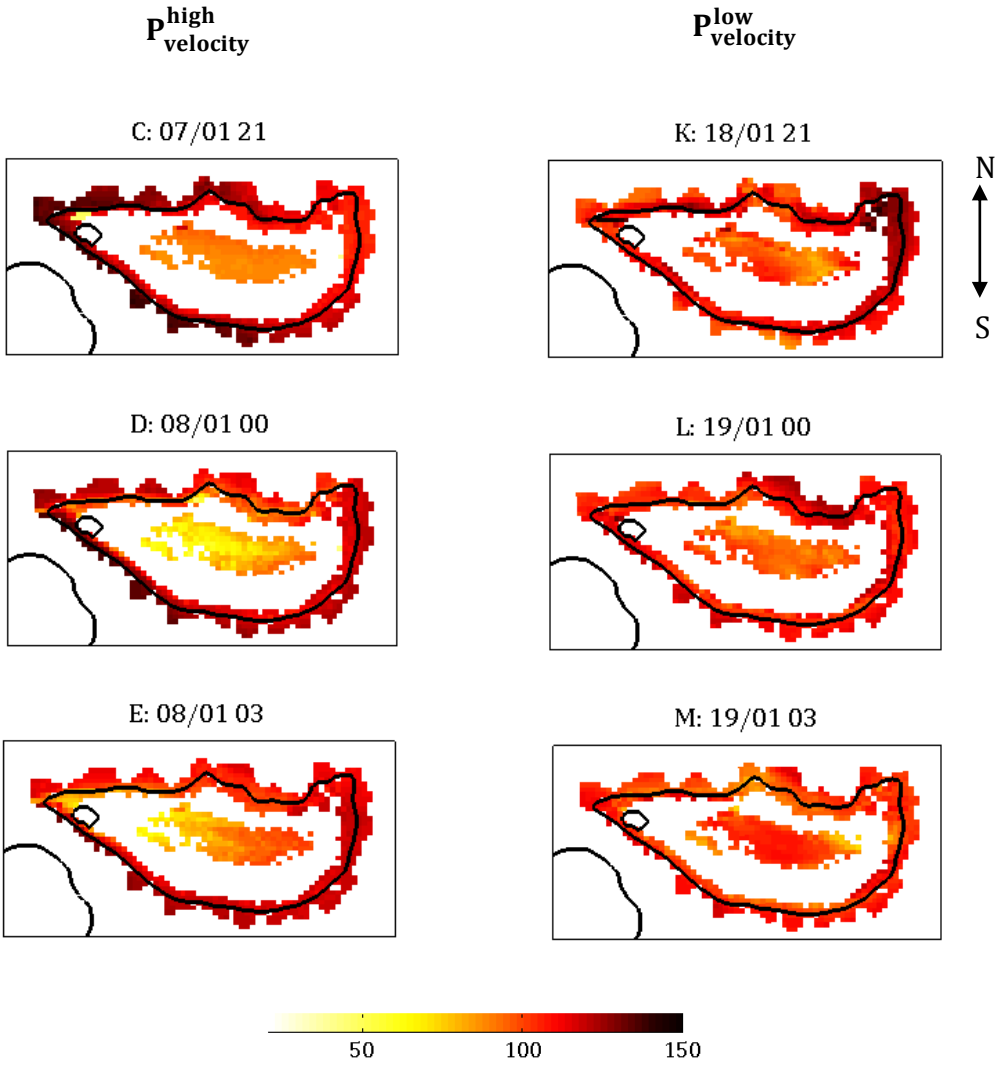

Figure 5.16: Potential uptake rate of organic nitrogen by corals through heterotrophic feeding (mg N m^{-2} d^{-1}). Note that the letter representing each panel corresponds to the time point identification in Figure 5.3.

5.3.5 Water column change in pH

Photosynthetic processes, here represented by DIC uptake, may influence water pH over the reef. This was visible in $P^{low}_{velocity}$ where the pH was reduced by 0.2 over the reef (Fig 5.18). This may seem like a small number, but putting it into context, ocean acidification due to increased levels of CO_2 in the atmosphere have caused a global drop of ocean pH of 0.1 since the beginning of the industrial revolution (Sabine et al. 2004).

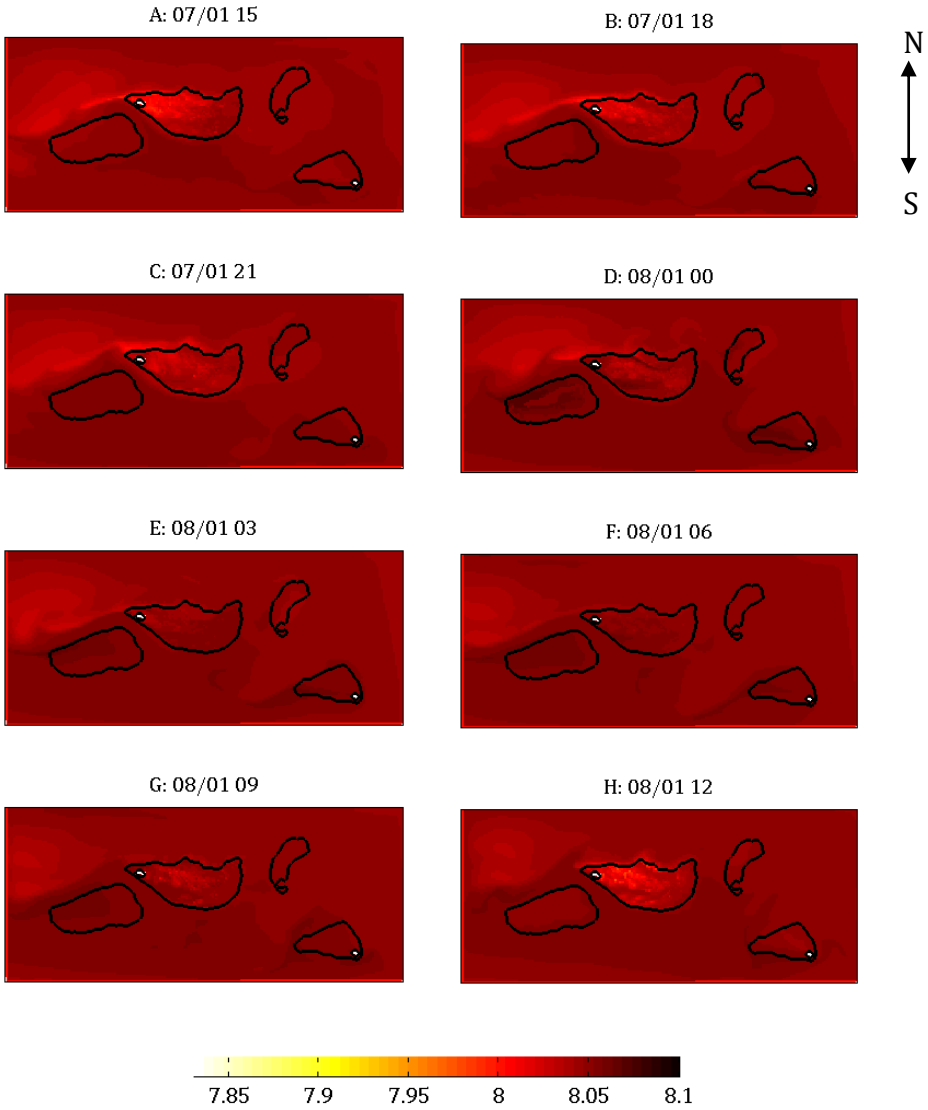

Figure 5.17: Surface water pH during $P^{high}_{velocity}$.

During $P_{velocity}^{high}$ a decrease in pH of less than 0.1 was detected (Fig. 5.17). The reason for the greater reduction in pH during $P_{velocity}^{low}$ was due to that the water remained over the reef for longer periods of time, during which calcification and respiration could lower the pH. Although not shown here the aragonite saturation state of the water followed the same pattern as the pH for all output points.

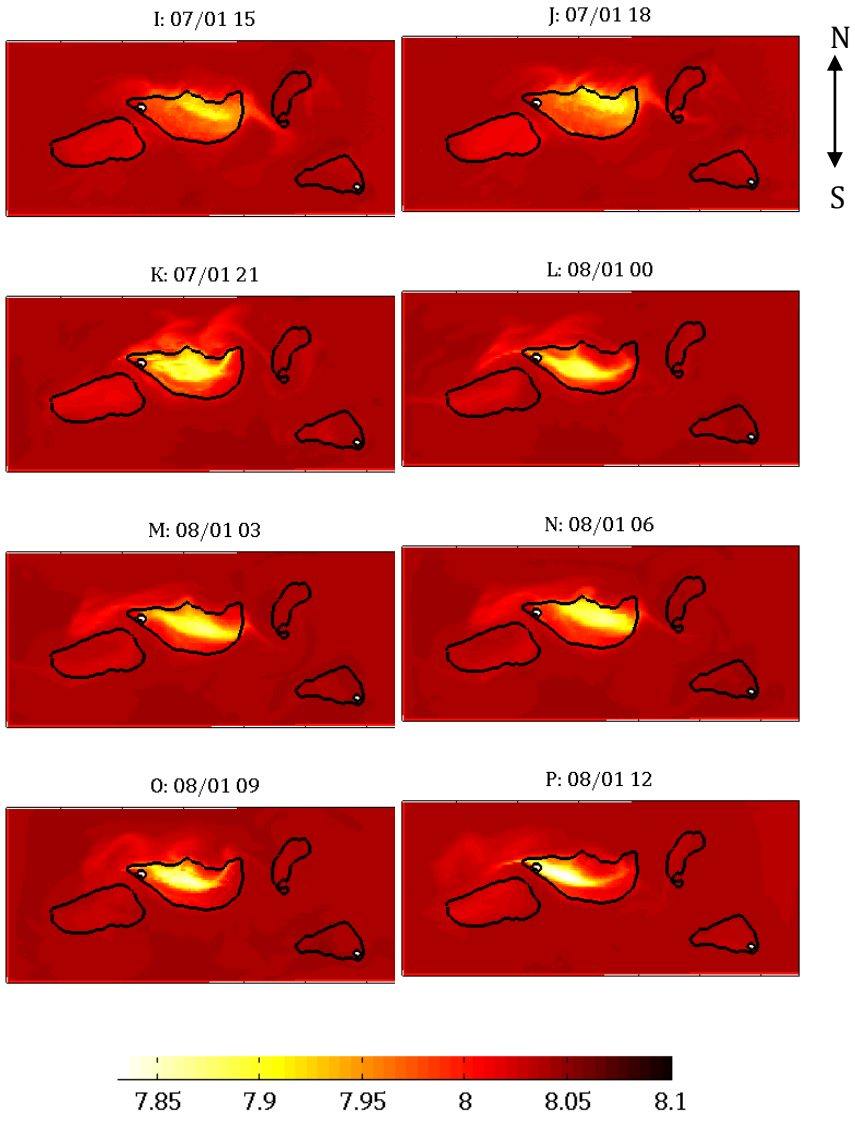

Figure 5.18: Surface water pH during $P_{velocity}^{low}$.

The change in pH and aragonite saturation should coincide with a change in DIN concentration, and hence DIN uptake. In turn DIN uptake was dependent on the mass transfer limitation associated with water velocity and surface roughness.

As the reef structure influences the hydrodynamics above and surrounding the reef, rates of uptake varied with location across the reef. To assess if there was any difference in uptake of DIN depending on location on the reef, we analysed a transect across the whole reef in an east-west direction so as to include both the reef crest and slope on both sides of the reef and the deep lagoon with coral bommies. Two time points (H and O, see Fig. 5.3) were selected (one from each period). The selected time points had the common features of daylight and a dominant east to west current direction.

The map in Figure 5.19A shows the location of the transact, the red line, and colour and contours indicate water depth. The top two panels (Fig. 5.19 B and C) show the change in pH and water age, respectively, along the transect. In $P_{velocity}^{high}$ (Fig. 5.19 B) the pH only showed a small reduction (less than 0.1) as the water moved over the reef towards the west, whereas the water age on the other hand, showed an increase in the same direction. Due to the current strength the water age remained low as the water moved across the entire reef in less than 10 h. In $P_{velocity}^{low}$ the pH was reduced by almost 0.2 in the deep lagoon. The pH changed with the opposite change in water age, hence lower pH seemed to be linked to older water. In $P_{velocity}^{low}$ the age of the water increased in the current direction until reaching the middle of the lagoon where it started to decline. This decline indicated that younger water was mixed into the east-west flow from another direction, in this case the north-east.

The DIN concentration was reduced over the reef for both periods. In $P_{velocity}^{high}$ the changes in concentration were stronger and more abrupt than in $P_{velocity}^{low}$, which was a result of a higher uptake rate due to water velocity in $P_{velocity}^{high}$, whereas the

reduction in DIN in $P^{low}_{velocity}$ took place at a lower rate, but over a longer period of time.

A: Transect

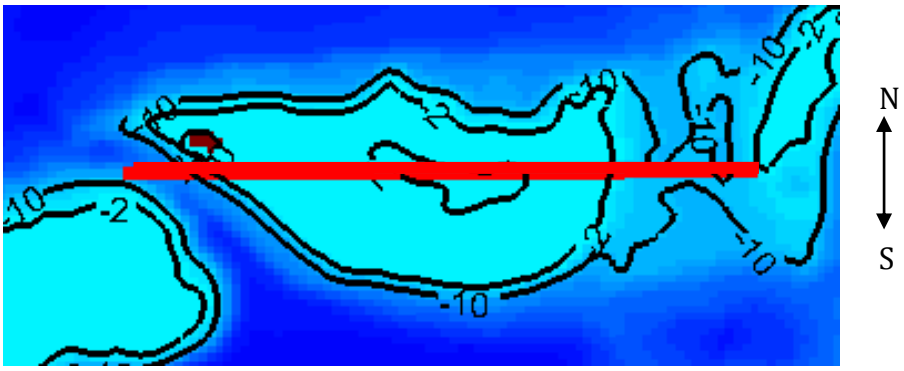

B: 8th January 12:00 h (High flow)

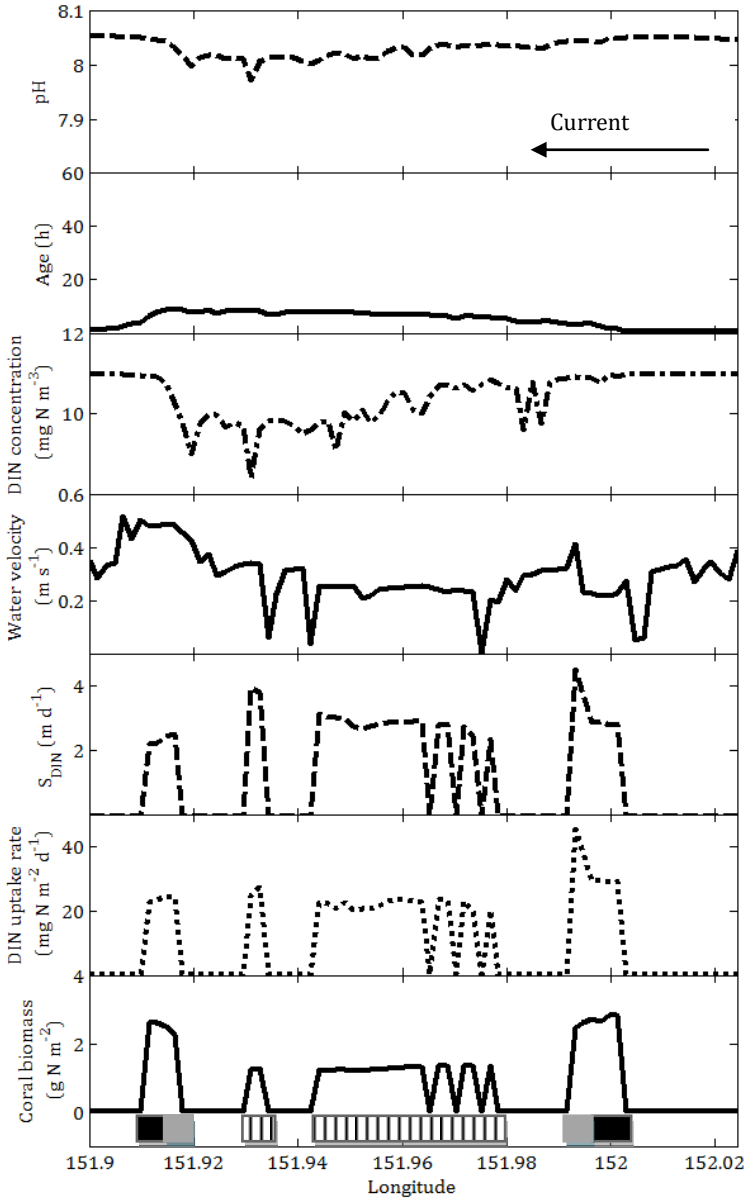

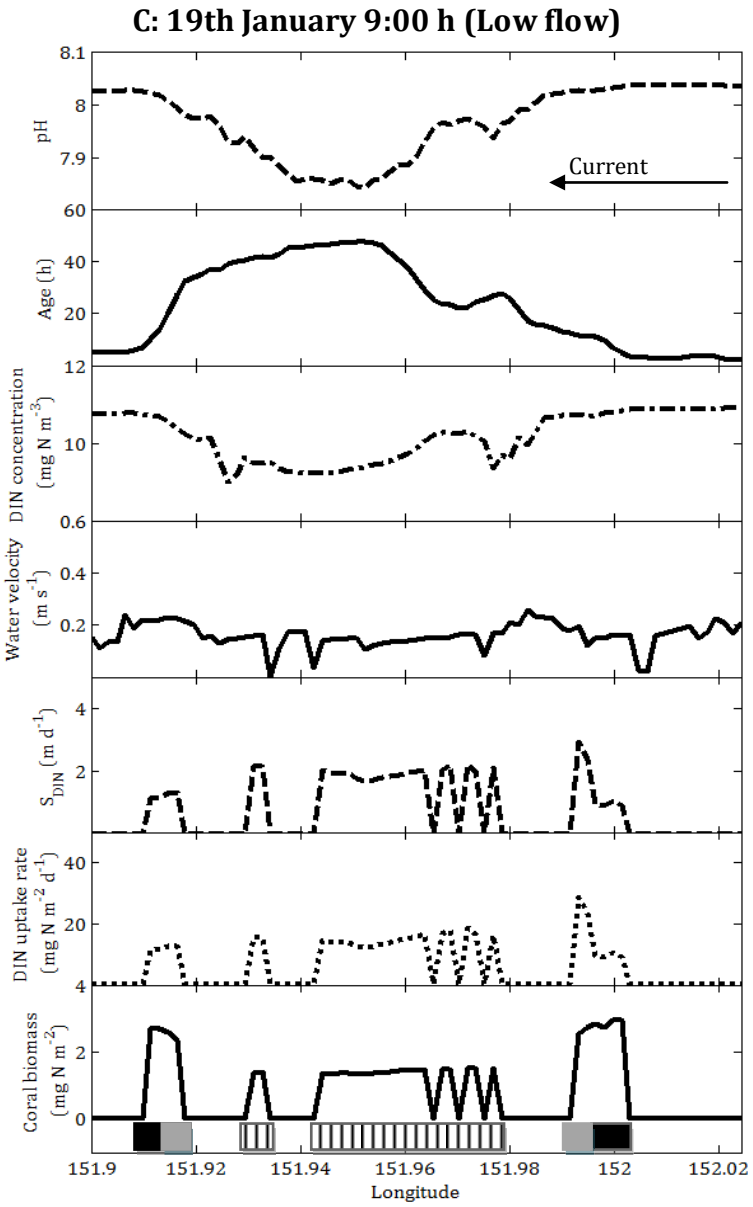

Figure 5.19: Profile of DIN uptake by the coral community, and change DIN concentration, pH and water age at the surface of the water column, as well as water velocity directly over the substrate. A) red line shows the location of the profile over Heron Reef. Water velocity, pH, water age, DIN concentration in the water column, DIN uptake over the coral population and coral host N biomass along the transect for $P_{velocity}^{high}$ (B), and $P_{velocity}^{low}$ (C). The arrow indicates the direction of the current. At the bottom of the panels showing biomass different greyscales indicate different parts of the reef; black=reef slope, gray=reef crest and dashed=bommies.

Water velocity above the corals was higher in $P_{velocity}^{high}$, but the local change in water velocity showed a similar pattern between the two flow periods. However, water velocity on its own did not explain the pattern of DIN uptake. Plotting mass transfer rate coefficient of DIN (S_{DIN}), a function of water velocity and surface roughness, over the corals along the transect showed a strong similarity to DIN uptake. The mass transfer rate coefficient explained why the back reef (west crest and slope) had a lower DIN uptake compared to the fore reef (east crest and slope) even though the water velocity was stronger at the back reef and all the other physical factors were similar to the fore reef. The mass transfer rate was higher or equal over the bommies and the reef crest and slope; however, the DIN uptake was relatively less. This depended on the effective projected area (A_{eff}) which was on average 0.97 at the reef crest and slope and 0.79 at the bommies, as well as the reduction in DIN concentration within the lagoon.

5.4 DISCUSSION

Incorporating the coral model into the Heron Island hydro-chemical model showed that the coral community influenced the environment by altering the nutritional status and chemistry of the water column above the reef. Having the coral as the only living organism in the model had the advantage of allowing us to understand how the coral interacted with the physical environment and to assess the coral contribution to the nutrient dynamics of the model. However, corals are far from the only important organism on a coral reef, and to better understand the nutrient dynamics other key organisms such as phytoplankton, zooplankton, microalgae, vertebrates, bacteria etc. should be considered.

The outcome of this modelling effort highlighted the importance of water flow to the reef nutrient dynamics. Comparing a 24 h period dominated by high water velocity to one with predominantly low water velocity showed that the lower

water velocity reduced the exchange of the water between the reef lagoon and the surrounding ocean. Hence, biological processes had more time to change the nutritional and chemical status of the reef water, even though lower water velocity also meant lower uptake rates of DIN and symbiont growth the results showed that pH, DIN and PON concentration greatly altered during periods of low water flow. Additionally, the reversal of the tide during the low flow period contributed to retaining the water above the reef. The growth rate where found to be mass transfer limited, and directly dependent on the water velocity and bottom shear stress in the model.

5.4.1 Comparison with process-based field observations

The modelled concentration of DIN in the water column above the reef, with values ranging between 9 – 11 mg m^{-3}, was of the same magnitude as recorded field measurements of 9.9 mg m^{-3} (Wyatt et al. 2012), 9.1 mg m^{-3} (Koop et al. 2001), 8.9 mg m^{-3} (Atkinson et al. 2001) and 4.9 mg m^{-3} (Naumann et al. 2010). Uptake of DIN by the coral is influenced by a series of factors such as DIN concentrations, bottom friction, water velocity and coral biomass. As a result, a direct comparison between modelled DIN uptake and measured uptake rates is problematic. Comparing the DIN mass transfer rate coefficient (S_{DIN}) gets around this issue as S_{DIN} is dependent on water velocity and surface roughness alone. The modelled S_{DIN} ranged between 1 - 5 m d^{-2}, which in accordance with values found in flume experiments with laminar flow such as, Bilger and Atkinson (1995) whom estimated a mass transfer coefficient of 2.2 – 12.7 m d^{-1} for a water flow of 0.04 - 0.4 m s^{-1} or Thomas and Atkinson (1997) who found nitrogen uptake to have a rate coefficient of 1.38 – 12.4 m d^{-1} for similar water velocities. However, studies that have taken wave action into account have found higher uptake rates, with rate coefficients ranging between 9 – 16 m d^{-1} (Falter et al. 2004). Waves were accounted for in the Heron Island model in form of an addition to the water velocity, but the model did not account for the turbulence that may arise from waves breaking over the reef rim.

Assessing the PON concentration and the PON uptake by the coral community in comparison to the literature values was difficult, as in reality PON would include both detrital as well as living organisms such as phytoplankton, zooplankton and bacteria. The heterotrophic feeding rate did however seem to be within reason with values ranging between 20-90 mg N m^{-2} d^{-1}. This brackets the feeding rate estimated by Houlbrèque and Ferrier-Pagès (2009) of 37 mg N m^{-2} d^{-1}. The localized high PON concentration seen during the low-velocity period was associated with mucus being released from the coral. The released mucus was assumed to become incorporated into the PON concentration in the water column, hence it immediately became a source of food for the coral. This may be a debatable assumption;, however, coral mucus has been shown to be an important source of nutrient within the reef community (Wild et al. 2004a; Bythell and Wild 2011). The modelled mucus release ranged between 3 and 18 mg N m^{-2} d^{-1}. Naumann et al. (2010) measured mucus release varying between 0.96 – 12 mg N m^{-2} d^{-1} depending on coral species and season.

5.4.2 Analysis of model assumptions

One assumption made in this model was that all uptake and release of nutrient took place at the Redfield ratio of C/N/P. This is a crude assumption for corals and should be considered with care. Many of the coral's processes have a dynamic C/N ratio. For example the C/N ratio of coral mucus may vary between 5 and 20 mol C mol N^{-1} with a mean of 13 mol C mol N^{-1} (Naumann et al. 2010) which is a significantly higher C/N ratio than the Readfield ratio of 6.6 mol C mol N^{-1}. Thus we may be overestimating the nitrogen contribution of coral mucus to the environment. This does not impact the model greatly under the current conditions with corals being the only living organism in the system. However, if other organisms were to be included this potential over estimation of N release from the corals should be further investigated. Likewise, translocation of photosynthates within the coral is unlikely to occur at the Redfield ratio, as the compounds that are translocated consist mostly of glycerol (Sutton and Hoegh-Guldberg 1990), lipids

(Kellogg and Patton 1983) and amino acids (Grant et al. 1997; Venn et al. 2008) with a suggested C/N ratio of 23 (Falkowski et al. 1993). Adding reserves of N and C in the coral host and symbiont would allow for flexible C/N ratios, which for example would make it possible to release mucus high in C during times when photosynthesis is high but N supply is low.

Better understanding the initial conditions used to start the model or alternatively running the spin-up simulation for a much longer period of time would be preferred, allowing the coral state variables to reach some steady state. Due to the computationally expensive nature of the model this was not possible within the timeframe of this project. Additionally, refining the assumptions made for coral mortality, respiration and mucus production would aid in the interpretation of the model on a symbiont-host scale.

A substantial part of the gross primary production on a coral reef comes from Scleractinian corals (Leclercq et al. 2002). Even though the coral model was a simplified version of the GBR13 model it did demonstrate that the coral were able to strongly influence the reef biogeochemical environment, and this highlight the importance of including actual coral processes into ecosystem models on a reef scale. On the other hand, this study also showed that hydrodynamics were essential to the coral processes indicating that mass transfer limitation associated with currents and surface properties should in the future be considered when using the more detailed GBR13 model.

CHAPTER 6:

GENERAL DISCUSSION

6. General Discussion

In this thesis, a mathematical model of coral symbiosis in a changing environment was developed. By synthesizing our current knowledge of the coral-algae interaction and the effects of external forcings into numerical relationships, a model was derived which was able to reproduce both field and laboratory experiments, as well as simulate scenarios with external forcing varying in combination, strength and duration that may be difficult to achieve in a laboratory environment. Numerical models of such systems in which there are a multitude of processes interacting with each other have become an increasingly popular scientific tool over the past decades, particularly in climate studies where the models need to be able to recreate past events (hindcast) and simulate future (forecast) scenarios (Kattenberg et al. 1996; Randall et al. 2007). The recent surge in modelling applications is a result of an increasing knowledge base and increasing computer capacity, allowing for the development of increasingly complex models.

Modelling physiological responses of living organisms to their external environment, and their roles within the ecosystem is still a recent area of research. Such modelling requires a deep understanding of the organism, as well as the interaction with other organisms and their environment. Models of plankton community dynamics are good examples of how to structure and describe an ecosystem with different organisms of varying trophic levels interacting with each other (Franks 2002; Baird et al. 2003). However, describing the symbiotic relationship between a cnidarian host and algal symbiont proved more complicated, particularly as we aimed to use a mechanistic approach to simulste many of the physiological processes. In the following section the process of structuring the model will be discussed.

6.1 STRUCTURING THE MODEL

To construct this model of the coral-algae interaction using a mechanistic approach, an in-depth understanding of the physiological and biochemical processes was needed. To gain this understanding we had to look beyond the coral system, to other symbiotic relationships, as well as free-living algae and aposymbiotic cnidarians (Kellogg and Patton 1983; Roberts et al. 2001; Suggett et al. 2008). For example, several of the symbiont processes, including components of the photosystem, were derived using information from cultured *Symbiodinium* (Suggett et al. 2008) or other free-living phytoplankton (Ross et al. 2008; Ross and Geider 2009). Ideally as research progresses and more coral host data become available the processes based on non-coral organisms or empirical relationships will be validated or rectified.

Constructing a model with the level of complexity seen in the coupled GBR13 photoinhibition model (GBR13-photo) meant that the model was developed in steps, starting with the basic features of the host and the symbiont, as well as their interaction. By first developing the coral symbiont nutrient model GBR13 (Chapter 2) and then building and improving on this model (Chapter 3 and 4) allowed the model to evolve logically and to ensure that each model component behaved and interacted with each other in a reasonable manner. Throughout the construction of this model, decisions on the level of model complexity have had to be made. Deciding on the level of model complexity involves selecting which processes we deemed important and should be represented in the model; however, including too many processes in the interpretation becomes difficult. Additionally, there is always a level of uncertainty to all processes, hence adding a few processes at the time and evaluating each process was the preferred method used in this study. An example, of a highly complex model is that photosystem model proposed by Kroon and Thoms (2006) which included all steps of linear and cyclic electron flow in photosystem I and II. Arguably they made a detailed description of the electron transport through the photosystem; however, the high model complexity and vast number of state variables makes it undesirable to be used as a representation of the photosystem in a model where the aim is to quantify physiological processes

like growth, pigment synthesis and mortality. In contrast, there are other models that use photosynthesis-irradiance curve (PI-curves) to represent photosynthesis as a function of light (Neale and Richerson 1987; Zimmerman et al. 1987). This might also not be ideal as parameters such as temperature, nutrient and pH are known to effect photosynthetic output (Jones et al. 2000; Crawley et al. 2010; Hoogenboom et al. 2012). We aimed to find a middle ground for each process. For example the photosystem is represented but does not include all details and every redox reaction involved in electron transport.

The basic GBR13 model contained the main physiological processes taking place within the coral that we deemed as important under "non-stress" conditions, including synthesis of new tissues, photosynthesis, respiration, translocation of photosynthates, calcification and mucus production (Chapter 2). The model was used to simulate the metabolic advantage of having two interchangeable sources of nutrient of, which experimental work previously have shown to be of critical importance for coral survival (Wang and Douglas 1998; Yellowlees et al. 2008). As the GBR13 model did not include any temperature dependence and could not simulate damage caused by high light intensities, it simply allowed us to focus on exploring the potential mutualistic benefits of trophic energy partitioning.

Due to the imminent threat of climate change to coral reef, the main focus of coral research has been to understand the impact of environmental change, including elevated sea surface temperatures (SST) and ocean acidification (Hoegh-Guldberg 2004; Hoegh-Guldberg et al. 2007). This made the parameterisation and validation of the coupled GBR13-photoinhibition model (GBR13-photo) easier, as there were several published experimental datasets available to which the model could be fitted and validated (Chapter 3). An important step when making the photoinhibition model comparable to experimental studies was finding the physical processes in the model which represented the commonly used fluorometry measurements such as maximum quantum yield (Fv/Fm), effective quantum yield of PSII (Y(II)), non-photochemical quenching Y(NPQ) and non-regulated heat dissipation Y(NO) (Kramer et al. 2004). These measurements tell us about the state of the photosystem; however, due to the fact that they are based on

ratios, fluorescence measurements are unitless and therefore difficult to assign to a certain physiological processes (Schreiber et al. 1995). Defining Fv/Fm as the maximum potential efficiency of the photosystem (Q_a/Q_t), Y(II) as the actual potential of the photosystem (Q_{ox}/Q_t), Y(NPQ) as the ratio of photosynthetic to heat dissipating pigments ($D_t/(D_t+D_d+ Chl)$) and Y(NO) based on the assumption Y(II)+ Y(NPQ)+ Y(NO)=1 (Kramer et al. 2004) proved to be efficient definitions of these measurements. However, under circumstances of prolonged heat and light stress these definitions would become somewhat unrealistic as Y(NPQ) reached its maximum and reduction and inhibition caused the Y(II) to approached zero which result in Y(NO) approaching an unrealistic levels.

While developing the GBR13-photo model it became apparent that the process of translocation of photosynthates and the uptake of dissolved inorganic carbon (DIC) and dissolved inorganic nitrogen (DIN) were essential processes that could influence the outcome of the model. How these processes operate and what controls them are still not fully understood (Fitt 2000). At the start of this modelling exercise, the uptake of inorganic C was thought to be diffused into the coral host tissue and the translocation was controlled by the symbiont as suggested by Muscatine and D'elia (1978). DIN was released at a set rate to allow control over the amount of N entering the coral. In Chapter 4, the DIN and DIC rates were reconsidered and improved using a dataset provided by Pernice et al. (in prep.). As this experimental dataset used the sea anemone *Aiptasia pulchella,* we also had the opportunity to apply the model to an organism other than a coral. As no DIC uptake was detected in an aposymbiotic *A. pulchella,* the conclusion was drawn that the uptake of inorganic C was driven by the symbiont, and the model processes were changed accordingly. Additionally, previous studies have shown a similar result for DIN (Koop et al. 2001; Pernice et al. 2012). The translocation process was also modified to equal the host driven translocation plus the excess photosynthates which the symbiont could not utilize. These changes to the translocation rate was critical to deliver a high percentage of photosynthates which were being translocated to the host as suggested in literature (Muscatine et al. 1981; Edmunds and Davies 1986; Edmunds and Davies 1989; Tremblay et al.

2012). These changes proved to be a good addition to the model, as by only changing one parameter, the model could reproduce an experimentally derived coral carbon budget (Tremblay et al. 2012).

6.2 ECOSYSTEM SCALE MODELLING

One of the initial objectives for developing this model was to be able to use it as a foundation for coral physiology in an ecosystem model at a reef scale (Chapter 5). In a real coral reef ecosystem there is a large number of processes interacting and linking animals, plants and the physical environment. Ecosystem models are important tools to assess consequences of anthropogenic activities (Fulton et al. 2003). Due to the multitude of processes that take place within an ecosystem it is important to consider the complexity of the model, and with care evaluate which processes to include (Fulton et al. 2003). On a coral reef the Scleractinian coral community is known to influence the nutrient load, as well as the chemistry in the water column and the sediment (Wild et al. 2004a; Wild et al. 2005b; Wyatt et al. 2012). Incorporating the full GBR13-photo model into the coupled hydrodynamic-chemistry model of Heron Island Reef developed by CSIRO (Mongin and Baird, submitted) was not possible due to the already computationally expensive nature of such a model. Evaluating the model with corals as the only living organism showed that the coral community could significantly alter the nutrient dynamics, as well as the pH and aragonite saturation of the reef water. However, introducing other organisms into the model would likely change this dynamic both to the corals advantage (added sources or redistribution of nutrient sources) and disadvantage (competition or nutrient and space). There is still much work that could be done to improve the coral processes in the Heron Island Reef model, for example introducing energy reserves which could be used by the coral during low-nutrient periods. An additional process that would have been good to include in the model is wave action, as it has been shown that turbulence caused by waves can enhance coral nutrient uptake (Falter et al. 2004; Zhang et al. 2011).

Even though the coral model incorporated into the Heron model was very simple in comparison to the GBR13-photo model and it did not capture temperature dependence due to the lack of the photoinhibition model, the model showed the importance of the coral community to the nutrient dynamics on the reef. The coral model is currently being incorporated into the modelling effort eReefs a Australian initiative that aims to create a model of the Great Barrier Reef (CSIRO).

6.3 MODEL APPLICATION AND USE

The GBR13-photo model developed here is applicable to several organisms and can with only minor changes be used for different species and even other organisms. The advantage of a model like this is that it can be used to test all kinds of combinations of external forcings and simulate what will happen over time scales of hours to years, experiments that would be difficult to set up in reality. A model such as GBR13-photo model can be used to simulate more than responses to environmental conditions; it can also be used to shed light on processes which we do not understand, or have yet to be agreed upon by researchers. An example of this is the disagreement about the repair rate of D1 protein in the photosystem, whether it is up- or down-regulated as a function of stress (discussed in Chapter 3). The model could also be used as a tool to try to optimize processes in biofuel production, for example finding the optimal light, temperature and nutrient concentrations to maximize growth rate.

The model can be used to evaluate existing frameworks and relationships used to assess coral health or bleaching risk such as Degree Heating Days (DHD). An interesting outcome of Chapter 3 was the indication that heterotrophy could reduce the effect of bleaching. The model outputs were consistent with the "DHD theory" (Maynard et al. 2008a; Maynard et al. 2008b) with exception of periods with high nutrient availability (Chapter 3). A possible improvement to the DHD index could be to use satellite chlorophyll measurements to represent the organic

nutrient concentration, as plankton blooms are often associated with both high DOM and zooplankton (Baird et al. 2004b; Wyatt et al. 2010).

6.4 FUTURE DIRECTIONS AND RESEARCH

One major consequence of climate change is ocean acidification (Guinotte and Fabry 2008; Doney et al. 2009). A reduction in pH is known to influence coral's ability to calcify, as well as having an adverse effect on photosynthetic rates (Anthony et al. 2008; Crawley et al. 2010). Including pH dependence into the model that influences the calcification, as well as the photosynthetic processes would be a great advantage when trying to simulate the impact of climate change in the coral community. However, the processes taking place inside the corals, in particular within the celenteron are still not fully understood, but are likely to be important as the chemistry inside to coral body cavity and celenteron may be significantly different from that of the water column (Al-Horani 2005). As the processes become clearer, adding them to this model would become easier. During the development of this model, we decided that introducing pH in addition to temperature, light and nutrient dependence would complicate the model too much and introduce too many uncertainties, particularly as the understanding of the physiological impacts of pH were still in strong debate with no consistent hypothesis.

The other major component missing from this model is reproduction. Corals are known to put a large amount of energy into producing gametes (Richmond 1987; Ward 1995; Jokiel 1998). Corals are known to spawn during a short period each year, and the release of gametes is often synchronised, particularly within a species but sometimes also over a whole reef (Penland et al. 2004). We did not regard this as an essential process, as most of our simulation did not extend across seasons. However, setting up the model with a production and release of gametes would not be too difficult, and when running the model for different seasons it

would be important to take this into consideration, as the energy partitioned to reproduction is significant.

There are still physiological and biochemical processes within the cnidarian-algae association that ideally would be incorporated into this model, such as photorespiration and alternative electron transport paths in the photosystem, as well as transfer of reactive oxygen to the host and host antioxidant systems. As discussed in Chapter 4 another useful addition to the model would be an adjustment of the internal light field as a function of scattering by the skeleton and absorption by pigments model (Enríquez et al. 2005; Wangpraseurt et al. 2012).

For further use of the model, developing a more user-friendly version of this model, where one could easily alter the model to represent a coral, anemone a free-living algae or an aposymbiotic cnidarian, would be ideal. This would be a time-consuming task, but important if anyone not familiar with programming were to use it.

7. Supplementary Material

This supplementary section gives the methods for deriving the experimental data used in chapter 4. Text provided by Mathieu Pernice.

7.1 ISOTOPIC INCUBATION

To quantify the assimilation of dissolved inorganic carbon by the different cellular compartments (gastroderm, epiderm and symbiotic zooxanthellae), individual anemones were exposed to two experimental treatments (isotopic labelling and control treatments). Symbiotic and aposymbiotic anemones were randomly distributed in 6 independent small aquaria (10 L; three tank replicates per treatment; closed water system; continuously stirred using 1 one powerhead pump for each tank) and incubated for four hours. For the isotopic labeling, artificial seawater was amended by adding $NaH^{13}CO_3$ powder (^{13}C isotopic abundance of 99%, commercially available from Sigma) to a final concentration of 2 mM. A total of 6 anemones were randomly removed from the treatment and control tanks at T=0, 4 hours and 12 hours, respectively. A subset of 6 tentacles was removed from each individual anemone and chemically fixed for NanoSIMS analysis. The rest of the animal was snap-frozen in liquid nitrogen and stored at -80°C for further analysis on total carbon content. For NanoSIMS analysis, *Aiptasia* tentacles were chemically fixed 24h at 4°C by immersion in a solution containing 2.5% glutaraldehyde and 1 % formaldehyde in PBS-sucrose buffer (0.1 M phosphate, 0.65 M sucrose, 2.5 mM $CaCl_2$), pH 7.5. Samples were then stored in PBS-sucrose buffer (0.1 M phosphate, 0.65 M sucrose, 2.5 mM $CaCl_2$), pH 7.5 at 4°C for 3 three days until further processing for TEM and NanoSIMS analyses.

7.2 TISSUE PREPARATION FOR TEM AND NANOSIMS ANALYSES

Aiptasia tentacles were sectioned and embedded in 1.5% agarose (1) at 4°C and pH 7.5 in Sörensen 0.1 M buffer and post-fixed 1 hour at RT in 1% OsO4 in Sörensen phosphate buffer (0.1 M). Tissue samples were then dehydrated in an increasing

series of ethanol concentrations (50%, 70%, 90% and 100%) and stored in acetone until resin embedding. Samples were embedded in Spurr resin, oriented under a microscope, cut into 100-120 nm sections using an Ultracut E microtome (Leica Microsystems, Australia) and mounted onto finder grids for Transmission Electron Microscopy (ProsciTech, Australia) counterstained with uranyl acetate 2% (10 min) and Reynold's lead citrate (10 min).

7.3 TEM ANALYSES

The different regions of interest within the tissue sections were mapped and imaged at the Centre for Microscopy and Microanalysis (the University of Sydney, Sydney, Australia) using a JEOL JEM1400 Transmission Electron Microscope (JEOL, Korea LTD) operated at 80 kV accelerating voltage. After TEM mapping and imaging of the tissue, the TEM Grids were mounted on 10 mm aluminum stubs and gold-coated for further NanoSIMS analyses.

7.4 NANOSIMS ANALYSES

The regions of interest within the tissue sections were imaged with a NanoSIMS ion microprobe in order to quantify the distribution of newly fixed ^{13}C within symbiotic and aposymbiotic anemones. Samples were bombarded with a 16 keV primary ion beam of (1-3 pA) Cs^+ focused to a spot size of about 100-150 nm on the sample surface. Secondary molecular ions $^{12}C^{12}C^-$ and $12C^{13}C^-$ were simultaneously collected in electron multipliers at a mass resolution (M/M) of about 9000, enough to resolve potential problematic interferences. Charge compensation was not necessary. Typical images of 35×35 µm with 256×256 pixels for $^{12}C^{12}C$- and $^{12}C^{13}C^-$, respectively, were obtained by rastering the primary beam across the sample with a dwell-time of 5 milliseconds. After drift correction, the $^{13}C/^{12}C$ maps were obtained by taking the ratio between the $^{12}C^{13}C^-$ and $^{12}C^{12}C$ images. Unlabelled *Aiptasia* tissue with dinoflagellate symbionts was used as an internal standard and was measured every day of NanoSIMS analyses.

8. REFERENCES

Ahmad, W., and D. Neil. 1994. An evaluation of Landsat Thematic Mapper (TM) digital data for discriminating coral reef zonation: Heron Reef (GBR). International Journal of Remote Sensing **15:** 2583-2597.

Al-Horani, F. 2005. Effects of changing seawater temperature on photosynthesis and calcification in the scleractinian coral Galaxea fascicularis, measured with O 2, Ca 2+ and pH microsensors. Scientia Marina **69**.

Al-Horani, F. A., S. M. Al-Moghrabi, and D. De Beer. 2003. The mechanism of calcification and its relation to photosynthesis and respiration in the scleractinian coral Galaxea fascicularis. Marine Biology **142:** 419-426.

Al-Moghrabi, S., D. Allemand, J. Couret, and J. Jaubert. 1995. Fatty acids of the scleractinian coral Galaxea fascicularis: effect of light and feeding. Journal of Comparative Physiology B: Biochemical, Systemic, and Environmental Physiology **165:** 183-192.

Al-Moghrabi, S., C. Goiran, D. Allemand, N. Speziale, and J. Jaubert. 1996. Inorganic carbon uptake for photosynthesis by the symbiotic coral-dinoflagellate association II. Mechanisms for bicarbonate uptake. Journal of Experimental Marine Biology and Ecology **199:** 227-248.

Allemand, D. and others 2004. Biomineralisation in reef-building corals: from molecular mechanisms to environmental control. Comptes Rendus Palevol **3:** 453-467.

Alongi, D. M., F. Tirendi, and A. Goldrick. 1996. Organic matter oxidation and sediment chemistry in mixed terrigenous-carbonate sands of Ningaloo Reef, Western Australia. Marine chemistry **54:** 203-219.

Anthony, K., and S. Connolly. 2004. Environmental limits to growth: physiological niche boundaries of corals along turbidity–light gradients. Oecologia **141:** 373-384.

Anthony, K., and K. Fabricius. 2000. Shifting roles of heterotrophy and autotrophy in coral energetics under varying turbidity. Journal of Experimental Marine Biology and Ecology **252:** 221-253.

Anthony, K. R. N., M. O. Hoogenboom, J. A. Maynard, A. G. Grottoli, and R. Middlebrook. 2009. Energetics approach to predicting mortality risk from environmental stress: a case study of coral bleaching. Functional Ecology **23:** 539-550.

Anthony, K. R. N., D. I. Kline, G. Diaz-Pulido, S. Dove, and O. Hoegh-Guldberg. 2008. Ocean acidification causes bleaching and productivity loss in coral reef builders. Proceedings of the National Academy of Sciences **105:** 17442-17446.

Apel, K., and H. Hirt. 2004. Reactive oxygen species: metabolism, oxidative stress, and signal transduction. Annu. Rev. Plant Biol. **55:** 373-399.

Asada, K. 1996. Radical production and scavenging in the chloroplasts. Photosynthesis and the Environment **5:** 123-150.

Asada, K. 2006. Production and scavenging of reactive oxygen species in chloroplasts and their functions. Plant physiology **141:** 391-396.

Atkinson, M., and R. Bilger. 1992. Effects of water velocity on phosphate uptake in coral reef-flat communities. Limnology and Oceanography **37:** 273-279.

Atkinson, M., J. Falter, and C. Hearn. 2001. Nutrient dynamics in the Biosphere 2 coral reef mesocosm: water velocity controls NH 4 and PO 4 uptake. Coral Reefs **20:** 341-346.

Baird, A., R. Bhagooli, P. Ralph, and S. Takahashi. 2009. Coral bleaching: the role of the host. Trends in Ecology & Evolution **24:** 16-20.

Baird, M., and M. Atkinson. 1997. Measurement and prediction of mass transfer to experimental coral reef communities. Limnology and Oceanography **42:** 1685-1693.

Baird, M., M. Roughan, R. Brander, J. Middleton, and G. Nippard. 2004a. Mass-transfer-limited nitrate uptake on a coral reef flat, Warraber Island, Torres Strait, Australia. Coral Reefs **23:** 386-396.

Baird, M., S. Walker, B. B. Wallace, I. Webster, and J. Parslow. 2003. The use of mechanistic descriptions of algal growth and zooplankton grazing in an estuarine eutrophication model. Estuarine, Coastal and Shelf Science **56:** 685-695.

Baird, M. E., P. R. Oke, I. M. Suthers, and J. H. Middleton. 2004b. A plankton population model with biomechanical descriptions of biological processes in an idealised 2D ocean basin. Journal of Marine Systems **50:** 199-222.

Baird, M. E., P. J. Ralph, F. Rizwi, K. Wild-Allen, and A. D. Steven. 2013. A dynamic model of the cellular carbon to chlorophyll ratio applied to a batch culture and a continental shelf ecosystem. Limnol. Oceanogr **58:** 1215-1226.

Berking, S. 2007. Generation of bilateral symmetry in Anthozoa: A model. Journal of Theoretical Biology **246:** 477-490.

Bilger, R., and M. Atkinson. 1995. Effects of nutrient loading on mass-transfer rates to a coral-reef community. Limnology and Oceanography **40:** 279-289.

Borell, E. M., and K. Bischof. 2008. Feeding sustains photosynthetic quantum yield of a scleractinian coral during thermal stress. Oecologia **157:** 593-601.

Borell, E. M., A. R. Yuliantri, K. Bischof, and C. Richter. 2008. The effect of heterotrophy on photosynthesis and tissue composition of two scleractinian corals under elevated temperature. Journal of Experimental Marine Biology and Ecology **364:** 116-123.

Boussinesq, J. 1877. Essai sur la théorie des eaux courantes. Imprimerie nationale.

Brown, B., R. Dunne, M. Goodson, and A. Douglas. 2000. Marine ecology: bleaching patterns in reef corals. Nature **404:** 142-143.

Brown, B. E. 1997. Coral bleaching: causes and consequences. Coral Reefs **16:** S129-S138.

Brown, B. E., and J. C. Bythell. 2005. Perspectives on mucus secretion in reef corals. Marine Ecology Progress Series **296:** 291-309.

Bythell, J. C. 1990. Nutrient Uptake in the Reef-building Coral Acropora Palmata at Natural Envi Ental „, Concentrations Protectea r. Mar. Ecol. Prog. Ser **68:** 65-69.

Bythell, J. C., and C. Wild. 2011. Biology and ecology of coral mucus release. Journal of Experimental Marine Biology and Ecology **408:** 88-93.

Chen, D., and A. Krol. 1997. Hydrogeology of Heron Island, Great Barrier Reef, Australia. Geology and Hydrogeology of Carbonate Islands **54:** 867-884.

Clark, K. B., and K. R. Jensen. 1982. Effects of temperature on carbon fixation and carbon budget partitioning in the zooxanthellal symbiosis of *Aiptasia pallida*(Verrill). Journal of Experimental Marine Biology and Ecology **64:** 215-230.

Connolly, S., M. Lopez-Yglesias, and K. R. Anthony. 2012. Food availability promotes rapid recovery from thermal stress in a scleractinian coral. Coral Reefs **31:** 951-960.

Cook, C. B., G. Muller-Parker, and C. F. D'elia. 1992. Ammonium enhancement of dark carbon fixation and nitrogen limitation in symbiotic zooxanthellae: Effects of feeding and starvation of the sea anemone Aiptasia pallida. Limnology and Oceanography **37:** 131-139.

Crawley, A., D. I. Kline, S. Dunn, K. E. N. Anthony, and S. Dove. 2010. The effect of ocean acidification on symbiont photorespiration and productivity in *Acropora formosa*. Global Change Biology **16:** 851-863.

Crossland, C. 1987. In situ release of mucus and DOC-lipid from the corals Acropora variabilis and Stylophora pistillata in different light regimes. Coral Reefs **6:** 35-42.

D'elia, C., S. Domotor, and K. Webb. 1983. Nutrient uptake kinetics of freshly isolated zooxanthellae. Marine Biology **75:** 157-167.

Davies, P. 1991. Effect of daylight variations on the energy budgets of shallow-water corals. Marine Biology **108:** 137-144.

Davy, S., and C. Cook. 2001a. The relationship between nutritional status and carbon flux in the zooxanthellate sea anemone Aiptasia pallida. Marine Biology **139:** 999-1005.

Davy, S., K. Withers, and R. Hinde. 2006. Effects of host nutritional status and seasonality on the nitrogen status of zooxanthellae in the temperate coral Plesiastrea versipora (Lamarck). Journal of Experimental Marine Biology and Ecology **335:** 256-265.

Davy, S. K., and C. B. Cook. 2001b. The influence of 'host release factor' on carbon release by zooxanthellae isolated from fed and starved *Aiptasia pallida* (Verrill). Comparative Biochemistry and Physiology Part A: Molecular & Integrative Physiology **129:** 487-494.

De'ath, G., J. Lough, and K. Fabricius. 2009. Declining coral calcification on the Great Barrier Reef. Science **323:** 116.

Domotor, S., and C. D'elia. 1986. Cell-size distributions of zooxanthellae in culture and symbiosis. The Biological Bulletin **170:** 519-525.

Doney, S., V. Fabry, R. Feely, and J. Kleypas. 2009. Ocean acidification: the other CO_2 problem. Marine Science **1:** 169-192.

Donner, S., T. Knutson, and M. Oppenheimer. 2007. Model-based assessment of the role of human-induced climate change in the 2005 Caribbean coral bleaching event. Proceedings of the National Academy of Sciences **104:** 5483.

Downs, C., J. E. Fauth, J. C. Halas, P. Dustan, J. Bemiss, and C. M. Woodley. 2002. Oxidative stress and seasonal coral bleaching. Free Radical Biology and Medicine **33:** 533-543.

Ducklow, H., W, and R. Mitchell. 1979. Bacterial Populations and Adaptations in the Mucus Layers on Living Corals. American Society of Limnology and Oceanography **24:** 715-725.

Dugdale, R., and F. Wilkerson. 1986. The use of N to measure nitrogen uptake in eutrophic oceans; experimental considerations. Limnology and Oceanography **31:** 673-689.

Dunn, S. R., M. Pernice, K. Green, O. Hoegh-Guldberg, and S. G. Dove. 2012. Thermal stress promotes host mitochondrial degradation in symbiotic cnidarians: are the batteries of the reef going to run out? PloS one **7:** e39024.

Duyens, L. 1956. The flattering of the absorption spectrum of suspensions, as compared to that of solutions. Biochimica et Biophysica Acta **19:** 1-12.

Edmunds, P., and P. Davies. 1986. An energy budget for *Porites porites* (Scleractinia). Marine Biology **92:** 339-347.

Edmunds, P., and P. Davies. 1989. An energy budget for *Porites porites* (Scleractinia), growing in a stressed environment. Coral Reefs **8:** 37-43.

Enríquez, S., E. R. Méndez, and R. Iglesias-Prieto. 2005. Multiple scattering on coral skeletons enhances light absorption by symbiotic algae. Limnology and Oceanography **50:** 1025-1032.

Epp, L., I. Smid, and P. Tardent. 1986. Synthesis of the mesoglea by ectoderm and endoderm in reassembled hydra. Journal of Morphology **189:** 271-279.

Everett, J. D., M. E. Baird, and I. M. Suthers. 2007. Nutrient and plankton dynamics in an intermittently closed/open lagoon, Smiths Lake, south-eastern Australia: An ecological model. Estuarine, Coastal and Shelf Science **72:** 690-702.

Eynaud, Y., R. M. Nisbet, and E. B. Muller. 2011. Impact of excess and harmful radiation on energy budgets in scleractinian corals. Ecological Modelling **222:** 1315-1322.

Falkowski, P., Z. Dubinsky, L. Muscatine, and L. Mccloskey. 1993. Population control in symbiotic corals. Bioscience **43:** 606-611.

Falkowski, P., Z. Dubinsky, L. Muscatine, and J. Porter. 1984. Light and the bioenergetics of a symbiotic coral. Bioscience **34:** 705-709.

Falkowski, P., J. Raven, and E. Laws. 2007. Aquatic photosynthesis. Princeton University Press.

Falter, J. L., M. J. Atkinson, and M. A. Merrifield. 2004. Mass-transfer limitation of nutrient uptake by a wave-dominated reef flat community. Limnology and Oceanography **49:** 1820-1831.

Fautin, D., and R. Mariscal. 1991. Cnidaria: Anthozoa. Wiley: New York **vol. 2:** 357.

Ferrer, L. M., and A. M. Szmant. 1988. Nutrient regeneration by the endolithic community in coral skeletons. Proceedings of the 6th International Coral Reef Symposium **3:** 1-4.

Ferrier-Pagès, C., C. Rottier, E. Beraud, and O. Levy. 2010. Experimental assessment of the feeding effort of three scleractinian coral species during a thermal stress: Effect on the rates of photosynthesis. Journal of Experimental Marine Biology and Ecology **390:** 118-124.

Ferrier-Pagès, C., J. Witting, E. Tambutté, and K. P. Sebens. 2003. Effect of natural zooplankton feeding on the tissue and skeletal growth of the scleractinian coral *Stylophora pistillata*. Coral Reefs **22:** 229-240.

Fitt, W. 2000. Cellular growth of host and symbiont in a cnidarian-zooxanthellar symbiosis. Biol Bull **198:** 110-120.

Fitt, W., and C. Cook. 2001. The effects of feeding or addition of dissolved inorganic nutrients in maintaining the symbiosis between dinoflagellates and a tropical marine cnidarian. Marine Biology **139:** 507-517.

Fitt, W., F. Mcfarland, M. Warner, and G. Chilcoat. 2000. Seasonal patterns of tissue biomass and densities of symbiotic dinoflagellates in reef corals and relation to coral bleaching. Limnology and Oceanography **45:** 677-685.

Fitt, W. K., H. J. Spero, J. Halas, M. W. White, and J. W. Porter. 1993. Recovery of the coral *Montastrea annularis* in the Florida Keys after the 1987 Caribbean "bleaching event". Coral Reefs **12:** 57-64.

Flores-Ramírez, L. A., and M. A. Liñán-Cabello. 2007. Relationships among thermal stress, bleaching and oxidative damage in the hermatypic coral, *Pocillopora*

capitata. Comparative Biochemistry and Physiology Part C: Toxicology & Pharmacology **146:** 194-202.

Fowler, S. W., and G. A. Knauer. 1986. Role of large particles in the transport of elements and organic compounds through the oceanic water column. Progress in Oceanography **16:** 147-194.

Franks, P. 2002. NPZ Models of Plankton Dynamics: Their Construction, Coupling to Physics, and Application. Journal of Oceanography **58:** 379-387.

Fulton, E. A., A. D. M. Smith, and C. R. Johnson. 2003. Effect of complexity on marine ecosystem models. Marine Ecology Progress Series **253:** 1-16.

Furla, P., I. Galgani, I. Durand, and D. Allemand. 2000. Sources and mechanisms of inorganic carbon transport for coral calcification and photosynthesis. J Exp Biol **203:** 3445-3457.

Gates, R., G. Baghdasarian, and L. Muscatine. 1992. Temperature stress causes host cell detachment in symbiotic cnidarians: implications for coral bleaching. The Biological Bulletin **182:** 324-332.

Gates, R. D., O. Hoegh-Guldberg, M. J. Mcfall-Ngai, K. Y. Bil, and L. Muscatine. 1995. Free amino acids exhibit anthozoan" host factor" activity: they induce the release of photosynthate from symbiotic dinoflagellates in vitro. Proceedings of the National Academy of Sciences **92:** 7430-7434.

Gattuso, J., D. Allemand, and M. Frankignoulle. 1999. Photosynthesis and Calcification at Cellular, Organismal and Community Levels in Coral Reefs: A Review on Interactions and Control by Carbonate Chemistry. Amer. Zool. **39:** 160-183.

Geider, R., H. Macintyre, and T. Kana. 1998. A dynamic regulatory model of phytoplanktonic acclimation to light, nutrients, and temperature. Limnology and Oceanography **43:** 679-694.

Godinot, C., F. Houlbrèque, R. Grover, and C. Ferrier-Pagès. 2011. Coral uptake of inorganic Phosphorus and Nitrogen negatively affected by simultaneous changes in temperature and pH. PloS one **6:** e25024.

Goiran, C., S. Al-Moghrabi, D. Allemand, and J. Jaubert. 1996. Inorganic carbon uptake for photosynthesis by the symbiotic coral/dinoflagellate association I. Photosynthetic performances of symbionts and dependence on sea water bicarbonate. Journal of Experimental Marine Biology and Ecology **199:** 207-225.

Gorbunov, M. Y., Z. S. Kolber, M. P. Lesser, and P. G. Falkowski. 2001. Photosynthesis and photoprotection in symbiotic corals. Limnology and Oceanography **46:** 75-85.

Gourlay, M., and J. L. Hacker. 1999. Influence of waves and winds on reef-top currents at Heron Island, Southern Great Barrier Reef, p. 209. Coasts & Ports 1999: Challenges and Directions for the New Century; Proceedings of the 14th Australasian Coastal and Ocean Engineering Conference and the 7th Australasian Port and Harbour Conference. National Committee on Coastal and Ocean Engineering, Institution of Engineers, Australia.

Gourlay, M. R., and G. Colleter. 2005. Wave-generated flow on coral reefs—an analysis for two-dimensional horizontal reef-tops with steep faces. Coastal Engineering **52:** 353-387.

Grant, A. J., M. Rémond, J. People, and R. Hinde. 1997. Effects of host-tissue homogenate of the scleractinian coral Plesiastrea versipora on glycerol metabolism in isolated symbiotic dinoflagellates. Marine Biology **128:** 665-670.

Grottoli, A. G., L. J. Rodrigues, and J. E. Palardy. 2006a. Heterotrophic plasticity and resilience in bleached corals. Nature **440:** 1186-1189.

Grottoli, A. G., L. J. Rodrigues, and J. E. Palardy. 2006b. Heterotrophic plasticity and resilience in bleached corals, p. 1186-1189. Nature Publishing Group.

Grover, R., J.-F. Maguer, S. Reynaud-Vaganay, and C. Ferrier-Pages. 2002. Uptake of ammonium by the scleractinian coral Stylophora pistillata: effect of feeding, light, and ammonium concentrations. Limnology and Oceanography **47:** 782-790.

Guinotte, J., and V. Fabry. 2008. Ocean acidification and its potential effects on marine ecosystems. Annals of the New York Academy of Sciences **1134:** 320-342.

Gustafsson, M. S. M., M. E. Baird, and P. J. Ralph. 2013. The interchangeability of autotrophic and heterotrophic nitrogen sources in Scleractinian coral symbiotic relationships: A numerical study. Ecological Modelling **250:** 183-194.

Gustafsson, M. S. M., M. E. Baird, and P. J. Ralph. in press. Photoinhibition and bleaching in Scleractinian coral as a function of light, temperature and heterotrophy. Limnol Oceanogr.

Halliwell, B. 1991. Oxygen radicals: their formation in plant tissues and their role in herbicide damage. Topics in photosynthesis **10:** 87-129.

Haney, J. D. 1996. Modeling phytoplankton growth rates. Journal of Plankton Research **18:** 63.

Havaux, M., and F. Tardy. 1996. Temperature-dependent adjustment of the thermal stability of photosystem II in vivo: possible involvement of xanthophyll-cycle pigments. Planta **198:** 324-333.

Hearn, C., M. Atkinson, and J. Falter. 2001. A physical derivation of nutrient-uptake rates in coral reefs: effects of roughness and waves. Coral Reefs **20:** 347-356.

Heidelberg, K., K. Sebens, and J. Purcell. 2004. Composition and sources of near reef zooplankton on a Jamaican forereef along with implications for coral feeding. Coral Reefs **23:** 263-276.

Hennige, S. J., M. P. Mcginley, A. G. Grottoli, and M. E. Warner. 2011. Photoinhibition of *Symbiodinium* spp. within the reef corals *Montastraea faveolata* and *Porites astreoides*: implications for coral bleaching. Marine Biology **158:** 2515-2526.

Herzfeld, M. 2006. An alternative coordinate system for solving finite difference ocean models. Ocean Modelling **14:** 174-196.

Herzfeld, M., J. Andrewartha, and P. Sakov. 2010. Modelling the physical oceanography of the D'Entrecasteaux Channel and the Huon Estuary, south-eastern Tasmania. Marine and Freshwater Research **61:** 568-586.

Hill, R., C. M. Brown, K. Dezeeuw, D. A. Campbell, and P. J. Ralph. 2011. Increased rate of D 1 repair in coral symbionts during bleaching is insufficient to counter accelerated photo-inactivation. Limnology and Oceanography **56:** 139-146.

Hill, R., A. Larkum, C. Frankart, M. Kühl, and P. Ralph. 2004. Loss of functional Photosystem II reaction centres in zooxanthellae of corals exposed to bleaching conditions: using fluorescence rise kinetics. Photosynthesis Research **82:** 59-72.

Hill, R. and others 2012. Light-induced dissociation of antenna complexes in the symbionts of scleractinian corals correlates with sensitivity to coral bleaching. Coral Reefs **31:** 963-975.

Hoegh-Guldberg, O. 1999. Climate change, coral bleaching and the future of the world's coral reefs. Marine & Freshwater Research **50:** 839-866.

Hoegh-Guldberg, O. 2004. Coral reefs in a century of rapid environmental change. Symbiosis **37:** 1-31.

Hoegh-Guldberg, O., and R. J. Jones. 1999. Photoinhibition and photoprotection in symbiotic dinoflagellates from reef-building corals. Marine Ecology Progress Series **183:** 73-86.

Hoegh-Guldberg, O. and others 2007. Coral reefs under rapid climate change and ocean acidification. Science **318:** 1737.

Hoogenboom, M. O., D. A. Campbell, E. Beraud, K. Dezeeuw, and C. Ferrier-Pagès. 2012. Effects of Light, Food Availability and Temperature Stress on the Function of Photosystem II and Photosystem I of Coral Symbionts. PloS one **7:** e30167.

Horton, H. R., L. A. Moran, R. S. Ochs, J. D. Rawn, and K. G. Scrimgeour. 2002. Principles of biochemistry. Prentice Hall Upper Saddle River, NJ.

Houlbrèque, F., and C. Ferrier-Pagès. 2009. Heterotrophy in tropical scleractinian corals. Biological Reviews **84:** 1-17.

Houlbreque, F., E. Tambutte, D. Allemand, and C. Ferrier-Pages. 2004a. Interactions between zooplankton feeding, photosynthesis and skeletal growth in the scleractinian coral Stylophora pistillata. J Exp Biol **207:** 1461-1469.

Houlbrèque, F., E. Tambutté, and C. Ferrier-Pagès. 2003. Effect of zooplankton availability on the rates of photosynthesis, and tissue and skeletal growth in the scleractinian coral Stylophora pistillata. Journal of Experimental Marine Biology and Ecology **296:** 145-166.

Houlbreque, F., E. Tambutte, C. Richard, and C. Ferrier-Pages. 2004b. Importance of a micro-diet for scleractinian corals. Marine Ecology Progress Series **282:** 151-160.

Hughes, A., A. Grottoli, and T. Pease. 2008. Recovery from bleaching: Autotrophic and heterotrophic carbon acquisition in two Hawaiian corals during recovery from thermally-induced bleaching. American Geophysical Union, 2000 Florida Ave., N. W. Washington DC 20009 USA.

Hughes, A. B. 2011. Amino Acids, Peptides and Proteins in Organic Chemistry, Building Blocks, Catalysis and Coupling Chemistry. Wiley-VCH.

Hughes, T. 1989. Community structure and diversity of coral reefs: the role of history. Ecology **70:** 275-279.

Hughes, T. and others 2003. Climate change, human impacts, and the resilience of coral reefs. Science **301:** 929-933.

Iglesias-Prieto, R., J. Matta, W. Robins, and R. Trench. 1992. Photosynthetic response to elevated temperature in the symbiotic dinoflagellate Symbiodinium microadriaticum in culture. Proceedings of the National Academy of Sciences of the United States of America **89:** 10302-10305.

Johannes, R. and others 1972. The metabolism of some coral reef communities: a team study of nutrient and energy flux at Eniwetok. Bioscience **22:** 541-543.

Jokiel, P. 1998. Energetic cost of reproduction in the coral Pocillopora damicornis: a synthesis of published data. Reproduction in Reef Corals Results of the 1997 Edwin W. Pauley Summer Program in Marine Biology**:** 38.

Jones, R. 2008. Coral bleaching, bleaching-induced mortality, and the adaptive significance of the bleaching response. Marine Biology **154:** 65-80.

Jones, R., O. Hoegh-Guldberg, A. Larkum, and U. Schreiber. 1998. Temperature-induced bleaching of corals begins with impairment of the CO_2 fixation mechanism in zooxanthellae. Plant Cell and Environment **21:** 1219-1230.

Jones, R. J., S. Ward, A. Y. Amri, and O. Hoegh-Guldberg. 2000. Changes in quantum efficiency of Photosystem II of symbiotic dinoflagellates of corals after heat stress, and of bleached corals sampled after the 1998 Great Barrier Reef mass bleaching event. Marine and Freshwater Research **51:** 63-71.

Kattenberg, A. and others 1996. Climate models—projections of future climate. Climate Change 1995: The Science of Climate Change. Contribution of Working Group I to the Second Assessment Report of the Intergovernmental Panel on Climate Change**:** 285-357.

Kellogg, C. A. 2004. Tropical Archaea: diversity associated with the surface microlayer of corals. Marine Ecology Progress Series **273:** 81-88.

Kellogg, R., and J. Patton. 1983. Lipid droplets, medium of energy exchange in the symbiotic anemone Condylactis gigantea: a model coral polyp. Marine Biology **75:** 137-149.

Kirk, J. 1975. A theoretical analysis of the contribution of algal cells to the attenuation of light within natural waters II. Spherical cells. New Phytologist **75:** 21-36.

Kirk, J. T. O. 1994. Light and photosynthesis in aquatic ecosystems, 2nd ed. Cambridge University Press.

Kleypas, J., R. Buddemeier, D. Archer, J. Gattuso, C. Langdon, and B. Opdyke. 1999. Geochemical consequences of increased atmospheric carbon dioxide on coral reefs. Science **284:** 118.

Kleypas, J., R. Buddemeier, and J. Gattuso. 2001. The future of coral reefs in an age of global change. International Journal of Earth Sciences **90:** 426-437.

Koop, K. and others 2001. ENCORE: the effect of nutrient enrichment on coral reefs. Synthesis of results and conclusions. Marine Pollution Bulletin **42:** 91-120.

Kopp, C. and others 2013. Highly Dynamic Cellular-Level Response of Symbiotic Coral to a Sudden Increase in Environmental Nitrogen. mBio **4**.

Kramer, D. M., G. Johnson, O. Kiirats, and G. E. Edwards. 2004. New fluorescence parameters for the determination of QA redox state and excitation energy fluxes. Photosynthesis Research **79:** 209-218.

Kroon, B. M. A., and S. Thoms. 2006. From electron to biomass: A mechanistic model to describe phytoplankton photosynthesis and stready-state growth rates. Journal of Phycology **42:** 593-609.

Lajeunesse, T. 2002. Diversity and community structure of symbiotic dinoflagellates from Caribbean coral reefs. Marine Biology **141:** 387-400.

Lajeunesse, T. C., G. Lambert, R. A. Andersen, M. A. Coffroth, and D. W. Galbraith. 2005. *Symbiodinium* (Pyrrhophyta) genome sizes (DNA content) are smallest among dinoflagellates. Journal of Phycology **41:** 880-886.

Leclercq, N., J. Gattuso, and J. Jaubert. 2002. Primary production, respiration, and calcification of a coral reef mesocosm under increased CO 2 partial pressure. Limnology and Oceanography **47:** 558-564.

Leggat, W., M. Badger, and D. Yellowlees. 1999. Evidence for an inorganic carbon-concentrating mechanism in the symbiotic dinoflagellate Symbiodinium sp. Plant physiology **121:** 1247.

Lesser, M., and J. Farrell. 2004. Exposure to solar radiation increases damage to both host tissues and algal symbionts of corals during thermal stress. Coral Reefs **23:** 367-377.

Lesser, M. P. 2004. Experimental biology of coral reef ecosystems. Journal of Experimental Marine Biology and Ecology **300:** 217-252.

Lesser, M. P. 2006. Oxidative stress in marine environments: biochemistry and physiological ecology. Annu. Rev. Physiol. **68:** 253-278.

Lesser, M. P., M. Slattery, M. Stat, M. Ojimi, R. D. Gates, and A. Grottoli. 2010. Photoacclimatization by the coral Montastraea cavernosa in the mesophotic zone: light, food, and genetics. Ecology **91:** 990-1003.

Lewis, J., and W. Price. 1975. Feeding mechanisms and feeding strategies of Atlantic reef corals. Journal of Zoology **176:** 527-544.

Levy, O., Y. Achituv, Y. Yacobi, N. Stambler, and Z. Dubinsky. 2006. The impact of spectral composition and light periodicity on the activity of two antioxidant enzymes (SOD and CAT) in the coral *Favia favus*. Journal of Experimental Marine Biology and Ecology **328:** 35-46.

Lilley, R., P. J. Ralph, and A. W. D. Larkum. 2010. The determination of activity of the enzyme Rubisco in cell extracts of the dinoflagellate alga *Symbiodinium* sp. by manganese chemiluminescence and its response to short-term thermal stress of the alga. Plant, Cell & Environment **33:** 995-1004.

Loya, S., N. Yamazato, and W. Sambali. 2001. Coral bleaching: the winners and the losers. Ecology Letters **4:** 122-131.

Mackay, R., and M. Khalil. 2000. Greenhouse gases and global warming. Trace gas emissions and plants**:** 1–28.

Marshall, A., and O. Wright. 1993. Confocal laser scanning light microscopy of the extra-thecal epithelia of undecalcified scleractinian corals. Cell and Tissue Research **272:** 533-543.

Marshall, H. L., R. J. Geider, and K. J. Flynn. 2000. A mechanistic model of photoinhibition. New Phytologist **145:** 347-359.

Marshall, P., and A. Baird. 2000. Bleaching of corals on the Great Barrier Reef: differential susceptibilities among taxa. Coral Reefs **19:** 155-163.

Marubini, F., and B. Thake. 1999. Bicarbonate addition promotes coral growth. Limnology and Oceanography **44:** 716-720.

Maynard, J., K. Anthony, P. Marshall, and I. Masiri. 2008a. Major bleaching events can lead to increased thermal tolerance in corals. Marine Biology **155:** 173-182.

Maynard, J. A. and others 2008b. ReefTemp: an interactive monitoring system for coral bleaching using high-resolution SST and improved stress predictors. Geophysical Research Letters **35:** L05603.

Mcginty, E. S., J. Pieczonka, and L. D. Mydlarz. 2012. Variations in reactive oxygen release and antioxidant activity in multiple *Symbiodinium* types in response to elevated temperature. Microbial ecology **64:** 1000-1007.

Mehler, A. H., and A. H. Brown. 1952. Studies on reactions of illuminated chloroplasts. III. Simultaneous photoproduction and consumption of oxygen studied with oxygen isotopes. Archives of biochemistry and biophysics **38:** 365-370.

Mongin, M., and M. Baird. submitted. The interacting effects of photosynthesis, calcification and water circulation on carbon chemistry variability on a coral reef at: a modelling study. Ecological Modelling.

Monismith, S. G. and others 2010. Flow effects on benthic grazing on phytoplankton by a Caribbean reef. Limnology and Oceanography **55:** 1881-1892.

Moya, A. and others 2008. Carbonic Anhydrase in the Scleractinian Coral Stylophora pistillata. Journal of Biological Chemistry **283:** 25475-25484.

Muller-Parker, G., C. Cook, and C. D'elia. 1994a. Elemental composition of the coral *Pocillopora damicornis* exposed to elevated seawater ammonium. Pacific Science **48:** 234-246.

Muller-Parker, G., and C. D'elia. 1997. Interactions between corals and their symbiotic algae. Life and death of coral reefs**:** 96–133.

Muller-Parker, G., L. Mccloskey, O. Hoegh-Guldberg, and P. Mcauley. 1994b. Effect of ammonium enrichment on animal and algal biomass of the coral Pocillopora damicornis.

Muller, E. B., S. a. L. M. Kooijman, P. J. Edmunds, F. J. Doyle, and R. M. Nisbet. 2009. Dynamic energy budgets in syntrophic symbiotic relationships between heterotrophic hosts and photoautotrophic symbionts. Journal of Theoretical Biology **259:** 44-57.

Murata, N., S. Takahashi, Y. Nishiyama, and S. I. Allakhverdiev. 2007. Photoinhibition of photosystem II under environmental stress. Biochimica et Biophysica Acta (BBA) - Bioenergetics **1767:** 414-421.

Murray, A., and J. Parslow. 1997. Port Phillip Bay integrated model: final report. Canberra, A.C.T.: Technical report CSIRO.

Muscatine, L. 1990. The role of symbiotic algae in carbon and energy flux in reef corals. Ecosystems of the world **25:** 75-87.

Muscatine, L., and C. D'elia. 1978. The uptake, retention, and release of ammonium by reef corals. Limnology and Oceanography **23:** 725-734.

Muscatine, L., D. Grossman, and J. Doino. 1991. Release of symbiotic algae by tropical sea anemones and corals after cold shock. Marine ecology progress series. Oldendorf **77:** 233-243.

Muscatine, L., L. Mccloskey, and R. Marian. 1981. Estimating the daily contribution of carbon from zooxanthellae to coral animal respiration. Limnology and Oceanography **26:** 601-611.

Muscatine, L., and J. Porter. 1977. Reef corals: mutualistic symbioses adapted to nutrient-poor environments. Bioscience **27:** 454-460.

Muscatine, L., J. W. Porter, and I. R. Kaplan. 1989. Resource partitioning by reef corals as determined from stable isotope composition. Marine Biology **100:** 185-193.

Naumann, M., A. Haas, U. Struck, C. Mayr, M. El-Zibdah, and C. Wild. 2010. Organic matter release by dominant hermatypic corals of the Northern Red Sea. Coral Reefs **29:** 649-659.

Neale, P. J., and P. J. Richerson. 1987. Photoinhibition and the diurnal variation of phytoplankton photosynthesis—I. Development of a photosynthesis—

irradiance model from studies of in situ responses. Journal of Plankton Research **9:** 167-193.

Orr, J. and others 2005. Anthropogenic ocean acidification over the twenty-first century and its impact on calcifying organisms. Nature **437:** 681-686.

Peng, S. E. and others 2008. Isolation of tissue layers in hermatypic corals by N-acetylcysteine: morphological and proteomic examinations. Coral Reefs **27:** 133-142.

Penland, L., J. Kloulechad, D. Idip, and R. Van Woesik. 2004. Coral spawning in the western Pacific Ocean is related to solar insolation: evidence of multiple spawning events in Palau. Coral Reefs **23:** 133-140.

Pernice, M. and others 2012. A single-cell view of ammonium assimilation in coral–dinoflagellate symbiosis. The ISME Journal.

Ragni, M., R. L. Airs, S. J. Hennige, D. J. Suggett, M. E. Warner, and R. J. Geider. 2010. PSII photoinhibition and photorepair in *Symbiodinium* (Pyrrhophyta) differs between thermally tolerant and sensitive phylotypes. Mar Ecol Prog Ser **406:** 57-70.

Randall, D. A. and others 2007. Climate models and their evaluation. Climate change **323**.

Raven, J. A. 2003. Inorganic carbon concentrating mechanisms in relation to the biology of algae. Photosynthesis Research **77:** 155-171.

Raven, J. A. 2011. The cost of photoinhibition. Physiologia Plantarum **142:** 87-104.

Raven, J. A., C. S. Cockell, and C. L. De La Rocha. 2008. The evolution of inorganic carbon concentrating mechanisms in photosynthesis. Philosophical Transactions of the Royal Society B: Biological Sciences **363:** 2641-2650.

Redfield, A. C., B. H. Ketchum, and F. A. Richards. 1963. The influence of organisms on the composition of sea-water. The sea: ideas and observations on progress in the study of the seas **2**.

Reynaud, S., N. Leclercq, S. Romaine-Lioud, C. Ferrier-Pagés, J. Jaubert, and J. Gattuso. 2003. Interacting effects of CO_2 partial pressure and temperature

on photosynthesis and calcification in a scleractinian coral. Global Change Biology **9:** 1660-1668.

Richmond, R. 1987. Energetic relationships and biogeographical differences among fecundity, growth and reproduction in the reef coral Pocillopora damicornis. Bulletin of Marine Science **41:** 594-604.

Roberts, C. and others 2002. Marine biodiversity hotspots and conservation priorities for tropical reefs. Science **295:** 1280.

Roberts, J., L. Fixter, and P. Davies. 2001. Ammonium metabolism in the symbiotic sea anemone Anemonia viridis. Hydrobiologia **461:** 25-35.

Roberts, J. M., A. J. Wheeler, and A. Freiwald. 2006. Reefs of the deep: the biology and geology of cold-water coral ecosystems. Science **312:** 543.

Roelfsema, C., S. Phinn, and W. Dennison. 2002. Spatial distribution of benthic microalgae on coral reefs determined by remote sensing. Coral Reefs **21:** 264-274.

Rosenberg, E., O. Koren, L. Reshef, R. Efrony, and I. Zilber-Rosenberg. 2007. The role of microorganisms in coral health, disease and evolution. Nat Rev Micro **5:** 355-362.

Ross, O., and R. Geider. 2009. New cell-based model of photosynthesis and photo-acclimation: accumulation and mobilisation of energy reserves in phytoplankton. Mar Ecol Prog Ser **383:** 53-71.

Ross, O., C. Moore, D. Suggett, H. Macintyre, and R. Geider. 2008. A model of photosynthesis and photo-protection based on reaction center damage and repair. Limnology and Oceanography **53:** 1835-1852.

Sabine, C. L. and others 2004. The oceanic sink for anthropogenic CO2. Science **305:** 367-371.

Saragosti, E., D. Tchernov, A. Katsir, and Y. Shaked. 2010. Extracellular production and degradation of superoxide in the coral *Stylophora pistillata* and cultured *Symbiodinium*. PloS one **5:** e12508.

Schreiber, U., H. Hormann, C. Neubauer, and C. Klughammer. 1995. Assessment of photosystem II photochemical quantum yield by chlorophyll fluorescence quenching analysis. Functional Plant Biology **22:** 209-220.

Sebens, K., S. Grace, B. Helmuth, E. Maney Jr, and J. Miles. 1998. Water flow and prey capture by three scleractinian corals, Madracis mirabilis, Montastrea cavernosa and Porites porites, in a field enclosure. Marine Biology **131:** 347-360.

Shashar, N., Y. Cohen, Y. Loya, and N. Sar. 1994. Nitrogen fixation (acetylene reduction) in stony corals - Evidence for coral-bacteria interactions. Marine Ecology Progress Series **111:** 259-264.

Shick, J. M. 1991. A functional biology of sea anemones. Chapman & Hall.

Smith, D., D. Suggett, and N. Baker. 2005. Is photoinhibition of zooxanthellae photosynthesis the primary cause of thermal bleaching in corals? Global Change Biology **11:** 1-11.

Stat, M., D. Carter, and O. Hoegh-Guldberg. 2006. The evolutionary history of< i> Symbiodinium</i> and scleractinian hosts—Symbiosis, diversity, and the effect of climate change. Perspectives in Plant Ecology, Evolution and Systematics **8:** 23-43.

Steen, R. G., and L. Muscatine. 1987. Low temperature evokes rapid exocytosis of symbiotic algae by a sea anemone. The Biological Bulletin **172:** 246-263.

Stimson, J. 1997. The annual cycle of density of zooxanthellae in the tissues of field and laboratory-held Pocillopora damicornis (Linnaeus). Journal of Experimental Marine Biology and Ecology **214:** 35-48.

Suggett, D. J., M. E. Warner, D. J. Smith, P. Davey, S. Hennige, and N. R. Baker. 2008. Photosynthesis and production of hydrogen peroxide by *Symbiodinium* (Pyrrhophyta) phylotypes with different thermal tolerances. Journal of Phycology **44:** 948-956.

Sutton, D., and O. Hoegh-Guldberg. 1990. Host-zooxanthella interactions in four temperate marine invertebrate symbioses: assessment of effect of host extracts on symbionts. The Biological Bulletin **178:** 175-186.

Szmant-Froelich, A., and M. E. Pilson. 1977. Nitrogen excretion by colonies of the temperate coral Astrangia danae with and without zooxanthellae, p. 417-423. Proc. 3rd Int. Coral Reef Symp.

Takahashi, S., T. Nakamura, M. Sakamizu, R. Woesik, and H. Yamasaki. 2004. Repair machinery of symbiotic photosynthesis as the primary target of heat stress for reef-building corals. Plant and cell physiology **45:** 251-255.

Takahashi, S., S. Whitney, S. Itoh, T. Maruyama, and M. Badger. 2008. Heat stress causes inhibition of the de novo synthesis of antenna proteins and photobleaching in cultured Symbiodinium. Proceedings of the National Academy of Sciences **105:** 4203-4208.

Takahashi, S., S. M. Whitney, and M. R. Badger. 2009. Different thermal sensitivity of the repair of photodamaged photosynthetic machinery in cultured *Symbiodinium* species. Proceedings of the National Academy of Sciences **106:** 3237-3242.

Tambutte, E., D. Allemand, E. Mueller, and J. Jaubert. 1996. A compartmental approach to the mechanism of calcification in hermatypic corals. Journal of Experimental Biology **199:** 1029.

Tambutté, S. and others 2007. Characterization and role of carbonic anhydrase in the calcification process of the azooxanthellate coral Tubastrea aurea. Marine Biology **151:** 71-83.

Tanaka, Y., H. Ogawa, and T. Miyajima. 2011. Bacterial decomposition of coral mucus as evaluated by long-term and quantitative observation. Coral Reefs **30:** 443-449.

Tchernov, D. and others 2004. Membrane lipids of symbiotic algae are diagnostic of sensitivity to thermal bleaching in corals. Proceedings of the National Academy of Sciences of the United States of America **101:** 13531-13535.

Titlyanov, E., and T. Titlyanova. 2002. Reef-building corals—symbiotic autotrophic organisms: 1. General structure, feeding pattern, and light-dependent distribution in the shelf. Russian Journal of Marine Biology **28:** 1-15.

Tremblay, P., R. Grover, J. F. Maguer, L. Legendre, and C. Ferrier-Pagès. 2012. Autotrophic carbon budget in coral tissue: a new 13C-based model of photosynthate translocation. The Journal of Experimental Biology **215:** 1384-1393.

Ulstrup, K., P. Ralph, A. Larkum, and M. Kühl. 2006. Intra-colonial variability in light acclimation of zooxanthellae in coral tissues of *Pocillopora damicornis*. Marine Biology **149:** 1325-1335.

Wang, J., and A. Douglas. 1998. Nitrogen recycling or nitrogen conservation in an alga-invertebrate symbiosis? Journal of Experimental Biology **201:** 2445-2453.

Wang, J., and A. Douglas. 1999. Essential amino acid synthesis and nitrogen recycling in an alga–invertebrate symbiosis. Marine Biology **135:** 219-222.

Wangpraseurt, D., A. W. Larkum, P. J. Ralph, and M. Kühl. 2012. Light gradients and optical microniches in coral tissues. Frontiers in Microbiology **3:** 316.

Ward, S. 1995. Two patterns of energy allocation for growth, reproduction and lipid storage in the scleractinian coral Pocillopora damicornis. Coral Reefs **14:** 87-90.

Warner, M., W. Fitt, and G. Schmidt. 1999. Damage to photosystem II in symbiotic dinoflagellates: a determinant of coral bleaching. Proceedings of the National Academy of Sciences **96:** 8007-8012.

Webb, K., W. Dupaul, W. Wiebe, W. Sottile, and R. Johannes. 1975. Enewetak (Eniwetok) Atoll: aspects of the nitrogen cycle on a coral reef. Limnology and Oceanography**:** 198-210.

Webster, N. S. and others 2004. Metamorphosis of a Scleractinian Coral in Response to Microbial Biofilms. Appl. Environ. Microbiol. **70:** 1213-1221.

Weis, V. M. 2008. Cellular mechanisms of Cnidarian bleaching: stress causes the collapse of symbiosis. Journal of Experimental Biology **211:** 3059.

Venn, A. A., J. E. Loram, and A. E. Douglas. 2008. Photosynthetic symbioses in animals. J. Exp. Bot. **59:** 1069-1080.

Venn, A. A., M. A. Wilson, H. G. Trapido-Rosenthal, B. J. Keely, and A. E. Douglas. 2006. The impact of coral bleaching on the pigment profile of the symbiotic alga, Symbiodinium. Plant, Cell & Environment **29:** 2133-2142.

Veron, J. E. N., and M. Stafford-Smith. 2000. Corals of the World. Corals of the World Australian Institute of Marine Science: Townsville.

Wild, C., M. Huettel, A. Klueter, S. Kremb, M. Rasheed, and B. Jørgensen. 2004a. Coral mucus functions as an energy carrier and particle trap in the reef ecosystem. Nature **428:** 66-70.

Wild, C. and others 2005a. Benthic metabolism and degradation of natural particulate organic matter in carbonate and silicate reef sands of the northern Red Sea. Marine Ecology Progress Series **298:** 69-78.

Wild, C., M. Rasheed, U. Werner, U. Franke, R. Johnstone, and M. Huettel. 2004b. Degradation and mineralization of coral mucus in reef environments. Marine Ecology Progress Series **267:** 159-171.

Wild, C., H. Woyt, and M. Huettel. 2005b. Influence of coral mucus on nutrient fluxes incarbonate sands. Marine Ecology Progress Series **287:** 87-98.

Wilkerson, F., and R. Trench. 1986. Uptake of dissolved inorganic nitrogen by the symbiotic clam Tridacna gigas and the coral Acropora sp. Marine Biology **93:** 237-246.

Wilkinson, C. [ed.]. 2002. Status of coral reefs of the world. Australian Institute of Marine Science.

Wilkinson, C., D. M. B. Williams, P. Sammarco, R. Hogg, and L. Trott. 1984. Rates of nitrogen fixation on coral reefs across the continental shelf of the central Great Barrier Reef. Marine Biology **80:** 255-262.

Von Liebig, J., and L. P. B. Playfair. 1840. Chemistry in its Application to Agriculture and Physiology. Taylor and Walton, London.

Wooldridge, S. 2009. A new conceptual model for the warm-water breakdown of the coral–algae endosymbiosis. Marine and Freshwater Research **60:** 483-496.

Wooldridge, S. A., and T. J. Done. 2009. Improved water quality can ameliorate effects of climate change on corals. Ecological Applications **19:** 1492-1499.

Wyatt, A. S., J. L. Falter, R. J. Lowe, S. Humphries, and A. M. Waite. 2012. Oceanographic forcing of nutrient uptake and release over a fringing coral reef. Limnol Oceanogr **57:** 401-419.

Wyatt, A. S., R. J. Lowe, S. Humphries, and A. M. Waite. 2010. Particulate nutrient fluxes over a fringing coral reef: relevant scales of phytoplankton production and mechanisms of supply. Mar. Ecol. Prog. Ser **405:** 113-130.

Yellowlees, D., T. a. V. Rees, and W. Leggat. 2008. Metabolic interactions between algal symbionts and invertebrate hosts. Plant, Cell & Environment **31:** 679-694.

Yonge, C. M., and A. Nicholls. 1931. The structure, distribution and physiology of the zooxanthellae. British Museum.

Zhang, Z., R. Lowe, J. Falter, and G. Ivey. 2011. A numerical model of wave-and current-driven nutrient uptake by coral reef communities. Ecological Modelling **222:** 1456-1470.

Zhu, B., G. Wang, B. Huang, and C. Tseng. 2004. Effects of temperature, hypoxia, ammonia and nitrate on the bleaching among three coral species. Chinese Science Bulletin **49:** 1923-1928.

Zimmerman, R., J. B. Soohoo, J. Kremer, and D. D'argenio. 1987. Evaluation of variance approximation techniques for non-linear photosynthesis—irradiance models. Marine Biology **95:** 209-215.